Multifunctional water-soluble phosphorus dendrimers

– synthesis and surface applications –

Dissertation zur Erlangung des Grades

"Doktor der Naturwissenschaften"

am Fachbereich Biologie
der Johannes Gutenberg-Universität
in Mainz

vorgelegt von

Edwin Ronald de Jong
geboren in Gouda, die Niederlande

Mainz, 2010

Die vorliegende Arbeit wurde in der Zeit von April 2007 bis März 2010 am Laboratoire de Chimie de Coordination (CNRS, Toulouse, Frankreich) und am Max-Planck-Institut für Polymerforschung (Mainz) angefertigt.

Verteidigt am 30.03.2010 an der Johannes Gutenberg Universität, Mainz.

to my family and Vesna

Abstract – Zusammenfassung

Dendrimers are polymeric macromolecules with a regularly branched structure and are synthesised in an iterative fashion. Due to their monodispersity, well-defined shape and extremely high functionality, dendrimers are ideal nano-sized objects for functional and biocompatible surface coatings, biosensing and biomedicine. This dissertation describes the synthesis of ten novel water-soluble phosphorus containing dendrimers and their application in different biological and biomimetic systems. The dendrimers can be divided into two classes; the first type contains either a ferrocene at the core or 24 ferrocenes in the branches. They showed reversible reduction-oxidation behaviour and might be applied in electronic multilayered architectures. Dendrimers of the second class carry a dithiolane functionalised core that can strongly bind to noble metals, like gold substrates. Although such dendrimer coated substrates were unable to tether defect-free lipid bilayer membranes, the coatings were successfully applied for culturing Human Osteoblast cells. The cell adhesion to a coating of polycationic dendrimers was so strong that cell division could not take place, specifically evoking apoptosis. The polyanionic dendrimers, however, promoted excellent cell adhesion and proliferation. Therefore, the practical application of such macromolecular architectures can be envisioned, such as in dendrimer coatings for tissue engineering and or medical implants.

Dendrimere sind polymere Makromoleküle mit einer wohl definierten Struktur. Dank ihrer Monodispersität, hohen Verästelung und sehr hohen Funktionalität sind Dendrimere ideale nanoskopische Objekte für die Beschichtung von hochfunktionellen, biokompatibelen Oberflächen zur Anwendung in Biosensorik und Biomedizin. Im Rahmen dieser Dissertation wurden zehn neue wasserlösliche phosphorhaltige Dendrimere synthetisiert. Mögliche Anwendungen in biologischen und biomimetischen Systemen wurden untersucht und diskutiert. Die synthetisierten Dendrimere können in zwei Klassen unterteilt werden. Dendrimere der ersten Klasse tragen entweder zentral ein Ferrocen oder insgesamt 24 Ferrocen-Moleküle in den Ästen.

Diese Denrimere zeigen ein reversibles Reduktions- und Oxidationsverhalten und könnten damit in elektronische Multischichtsysteme inkorporiert werden. Dendrimere der zweiten Klasse tragen ein Dithiolan im Zentrum. Somit konnten Edelmetalle, wie zum Beispiel Goldoberflächen, mit einer Dendrimerschicht funktionalisiert werden. Die erhaltenen Strukturen konnten leider nicht die Bildung einer defektfreien Lipidmembrane unterstützen. Sie förderten allerdings die Adhäsion humaner Osteoblastzellen. Die Zelladhäsion auf Schichten aus polykationischen Dendrimeren war so stark, dass Zellteilung nicht länger möglich war und sogar spezifisch Apoptose hervorrief. Polyanionische Dendrimere dagegen führten zu exzellenter Zelladhesion und -proliferation. Die erhaltenen makromolekularen Architekturen können somit als mögliche Oberflächenbeschichtungen, zum Beispiel für Humanimplantate, Anwendung finden.

List of Abbreviations

AC	alternating current
ADP	Adenosine diphosphate
AFM	Atomic Force Microscopy
ATP	Adenosine triphosphate
ATR	Attenuated Total Reflectance
BLM	black lipid membrane
CA	contact angle
CCD	charge-coupled device
CcO	Cytochrome c oxidase
Cp	cyclopentadienyl
CPE	Constant Phase Element
CV	Cyclic Voltammetry
DAPI	4',6-diamidino-2-phenylindole dihydrochloride
DC	direct current
DCM	dichloromethane
DDM	dodecyl-β-D-maltoside
DE	dendritic effect
DEEDA	N,N-diethylethylenediamine
DIPEA	diisopropylethylamine
DMF	dimethylformamide
DNA	deoxyribonucleic acid
DphyPC	1,2-di-O-phytanoyl-sn-glycero-3-phosphocholine
EIS	Electrochemical Impedance Spectroscopy
ET	electron transfer
FRAP	Fluorescence Recovery After Photobleaching
G_n	generation number n
GUV	Giant Unilamellar Vesicle
hBLM	hybrid bilayer lipid membrane
HIS tag	hexahistidine tag
HOB	Human Osteoblast
HPLC	High Performance Liquid Chromatography
ITO	Indium Tin Oxide
LB / LS	Langmuir Blodgett / Langmuir Schäfer
LbL	layer-by-layer
LCC	Laboratoire de Chimie de Coordination
MeOH	methanol
MHTPC	N-methyldichloro thiophosphorhydrazide (methylhydrazide thiophosphoryl chloride)
MPI-P	Max Planck Institute for Polymer Research
MRI	Magnetic Resonance Imaging
*n*BuLi	*n*-butyllithium
NK cell	Natural Killer cell
NMR	Nuclear Magnetic Resonance
NP	nanoparticle
NT	nanotube
OLED	Organic Light Emitting Device
PAMAM	polyamidoamine
PDMS	polydimethylsiloxane
PEG (=PEO)	polyethyleneglycol (= -oxide)
PEI	Polyethyleneimide
p-HBA	para-hydroxybenzaldehyde
PPI	polypropyleneimine
PTFE	polytetrafluorethylene
QCM-D	Quartz Crystal Microbalance (Dissipation)
RGD	$(\text{arginine-glycine-aspartic acid})_n$ sequence
RSE	rapid solvent exchange
RT	room temperature
SAM	self assembled monolayer
SEIRAS	Surface Enhanced InfraRed Absorption spectroscopy
SPR	Surface Plasmon Resonance
SUV	small unilamellar vesicle
tBLM	tethered bilayer lipid membrane
TBTU	O-(benzotriazol-1-yl)-N,N,N',N'-tetramethyl uronium tetrafluoroborate
*t*BuLi	*tert*-butyllithium
THF	tetrahydrofuran
TIR	Total Internal Reflection
TPA	Two Photon Absorption
TPEF	Two Photon Excitation Fluorescence
TSG	template stripped gold
VF	Vesicle Fusion

Table of Contents

1 Introduction

In this chapter a general overview on dendrimers is given. The objective is not to provide an exhaustive review on all dendrimer applications, but rather to describe basic concepts and their relation to characteristics of dendrimers. The focus lies on the relationship between synthetic approach, the final structure and the physical and chemical properties of dendrimers. Applications related to the work performed in this thesis are discussed in greater detail in Chapters 3-6 in order to present the experimental findings in their broader perspective.

1.1 Dendrimers

1.1.1 A brief history: the first two decades

Dendrimers appeared in 1978 as so-called "cascade molecules" reported by Vögtle *et al* [3], who recognised the analogy with a waterfall progressively splitting up into multiple smaller waterfalls [8]. The synthetic approach towards these cascade molecules [4-7] comprised two steps; the first one is a Michael addition where a di- (or poly-) amine becomes a tetra- (or poly-) nitrile and the second step is the reduction of the nitriles into primary amines. This sequence of reactions can be carried out repeatedly to obtain, for the first time, regularly branched molecules that have many arms. Despite this synthetic novelty, the development of this type of molecules experienced a slow start due to synthetic and subsequent analytic obstacles (purification). In the early eighties, the development of dendrimers progressed with Denkewalter (polylysine [9]), Maciejewski (densely packed cascade-like polymers [10]), De Gennes and Hervet (starburt-limited generation [11]) and Tomalia [12-14]. Tomalia *et al.* synthesised branched "Starburst" polyamidoamine (PAMAM) molecules and coined the name *dendrimers*, which is derived from the greek words *dendron* (tree) and *meros* (part). These

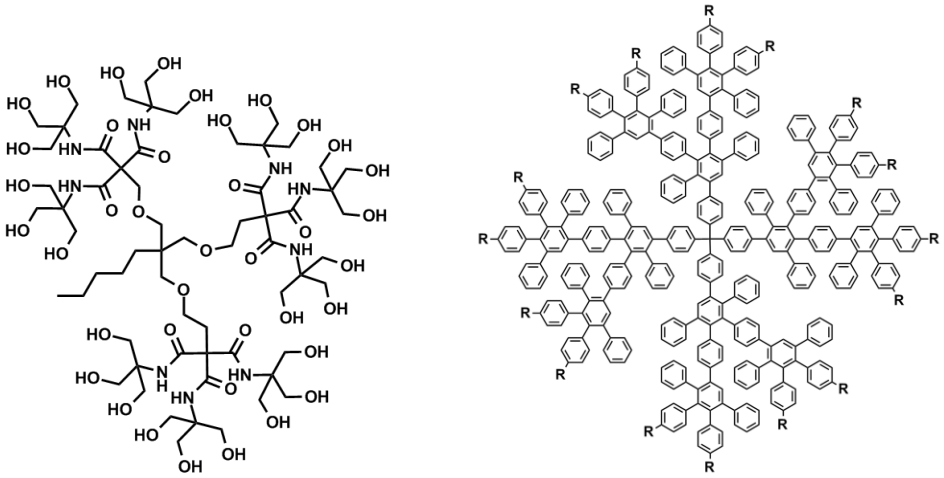

Fig. 1.1 – Left: Newkome's arborol [1]. Right: a Müllen-type shape persistent polyphenylene dendrimer [2].

dendrimers were the first ones to become commercially available [15]. In the same year, Newkome *et al.* [1] synthesised what he called “arborols”; water-soluble hydroxy terminated dendrimers (Fig. 1.1).

The first convergent (see 1.2.2) polyarylether dendrimers were synthesised by Fréchet and Hawker [16]. In the same year, Miller and Neenan [17] prepared aryl based dendrimers in a convergent manner. The first dendrimers containing heteroatoms (silicon [18], phosphorus [19]) were prepared soon after and in 1994 [20], Majoral and Caminade reported their first phosphorus containing dendrimers [21-23]. Soon after, Müllen prepared the first polyphenylene dendrimers, which were the first shape persistent dendrimers [2, 24] (Fig. 1.1).

1.1.2 Dendritic architectures

Dendrimers are polymeric macromolecules that are synthesised in a radial, stepwise fashion. They are built starting from a core that allows for the attachment of multiple branches. This multiplicity can be chosen nearly arbitrarily [25]. As schematically depicted in Fig. 1.2, the iterative synthesis occurs in cycles of two reactions (branch unit and divergent point) that together complete a generation. The generation number is indicated with G_n. The divergent points are responsible for an exponential increase of peripheral groups, whose number can be defined as $N_c.N_{div}{}^G$ where N_c is the multivalency of the core, N_{div} the multivalency of the divergent points and G the generation number. The use of the terms surface- or end groups as an alternative for peripheral or terminal groups may become inappropriate when branches fold inwards and no longer represent the outside layer of the dendrimer. Within the dendrimer, there are voids that can be filled with solvent or other small molecules. These voids can be exploited and already find their application for drugs delivery [26-28] and nanoparticle synthesis [29].

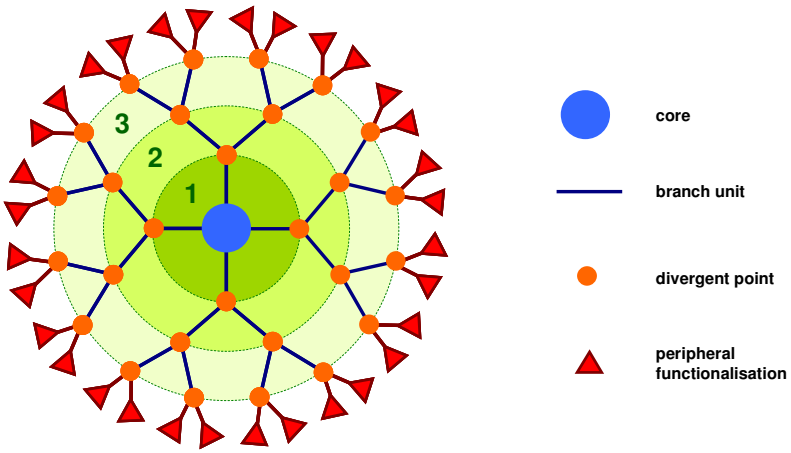

Fig. 1.2 – A generation 3 (G_3) dendrimer with a tetravalent core and 32 functional groups. The numbers indicate the generations. In green, internal voids are indicated.

Fig. 1.2 shows only one type of dendritic architecture, but there are a few other architectures worth mentioning (Fig. 1.3). The simplest of them is the dendron, which has a functional core. Multiple dendrons can be combined in a convergent approach to a dendrimer. If the dendrons are differently functionalised and attached to a core, the result is an asymmetric Janus-type dendrimer [30-31]. Linear polymers can be dendronised by reacting dendrons with their focal point to their backbones.

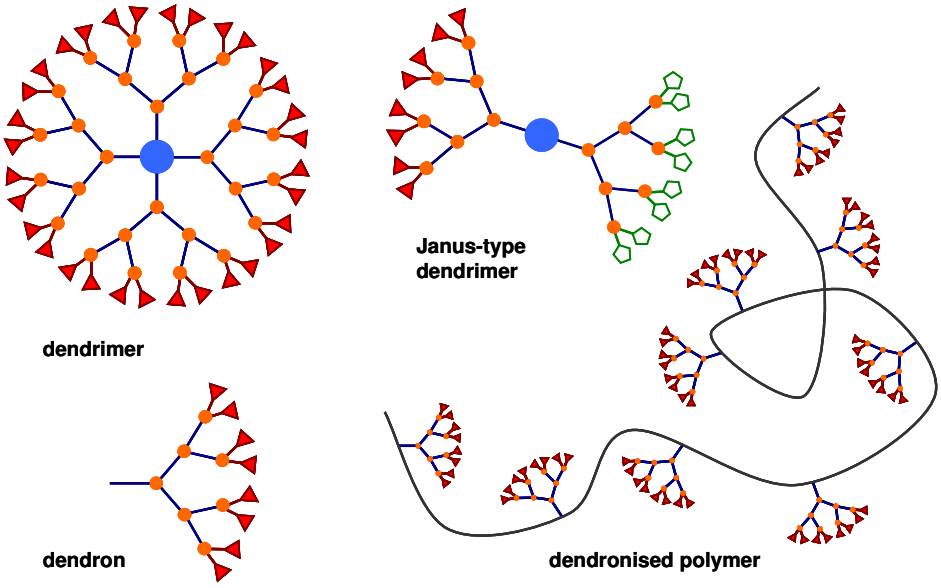

Fig. 1.3 – Different dendritic architectures: dendrons can be combined in different ways and can be used to functionalise other macromolecules.

1.1.3 Perfection and its limitations

Dendrimers can be distinguished from for instance hyperbranched polymers by their absolute monodispersity. Whereas hyperbranched polymers are formed by the rather uncontrolled polymerisation of monomers, dendrimers are synthesised in a stepwise fashion while having full control over the degree of branching. This was described by Frechet *et al.* who prepared polyester quasi-dendrimers in a one-pot reaction [32]. Dendrimers possess a degree of branching that equals 1.

The theory of de Gennes [11] states that dendritic growth continues in a defect free manner until the generation at which the available surface for new units becomes limiting. This phenomenon is known under the name "Starburst limited effect" and for this reason ideally branched G_5 polyethyleneimine dendrimers, for example, do not exist [14]. This model, however, falls short in explaining how G_{12} phosphorus dendrimers, the largest dendrimers ever synthesised [33], could be synthesised defect free. At higher generations, due to steric crowding, peripheral groups can start folding back [34]. This does not necessarily immediately lead to non-quantitative conversion of the end groups as the dendrimer interior is still available for chemical reactions. At even higher generations, however, backfolding introduces imperfections in the dendritic structure. Moreover, backfolding may not be possible when bulky terminal groups are used [35-37]. This problem can be overcome by introducing a tether-lengthening strategy that provides more space at the dendrimer periphery. This shows that it is the available interior space that is limiting rather than the peripheral surface area.

1.2 Dendrimers: Synthesis and Species

Dendrimers can be prepared in a bottom-up and top-down approach, which are the divergent and convergent syntheses, respectively. The former starts with a core unit onto which the branch units and divergent points are grafted in a layer-wise fashion. The latter approach involves the attachment of

dendrons to a core. Whichever methodology is used to synthesise dendrimers, the reactions involved must always be quantitative, quick and must only have by-products that are easily removable by a washing or precipitation work-up. Here, both the divergent and convergent method with their issues and advantages are described.

1.2.1 Divergent Synthesis

PAMAM dendrimers are by far the most frequently used dendrimers, because they are commercially available. Their synthesis is a divergent process [13]. Starting from an ethylenediamine core, the repetitive steps are a Michael addition of amines to the double bond of methylacrylate and the formation of amide bonds between the terminal esters and ethylenediamine (Fig. 1.4). Repeating these two steps leads to large dendrimers up to generation 10.

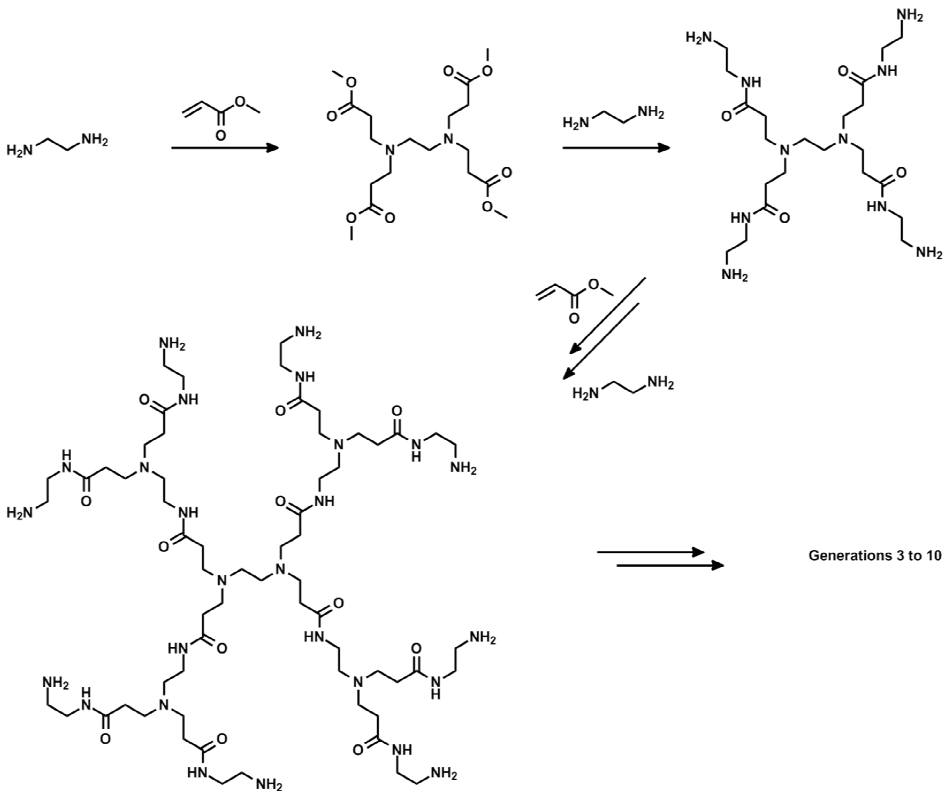

Fig. 1.4 – Divergent synthesis of PAMAM dendrimers comprises a Michael addition and an amidation as the alternating reactions [13].

Divergent synthesis enables the preparation of high generation dendrimers, but the number of reactions at higher generations increases exponentially also the time required for completion increases. As discussed before, above a certain threshold generation defects appear in the dendrimer that grow in number when the generation is increased. This leads to a loss of monodispersity [38-39]. Despite this drawback, most dendrimers are synthesised in a divergent fashion. Phosphorus dendrimers can also be synthesised in a divergent manner. Their synthesis is discussed in detail in section 3.3.

1.2.2 Convergent Synthesis

As a solution to the statistical defects that are introduced with the divergent methodology at higher generations, convergent synthesis attaches complete dendrons to a core. This approach allows for larger defect free dendrimers, but also in this case the generation number is limited; if the dendrons become too large the core will only be partially functionalised. The convergent method also decreases the required reaction time at higher generations. Fréchet *et al.* developed a method [16, 40] that progressively works towards the core,

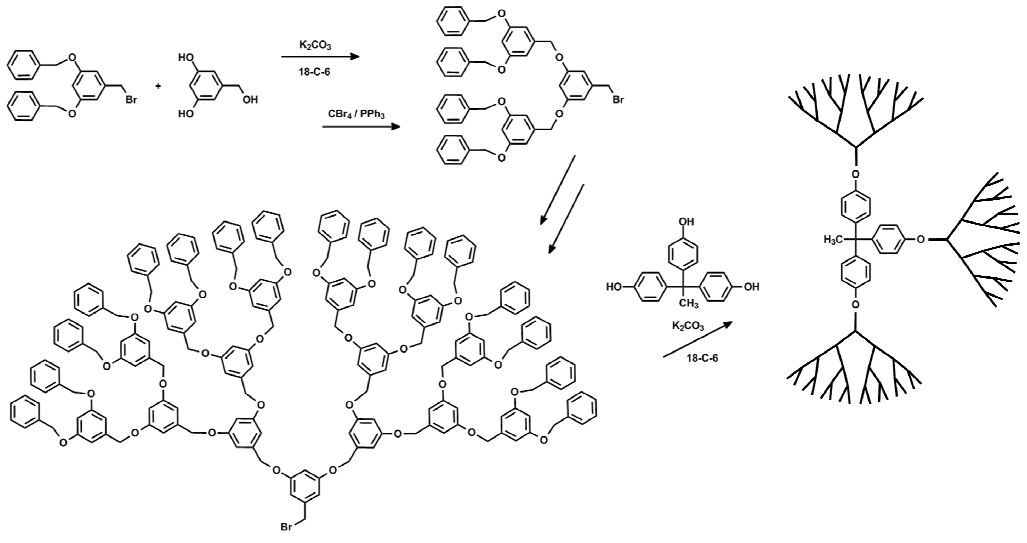

Fig. 1.5 – Convergent synthesis of arylether dendrimers until the 4th generation

starting from the peripheral groups. This process is depicted in Fig. 1.5 for arylether dendrimers.

The synthesis involves only two different reactions, namely the condensation of two benzylic bromines with two phenolic groups of 3,5-dihydroxybenzyl alcohol and the activation of the methyl alcohol into the corresponding bromide. Comparing the divergent and convergent method in terms of the total number of necessary reactions for obtaining a G_4 dendrimer (93 vs. 9) clearly shows the efficacy of the convergent approach.

Convergent synthesis also enables the preparation of asymmetric dendrimers bearing different wedges on the same core [30-31, 41]. Moreover, the addition of the same wedges to different cores immediately gives access to entirely new dendrimers in only one reaction step [42].

1.2.3 Water-soluble dendrimers

Dendrimers are required to be water-soluble when they are to be applied in biological systems or in water compatible materials [43]. With PAMAM dendrimers as an exception, dendrimers generally exhibit an apolar character and therefore need to be explicitly functionalised in order to be water-soluble. Some dendrimers are charged within the cascade structure [44], but most of them bear their water-soluble groups on their periphery. These groups include sugars [45], poly- or oligo ethyleneglycols [46-47], hydroxyls [48] and ionic moieties [44, 49].

Water-soluble dendrimers that are built on an apolar backbone have an intrinsic ambivalent character. Whereas some act like nanometric sponges [50], others assemble into well defined multimolecular architectures [51-53]. An extended introduction to water-soluble phosphorus dendrimers is given in Chapter 3.

1.3 Dendrimers: Features and Functionality

Dendrimers can be functionalised on a very precise location, thanks to the extremely well-defined structure and shape of the molecule. Asymmetric dendrimers prepared through a convergent synthesis were already discussed above. In most cases, however, the functional groups of dendrimers are located at either the core, the periphery, in the branches or complexed inside the dendrimer cavities. This section provides only a few examples of functional phosphorus dendrimers as section 4.1 gives many examples of organometallic dendrimers with metals at different locations. This chapter shows that a quasi-unlimited number of entirely different dendrimers can be synthesised and turned into highly functional, specific and efficient tools that can be applied in virtually all fields of chemistry, physics and biology.

1.3.1 Core

By shielding off the outside, dendrimer wedges often form a “microclimate” within the dendrimer. The outer part of the dendrons make up a dense layer that can be regarded as a protective shell [54]. This can be used to protect the core from the environment or to enhance its function. There are many fluorescent dendrimers that require such a microclimate in aqueous solution [55]. One example is given in Fig. 1.6, where a G_3 dendrimer is depicted that bears a core that shows two-photon absorption [56].

Two photon excited fluorescence (TPEF) finds its applications in biological and medical imaging. In contrast to single photon fluorescence, TPEF has significant advantages. First of all, it is possible to excite dyes in a spatially confined manner and TPEF reduces background fluorescence by using near-infrared excitation wavelengths. Moreover, it is possible to work deep inside tissue due to the large penetration depth of the excitation beam. However, most two-photon dyes are very lipophilic and therefore interaction with water leads to aggregation of the dye and it opens non-radiative decay pathways, both resulting in a greatly decreased quantum yield and fluorescence.

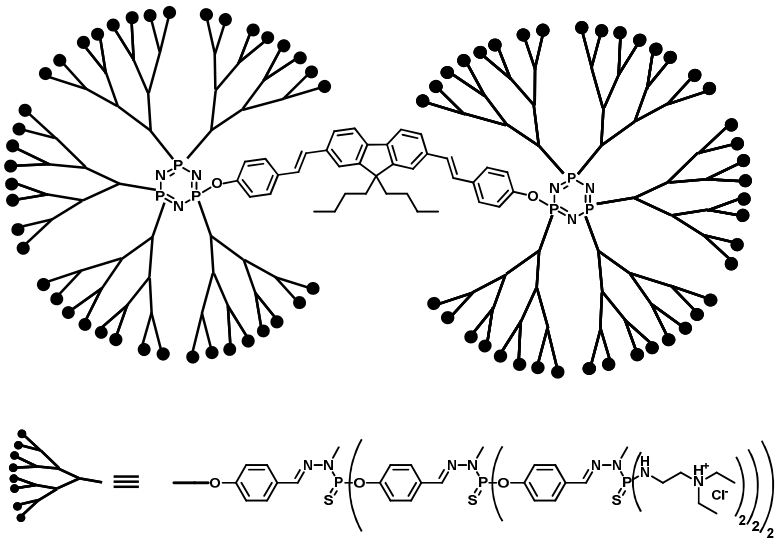

Fig. 1.6 – Water-soluble G_3 dendrimer with a decavalent two-photon absorption core [56].

Therefore, the dye requires a protective environment that is biocompatible and water-soluble. The G_3 dendrimer in Fig. 1.6 has a hydrophobic interior that stabilises the two-photon dye. Additionally, it has a polycationic periphery that makes the dendrimer water-soluble and that enables it, assisted by the hydrophobic interior, to pass biological membranes. This dendritic TPA dye was successfully applied for in-vivo imaging of the olfactory system of rats [56].

1.3.2 Periphery

Higher generation dendrimers that are functionalised at their periphery possess a higher density of functional groups than their linear or randomly (hyper-) branched analogues [57]. In networks or solutions of linear or branched polymers, the functional groups are to a large extent shielded by the polymer backbone and therefore not exposed to their target analyte. Peripherally tailored dendrimers, however, expose all their functionality outwards, resulting in very strong and efficient interactions with their environment.

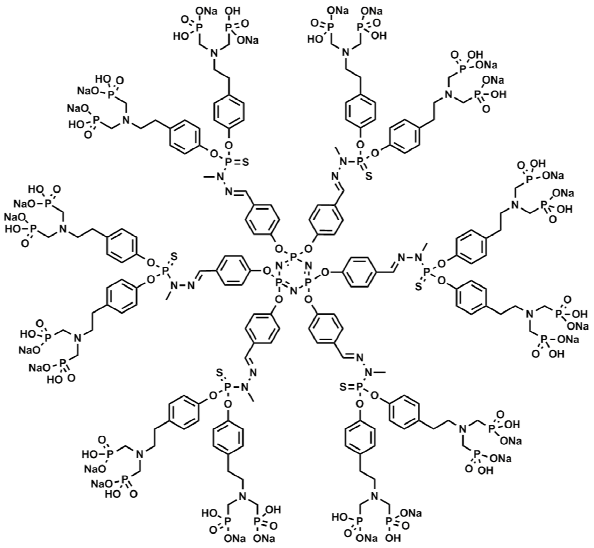

Fig. 1.7 – G_1 dendrimer capped with 12 peripheral aminobis (methylenephosphonic acid) [58].

In Fig. 1.7, a G_1 dendrimer is depicted that bears 12 peripheral bisphosphonates. These water-soluble dendrimers were found to stimulate and activate the human adaptive immune system [58-59]. In particular the number of Natural Killer (NK) cells, which play a crucial role in the first stages of an innate immune system response [59-60], were multiplied in large numbers and in a highly selective fashion. NK cells require an external stimulus before they multiply and actively reject tumours and virally infected cells. Until recently, artificially increasing the number of blood immune cells was accomplished through the addition of biologically produced molecules, which are poorly available. It was, however, shown that small molecules like pyrophosphates (referred to as phosphoantigens) [61] and amino bisphosphonates [62] can activate a subset of lymphocytes. As phosphonate-termined dendrimers are not recognised and degraded by phospholipases [63] and phosphatases [64] and because of their much higher activity than their smaller monomer analogues, they are ideal candidates for *in vivo* application. In contrast to the known ligands for NK cell activation [65], these dendrimers do not cause any unwanted side effects. Moreover, they could be used for the industrial production of NK cells, which can be used for NK cell therapies that counter infectious and malignant diseases.

1.3.3 Branches and cavities

Finally, also dendrimer branches and the internal cavities can be exploited to carry out precise functions. Dendrimers can be considered nanosized containers that can contain guest molecules [67]. This is interesting for transport and delivery functions. Encapsulation, however, does not necessarily require special chemical functions inside the dendrimer. One example, that involves special chemical functionalities in the branches, is the stacking of dendrimers into columnar assemblies yielding liquid crystalline materials through a strong intermolecular interaction between the dendrimer branches [68-69]. Dendrimer branches can also be used for the internalisation and complexation of metals, which can be applied for the synthesis of metal nanoparticles with an extremely narrow size distribution [29, 70-71]. An example of such a dendrimer is given in Fig. 1.8 where a dendrimer is depicted that selectively complexes gold to its cascade structure [66]. The dendrimer was synthesised using a regioselective approach [72]: the selective modification of the dendrimer backbone structure in order to enable additional dendritic growth inside the dendrimer cavities. The depicted dendrimer (Fig. 1.8) contains three different divergent points based on a pentavalent phosphorus atom: the P=S linkage, the P=N-P=S linkage and the P=N-P=N-P=S linkage of which the latter two can coordinate gold due to their

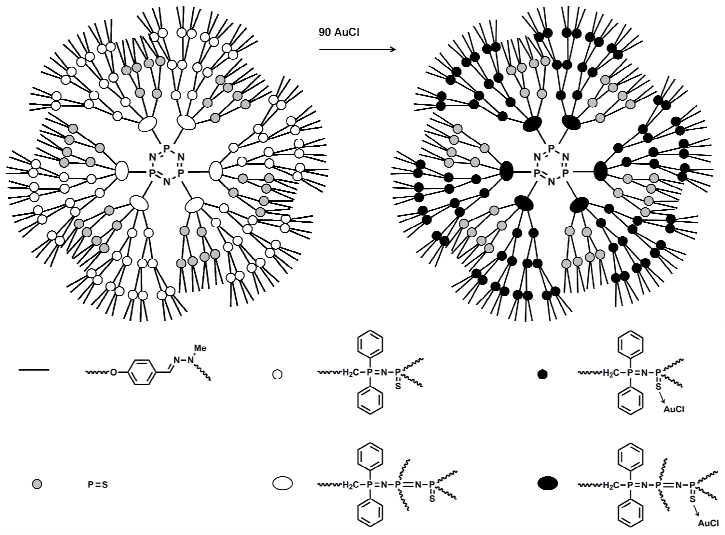

Fig. 1.8 – Regioselectively modified G_3 phosphorus containing dendrimer with branches that complex gold [66].

ability to separate charge along the small conjugated system. The P=S linkages that were used in the post-modification of the dendrimer branches at G_0 show no affinity for gold. The complexation of gold in such a controlled manner opens the possibility to synthesise gold nanoparticles with controlled size by reducing the gold ions to metallic gold, which cluster together to form well-defined particles [29].

1.3.4 The dendritic effect

A particularly interesting feature of dendrimers is that their activity or interactions sometimes are generation-dependent chemical or physical phenomena. This is very often indicated with the term “dendritic effect” (DE) [8, 73] and the DE is encountered in virtually all fields of application (guest encapsulation [74-75], metal and non-metal mediated catalysis [76-78], electrochemistry [79-80], biology [81-82]). The DE can be positive or negative, referring to an increase or decrease in activity with generation number. In general, the dendritic effect is assigned to the combination of structural flexibility of the branches, the cooperative multivalency and the surface density of the peripheral moieties. From a molecular design point of view, it would be very helpful to be able to predict whether or not a dendritic effect would occur. This is, however, dependent on many parameters, including molecular structure, generation number, temperature, solvents, guest molecules etc. Flexible or rigid linear spacers usually decrease the dendritic effect. In certain cases, for example for electrochemical and photo-physical phenomena, the dendritic effect can be predicted or even predetermined. Molecular recognition and catalysis, on the other hand, do usually not allow for such predictions due to the complexity of the chemical reaction mechanisms. Although often a positive correlation between effect and generation number is observed, larger is not necessarily synonym for more active, which is explained by the steric crowding and resulting inflexibility of the peripheral groups.

1.4 Scope and objectives of this thesis

Dendrimers are polymeric macromolecules that are synthesised in a repetitive fashion, which gives full control over a monodisperse size, the shape, position-specific functionalisation and physical and chemical properties. Thanks to this level of control over features and to the peripheral multivalency, dendrimers are being applied in materials science, biology, optics, medicine and electronics.

This thesis aims at the synthesis and application of new phosphorus containing dendrimers that contribute to the field of functional surface coatings. The envisioned coatings should have the following functions:

- ✓ preparing surfaces for their application in aqueous and biological systems
- ✓ enabling or enhancing electronic communication between electrode and solution

All dendrimers should therefore be water-soluble. The both above mentioned concepts are addressed by the synthesis and application of two different dendrimer families.

One should be able to covalently bind to gold (and other materials') surfaces and make a hydrophilic coating functionalised with cationic or anionic groups. These coatings can find their application as template for *molecular Lego*: electrostatically constructed multilayered systems as well as new biocompatible surface for cell culture, tissue engineering or implant integration.

The other class of dendrimers carries ferrocenyl groups within the cascade structure or at the core for their deposition on surfaces through electrostatic interactions. These dendrimers were also synthesised in polycationic and

polyanionic form. The dendrimers should mediate electrochemically between solution and electrode through their reversible redox activity. This could find an application in nanoscale sensing.

Chapter 2 gives an overview of the most relevant techniques and methods that were applied during characterisation and application of the dendrimer coated surfaces. The syntheses of the 10 different gold-binding and ferrocene-containing dendrimers are elaborated in Chapters 3 and 4, respectively, and their preliminary characterisation is described in the context of their broader field of application. Chapter 5 and 6 describe the applications of the gold-binding dendrimers with regard to tethered lipid membranes and biocompatibility towards Human Osteoblast cells.

The dendrimer syntheses were carried out at the CNRS institute for Coordination Chemistry (Laboratoire de Chimie de Coordination) under the direction of Dr. Jean-Pierre Majoral and Dr. Anne-Marie Caminade. The characterisations and applications were investigated at the Max-Planck Institute for Polymer Research under the direction of Dr. Ingo Köper and Prof. Dr. Wolfgang Knoll.

1.5 Bibliography

[1] G.R. Newkome, Z.-Q. Yao, G.R. Baker, V.K. Gupta, Journal of Organic Chemistry 50 (1985) 2003.
[2] G. Mihov, D. Grebel-Koehler, A. Lubbert, G.W.M. Vandermeulen, A. Herrmann, H.A. Klok, K. Mullen, Bioconjugate Chem 16/2 (2005) 283.
[3] E. Buhleier, W. Wehner, F. Vögtle, Synthesis 1978/02 (1978) 155.
[4] A.J. Boydston, Y.S. Yin, B.L. Pagenkopf, J Am Chem Soc 126/33 (2004) 10350.
[5] N. Feuerbacher, F. Vogtle, Top Curr Chem 197 (1998) 1.
[6] P.A. Jacobi, H. Liu, J Am Chem Soc 121/9 (1999) 1958.
[7] Y.M. Zhao, R.R. Tykwinski, J Am Chem Soc 121/2 (1999) 458.
[8] F. Vögtle, G. Richardt, N. Werner, Dendritische Moleküle, Teubner Verlag, Wiesbaden, 2007.
[9] R.G. Denkewalter, J.F. Kolc, W.J. Lukasavage, U.S. Patent 4.360.646 (1979).
[10] M. Maciejewski, Journal of Macromolecular Science, part A: Pure and Applied Chemistry A17(4) (1982) 689.
[11] P.-G. de Gennes, H. Hervet, Journal de Physique Lettres (fr) 44 (1983) L351.
[12] D.A. Tomalia, H. Baker, J. Dewald, M. Hall, G. Kallos, S. Martin, J. Roeck, J. Ryder, P. Smith, Macromolecules 19/9 (1986) 2466.
[13] D.A. Tomalia, H. Baker, J. Dewald, M. Hall, G. Kallos, S. Martin, J. Roeck, J. Ryder, P. Smith, Polymer Journal 17 (1985) 117.
[14] D.A. Tomalia, A.M. Naylor, W.A.G. III, Angew Chem Int Ed 29 (1990) 138.

[15] R. Esfand, D.A. Tomalia, Drug Discovery Today 6/8 (2001) 427.
[16] C. Hawker, J.M. Frechet, Chem Commun??/15 (1990) 1010.
[17] T.M. Miller, T.X. Neenan, Chem Mater 2/4 (1990) 346.
[18] E.A. Rebrov, A.M. Muzafarov, V.S. Papkov, A.A. Zhdanov, Doklady Akademii Nauk SSSR 309/2 (1989) 376.
[19] K. Rengan, R. Engel, Journal of the Chemical Society-Perkin Transactions 1/5 (1991) 987.
[20] N. Launay, A.-M. Caminade, R. Lahana, J.-P. Majoral, Angewandte Chemie International Edition in English 33/15-16 (1994) 1589.
[21] C. Galliot, D. Prevote, A.M. Caminade, J.P. Majoral, J Am Chem Soc 117/20 (1995) 5470.
[22] N. Launay, C. Galliot, A.M. Caminade, J.P. Majoral, Bulletin De La Societe Chimique De France 132/11 (1995) 1149.
[23] M. Slany, M. Bardaji, M.J. Casanove, A.M. Caminade, J.P. Majoral, B. Chaudret, J Am Chem Soc 117/38 (1995) 9764.
[24] F. Morgenroth, E. Reuther, K. Mullen, Angewandte Chemie-International Edition in English 36/6 (1997) 631.
[25] M. Fischer, F. Vogtle, Angew Chem Int Edit 38/7 (1999) 885.
[26] S.H. Bai, C. Thomas, A. Rawat, F. Ahsan, Critical Reviews in Therapeutic Drug Carrier Systems 23/6 (2006) 437.
[27] A. D'Emanuele, D. Attwood, Advanced Drug Delivery Reviews 57/15 (2005) 2147.
[28] N.K. Jain, U. Gupta, Expert Opinion on Drug Metabolism & Toxicology 4/8 (2008) 1035.
[29] R. Sardar, A.M. Funston, P. Mulvaney, R.W. Murray, Langmuir 25/24 (2009) 13840.
[30] V. Maraval, A. Maraval, G. Spataro, A.M. Caminade, J.P. Majoral, D.H. Kim, W. Knoll, New J Chem 30/12 (2006) 1731.
[31] V. Maraval, R.M. Sebastian, F. Ben, R. Laurent, A.M. Caminade, J.P. Majoral, Eur J Inorg Chem (7) (2001) 1681.
[32] C.J. Hawker, R. Lee, J.M.J. Frechet, J Am Chem Soc 113/12 (1991) 4583.
[33] M.-L. Lartigue, B. Donnadieu, C. Galliot, A.-M. Caminade, J.-P. Majoral, J.-P. Fayet, Macromolecules 30/23 (1997) 7335.
[34] D. Astruc, C. Ornelas, J. Ruiz, Chem-Eur J 15/36 (2009) 8936.
[35] D. Boris, M. Rubinstein, Macromolecules 29/22 (1996) 7251.
[36] R.L. Lescanec, M. Muthukumar, Macromolecules 23/8 (1990) 2280.
[37] M.L. Mansfield, L.I. Klushin, Macromolecules 26/16 (1993) 4262.
[38] G.R. Newkome, C.D. Weis, C.N. Moorefield, I. Weis, Macromolecules 30/8 (1997) 2300.
[39] J.C. Hummelen, J.L.J. vanDongen, E.W. Meijer, Chem-Eur J 3/9 (1997) 1489.
[40] C.J. Hawker, J.M.J. Frechet, J Am Chem Soc 112/21 (1990) 7638.
[41] K.L. Wooley, C.J. Hawker, J.M.J. Frechet, J Am Chem Soc 115/24 (1993) 11496.
[42] K. Yamamoto, J Polym Sci Pol Chem 43/17 (2005) 3719.
[43] U. Gupta, H.B. Agashe, A. Asthana, N.K. Jain, Biomacromolecules 7/3 (2006) 649.
[44] A.M. Caminade, C.O. Turrin, R. Laurent, C. Rebout, J.P. Majoral, Polymer International 55 (2006) 1155.
[45] P. Wu, X. Chen, N. Hu, U.C. Tam, O. Blixt, A. Zettl, C.R. Bertozzi, Angew Chem Int Edit 47/27 (2008) 5022.
[46] M.W.P.L. Baars, R. Kleppinger, M.H.J. Koch, S.-L. Yeu, E.W. Meijer, Angewandte Chemie International Edition 39/7 (2000) 1285.
[47] S.M. Ryan, G. Mantovani, X.X. Wang, D.M. Haddleton, D.J. Brayden, Expert Opinion on Drug Delivery 5/4 (2008) 371.
[48] A.E. Beezer, A.S.H. King, I.K. Martin, J.C. Mitchel, L.J. Twyman, C.F. Wain, Tetrahedron 59/22 (2003) 3873.
[49] A.M. Caminade, J.P. Majoral, Prog Polym Sci 30/3-4 (2005) 491.
[50] J. Leclaire, Y. Coppel, A.M. Caminade, J.P. Majoral, J Am Chem Soc 126 (2004) 2304.
[51] B.S. Kim, O.V. Lebedeva, D.H. Kim, A.M. Caminade, J.P. Majoral, W. Knoll, O.I. Vinogradova, Langmuir 21/16 (2005) 7200.
[52] D.H. Kim, P. Karan, P. Goring, J. Leclaire, A.M. Caminade, J.P. Majoral, U. Gosele, M. Steinhart, W. Knoll, Small 1/1 (2005) 99.
[53] T. Emrick, J.M.J. Fréchet, Curr Opin Colloid In 4/1 (1999) 15.
[54] C.B. Gorman, J.C. Smith, Acc Chem Res 34/1 (2001) 60.

[55] A.-M. Caminade, A. Hameau, J.-P. Majoral, Chemistry - A European Journal 15/37 (2009) 9270.
[56] T.R. Krishna, M. Parent, M.H.V. Werts, L. Moreaux, S. Gmouh, S. Charpak, A.-M. Caminade, J.-P. Majoral, M. Blanchard-Desce, Angewandte Chemie International Edition 45/28 (2006) 4645.
[57] A.S. Abd-El-Aziz, E.K. Todd, Coordin Chem Rev 246/1-2 (2003) 3.
[58] O. Rolland, C.O. Turrin, A.M. Caminade, J.P. Majoral, New J Chem 33/9 (2009) 1809.
[59] L. Griffe, M. Poupot, P. Marchand, A. Maraval, C.-O. Turrin, O. Rolland, P. Métivier, G. Bacquet, J.-J. Fournié, A.-M. Caminade, R. Poupot, J.-P. Majoral, Angewandte Chemie International Edition 46/14 (2007) 2523.
[60] M. Poupot, L. Griffe, P. Marchand, A. Maraval, O. Rolland, L. Martinet, F.E. L'Faqihi-Olive, C.O. Turrin, A.M. Caminade, J.J. Fournie, J.P. Majoral, R. Poupot, Faseb Journal 20/13 (2006) 2339.
[61] M. Poupot, J.-J. Fournié, Immunology Letters 95/2 (2004) 129.
[62] V. Kunzmann, E. Bauer, J. Feurle, F.W. Tony, Hans-Peter, M. Wilhelm, Blood 96/2 (2000) 384.
[63] W.K. Born, C.L. Reardon, R.L. O'Brien, Current Opinion in Immunology 18/1 (2006) 31.
[64] Y. Xu, S.A. Lee, T.G. Kutateladze, D. Sbrissa, A. Shisheva, G.D. Prestwich, J Am Chem Soc 128/3 (2005) 885.
[65] A. Moretta, C. Bottino, M. Vitale, D. Pende, C. Cantoni, M.C. Mingari, R. Biassoni, L. Moretta, Annual Review of Immunology 19/1 (2001) 197.
[66] C. Larre, B. Donnadieu, A.M. Caminade, J.P. Majoral, Chem-Eur J 4/10 (1998) 2031.
[67] J. Jansen, E.M.M. Debrabandervandenberg, E.W. Meijer, Science 266/5188 (1994) 1226.
[68] B. Donnio, S. Buathong, I. Bury, D. Guillon, Chem Soc Rev 36/9 (2007) 1495.
[69] B. Donnio, D. Guillon, Adv Polym Sci 201 (2006) 45.
[70] R.M. Crooks, M. Zhao, L. Sun, V. Chechik, L.K. Yeung, Acc Chem Res 34/3 (2001) 181.
[71] M.C. Daniel, D. Astruc, Chem Rev 104/1 (2004) 293.
[72] C. Galliot, C. Larré, A.-M. Caminade, J.-P. Majoral, Science 277/5334 (1997) 1981.
[73] G.R. Newkome, C.N. Moorefield, F. Vogtle, Dendrimer and Dendrons: Concepts, Syntheses and Applications, VCH, Weinheim, 2001.
[74] C.A. Schalley, C. Verhaelen, F.-G. Klärner, U. Hahn, F. Vögtle, Angewandte Chemie International Edition 44/3 (2005) 477.
[75] G.P. Perez, R.M. Crooks, Electrochemical Society: Interface (2001) 34.
[76] G.E. Oosterom, J.N.H. Reek, P.C.J. Kamer, P.W.N.M.v. Leeuwen, Angewandte Chemie International Edition 40/10 (2001) 1828.
[77] D. Tomalia, P.R. Dvornic, Nature 372/6507 (1994) 617.
[78] R. van Heerbeek, P.C.J. Kamer, P.W.N.M. van Leeuwen, J.N.H. Reek, Chem Rev 102/10 (2002) 3717.
[79] H.-F. Chow, I.Y.K. Chan, P.-S. Fung, T.K.K. Mong, M.F. Nongrum, Tetrahedron 57/8 (2001) 1565.
[80] C. Valerio, J.-L. Fillaut, J. Ruiz, J. Guittard, J.-C. Blais, D. Astruc, J Am Chem Soc 119/10 (1997) 2588.
[81] D. Fischer, T. Bieber, Y.X. Li, H.P. Elsasser, T. Kissel, Pharm Res 16/8 (1999) 1273.
[82] D. Fischer, Y.X. Li, B. Ahlemeyer, J. Krieglstein, T. Kissel, Biomaterials 24/7 (2003) 1121.

2 Methods

This chapter describes the most important methods and techniques that were employed in this work. It aims at combining fundamental understanding and a few practical examples.

2.1 Surface Plasmon Resonance Spectroscopy

Surface Plasmon Resonance (SPR) spectroscopy is a widely used technique to detect dielectric molecular layers at surfaces [1-3]. It allows for the sensitive and non-invasive characterisation of thin films as well as kinetic processes. Film thickness can be measured down to Ångstrom precision and solutes can be detected at extremely low concentrations (10^{-12} M) [4], depending on their molecular mass and refractive index. SPR can be applied in biosensors to monitor the construction of their usually complicated layered structure and for real-time detection of analyte binding.

2.1.1 Theory

When photons hit a thin noble metal film, they are usually reflected off the surface. However, under specific conditions, they can transfer their energy to electrons at the metal surface. If that happens, a propagating electron density wave at the interface between metal and dielectric is excited, the surface plasmon. The conditions for the excitation of this wave are resonance conditions, i.e. the x-component of the wave vector of the incident light matches exactly the x-component of the wave vector of the plasmon wave. The plasmon's field strength is very high at the interface and decays exponentially (as deduced next) into both media (metal and dielectric) with a dampening (also known as absorption) constant that depends on the used materials, excitation wavelength and arrangement of the setup. In the frequently employed Kretschmann setup [5] with 50 nm of gold evaporated on a glass slide and water as a dielectric medium, the dampening constant is

approximately 230 nm^{-1} [1, 3]. The experimental setup is discussed in more detail in 2.1.2.

As the electrons in a plasmon resonate out-of-plane at the surface, the electric component of the photons has to be oriented such that it has a momentum in the direction of electron resonance. The magnetic component is irrelevant. That means that only p-polarised light can be used for the plasmon excitation. However, as becomes clear from the following mathematical derivations, it is not the out-of-plane component of the wave vector that is responsible for the resonance, but the one in-plane in the direction of the plasmon propagation.

Let the incident photon propagation be represented by the wave vector $\boldsymbol{k}$ (k_x, k_y, k_z), with the photon travelling in the xy plane and y being the interface's normal. As p-polarised light has no electric field in the z direction, all z contributions will be omitted in the following derivations. The electric field of a travelling wave can be described as

$$E = E_0 \exp(j\omega t - j\mathbf{k}\cdot\mathbf{r}) \qquad \textbf{Eqn. 2.1}$$

with j being the imaginary unit defined as $j^2 = -1$, ω the angular frequency, t time and $\boldsymbol{r}=(x,y,z)$ the position of the wave vector. This complex description can be derived from the simple cosine description via Euler's rule. The wave vectors amplitude k is described by

$$k = \sqrt{k_x^2 + k_y^2 + k_z^2} = n\frac{2\pi}{\lambda} = n\frac{\omega}{c} \qquad \textbf{Eqn. 2.2}$$

with refractive index n, wavelength λ and c being the speed of light in vacuum. Considering a photon refracting on an interface between two media with different refractive index, Snell's law Eqn. 2.3 holds, from which Eqn. 2.4 follows by combination with Eqn. 2.2.

$$n_1 \sin\alpha = n_2 \sin\beta \qquad \textbf{Eqn. 2.3}$$

$$k_{x1} = k_{x2} \equiv k_x \qquad \textbf{Eqn. 2.4}$$

Combination of Eqn. 2.2 and Eqn. 2.4 yields an expression for the y component of the wave vector perpendicular to the interface

$$k_{y2}^2 = n_1^2\left(\frac{2\pi}{\lambda}\right)^2\left(\frac{n_2^2}{n_1^2} - \sin^2\alpha\right) \qquad \textbf{Eqn. 2.5}$$

If now sin $\alpha > n_2/n_1$, the right part of Eqn. 2.5 becomes negative and k_y therefore purely imaginary. This situation is called Total Internal Reflection (TIR). This results in an evanescent wave described as

$$E = E_0 \exp(-\kappa_{y2} y)\exp(j\omega t - jk_x x) \qquad \textbf{Eqn. 2.6}$$

in which the exponential decay of the electric field strength into medium 2 is accounted for by the first exponential with the κ_{y2} decay length. This evanescent field is not a plasmon, yet. This becomes clear in Fig. 2.1.

The dispersion relation describes which combinations of two experimentally adjustable parameters, ω and k_x, will lead to the excitation of a surface plasmon. The dispersion relation is defined by

$$\mathrm{Re}\{k_x\} = \frac{\omega}{c}\sqrt{\frac{\varepsilon_1(\omega)\varepsilon_2(\omega)}{\varepsilon_1(\omega)+\varepsilon_2(\omega)}} \qquad \textbf{Eqn. 2.7}$$

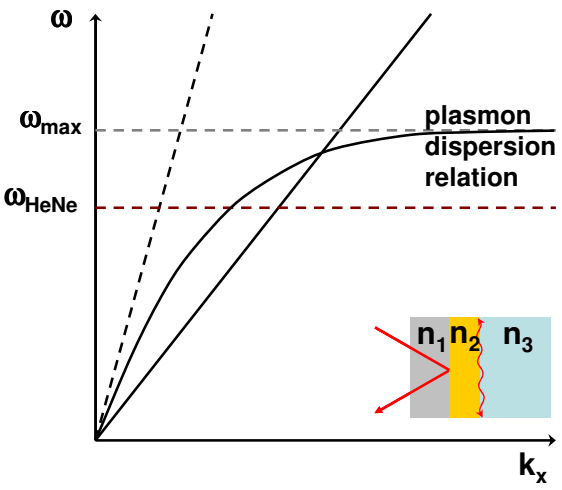

Fig. 2.1 – The dispersion relation for a surface plasmon. The two experimental values (ω and k_x) need to correlate via the dispersion relation in order to excite a plasmon. This correlation goes asymptotically to ω_{max}. The diagonal lines are "light lines", describing the dispersion relation between ω and maximum value feasible for k_x for the incident light. The slope of this line depends on n_1. All points located left of where the light line intersects with the dispersion relation offer a (ω, k_x) combination that will excite a surface plasmon.

The curve reaches a maximum angular frequency, which implies that frequencies higher (or wavelengths lower) than that value will not permit for the excitation of a plasmon. However, if medium 1 (with n_1 as defined in Fig. 2.1) is a low refractive material such as air, it still appears impossible to excite a plasmon. This can be explained by the dispersion relation of the incident light. This linear relation, the so-called light line, is depicted in Fig. 2.1 and defined by

$$\omega = ck_x\sqrt{\varepsilon_1} = ck_x n \qquad \textbf{Eqn. 2.8}$$

where k_x is now the maximum possible value for k_x (at an incidence angle of 90°) for each frequency. This implies that all values for k_x on the left side from that dispersion relation can be applied by varying the incident angle. For the excitation of a plasmon, the plasmon dispersion relation must have in common points with the left side of the light line. This is not the case when medium 1 is air, but for higher refractive index materials, like glass, it is possible. For this reason, it is necessary to couple the incident light into the system with a prism.

The propagation properties of the plasmon are dependent on the dielectric constants (and thus n) of all media around the metal film and their thicknesses. Any change of these parameters will cause a change in the angle of incident light at which the plasmon can be excited.

2.1.2 In practice

Essentially, the reflected light intensity is probed with a photodiode. Fig. 2.2 shows the typical experimental setup. In this Kretschmann configuration [2, 5-6], plasmons are excited via prism coupling. At most incidence angles, the laser light is reflected off the metal-prism interface, either by simple reflection or total internal reflection (TIR). At the angles where the momentum of the incoming light matches the plasmon requirements, destructive interference between the incoming and the back-coupled light leads to a minimum in

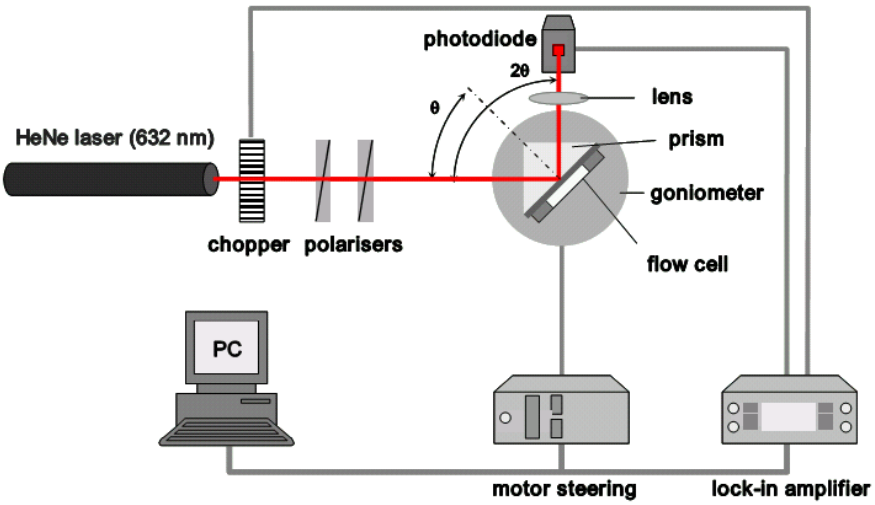

Fig. 2.2 – SPR setup in Kretschmann configuration [7].

reflected light intensity (Fig. 2.3). A 50 nm gold layer or 40 nm silver layer are commonly used as their optical dampening is lowest of all metals and they show the least broadening in the reflection minimum. Consequently, their experimental precision in determining the plasmon angle (θ_{spr}) is highest.

Fig. 2.3 shows as well how SPR can be used in a kinetic mode. By fixing the measuring angle θ to a value in the quasi-linear region left from the reflection minimum, the reflection intensity can be monitored with time. In this case the bold line represents the reflection before the addition (at approx t=1 min) of adsorbing molecules and the dashed line the reflection some time after addition. This allows for determining the end of an adsorption process. Overall, SPR is sensitive enough to detect the adsorption of sub-monolayers of molecules, provided they have a refractive index that is sufficiently different from the dielectric medium (usually water). However, both the thickness of the adsorbed film and its refractive index affect the shift in θ_{spr} and these two parameters cannot be measured independently with SPR. This implies that one of the parameters must be measured with a complementary technique.

For the quantitative evaluation of the θ_{spr} shift with respect to the changes in film thickness or refractive index, Fresnel equations are required [1-2]. These are the solutions of the Maxwell equations for the prism coupling and

multilayer system. The optical and thickness parameters must be inserted for all materials that the complete system consists of. This analysis was done using WINSPALL, developed at the MPI-P [8].

Apart from a laser, a polariser, a prism and a detector, the SPR setup also includes a second polariser (for adjusting the incident intensity). Moreover, in order to reduce the detrimental effects of (electrical and man-made) noise, a synchronous (coherent) detection principle is used. This implies the use of a chopper that lets through the measured signal at a certain frequency far away (kHz range) from the most regular types of noise-generating frequencies (artificial light, 50 or 100 Hz and radio waves). The incoming signal is compared to the chopper frequency by the lock-in amplifier and only the signal that exactly matches the chopper frequency is registered. This is depicted in Fig. 2.2. If SPR is to be used with a liquid medium a flow cell is used to regulate the addition of adsorbing molecules.

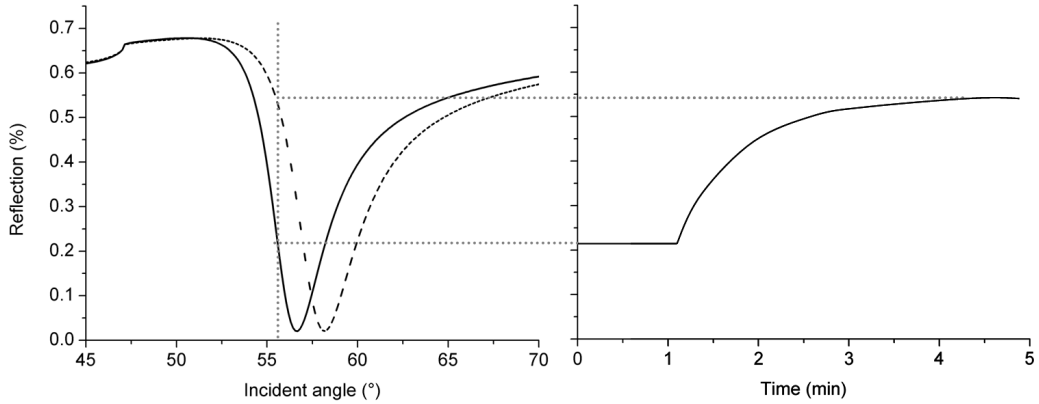

Fig. 2.3 – SPR schematically, in angular (left) and kinetic mode (right). During the adsorption process of an analyte, the reflection minimum shifts to higher angles (from solid to dashed line). At a fixed angle of observation, a change in reflected intensity represents the adsorption kinetics.

2.2 Electrochemical Impedance Spectroscopy

Dielectric Spectroscopy, or Electrochemical Impedance Spectroscopy (EIS), is a valuable technique for the electrochemical characterisation of coated electrodes. It measures the dielectric properties (energy storage and energy dissipation) of the coating by the application of an external electric field that interacts with the electric dipole moment of the coating. Dielectric systems with energy storage abilities are frequency dependent and therefore a frequency-response analysis of the sample provides a full dielectric characterisation. In the last decade, in its electrochemical context, EIS has become a standard method for the analysis of fuel cells [9-10], microstructured materials surfaces [11-12] and biomolecular interactions at interfaces [13-15]. Moreover, EIS is able to analyse chemical reactions as different intermediates dominate different frequency domains [16].

In practice, EIS probes the mobility of charges (electrons and ions) inside and close to the coating interfaces. By applying an electrical bias DC potential (voltage) with a small superimposed sinusoidal AC amplitude perturbation, the measured current shows an amplitude perturbation with the same frequency. In all cases, the measured system has a dissipative character (electrical resistance); they oppose current while dissipating energy (heating up). In the case of electrochemistry, where electrical double layers are present (2.2.1), the measured system has energy storage abilities (capacitive contributions) and will shift the current response in time with respect to the applied perturbation (phase shift). In nearly all electrochemical cases, the sample's frequency response can be modelled with an equivalent electrical circuit comprised of resistors and capacitors. This section discusses the basics of the technique EIS and the modelling of EIS spectra in an electrochemical context.

2.2.1 Theory

As for most electrochemical methods, EIS is generally carried out in a three electrode system (Fig. 2.4). An electrical potential is applied between the counter electrode and working electrode. The reference electrode holds a fixed potential that is used to fix the absolute value of the local potentials at both the working and counter electrode. The consequence of applying a potential is electrical current. One distinguishes between Faradaic and non-Faradaic current. The former arises when electrons cross the interface of solution and electrode (electron transfer), *i.e.* when reduction and oxidation reactions take place. The latter, non-Faradaic current, occurs when capacitive elements (elements that store charge) are charged and discharged. One example is the electrical double layer (Fig. 2.5).

An electrical double layer exists when a charged surface (electrode) is immersed into a polyelectrolyte solution. The co- and counter-ions in solution migrate to counteract the external electrical field. This gives rise to ion concentration profiles as sketched in Fig. 2.5. As the counter ions outnumber the co ions close to the electrode, the solution locally has a net charge with the sign opposite of the surface charge. Together, solution and surface make up the electrical double layer, which harbours charge. Any change in electrode

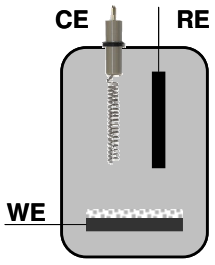

Fig. 2.4 – A three electrode system comprised of a coated working electrode (WE), counter electrode (CE) and reference electrode (RE).

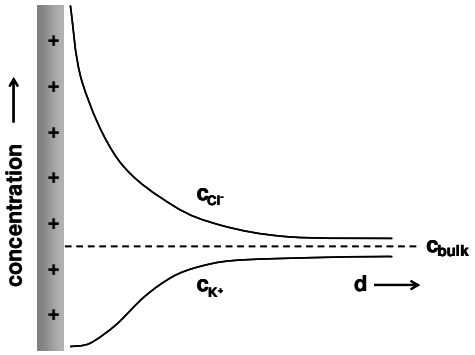

Fig. 2.5 – A simplified electrical double layer. A charged solution-electrode interface makes counter-ions migrate towards and co-ions migrate away from the interface. Charge is thus stored at both sides of this interface.

potential leads to charging or discharging of the double layer (a rearrangement of charges in the double layer), which gives rise to an electrical current. The (dis)charging of a capacitor is principally the same. Note that no electron transfer across the interface takes place.

With EIS, a sinusoidal AC potential, superimposed on a bias DC voltage, is applied between the working and counter electrode. The system's response is a sinusoidal current that is phase shifted with respect to the applied AC potential. In systems with capacitive characteristics, as derived hereafter, the current follows from the differential equation. As the shape of the current and potential are the same, the only relevant parameters are the amplitudes and the phase shift. These parameters are mathematically best described as a rotating vector in the complex plane. In this way, the sinusoidal shape disappears from the mathematics, the periodicity is replaced by complex exponentials (Eqn. 2.9 and Eqn. 2.10) and the differential equations become algebraic equations. This is schematically depicted in Fig. 2.6.

On the left hand side, the potential and current vectors turn around in the

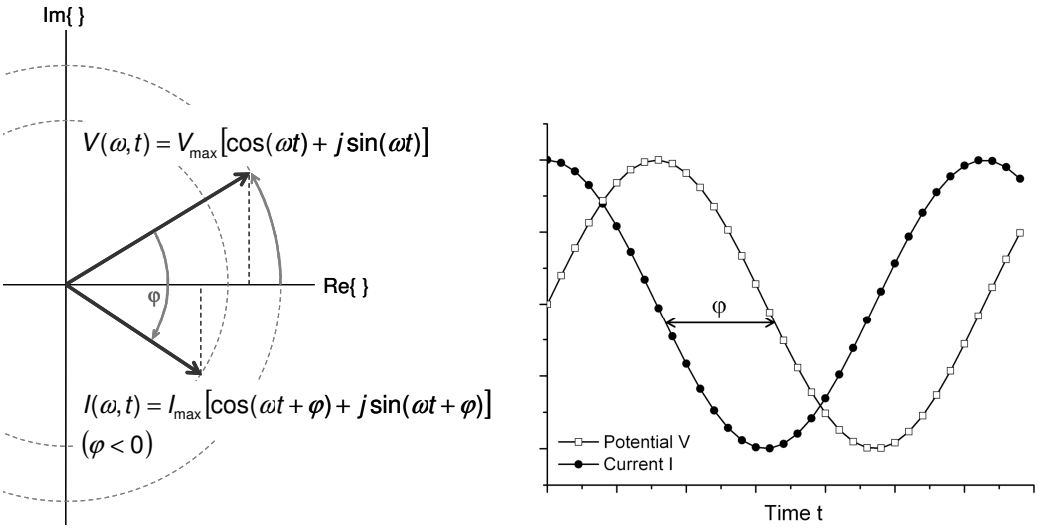

Fig. 2.6 – <u>Left:</u> the potential *V(ω,t)* and current *I(ω,t)* vectors plotted in the complex plane at time *t* and angular frequency *ω*. Both turn counter clockwise. The current runs behind with phase shift *φ*. The projections of the vectors on the real axis are Re{*V(ω,t)*}=V_{max}cos(*ωt*) and Re{*I(ω,t)*}=I_{max}cos(*ωt*+*φ*). V_{max} and I_{max} are the respective amplitudes of the sinosoids. <u>Right:</u> Re{*V*} and Re{*I*} plotted in time represent the applied potential and measured alternating current (AC).

complex plane; on the right hand side the projections of these vectors on the real axis are plotted, which represent the sinusoidal curves of the applied potential perturbation and the measured current. The complex notations of the applied potential perturbation and obtained current are

$$V(\omega,t) = V_{\max}\left[\cos(\omega t) + j\sin(\omega t)\right] = V_{\max}e^{j\omega t} \quad \textbf{Eqn. 2.9}$$

$$I(\omega,t) = I_{\max}\left[\cos(\omega t + \varphi) + j\sin(\omega t + \varphi)\right] = I_{\max}e^{j\omega t}e^{j\varphi} \quad \textbf{Eqn. 2.10}$$

With $j = \sqrt{-1}$ **Eqn. 2.11**

respectively, with ω being the angular frequency, t being time and φ being the phase shift. Note that φ has a negative sign. The vector projections on the real axes are in fact the applied potential perturbation and the measured current:

$$\mathrm{Re}\{V(\omega,t)\} = V_{\max}\cos(\omega t) \quad \textbf{Eqn. 2.12}$$

$$\mathrm{Re}\{I(\omega,t)\} = I_{\max}\cos(\omega t + \varphi) \quad \textbf{Eqn. 2.13}$$

As mentioned before, almost every electrochemical system can be represented by a network of resistors and capacitors. It is important to understand the differences in response of these elements to direct current (DC) and alternating current (AC). Under DC circumstances, the potential has a steady value and therefore a resistor follows Ohm's Law ($I=V/R$, with R being the resistance) and the capacitor harbours an amount of charge $Q=CV$, with C being the capacitance. In an AC situation, Ohm's Law is rewritten into

$$Z(\omega) = \frac{V(\omega,t)}{I(\omega,t)} \quad \textbf{Eqn. 2.14}$$

with Z being the impedance, the complex equivalent of resistance R. A resistor follows Ohm's Law and as it responds immediately to the applied potential (without giving rise to a phase shift, *i.e.* φ=0), the impedance of a resistor equals R. As a capacitor continuously charges and discharges due to the alternating potential, it impedes electrical current as well, giving rise to impedance and a phase shifted current response. Its DC definition ($Q=CV$) becomes

$$\frac{d}{dt}Q(t) = C\frac{d}{dt}V(t) \qquad \textbf{Eqn. 2.15}$$

and its impedance Z is not obvious anymore. Substitution of Eqn. 2.9 into Eqn. 2.15 gives the non-Faradaic current through a capacitor

$$I(t) = \frac{dQ(t)}{dt} = C\frac{dV(t)}{dt} = j\omega C V_{\max} e^{j\omega t} \qquad \textbf{Eqn. 2.16}$$

This allows us to derive the impedance of a capacitor by the ratio of potential over (Eqn. 2.9) and the current through (Eqn. 2.16) a capacitor using Eqn. 2.14.

$$Z(\omega) = \frac{V(\omega t)}{I(\omega t)} = \frac{1}{j\omega C}\frac{V_{\max}}{V_{\max}}\frac{e^{j\omega t}}{e^{j\omega t}} = \frac{1}{j\omega C} \qquad \textbf{Eqn. 2.17}$$

Therefore it can be concluded that EIS results can only be interpreted with complex mathematics once the studied system has a capacitive character. The latter equation also shows that impedance is time independent as all terms with time t disappear from the expressions. The impedance of a capacitor described in Eqn. 2.17 is a vector and therefore its absolute value (amplitude) and phase angle can be calculated. It can be derived that the current phase shift φ of a pure capacitor equals -½ π.

$$|Z| = \sqrt{Z\overline{Z}} = \sqrt{\mathrm{Re}\{Z(\omega)\}^2 + \mathrm{Im}\{Z(\omega)\}^2} = \sqrt{0^2 + \left(-\frac{1}{\omega C}\right)^2} = \frac{1}{\omega C} \qquad \textbf{Eqn. 2.18}$$

$$\varphi = \arctan\left(\frac{\mathrm{Im}\{Z(\omega)\}}{\mathrm{Re}\{Z(\omega)\}}\right) = \arctan\left(\frac{-\frac{1}{\omega C}}{0}\right) = -\frac{\pi}{2} \qquad \textbf{Eqn. 2.19}$$

The impedance of a capacitor is frequency dependent. For very low frequencies, a capacitor acts like an open circuit whereas for very high frequencies it acts like a short cut. This follows from the equations below, which are derived from Eqn. 2.17.

$$\lim_{\omega \to 0} Z(\omega) = \infty \qquad \textbf{Eqn. 2.20}$$

$$\lim_{\omega \to \infty} Z(\omega) = 0 \qquad \textbf{Eqn. 2.21}$$

2.2.2 Data representation

The objective of an EIS measurement is the representation of the investigated system in terms of an equivalent circuit and the interpretation of the values of the different components in terms of physical or chemical parameters. An example is given in Fig. 2.7 where a model membrane is sketched with its relevant equivalent circuit. The interface between the electrode and the rest of the system has no resistance, but charge separation takes place in the form of an electrical double layer. This is modelled as a capacitor. The lipid membrane also separates charge, but even very well-defined membranes leak a small current due to tiny defects and/or membrane dynamics that cause permeation of ions. This is a parallel process with a very high resistance. The solution contains electrolyte, which is represented by a small resistance.

The most common way of presenting EIS data is using the Bode plot together with either a Nyquist impedance plot or a Nyquist admittance plot. The Bode plot shows $|Z|$ of the system as well as the phase angle as a function of frequency. In practice, generally, there are only very few data points in the low frequency range and, as a consequence, the higher resistances cannot be clearly observed in the Bode plot. Therefore, a plot is required in which the data points in the low frequency range can be extrapolated on the basis of curve fitting to a well known equivalent circuit. This can be done with a

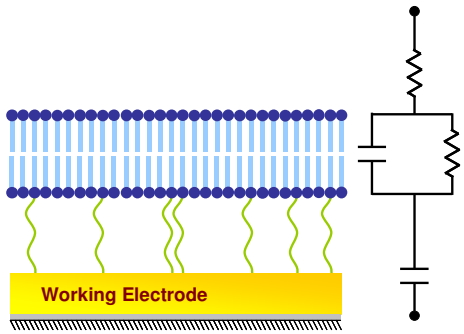

Fig. 2.7 – A model lipid bilayer membrane and its equivalent circuit comprised of resistors and capacitors.

Nyquist impedance plot, which gives Im{Z} against Re{Z}. A parallel RC element appears as a semicircle that approaches the real axis (where Im{Z}→0) at (0,0) and (R,0). This readily gives the value for R. Similarly, the admittance Re{Y} and Im{Y} can be plotted in the admittance Nyquist plot (the reciprocal impedance: $Y(\omega) = 1/Z(\omega)$) which gives the same information, but with enhanced insight in the high-frequency region. However, at high frequencies the relevant information can hardly be extracted on the linear scale of the Nyquist plots. This problem can be overcome by normalising both axes to the angular frequency. In this section a few simple model circuits are elaborated and the EIS output is given with Bode- and Nyquist plots.

Model 1: Resistor and capacitor in series

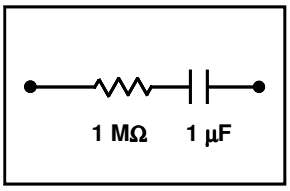

The first model system is comprised of a resistor and capacitor, which are connected in series. Like for resistances, the total impedance of multiple components in series is defined by

$$Z = Z_1 + Z_2 \qquad \textbf{Eqn. 2.22}$$

For this circuit the following expressions are found

$$Z(\omega) = R + \frac{1}{j\omega C} \text{ , therefore} \qquad \textbf{Eqn. 2.23}$$

$$\mathrm{Re}\{Z(\omega)\} = R \quad \text{and} \quad \mathrm{Im}\{Z(\omega)\} = -\frac{1}{\omega C}$$

$$|Z| = \sqrt{Z\overline{Z}} = R\sqrt{\frac{1+\omega^2\tau^2}{\omega^2\tau^2}} \qquad \textbf{Eqn. 2.24}$$

$$\varphi = \arctan\left(\frac{\mathrm{Im}\{Z(\omega)\}}{\mathrm{Re}\{Z(\omega)\}}\right) = \arctan\left(-\frac{1}{\omega\tau}\right) \qquad \textbf{Eqn. 2.25}$$

with τ equals RC (which has the dimension of time). With these expressions, the Bode plot and the Nyquist impedance plot can be readily constructed (Fig. 2.8). As was explained with Eqn. 2.20 and Eqn. 2.21, at very high frequencies, the impedance of the capacitor approaches zero. In this frequency range all

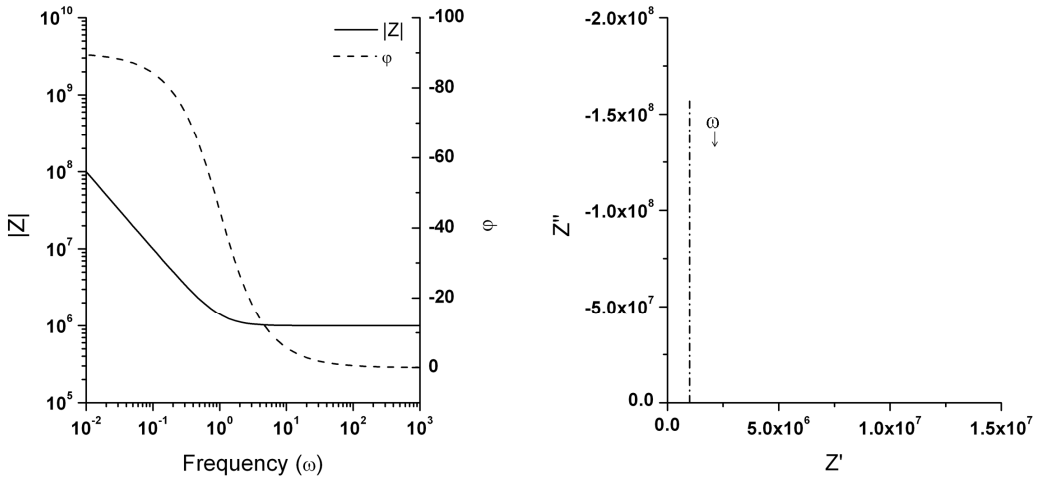

Fig. 2.8 – <u>Left:</u> the Bode plot shows the impedance (solid line) and the phase angle (dashed line). <u>Right:</u> the Nyquist plot returns Im{*Z*} (*Z*") against Re{*Z*} (*Z*').

impedance is dominated by the resistor (impedance is horizontal), which follows from Eqn. 2.24. At very low frequency the impedance of the capacity increases and it dominates the impedance of the total circuit. This manifests itself as a linear relationship between the logarithms of impedance and frequency, which directly follows from Eqn. 2.18. The phase angle therefore goes to -90° (-½π rad) where the impedance is dominated by the capacitor and goes to 0° where the resistor is dominant. The crossover frequency at which the switch between these "two faces" of this circuit occurs is at $\omega\tau = 1$. At this point the phase angle is exactly 45°.

The Nyquist plot shows Im{*Z*} against Re{*Z*}, often indicated with *Z*" vs. *Z*'. Re{*Z*} is independent of the frequency, but Im{*Z*} is not. Therefore, the Nyquist plot returns a straight line that approaches the real axis at *R*.

Model 2: Resistor and capacitor parallel

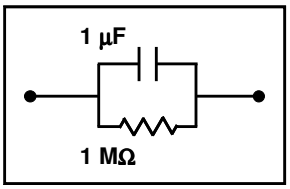

The second model is the parallel network of a resistor and a capacitor. Like resistors that are arranged parallelly, parallel impedances give the following total impedance

$$\frac{1}{Z} = \frac{1}{Z_1} + \frac{1}{Z_2} \qquad \textbf{Eqn. 2.26}$$

The necessary parameters of a parallel circuit are therefore expressed as

$$Z(\omega) = \frac{R}{1 + j\omega\tau} \text{ , therefore} \qquad \textbf{Eqn. 2.27}$$

$$\mathrm{Re}\{Z(\omega)\} = \frac{R}{1+\omega^2\tau^2} \quad \text{and} \quad \mathrm{Im}\{Z(\omega)\} = -\frac{\omega R\tau}{1+\omega^2\tau^2}$$

$$|Z| = \sqrt{Z\overline{Z}} = R\sqrt{\frac{1}{1+\omega^2\tau^2}} \qquad \textbf{Eqn. 2.28}$$

$$\varphi = \arctan\left(\frac{\mathrm{Im}\{Z(\omega)\}}{\mathrm{Re}\{Z(\omega)\}}\right) = \arctan(-\omega\tau) \qquad \textbf{Eqn. 2.29}$$

with τ equals RC. At high frequencies, the capacitor shortcuts the system and the impedance goes to zero. At low frequencies, the capacitor acts like an open circuit, making the resistor the only apparent element in the circuit. This returns the characteristic horizontal line at 1 MΩ for a frequency domain that is dominated by a resistor (see Eqn. 2.28). The Nyquist plot shows a semicircle with a diameter *R*, which describes all possible orientations of the impedance

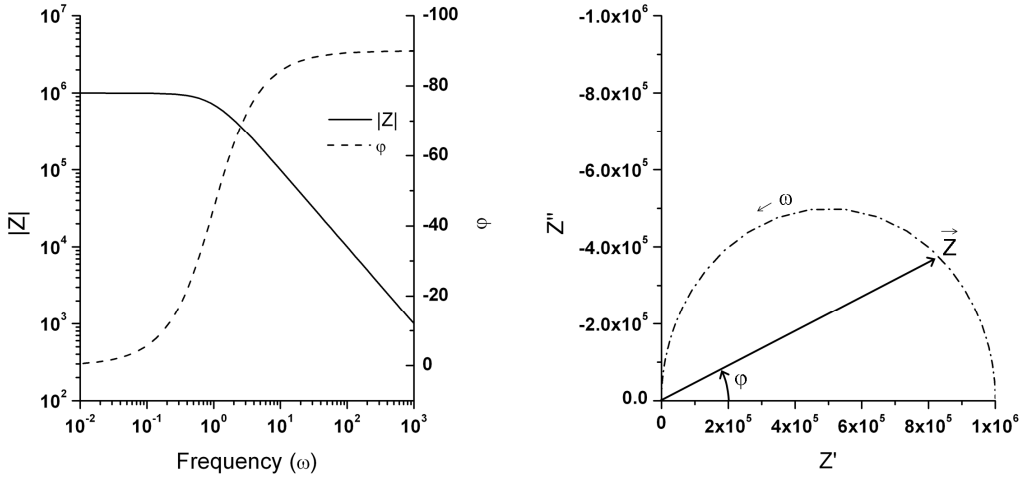

Fig. 2.9 – <u>Left:</u> the Bode plot shows the impedance (solid line) and the phase angle (dashed line). <u>Right:</u> the Nyquist plot returns Im{*Z*} (*Z*'') against Re{*Z*} (*Z*').

vector. The crossover between the two "faces" of the system appears again at $\omega\tau$=1.

Model 3: elements in series and parallel

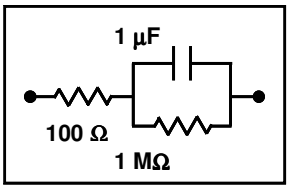

The last example model consists of a parallel network of a resistor and a capacitor with a second resistance connected in series. Also without working out the mathematics it is possible to draw the Bode and Nyquist plots.

At very high frequencies, the capacitor creates a bypass around the 1 MΩ resistor. Therefore, the impedance is 100 Ω and the phase angle is low. At very low frequencies, the capacitor acts like an open circuit, effectively creating a circuit with two resistors in series. This gives an impedance of 100 Ω + 1MΩ and a low phase shift. In between, in the parallel part of the network, current will preferably flow through the path of lowest impedance, which is through the capacitor. As the impedance of the capacitor is still very high compared to the 100 Ω resistor, the total impedance is dominated by the capacitor, giving rise to the high phase angle and linear (on log-log scale) relation between impedance and frequency. The two switches (between capacitive and resistive

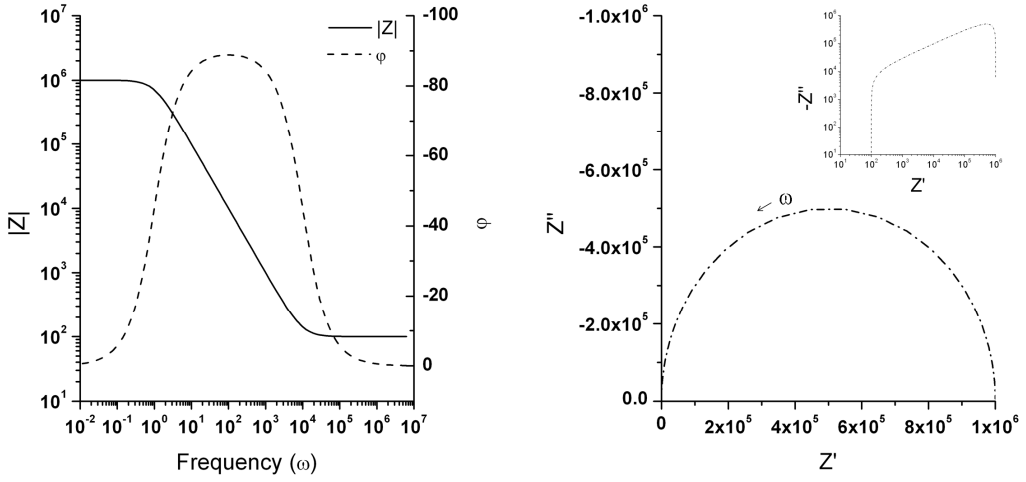

Fig. 2.10 – <u>Left:</u> the Bode plot shows the impedance (solid line) and the phase angle (dashed line). <u>Right:</u> the Nyquist plot returns Im{*Z*} (*Z*") against Re{*Z*} (*Z*').

dominance) represent the two RC times originating from the parallel and series network of the capacitor with either of the resistors. For both RC times, the switch occurs at $\omega\tau$=1.

The Nyquist plot shows almost the same semicircle as in Fig. 2.9, though it is shifted with 100 Ω on the real axis. On a linear scale this cannot be observed, which is the main disadvantage of the Nyquist plot. Therefore, the inset plots the same graph on log-log scale clearly showing the offset of 100 Ω.

2.2.3 Experimental

In this work, EIS has been conducted in combination with SPR spectroscopy. Therefore, a special measuring cell has been used that allows for the simultaneous prism coupled plasmon excitation on the gold electrode-water interface, for the application of an electrochemical potential between the working electrode and the counter electrode and for the application of different solutions with a regulated flow. The flow cell, depicted in Fig. 2.11, is made of Teflon for practical reasons: it is chemically inert, mechanically robust and easy to clean.

The working electrode (WE) is a gold coated glass slide or template stripped gold (TSG), onto which a prism can be mounted for the coupling of laser light into a surface plasmon. The front side is closed with a second, uncoated glass slide. The counter electrode (CE) is a platinum wire and the reference electrode (RE) is an Ag/AgCl electrode (Dri Ref 2, World Precision

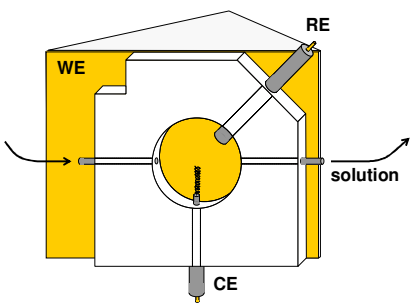

Fig. 2.11 – A Teflon flow cell with three electrodes. The working, reference and counter electrodes are indicated with WE, RE and CE, respectively. Different solutions can flow through. On the back side, a prism is mounted directly on the glass slide (WE), the front side is closed with another glass slide.

Instruments, Germany). The electrodes are connected to an Impedance Spectrometer (Autolab, PGSTAT12, The Netherlands) which regulates the applied voltages and frequencies between 100 kHz and 2 mHz. The measuring cell is placed inside a Faraday cage to reduce the noise from different sources (radio waves, electric network frequencies etc).

2.3 Cyclic Voltammetry

Cyclic Voltammetry (CV) is a dynamic electrochemical technique that studies electron transfer reactions between electrodes and reactant molecules, usually in a solution phase. It is used to study reaction mechanisms and for the characterisation of electrode surfaces. There are a number of parameters that influence the charge transfer process:

- ✓ The electrode potential
- ✓ Transport processes of material from and towards the electrodes
- ✓ Reactivity of the reactants (oxidation/reduction potentials)
- ✓ The physical characteristics of the electrodes

2.3.1 Theory

In CV, an alternating linearly shaped potential is applied between the working- and counter electrode (Fig. 2.12) so that a potential window of choice is scanned at a certain scan rate ν (Vs^{-1}). The resulting current provides information about the time constants involved in the reaction processes. When for example a redox molecule in solution is considered, the relevant time constants are the mass transport from and towards the electrode and the electron transfer rate at the electrode surface. The redox reaction that takes place involves the insertion into or acceptation of an electron from the electrode (as indicated in Fig. 2.12).

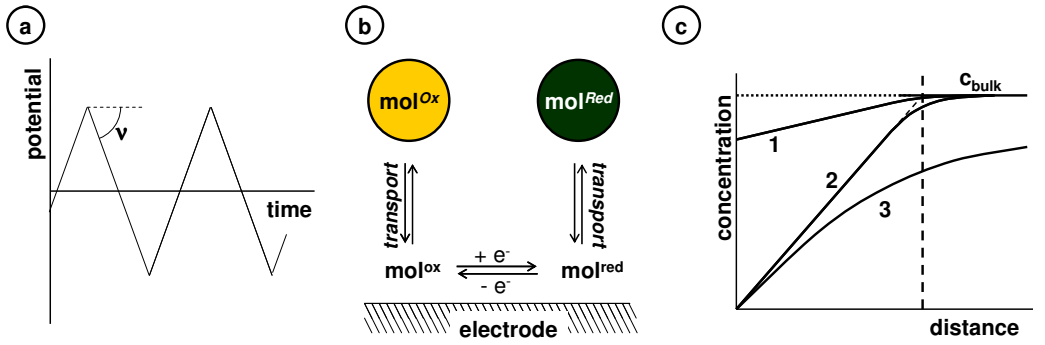

Fig. 2.12 – a: CV applies a zigzag potential in time. b: All dynamic processes and their time constants are revealed by analysing the current response. c: The concentration profile of the measured analyte changes with potential (described in text). The dashed line indicates the diffusion layer thickness.

The typical current response of a redox molecule in solution is given in Fig. 2.13. Here, only one electron is transferred across the electrode interface. In Fig. 2.13a-b only one linear voltage sweep is considered, starting at a low potential where the molecule is in its reduced state. Upon increasing the potential the statistical chance that the molecule injects an electron into the electrode increases, which initially gives rise to an exponential increase in the measured current. For entropic reasons, oxidised species diffuse away from the electrode and are being replaced by reduced species. This continuous process gives a linear concentration profile within the diffusion layer as sketched in Fig. 2.12c (line 1). Upon further increasing the potential, this concentration profile changes as close to the electrode the reduced species are quickly depleted (line 2). Further increasing the potential leads to gradual depletion of the reduced species in the diffusion layer (the region between the electrode and the dashed line), *i.e.* the reduced species do not diffuse quickly

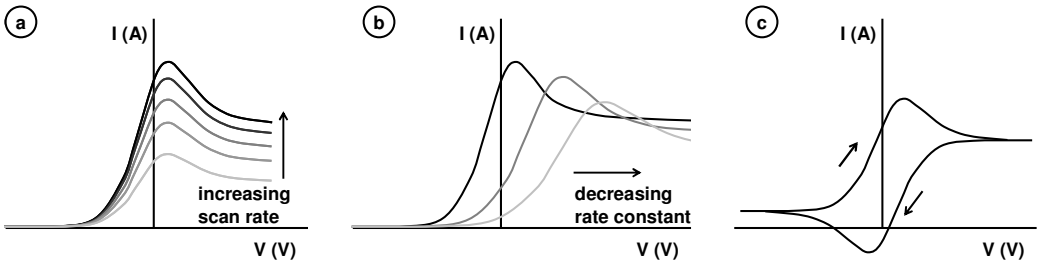

Fig. 2.13 – The typical current response in Cyclic Voltammetry. a: a single voltage sweep at different scan rates, b: a single voltage sweep at different electron transfer rates, c: a cyclic voltammogram.

enough to the electrode and the reaction becomes limited by diffusion (mass transport, line 3). This diffusion limitation leads to a peak current, as the measured current is linearly proportional to the concentration gradient [17]. The diffusion layer becomes thinner with increasing scan rate and the concentration gradients therefore steeper, which leads to higher currents (Fig. 2.13a). In the case that the electron transfer becomes the rate limiting factor (slower than the scan rate) and the current response is delayed, the peak current occur at higher potentials (Fig. 2.13b). When scanning back, the same behaviour is observed as in the forward scan, resulting in a negative peak current (reduction peak, Fig. 2.13c).

The relation between peak current and scan rate is captured in the empirical Randles-Sevcik equation:

$$i_p = (2.69 \cdot 10^5) n^{\frac{3}{2}} A c D^{\frac{1}{2}} \upsilon^{\frac{1}{2}} \qquad \textbf{Eqn. 2.30}$$

where i_p is the peak current (A), n is the number of transferred electrons per reaction, A is the electrode surface (cm^2), c s the bulk analyte concentration ($mol.cm^{-3}$), D is the diffusion constant (cm^2s^{-1}), n is the scan rate (Vs^{-1}) and the temperature is 25°C. This equation holds only for diffusion limited processes (fast electron transfer) [17] and provides information on the diffusion constant. The obtained voltammograms also readily give the standard redox potential, which is found at the potential exactly halfway between the oxidation and reduction peak.

2.3.2 Experimental

Cyclic voltammetry requires at least two electrodes (WE and RE), but very often an additional CE electrode is used. This is necessary when the working electrode has a larger surface [18]. In this work, a three electrode system was used. A gold coated glass slide constitutes the WE, the CE is a platinum wire and the RE is an Ag/AgCl electrode (Dri Ref 2, World Precision Instruments,

Germany). The used experimental setup is similar to the one employed for the EIS measurements (Fig. 2.11), allowing for the application of different solutions the measurement cell. The voltage sweeps are applied by an Autolab Potentiostat at controllable scan rates.

2.4 Contact Angle measurements

Hydrophilicity, hydrophobicity and solid surface topography can be assessed by placing a droplet of a liquid on top of the surface. This surface can be either solid or liquid. The shape of the droplet in the three-phase system (air is usually the third) is determined by interactions between the three interfaces in thermodynamic equilibrium.

In the case of a strong attractive interaction between the liquid and a solid surface, the droplet will tend to spread and show complete wetting of the surface. The contact angle is then usually between 0° and 30°. This is observed for instance for water on a hydrophilic glass substrate. When a water droplet is positioned on a hydrophobic surface (possessing low surface energy), the contact angle will be larger than 90°. On fluorinated materials like PTFE (Teflon), contact angles can go up to 120°.

The contact angle θ depends on the thermodynamic interplay between the three interfaces. This was described by Young [19]:

$$\gamma_{SV} - \gamma_{SL} - \gamma_{LV} \cos\theta = 0 \qquad \textbf{Eqn. 2.31}$$

with γ being the free surface energy of the interfaces between solid and vapour (SV), solid and liquid (SL) or liquid and vapour (LV), respectively. The surface

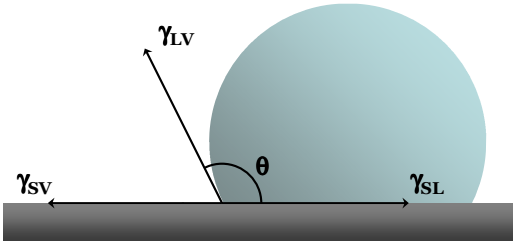

Fig. 2.14 – Schematic of Contact Angle measurement. A sessile droplet of water on a solid surface. The contact angle is indicated with θ.

energy equals the surface tension. This equation assumes a flat and chemically homogeneous surface.

2.5 Bibliography

[1] W. Knoll, Annu Rev Phys Chem 49 (1998) 569.
[2] H. Raether, Springer Tr Mod Phys 111 (1988) 1.
[3] R. Schasfoort, A. Tudos, Handbook of Surface Plasmon Resonance, The Royal Society of Chemistry, Cambridge, 2008.
[4] H. Chen, Y.-S. Gal, S.-H. Kim, H.-J. Choi, M.-C. Oh, J. Lee, K. Koh, Sensors and Actuators B: Chemical 133/2 (2008) 577.
[5] E. Kretschmann, H. Raether, Z Naturforsch Pt A A 23/12 (1968) 2135.
[6] J. Homola, Surface Plasmon Resonance-Based Sensors, Springer Berlin / Heidelberg, 2006.
[7] I. Vokenroth, Department of Chemistry, University of Bath, Bath, 2007.
[8] J. Worm, Implementation of Fresnel calculations for a layer system with anistropic dielectric and layer thickness values; and the graphical comparison with measured reflectivity data, Max-Planck Institute for Polymer Research, Mainz, 2001.
[9] Z. He, F. Mansfeld, Energy & Environmental Science 2/2 (2009) 215.
[10] X.Z. Yuan, H.J. Wang, J.C. Sun, J.J. Zhang, International Journal of Hydrogen Energy 32/17 (2007) 4365.
[11] A. Bieberle-Hutter, M. Sogaard, H.L. Tuller, Solid State Ionics 177/19-25 (2006) 1969.
[12] O. Fontaine, G. Trippe, C. Fave, J.C. Lacroix, H.N. Randriamahazaka, Journal of Electroanalytical Chemistry 632/1-2 (2009) 1.
[13] E. Katz, I. Willner, Electroanalysis 15/11 (2003) 913.
[14] I.O. K'Owino, O.A. Sadik, Electroanalysis 17/23 (2005) 2101.
[15] Y. Xu, G.F. Cheng, P.G. He, Y.Z. Fang, Electroanalysis 21/11 (2009) 1251.
[16] J. Otomo, X. Li, T. Kobayashi, C.-j. Wen, H. Nagamoto, H. Takahashi, Journal of Electroanalytical Chemistry 573/1 (2004) 99.
[17] A.J. Bard, L.R. Faulkner, Electrochemical Methods: Fundamentals and Applications, Wiley, New York, 2001.
[18] A.C. Fischer, Electrode Dynamics, Oxford University Press, Inc., Bath/New York, 1996.
[19] T. Young, Philosophical transactions of the Royal Society of London 95 (1805) 65.

3 Synthesis of water-soluble dendrimers for surface coatings

Thin film coatings of dendrimers find their applications in a wide variety of fields, ranging from nano-medicine to macro applications like water filtering. Immobilised dendrimers are exploited for their large number of peripheral functionalities, structural perfection and their conformational flexibility. In this chapter, the synthesis of four new G1 and G2 dendrimers is described bearing one dithiolane linker that can strongly bind to gold. Their peripheral charges are either cationic (quaternary amine) or anionic (sodium carboxylate), with G1 and G2 carrying 10 and 20 charges, respectively. These charges make all dendrimers exclusively water-soluble. The G1 dendrimers self assemble into 1 nm thin films on gold, whereas the G2 dendrimers have their dithiolane linker buried inside their interior, therefore unable to bind to gold.

3.1 Introduction

3.1.1 Surface coatings based on thiols and dithiolanes

Most of the materials we use in our daily life are organic, ranging from all plant and animal tissues and natural fabric polymers to synthetic polymers. Most of these materials are somehow related to solid or quasi-solid interfaces, which play vital roles in life. Examples are cell membranes and their associated proteins, water repellent lotus leafs and the gecko effect. In order to understand the functioning and characteristics of these highly complex biological surfaces and in order to be able to imitate them with technological applications, it is necessary to study simplified and well-defined artificial analogues. Cell membrane mimics can be tested on solid supports or free in solution as vesicles, as described in more detail in 5.1.2. Other systems are very often imitated on solid supports, like silicon crystals or evaporated gold. This introduction gives a few examples of organic coatings on solid surfaces while focussing on organothiols and dithiolanes related to the work performed in this chapter.

Self assembled monolayers

Self assembled monolayers (SAMs) constitute a very popular group of surface functionalisations. In most cases they are covalently bound to the surface, for instance by a gold-thiolate [1-2] or by a silane or vinyls attached to silicon (oxide, nitride or carbide) [3-6]. Organothiols (Fig. 3.1) and dithiolanes (Fig. 3.2) all have a similar structure, bearing a SH or a dithiolane (e.g. thioctic acid) at one end and a functional group (F) at the other end of one spacer (like an alkyl chain, oligophenylene or oligoethyleneoxide). The key advantage of SAMs is their relatively simple preparation and versatility compared to other monolayer deposition methods like Langmuir Blodgett transfer. The substrate is immersed into a thiol solution. Chemical reactions drive and fix the molecules to the surface and intermolecular interactions within the SAM regulate the lateral packing density. Fig. 3.2 shows one example of a SAM

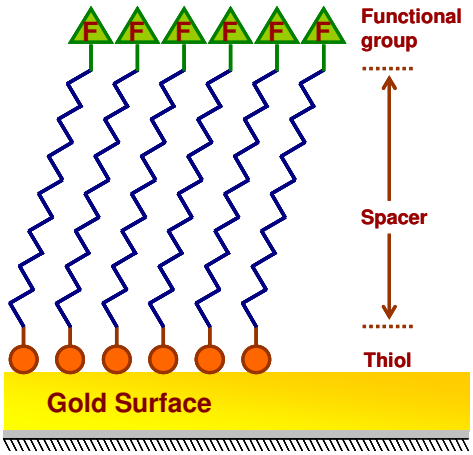

Fig. 3.1 – Schematic thiol SAM on gold.

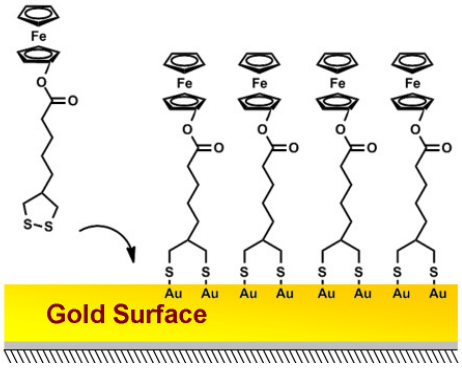

Fig. 3.2 – A ferrocene functionalised SAM anchored by a dithiolane (after [7])

functionalised with ferrocenes facing the solution [7]. Very often, SAMs merely serve as a functional template for more elaborate multilayered structures.

Not only planar substrates can be coated with self-assembling molecules, but also nanoparticles (NPs). One example is the coating of semiconductor quantum dots with dithiolane ligands [8].

3.1.2 Dendrimer coatings

By coating dendrimers to a surface it is possible to introduce a large variety of functionalities (chemical [9-10], optical [11], electrical [12] and biomedical [13-14]). When immobilised to a surface, their ability to contain small molecules in their interior and their enormous number of peripheral functionalities can be exploited to perform almost any function in a surface confined manner. Hereunder, a few examples are discussed.

Principally, there are two ways of coating a solid interface with a dendrimer layer. The first, a rather elaborate approach, is direct dendrimer synthesis on the surface. One example is the synthesis of PAMAM dendrons on magnetic nanoparticles [15] for binding biotin and streptavidin. Other examples include

fructose modified dendrimers that suppress apoptosis among hepatocytes [13] and dendrimer-like (hyperbranched) polymer films for biomineral synthesis [16]. This introduction, however, has its focus on dendrimers that bind to surfaces from solution through different interactions. A few examples of dendrimer based coatings are elaborated while discriminating between coatings on different surface architectures.

Dendrimers on planar surfaces

Biocompatible materials composed of polymers such as poly(DL-lactide-co-glycolide) or derivatives of cellulose, collagen, fibronectin etc. have been used as a solid platform for the release of drugs like hormones, nicotine and anti-hypertensives [18-21]. Similarly active coatings have been prepared containing loosely immobilised PAMAM dendrimers for eukaryotic gene transfection [14]. Dendrimer-DNA complexes are slowly released from the polymer surface coating and taken up by eukaryotic cells through their membrane.

Orthogonally to DNA transfection is DNA recognition and detection. Phosphorus dendrimers were immobilised by a condensation reaction between their peripheral aldehyde functionality and an aminosilane coated glass slide [17]. The so-called dendrislide (Fig. 3.3) possesses a reactive 100 Å layer that can covalently immobilise amino-modified DNA strands. The resulting DNA chips operated at a very high sensitivity for hybridisation of dye-labelled complementary DNA strands and the limit of detection concentration was reported to be 0.1 pM. In a similar approach, amino-

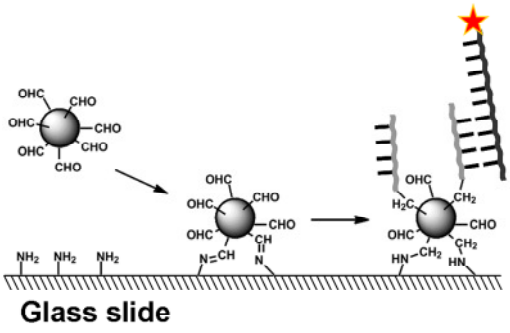

Fig. 3.3 – A schematic representation of a DNA hybridising "dendrislide" (after [17])

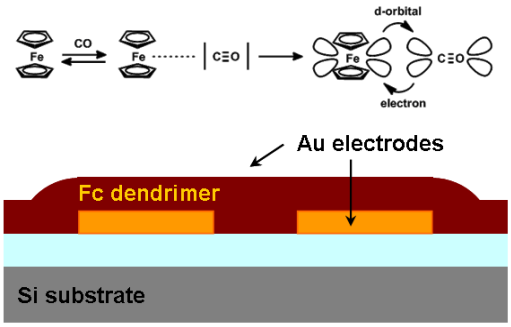

Fig. 3.4 – CO gas sensor. Ferrocene bearing dendrimers conduct when CO binds to the ferrocenes (after [12])

polyethylene glycol terminated dendrimers were used to enhance the DNA chip sensitivity [22].

The Crooks group [23] has investigated the possibility to use PAMAM dendrimers with amine functionality to tune the sensitivity of nanoporous aluminium towards the adsorption of volatile organic compounds. Where G6 dendrimers alone reduced the adsorption with 17%, a two-component layer consisting of the G6 dendrimer and a cross-linking linear polymer entirely blocked the vapour adsorption. Introducing selectivity into this system would result in selective gating towards vapour molecules and chemical sensing, as was shown by Advincula *et al.* [24] for solution based pH sensors and by Kim *et al.* [12] for CO gas sensors. The latter sensor was based on ferrocene terminated siloxane dendrimers, whose ferrocenes reversibly coordinate carbon monoxide in such a way that they become less conductive at a steady potential.

Dendrimers on nanosized objects

It is often problematic to keep nanoparticles (NPs) stable in solution. They have to be stabilised by a polymeric coating that enhances the solubility and prevents aggregation [25]. In the case of FeS NPs the synthesis was performed inside different G4 PAMAM dendrimers that stabilise the NPs and provide a template for the synthesis by complexation of Fe^{2+} ions to the amines in the dendrimer backbone [26]. Gold clusters were stabilised by further functionalising the present 11-mercaptoundecanoic acid/hexanethiolate monolayer into a PAMAM type dendrimer coating. This was done *via* either a convergent approach or a divergent approach [27].

In order to coat a gold object or surface with an organic layer, usually a thiol or dithiolane is used. One example is the coating of Au_{55} clusters [10] for the formation of perfectly organised Au_{55} superstructures. Au clusters of this size are interesting as sometimes their electronic behaviour reflects bulk material and in other cases single particles. Usually they are stabilised with phosphines or thiols [9], but these organic molecules can be outcompeted by thiol-terminated dendrimers [28-30]. The intention was to organise separate

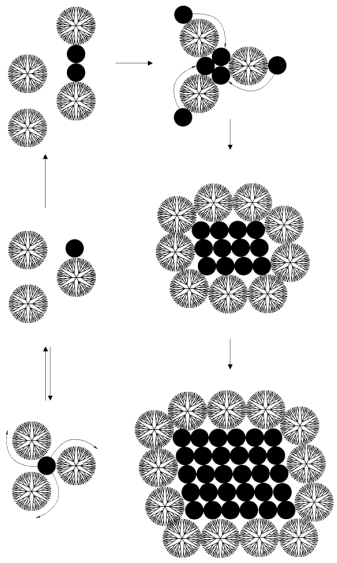

Fig. 3.5 - Gold clusters form perfect microcrystals when assisted by thiol-terminated G4 phosphorus dendrimers [10]

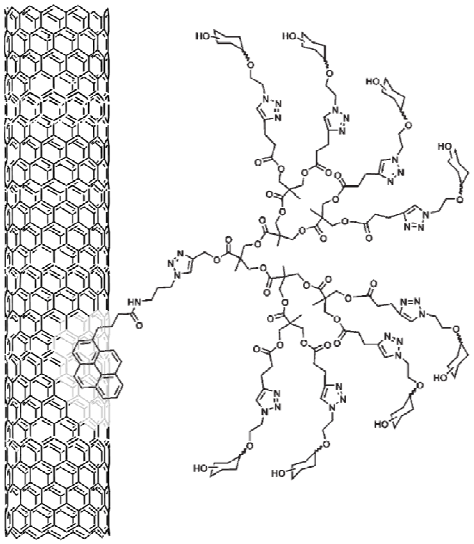

Fig. 3.6 – Glycodendrimer coated carbon nanotube anchored by a perylene (after [33])

clusters networked by the dendrimers, but the dendrimers were expelled and ultimately only covered the outside of the microcrystals (coalesced clusters). The dendrimer coating, however, seemed to have actively mediated the formation of perfect microcrystals. Using monolayers [31] of the same dendrimers [9] or other thiol SAMs [32], it is also possible to arrange the clusters in a monolayer fashion. The difference is, however, the dendrimers' ability to rearrange the gold clusters into nanosized crystals (20 nm) if the monolayer is exposed to a dichloromethane atmosphere.

By modifying dendrimers with a perylene moiety it is possible to immobilise dendrimers through π-π interactions with aromatic materials such as carbon nanotubes (NTs). Surface modifications of these nano-objects, with for example synthetic glycopolymers, can also simultaneously reduce the cytotoxicity of NTs and enhance the interaction with bio-components [33-35]. Similarly, dendrimer coated carbon NTs have been used in biomedical applications [36-38] using glycodendrimers that mimic the glycans found at the cell-surface [33, 39-41]. Apart from biomedical applications, carbon NTs have been coated with dendrimers that bear photo-active groups [42], that

improve their solubility [45] and that carry chemical functionality for metal recognition [46].

Dendrimer hybrid nanostructures

As discussed above, dendrimers can be arranged in a monolayer fashion. However, exploiting the layer-by-layer (LbL) approach by Decher [47], it is possible to organise oppositely charged water-soluble dendrimers into soft multilayers. Due to the nearly complete charge overcompensation during the adsorption of one dendrimer layer it is possible to construct multilayer architectures with a quasi-unlimited number of layers. Additionally, it is possible to functionalise the multilayers through the incorporation of other charged entities or by chemical post-modification of the dendrimers' peripheral groups. This concept yields hybrid multilayers and was applied for the sensitive detection of DNA hybridisation [48], adhesion layer for fetal cortical rat neurons [49], photoluminescent TiO_2 containing multilayers [50], DNA/dendrimer [51] and polyelectrolyte/dendrimer [52] multilayers, dendrimer multilayers inside nanoporous gold for biosensing [53] and hybrid dendrimer/Au nanoparticles multilayers [54].

Beside solid supported architectures, also free-standing three-dimensional architectures could be built from phosphorus dendrimer containing multilayers. The principle of DNA/dendrimer and polyelectrolyte/dendrimer multilayers was extended to the fabrication of microcapsules [51-52]. Using nanoporous anodised aluminium as a template, nanotubes with a diameter of 400 nm and 20 dendrimer bilayers were obtained [43] after dissolving the template. This principle was further used to make organic/inorganic hybrid

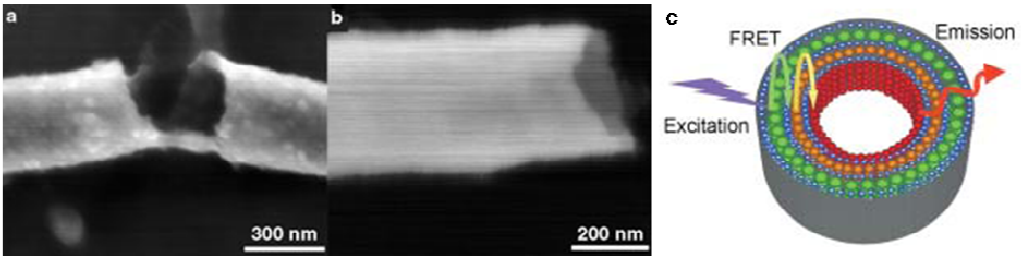

Fig. 3.7 – a,b: SEM images of dendrimer NTs, broken and open end, respectively [43]. c: schematic of dendrimer NT containing quantum dots for energy transfer and DNA hybridisation detection [44].

nanotubes containing quantum dots [44, 55]. These nanotubes could be used for ultra-sensitive detection of DNA hybridisation by arranging quantum dots with different emission wavelengths in an energy ramp manner. This allows for very efficient energy transfer and photon recycling, yielding an enhanced sensitivity.

3.2 Research Objectives & Approach

Organic surface coatings find a broad scope of applications, ranging from large scale industrial ship hull coatings that reduce bio-fouling thereby reducing energy consumption to 1 cm^2 lab-on-a-chip surfaces with ultrafine patterning for the analysis of a patient's risk factor concerning thousands of cancer types at once using one droplet of blood. This chapter focuses on the synthesis of novel dendrimers that can self-organise into monomolecular thin films. For that purpose, they require the following properties:

- ✓ Strong bonding to Gold
- ✓ Water solubility for their application in aqueous and biological environments.

The dendrimers are grown on a hexavalent hexachloride cyclotriphosphazene core in order to have a large number of peripheral functionalities at a low generation number. To meet the first requirement, the dendrimers were tailored with a dithiolane linker that is connected to the hexavalent core. The five remaining core connections are used for growing the dendrimer wedges. The wedges bear peripheral charges that are either polycationic or polyanionic. These charges render the dendrimers water-soluble. The generation number of the dendrimers must be adapted to the length of the dithiolane linker. It must be able to reach out from the core to a near gold surface for binding, sterically unhindered by the dendritic wedges. The objective of this chapter is the synthesis of dendrimers:

- ✓ Each with one dithiolane linker at the core
- ✓ Of generation 1 and generation 2
- ✓ With peripheral diethylethylene diamine hydrochlorides (polycationic dendrimers)
- ✓ Or with peripheral sodium carboxylates (polyanionic dendrimers)

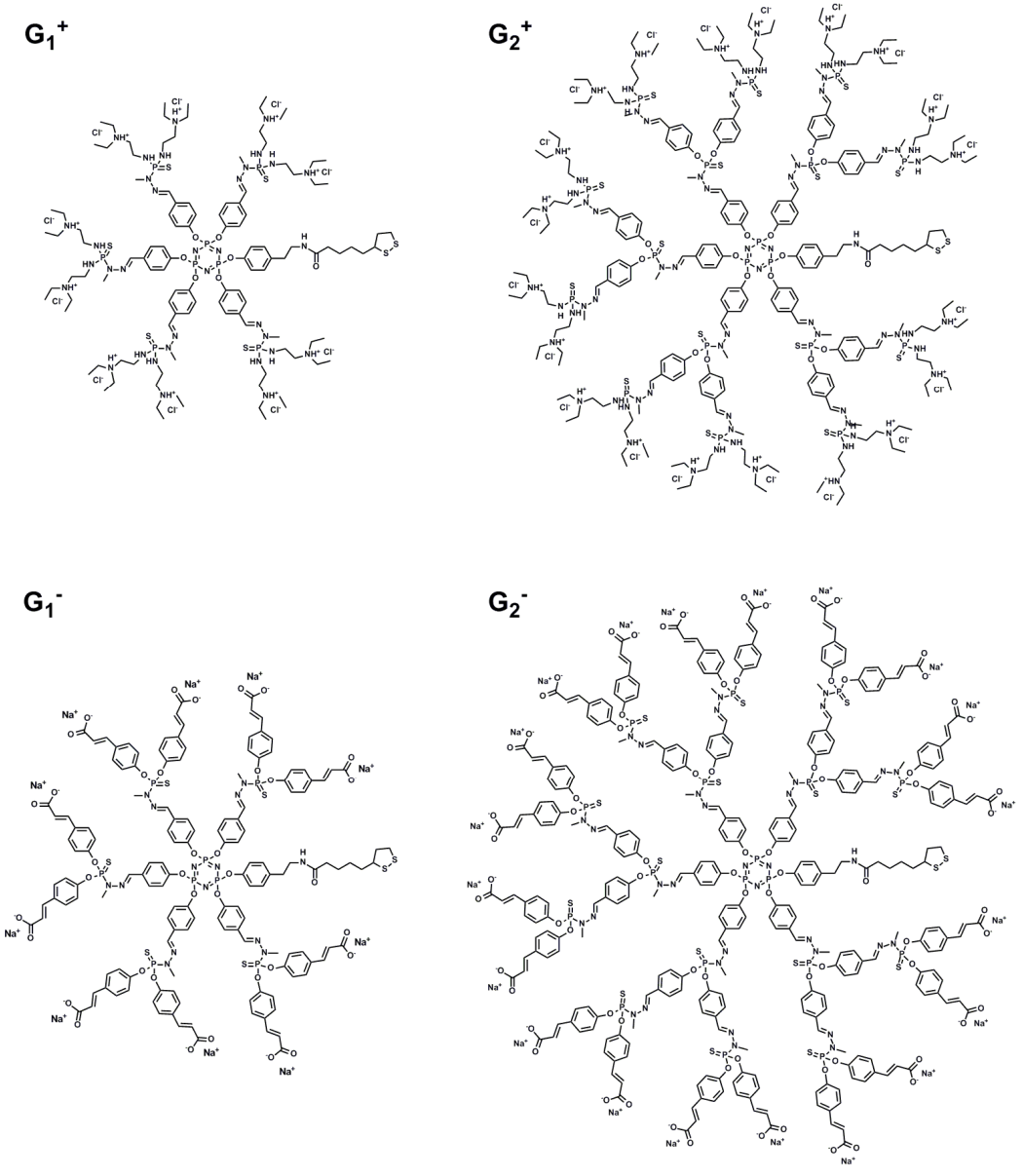

Fig. 3.8 – The four target dendrimers. Their nomenclature indicates the generation number and the sign of their peripheral charge.

The synthetic approach towards these four dendrimers followed the Majoral approach [56-57]. The target dendrimers are depicted in Fig. 3.8. The dendrimers were tested for their binding to gold surfaces.

3.3 Results and Discussion

In the next three sections the synthesis of water-soluble dendrimers with one dithiolane linker at the core and either 10 or 20 peripheral charges is discussed.

3.3.1 Synthesis of dithiolane functionalised core

For the synthesis of Majoral type dendrimers, three distinct building blocks are required. The first, the core, can be chosen arbitrarily ($PSCl_3$, N_3P_3, ...) , depending on the number of dendritic wedges (and therewith the final number of peripheral moieties) one pursues. For the purpose of coating surfaces with dithiolane containing dendrimers it is important to have a large number of peripheral charges at low generations. Taking into account that the thiolane linker is connected to the core and therefore already replaces one wedge it was chosen to construct dendrimers on the basis on cyclotriphosphazene hexachloride.

The second building block, p-hydroxybenzaldehyde (p-HBA), is responsible for the growth of the dendrimer size. It substitutes a chlorine under basic conditions, usually created with caesium carbonate. Basic conditions loosen the attachment of the proton of the phenol of p-HBA, resulting in a larger negative charge on the oxygen, which makes it more nucleophilic. As an alternative to the combination of p-HBA and Cs_2CO_3 one can use the sodium salt of p-HBA, synthesised by exchanging the phenol's proton for a sodium ion with sodium hydride under very dry (water free) conditions. This avoids the use of the rather expensive Cs_2CO_3. The reaction is given in Fig. 3.9. As the sodium salt of p-HBA is more reactive, it can also be a disadvantage.

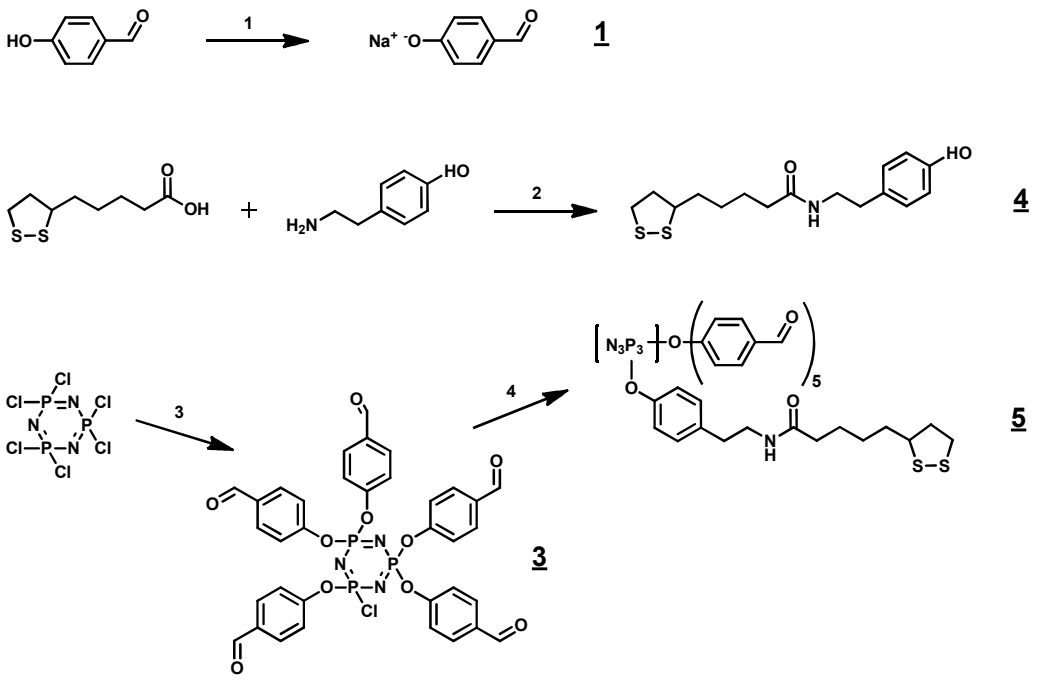

Fig. 3.9 – Synthetic route towards the N_3P_3 core functionalised with the dithiolane linker. (1) NaH in THF at -30°C, (2) DIPEA/TBTU in DMF at *RT*, (3) 1 in THF at 0°C, (4) 4/Cs_2CO_3 in THF at 0°C.

Moreover, working with NaH instead of Cs_2CO_3 is more dangerous since it can spontaneously ignite upon contact with moisture. Therefore, sometimes, p-HBA was still used in combination with caesium carbonate.

Principally, there are two ways to construct a cyclotriphosphazene core that carries one dithiolane linker and five benzaldehydes. The core that only carries the linker and no benzaldehydes appeared to be unstable for an unknown reason. Therefore, the pentasubstitution of the core was carried out first by stoichiometric addition of p-HBA, followed by the substitution of the last chlorine by the linker (Fig. 3.9). The relatively poor yield of the pentasubstitution can be explained by the formation of the hexa- and tetra substituted products as side products. These side products could be removed by column chromatography.

The dithiolane linker is synthesised from thioctic acid and tyramine by peptide coupling. First, thioctic acid was deprotonated by the base diisopropylethylamine (DIPEA) and turned into an activated ester with the uronium TBTU (O-(benzotriazol-1-yl)-N,N,N',N'-tetramethyluronium

tetrafluoroborate). Subsequently, tyramine was added and the selective reaction with its amine resulted in the amide **4**. This compound was coupled to the core by substituting the remaining chlorine under influence of the base Cs_2CO_3.

3.3.2 Dendrimer growth

The third standard building block for dendrimer synthesis is N-methyldichloro thiophosphorhydrazide (MHTPC, **2**). This hydrazide is made via the nucleophilic substitution of one of the three chlorines of

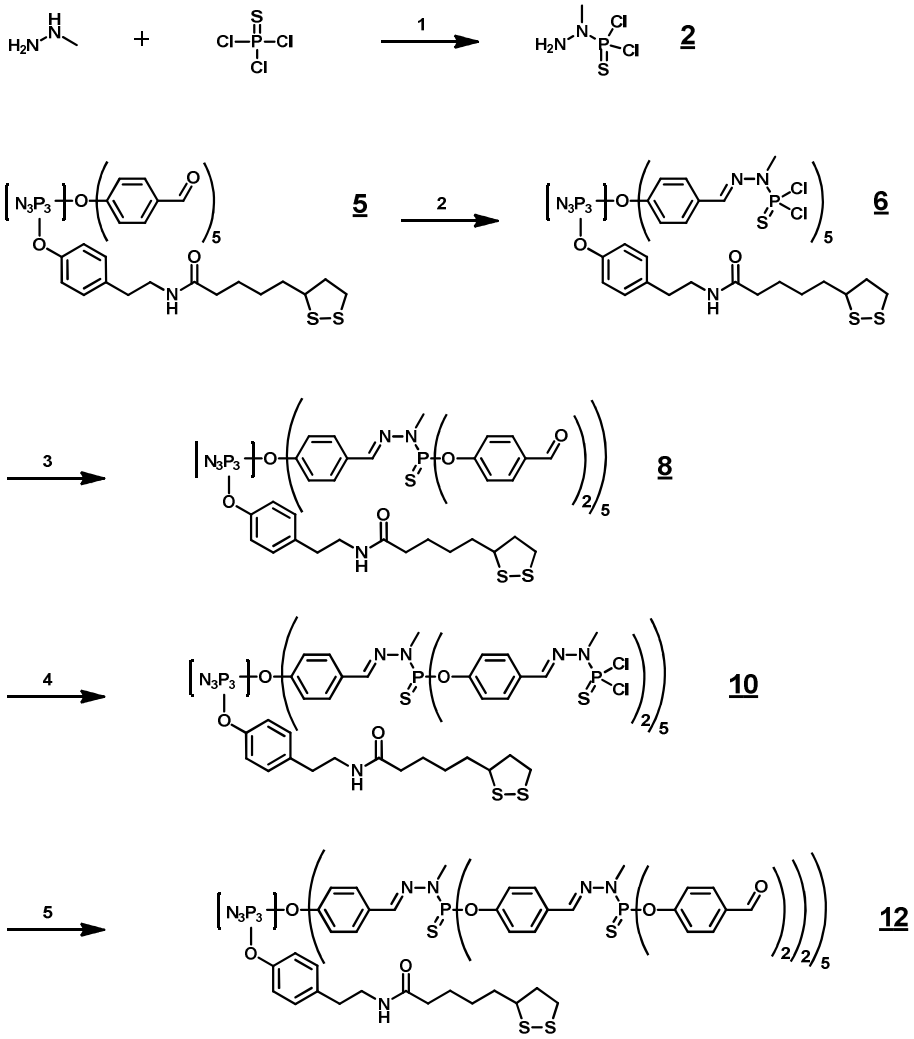

Fig. 3.10 – Synthesis scheme of dendritic growth with p-HBA and MHTPC on a N_3P_3 core. (1) in $CHCl_3$ at -60°C, (2,4) 2 in $CHCl_3$ at -60°C at *RT*, (3,5) p-HBA/Cs_2CO_3 in THF at *RT*.

thiophosphorylchloride and has to be stored as a cold, dilute chloroform solution in order to prevent polymerisation. The two chlorines of this molecule are responsible for the exponential growth of the dendrimer as it allows for the connection of twice as many peripheral benzaldehydes as a dendrimer of the previous generation contained (Fig. 3.10).

Every G_n' type dendrimer terminated with benzaldehydes can be further grown to a G_{n+1} type dendrimer by the condensation reaction with $5 \cdot 2^n$ equivalents of the hydrazide. In its turn, every G_n type dendrimer can be further grown into a G_n' type dendrimer by the previously discussed nucleophilic substitution of the terminal chlorines by $5 \cdot 2^n$ equivalents of p-HBA. This exponential growth is depicted in Fig. 3.10.

3.3.3 Rendering dendrimers water-soluble

As extensively described, phosphorus dendrimers can be made water-soluble [56, 58]. In order to make dendrimers polycationic, the numerous peripheral chlorines of hydrazide terminated dendrimers are substituted by the primary amine of N,N-diethylethylenediamine (DEEDA). The by-product of the nucleophilic substitution is HCl, which is immediately captured by the tertiary amine of DEEDA, as long as DEEDA is not present in excess. The resulting quaternary amine renders the dendrimer charged, which makes the dendrimer gradually precipitate from the THF solution during the reaction. The resulting dendrimer is only soluble in water (Fig. 3.11).

Polyanionic dendrimers can be synthesised departing from benzaldehyde terminated dendrimers. Through a Doebner-like reaction (Fig. 3.12) of the aldehyde with malonic acid, facilitated by a Lewis acid (piperidine), a cinnamic acid terminated dendrimers is synthesised [56, 58-61]. The Lewis acid attacks the carbonyl creating an alcohol. Simultaneously, the acidic proton of malonic acid, positioned at the central carbon, is removed by the basic solvent (pyridine) and the corresponding carbanion attacks the carbonyl

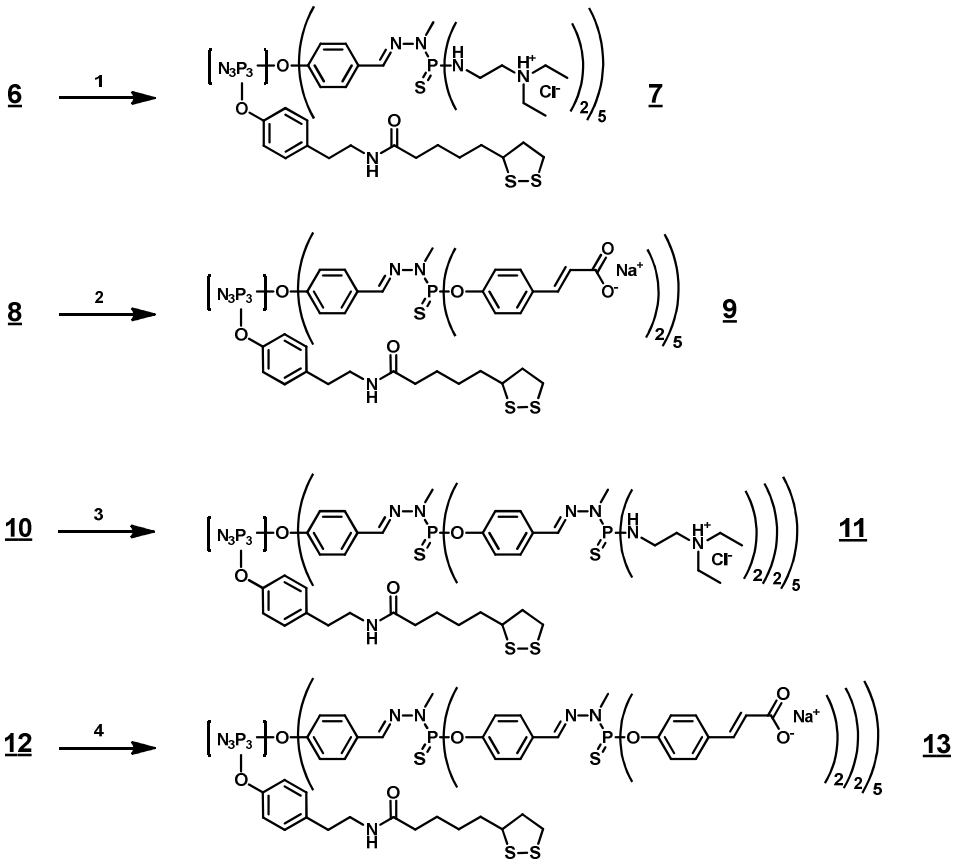

Fig. 3.11 – Synthesis of water-soluble dendrimers: periphery functionalisation with DEEDA or malonic acid. (1,3) DEEDA in THF at *RT*, (2,4) malonic acid/piperidine in pyridine at 95°C.

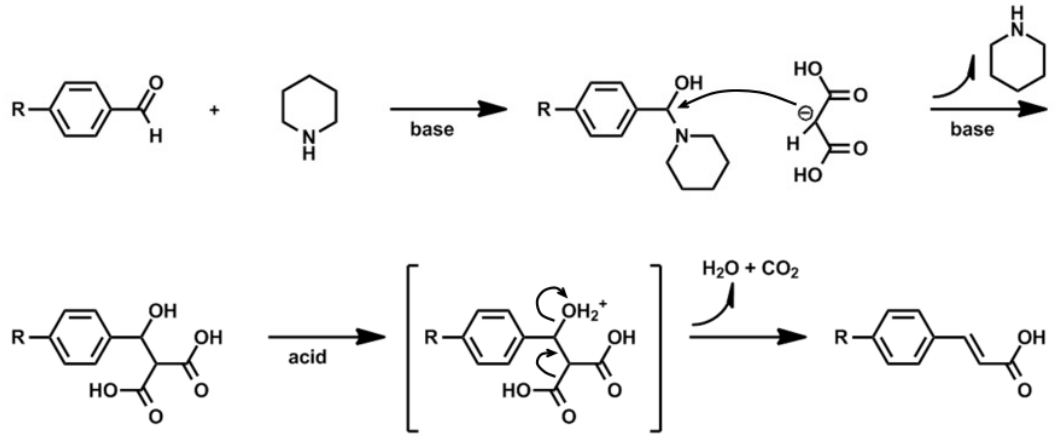

Fig. 3.12 – A Doebner-like reaction turning an unsaturated carbonyl into a cinnamic acid.

making piperidine leave again. Upon changing the pH to strongly acidic, the alcohol becomes protonated. A condensation takes place and carbon dioxide leaves as a gas. The protons of the resulting peripheral carboxylic acids are

exchanged for sodium ions by stoichiometric addition of sodium hydroxide. This renders the dendrimers water-soluble.

3.3.4 Surface Plasmon Resonance Spectroscopy

The adsorption process of the dendrimers to the gold coated slides was studied by SPR spectroscopy. This yielded an average thickness of the dendrimer layer and information about the kinetics of the adsorption process. For this experiment, a template stripped gold (TSG, 50 nm) sample was prepared and mounted into the spectrometer with a flow cell on the gold side. On the glass side, an $LaSFN_9$ prism was mounted with a small amount of refractive index matching oil (n=1.700) in between. Fig. 3.13 shows the result for negatively charged dendrimers, positively charged dendrimers gave a nearly identical response.

In the figure above, the normalised reflection is plotted against the incident angle. The solid line indicates an empty gold surface, whereas the dashed line represents the dendrimer coated surface after extensive rinsing with water. The dendrimers shifted the plasmon minimum to a higher angle with respect

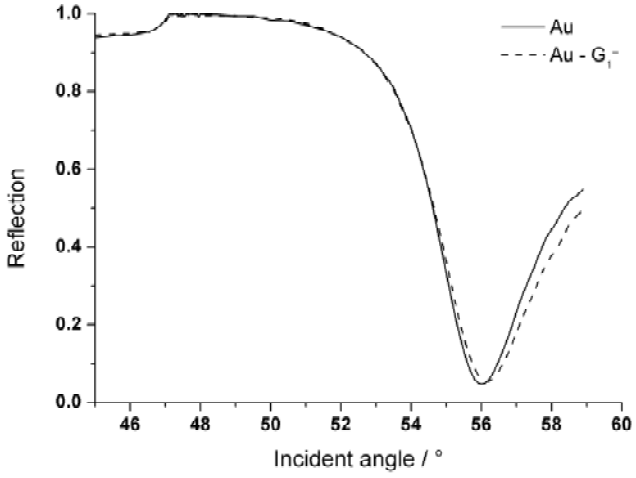

Fig. 3.13 – Angular SPR scan of a G_1^- dendrimer monolayer bound to gold (in water).

to the uncoated surfaces, indicating that the dendrimers both adhered to gold with a final film thickness of 1.0 nm.

As the change in layer thickness and refractive index due to an adsorption process are interrelated, it is impossible to determine either of them without measuring the other with a complementary technique. In this case, a dendrimer refractive index of 1.5 is assumed, based on the fact that organic molecules usually have very similar values [62]. Other fitting parameters include the gold thickness, its refractive index and the prism's refractive index. The gold parameters affect the depth and the width of the minimum. Changing the refractive index of the prism shifts the whole SPR curve on the angle axis and is the only parameter that affects the critical angle. As a TSG sample is constituted of different glass materials and glue of irregular thickness (which cannot be modelled), the theoretical location of the critical angle is uncertain. Fortunately, this is not a problem, as an error in the critical angle does not affect the interpretation of the fit in terms of dendrimer layer thickness.

Generation two dendrimers have also been tested for their adsorption onto flat planar gold surfaces. However, both the polycationic and polyanionic G_2 dendrimers were found to not adsorb at all. There are two facts that can be held responsible for this behaviour. Firstly, the dendrimers have an apolar interior that is shielded from the water by a hydrophilic shell. As the dithiolane moiety has a strong apolar character, it is energetically more favourable to bury this linker inside the dendrimer. Apparently, G_1 dendrimers were not able to shield the linker from the water and exposed the linker to the gold, which led to binding. Secondly, even if the dithiolane would be exposed to the aqueous environment, it would have been too short to sufficiently reach out to the gold and the interaction with gold would have been sterically too much hindered by the large dendrimer branches.

Modelling of the molecular structure of the dendrimers (MM2 energy minimalisation using Chemdraw 12) rendered a theoretical value for the dendrimers' diameters in vacuum [63]. This value was determined to be 2-3

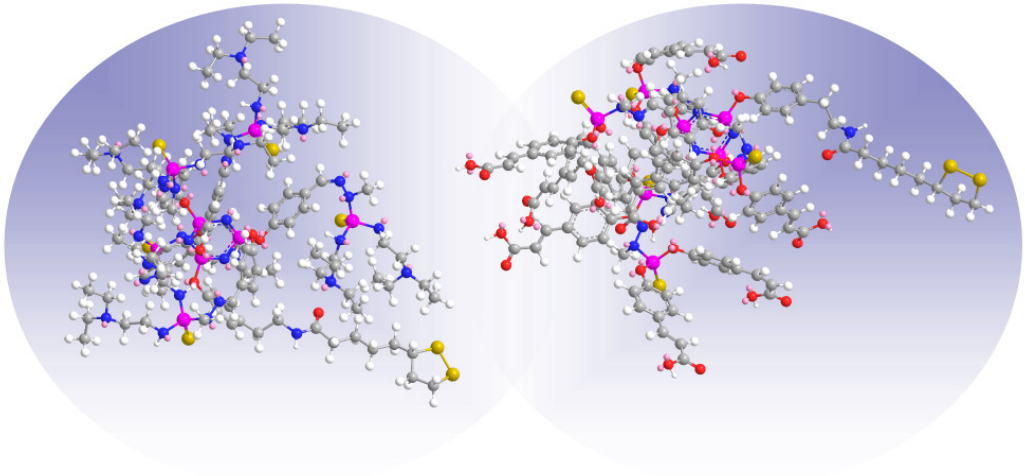

Fig. 3.14 – Three dimensional representation of the molecular structure of G_1^+ (right) and G_1^- (left) after running an energy minimalisation in vacuum.

nm for both of them. However, it must be kept in mind that solvents and ionic strength, which were not taken into account in this modelling, certainly [64] have an enormous influence on the shape of a dendrimer. As discussed before, the dendrimers have a hydrophobic core, which makes the dendrimer collapse upon contact with water in order to prevent too many energetically unfavourable interactions. The "vacuum value" calculated with the modelling may therefore well be overestimated. Moreover, it must be considered that SPR returns a value for the thickness that represents a surface average over the area where the plasmon is excited. Very often, layered systems of molecules are represented in a highly idealised fashion; molecules stacked like soldiers without any defects. This commonly results in an underestimation of the thickness per molecule. In the case of dendrimers, which almost certainly experience significant sterical hindrance during the adsorption process, a densely packed monolayer is probably far from reality. Thirdly, phosphorus dendrimers tend to flatten and slightly spread upon adsorption to a surface [43, 48] (unlike for example shape persistent polyphenylene dendrimers [65]), resulting in a layer thickness that is thinner than the "vacuum diameter" of the dendrimer. Hence, a measured layer thickness of 1.0 nm is here presumed to represent a monolayer with a packing density of close to 100%.

In short

Both applied dendrimers (G_1^+ and G_1^-) readily bound to the gold surfaces and formed a monolayer with an average coverage of approximately 100%. The required time to reach saturation was measured with SPR in the kinetic mode and was determined to be approximately two hours. Therefore, samples to be coated with dendrimers were incubated overnight and used the next morning after rinsing with extensive water and HPLC grade ethanol.

3.3.5 Contact Angle Measurements

In order to further characterise the dendrimer films on the gold samples, water contact angles were measured. This gives information about the hydrophilicity or hydrophobicity of the film. This property has a large influence on cell adhesion. On beforehand it is difficult to predict whether the dendrimers will render a polar or apolar surface, as they are only soluble in water despite the fact that their interior is lipophilic. With this experiment it is possible to qualitatively determine to what extent their interior is exposed to the aqueous environment.

After modification of the gold surfaces with a dendrimer monolayer, the contact angle changed from 33° to 52° and to 51° for the positively charged and negatively charged dendrimer, respectively. Whereas a clean, freshly stripped TSG surface is rather hydrophilic, the dendrimers made it more hydrophobic. This value is typically represents a surface that is neither hydrophilic nor hydrophobic. Surfaces coated with a SAM of alkane amonium-

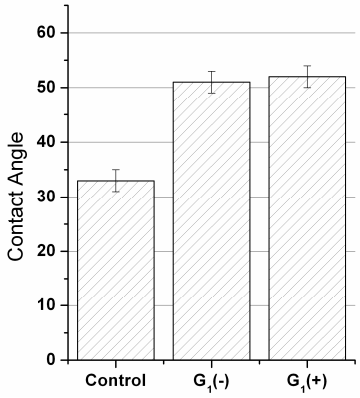

Fig. 3.15 – Water contact angles G1 dendrimer coated gold samples. Measurements on each sample were taken in 6-fold.

thiols or carboxylate-thiols exhibit lower contact angle values (at pH = 7; 30° [66] and 32° [67], respectively) than the dendrimers, despite the fact they bear identical "peripheral" functionalities. This implies that a significant proportion of the hydrophobic interior must be exposed to the water.

3.4 Synopsis and Conclusion

Four different phosphors dendrimers (Fig. 3.8) were synthesised at gram scale. All were soluble only in water due to their peripheral polycationic or polyanionic modifications. SPR spectroscopy revealed that only generation 1 dendrimers were able to bind to gold, which shows that the dithiolane linker is too short to efficiently bind to gold when it is attached to the core of a generation 2 dendrimer. For gold substrates coated with G1 polycationic and polyanionic dendrimers the water contact angles were 52° and 51°, respectively. These values indicate that the dendrimers' hydrophobic interiors are exposed to the aqueous environment.

3.5 Materials and Methods

In this section, all technical and experimental details are described. All water used is demineralised using MilliQ equipment and the resistivity was 18 MΩ.cm. All reactions were carried out under argon atmosphere and in freshly distilled solvents. All column chromatography was carried out with silica gel 60 as the static phase. All starting compounds were purchased from Aldrich, Merck or Fluka and used as received. Molecular weights are reported in g/mol.

3.5.1 Synthesis

Subscript in the NMR assignments indicates the generation number, superscript indicates either the numbering of the dithiolane linker as provided

with product 4 (between parentheses) or of the phenyl rings, where 1 is closest to the core and 4 farthest. Assignments labelled with [T] originate from the dithiolane linker.

1. p-hydroxybenzaldehyde sodium salt

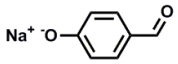

$C_7H_5NaO_2$

MW=122.1

A suspension of NaH (1.60 g, 66.7 mmol, 1.0 eq) in 50 mL THF was cooled to -30°C. To this, a 65 mL THF solution of p-hydroxybenzaldehyde (8.03 g, 65.8 mmol, 0.99 eq) was added dropwise. The reaction mixture was allowed to warm up to room temperature. The color changed from brown-beige to light yellow-green. After 1.5 hrs reaction time, the reaction mixture is quickly filtered with a Büchner funnel and the sodium salt is washed three times with dry diethyl ether. This yields 8.80 g (61 mmol, 92%) of a light yellow-green powder. No NMR data available.

2. N-methyldichloro thiophosphorhydrazide (MHTPC)

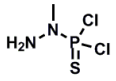

$C_1H_5P_1S_1Cl_2$

MW=151.0

In very dry glassware, 20 mL of thiophosphoryl chloride (193 mmol, 1.0 eq) were dissolved in 700 mL chloroform and cooled to -60°C. To this a solution of 20 mL monomethylhydrazine (379 mmol, 2.0 eq) in 44 mL chloroform was added very slowly using a dropping funnel while keeping the temperature constant at -60°C. The reaction was stirred overnight while allowing it to adopt room temperature slowly. After the night, the solution was filtered and transferred into a pre-cooled reception bottle. This solution contains only MHTPC and has a concentration of 0.24 M and it should be stored in the dark in the freezer.

$^{31}P\{^1H\}$-NMR (121.5 MHz, $CDCl_3$): **70.3** (s, P)

3. penta(4-formylphenoxy)-chlorocyclotriphosphazene

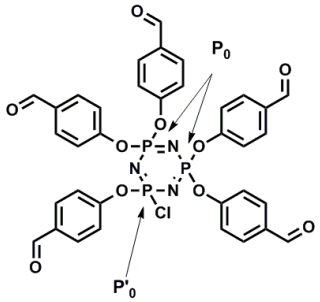

$C_{35}H_{25}ClN_3O_{10}P_3$

MW=776.0

In a Schlenk a dry 600 mL THF solution of hexachlorocyclotriphosphazene (2.87 g, 8.26 mmol, 1.0 eq) was cooled to 0°C and put under argon atmosphere. Stepwise **1** (6.17 g, 42.8 mmol, 5.2 eq) was added and the mixture was left to react overnight. The solids were removed from the reaction solution by centrifugation (30 min, 10k rpm) and the THF was evaporated under reduced pressure. The pentasubstituted core was separated from the tetra- and hexa substituted ones by means of column chromatography, applying a gradient (0% - 30%) of ethyl actetate in hexane as eluent. The yield was 4.0076 g (5.26 mmol, 63%) with the product being colorless oil that slowly turns into a white solid. The column still gave a small overlap of the penta- and hexasubstituted cores.

^{1}H-NMR (250 MHz, $CDCl_3$): **7.20** (m, 10H, C_o-H), **7.77** (m, 10H, C_m-H), **9.93** (2 s, 5H, CHO)

$^{31}P\{^1H\}$-NMR (101.3 MHz, $CDCl_3$): **5.2** (2 d, $^2J_{pp}$ = 86.2 Hz and 88.0 Hz, P_o), 20.8 (dd, $^2J_{pp}$ = 84.2 Hz and 88.8 Hz, P'_o)

$^{13}C\{^1H\}$-NMR (62.9 MHz, $CDCl_3$): **121.6** (m, C_o^2), **131.4** (s, C_o^3), **134.0** (m, C_o^4), **154.2** (m, C_o^1), **190.5** (2s, CHO).

4. 5-(1,2-dithiolan-3-yl)-N-[2-(4-hydroxyphenyl)ethyl]pentanamide

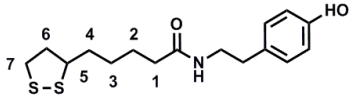

$C_{16}H_{23}NO_2S_2$

MW=325.5

In a Schlenk flask under argon atmosphere thioctic acid (2.509 g, 12.2 mmol, 1.23 eq) and DIPEA (diisopropylethylamine, 2.2 mL, 12.6 mmol, 1.27 eq) were dissolved in 20 mL dry dichloromethane and cooled down to -20°C. A 20 mL DMF solution of TBTU (3.634 g, 11.3 mmol, 1.14 eq) was added dropwise and the mixture was stirred for 30 minutes at room temperature. This mixture was added to a 10 mL DMF suspension of tyramine (1.356 g, 9.9 mmol, 1.0 eq) and the reaction was completed overnight at room temperature. The solvents were evaporated under reduced pressure. The product was diluted in dichloromethane and washed twice with a saturated aqueous $NaHCO_3$ solution and once with brine and finally dried over Na_2SO_4. The crude product was purified with column chromatography (1% MeOH in $CHCl_3$). This procedure quantitatively yielded a yellow solid.

^{1}H-NMR (300 MHz, $CDCl_3$): **1.39** (m, 2H, $C^{(3)}H_2$), **1.62** (m, 4H, $C^{(4)}H_2$ + $C^{(2)}H_2$), **1.87** (m, 1H, $C^{(6)}H_2$), **2.16** (t, 2H, CH_2CO, $^3J_{HH}$ = 7.4 Hz), **2.40** (m, 1H, $C^{(6)}H_2$), **2.72** (t, 2H, CH_2Ar, $^3J_{HH}$ = 7.0 Hz), **3.12** (m, 2H, CH_2S), **3.48** (m, 3H, CH-S + CH_2NH), **5.91** (t, 1H, NH, $^3J_{HH}$ = 5.7 Hz), **6.81** (d, 2H, arom., $^3J_{HH}$ = 8.4 Hz), **7.00** (d, 2H, arom., $^3J_{HH}$ = 8.4 Hz), **7.98** (s, 1H, OH)
^{13}C{^{1}H}-NMR (75.5 MHz, $CDCl_3$): **25.3** ($C^{(2/4)}H_2$), **28.9** ($C^{(3)}H_2$), **34.6** ($C^{(2/4)}H_2$), **35.0** (CH_2Ar), **36.4** (CH_2CO), **38.5** (CH_2S), **40.3** ($C^{(6)}H_2$), **40.5** (CH_2NH), **56.5** (CH), **115.7** (C_o^2), **129.7** ($C_o^{3,4}$), **155.3** C_o^1), **173.7** (NCO).
(All assignments are confirmed by a proton COSY, ^{1}H-^{13}C HMQC and ^{13}C J-mod spectra)

5. G'$_0$

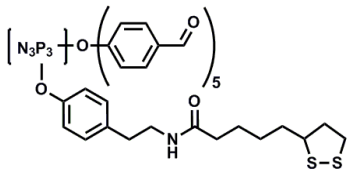

$C_{51}H_{47}N_4O_{12}P_3S_2$
MW=1065.0

A 150 mL THF solution of **3** (2.82 g, 3.64 mmol, 1.0 eq) and Cs_2CO_3 (1.79 g, 5.46 mmol, 1.5 eq) was cooled down to 0°C. A 20 mL THF solution of **4** (1.30 g, 4.00 mmol, 1.1 eq) was added and the reaction mixture was stirred overnight. The mixture was centrifuged (30 min, 10k rpm), the Cs_2CO_3 pellet

removed and the THF evaporated. The product was purified with column chromatography using an increasing gradient of ethyl acetate/hexane starting at a 1:1 ratio. This yielded the product (2.91 g, 2.72 mmol, 75%) as a yellow oil.

^{1}H-NMR (300 MHz, $CDCl_3$): **1.39** (m, 2H, $C^{(3)}H_2$), **1.62** (m, 4H, $C^{(4)}H_2$ + $C^{(2)}H_2$), **1.87** (m, 1H, $C^{(6)}H_2$), **2.16** (t, 2H, CH_2CO, $^{3}J_{HH}$ = 7.4 Hz), **2.40** (m, 1H, $C^{(6)}H_2$), **2.72** (t, 2H, CH_2Ar, $^{3}J_{HH}$ = 7.0 Hz), **3.12** (m, 2H, CH_2S), **3.48** (m, 3H, CH-S + CH_2NH), **5.91** (t, 1H, NH, $^{3}J_{HH}$ = 5.7 Hz), **6.89-7.74** (m, 24H, Ar)
^{31}P{^{1}H}-NMR (121.5 MHz, $CDCl_3$): **7.4** (m, P_o and P'_o)
^{13}C{^{1}H}-NMR (62.9 MHz, $CDCl_3$): **25.4** ($C^{(2/4)}H_2$), **28.8** ($C^{(3)}H_2$), **34.5** ($C^{(2/4)}H_2$), **34.7** (CH_2Ar), **36.5** (CH_2CO), **38.5** (CH_2S), **40.3** ($C^{(6)}H_2$), **41.0** (CH_2NH), **56.4** (CH), **120.7** (C_o^2 [T]), **121.3** (C_o^2), **129.9** (C_o^3 [T]), **131.4** (C_o^3), **133.7** (C_o^4), **136.6** (C_o^4 [T]), **155.3** (C_o^1), **173.7** (NCO), **190.5** (CHO).

6. G1

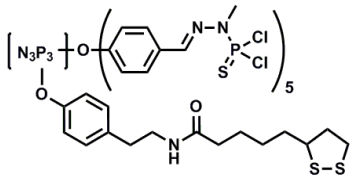

$C_{56}H_{62}N_{14}O_7P_8S_2$
MW=1869.3

A 56.7 mL 0.24 M solution of MHTPC (1.26 mmol, 5 eq.) in chloroform was added to a 50 mL solution of **5** (2.906 g, 2.72 mmol, 1.0 eq) in chloroform. After one night the amount of solvent was reduced to a few milliliters and added dropwise to a large amount of pentane. The product precipitates readily and the solvent was filtered of by means of a canula. This was repeated three times. The product was obtained as a white (pale yellow) solid in a yield of 4.68 g (2.50 mmol, 92%).

^{1}H-NMR (300 MHz, $CDCl_3$): **1.44** (m, 2H, $C^{(3)}H_2$), **1.66** (4H, $C^{(4)}H_2$ + $C^{(2)}H_2$), **1.92** (1H, $C^{(6)}H_2$), **2.12** (2H, CH_2CO), **2.45** (m, 1H, $C^{(6)}H_2$), **2.78** (2H, CH_2Ar), **3.16** (2H, CH_2S), **3.48** (3H, CH-S and CH_2NH), **5.47** (1H, NH), **6.89-7.74** (m, 24H, Ar).

$^{31}P\{^{1}H\}$-NMR (121.5 MHz, $CDCl_3$): **8.3** (s, P_o and P'_o), **62.4/62.6** (s, P_1 and P'_1)

$^{13}C\{^{1}H\}$-NMR (62.9 MHz, $CDCl_3$): **25.3** ($C^{(2/4)}H_2$), **28.9** ($C^{(3)}H_2$), **32.0** (d, P_1-N-CH_3, $^{2}J_{CP}$ = 13.2 Hz), **34.6** ($C^{(2/4)}H_2$), **35.2** (CH_2Ar), **36.4** (CH_2CO), **38.5** (CH_2S), **40.3** ($C^{(6)}H_2$), **41.0** (CH_2NH), **56.5** (CH), **121.1** (C_o^2 [T]), **121.4** (C_o^2), **128.6** (C_o^3), **129.7** (C_o^3 [T]), **131.3** (C_o^4), **140.7** (d, CH=N-N-P_o, $^{3}J_{CP}$ = 20.1 Hz), **151.7** (C_o^1), **173.0** (NCO).

7. G_1^+

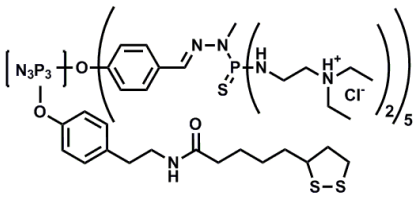

$C_{126}H_{222}N_{34}O_7P_8S_7Cl_{10}$

MW=3031

N,N-diethylethylenediamine (750 µL, 0.53 mmol, 0.99 eq) was added dropwise to a 150 mL THF solution of **6** (1.002 g, 5.36 mmol, 1.0 eq). The reaction was stirred at room temperature overnight. A white solid appeared during the reaction. The precipitate was washed with dry THF and diethylether and lyophilized. This yielded 1.226 g of a white powder (405 µmol, 76 %).

^{1}H-NMR (300 MHz, $CDCl_3$): **1.35** (m, 62H, $C^{(3)}H_2$ and NCH_2CH_3), **1.66** (m, 4H, $C^{(4)}H_2$ + $C^{(2)}H_2$), **1.92** (1H, $C^{(6)}H_2$), **2.12** (t, 2H, CH_2CO), **2.45** (m, 1H, $C^{(6)}H_2$), **2.78** (t, 2H, CH_2Ar), **3.16** (2H, CH_2S), **3.15-3.50** (m, 98H, CH-S and CH_2NH and P_1-N-CH_3 and CH_2), **6.80-7.81** (m, 29H, arom. and CH=N-N-P_1)

$^{31}P\{^{1}H\}$-NMR (121.5 MHz, $CDCl_3$): **8.5** (s, P_o and P'_o), **70.4** (s, P_1)

$^{13}C\{^{1}H\}$-NMR (75.5 MHz, $CDCl_3$): **7.9** (NCH_2CH_3), **25.4** ($C^{(2/4)}H_2$), **28.5** ($C^{(3)}H_2$), **31.4** (2d, P_1-N-CH_3, $^{2}J_{CP}$ = 10.6 Hz), **34.4** (d, $C^{(2/4)}H_2$), **35.5** (d, CH_2Ar), **36.2** (CH_2CO and CH_2-N-P_1), **38.0** (CH_2S), **40.0** ($C^{(6)}H_2$), **40.4** (CH_2NH [T]), **49.0** (P_1-N-CH_2CH_3), **52.2** (d, P_1-N-CH_2CH_2, $^{3}J_{CP}$ = 6.9 Hz), **56.5** (CH-S), **120.5** (C_o^2 [T]), **120.9** (C_o^2), **128.0** (C_o^3), **129.7** (C_o^3 [T]), **133.2** (d, C_o^4, $^{5}J_{CP}$ = 3.5 Hz), **136.4** (C_o^4 [T]), **140.7** (m, CH=N-N-P_1), **150.8** (m, C_o^1), **174.5** (NCO [T])

8. G_1'

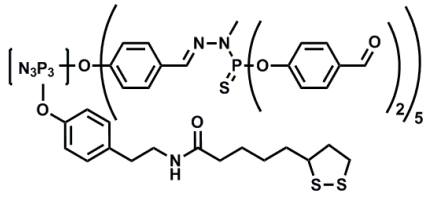

$C_{126}H_{112}N_{14}O_{27}P_8S_7$
MW=2725.2

In a Schlenk tube under argon atmosphere were mixed 4.68 g of **6** (2.50 mmol, 1.0 eq), 7.00 g of p-hydroxybenzaldehyde (57.4 mmol, 23 eq) and 16.25 g Cs_2CO_3 (50 mmol, 20 eq) and dissolved in 250 mL THF. The reaction mixture was stirred overnight at ambient temperature. The mixture was centrifuged, concentrated under reduced pressure, precipitated from pentane/ether and finally put on a small silica column to separate the product from the excessive amount of p-hydroxybenzaldehyde. Note that the 23 eq of p-hydroxybenzaldehyde was a clear mistake but without negative side effects. The precipitation could almost certainly have been carried out with (cold) methanol instead to yield a clean product. This procedure nevertheless yielded 5.97 g (88%) of product in the form of a pale yellow solid.

^{1}H-NMR (250 MHz, $CDCl_3$): **1.38** (m, 2H, $C^{(3)}H_2$), **1.57** (m, 4H, $C^{(4)}H_2$ + $C^{(2)}H_2$), **1.86** (m, 1H, $C^{(6)}H_2$), **2.06** (t, 2H, CH_2CO), **2.38** (m, 1H, $C^{(6)}H_2$), **2.70** (t, 2H, CH_2Ar), **3.06** (m, 2H, CH_2S), **3.36** (m, 18H, CH-S and CH_2NH and P_1-N-CH_3), **5.08** (s, 1H, NH), **6.89-7.84** (m, way too many H, aromatic and CH=N-N-$P_{1,2}$)
^{31}P{^{1}H}-NMR (101.3 MHz, $CDCl_3$): **8.2** (s, P_o and P'$_o$), **60.4** (s, P_1)
^{13}C{^{1}H}-NMR (62.9 MHz, $CDCl_3$): **25.6** ($C^{(2/4)}H_2$), **28.9** ($C^{(3)}H_2$), **32.9** (2d, P_1-N-CH_3, $^2J_{CP}$ = 12.8 Hz), **34.6** (d, $C^{(2/4)}H_2$), **35.1** (d, CH_2Ar), **36.3** (CH_2CO), **38.5** (CH_2S), **40.3** ($C^{(6)}H_2$), **40.5** (CH_2NH [T]), **56.5** (CH-S), **121.0** (C_o^2 [T]), **121.4** (C_o^2), **121.8** (d, C_2^2, $^3J_{CP}$ = 6.8 Hz), **128.3** (C_1^3), **129.7** (C_o^3), **131.5** (C_1^4), **131.8** (C_o^4 [T]), **133.7** (C_o^4), **140.7** (2d, CH=N-N-P_1, $^3J_{CP}$ = 13.4 Hz), **151.5** (2d, C_o^1, $^2J_{CP}$ = 7.0 Hz), **172.8** (NCO [T]), 190.7 (CHO).

9. G_1^-

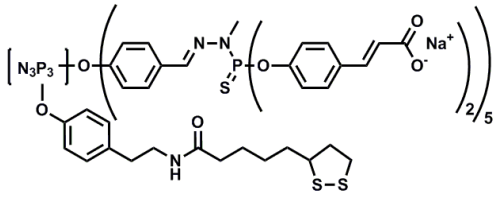

$C_{146}H_{122}N_{14}O_{37}P_8S_7Na_{10}$
MW=3365

Compound **8** (1.00 g, 0.367 mmol, 1.0 eq), 0.95 g of malonic acid (9.17 mmol, 25 eq) and 45 µL freshly distilled (on CaH_2) piperidine (0.459 mmol, 1.25 eq) were dissolved in 15 mL of freshly distilled pyridine (on CaH_2) and stirred overnight at 95°C. The mixture was then refluxed for 15 more minutes to remove the CO_2 and cooled down before precipitating it on ice cooled HCl (37%). The precipitate was subsequently washed with water (3 times) and ether (2 times) and dried under vacuum. In order to obtain the sodium salt, the product was taken into water and 12.25 mL of 0.1996 M NaOH (aq) (which is too much) were added dropwise yielding a slightly turbid solution. The overall yield was 0.811 g of the sodium salt (241 µmol, 66%).

^{1}H-NMR (300 MHz, DMSO-d6): **1.22** (m, 2H, $C^{(3)}H_2$), **1.42** (m, 4H, $C^{(4)}H_2$ + $C^{(2)}H_2$), **1.75** (m, 1H, $C^{(6)}H_2$), **1.96** (t, 2H, CH_2CO), **2.29** (m, 1H, $C^{(6)}H_2$), **2.58** (t, 2H, CH_2Ar), **3.04** (m, 2H, CH_2S), **3.27-3.41** (m, 18H, CH-S and CH_2NH and P_1-N-CH_3), **5.35** (s, 1H, NH), **6.40-7.92** (m, 89H, aromatic and CH=N-N-$P_{1,2}$ and CH=CH), **12.4** (COOH, 10H)
^{31}P{^{1}H}-NMR (121.5 MHz, DMSO-d6): **8.4** (s, P_o and P'_o), **62.0** (s, P_1)
^{13}C{^{1}H}-NMR (75.5 MHz, DMSO-d6): **25.5** ($C^{(2/4)}H_2$), **28.8** ($C^{(3)}H_2$), **33.4** (2d, P_1-N-CH_3, $^2J_{CP}$ = 11.9 Hz), **34.6** (d, $C^{(2/4)}H_2$), **34.9** (CH_2Ar), **35.7** (CH_2CO), **38.5** (CH_2S), **40.3** ($C^{(6)}H_2$) (DMSO), **40.5** (CH_2NH [T]) (DMSO), **56.5** (CH-S), **119.9** (Ar-*CH*=CH), **120.7** (C_o^2 [T]), **121.4** (C_o^2), **121.8** (d, C_2^2, $^3J_{CP}$ = 4.1 Hz), **125.4** (C_o^3 [T]), **128.7** (C_o^3), **130.2** (C_1^3), **132.2** (C_1^4), **132.4** (C_o^4), **137.2** (C_o^4 [T]), **141.1** (CH=N-N-P_1), **143.1** (CH=*CH*-COOH), **148.4** (C_o^1 [T]), **151.0** (C_o^1), **151.7** (C_1^1), **167.9** (COOH), **172.3** (NCO [T])

10. G_2

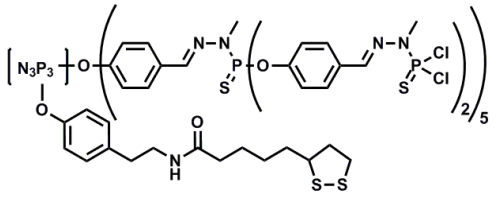

$C_{136}H_{142}N_{34}O_{17}P_{18}S_{17}Cl_{20}$

MW=4335

To an ice cooled 70 mL $CHCl_3$ solution of 3.97 g of compound **8** (1.46 mmol, 1.0 eq) were added 64 mL (0.24 M, 15.3 mmol, 10.5 eq) MHTPC in $CHCl_3$. The reaction mixture was stirred at room temperature for two hours and checked with NMR for completion. The volume of $CHCl_3$ was reduced and the mixture was precipitated from pentane several times until the excess of MHTPC was completely removed. This yielded 5.97 g (1.37 mmol, 94%) of product as a pale yellow solid.

^{1}H-NMR (250 MHz, $CDCl_3$): **1.35** (m, 2H, $C^{(3)}H_2$), **1.61** (m, 4H, $C^{(4)}H_2$ + $C^{(2)}H_2$), **1.88** (m, 1H, $C^{(6)}H_2$), **2.03** (t, 2H, CH_2CO), **2.42** (m, 1H, $C^{(6)}H_2$), **2.72** (t, 2H, CH_2Ar), **3.13** (m, 2H, CH_2S), **3.28-3.50** (m, 48H, CH-S and CH_2NH and $P_{1,2}$-N-CH_3), **5.70** (s, 1H, NH), **6.98-7.73** (m, 79H, aromatic and CH=N-N-$P_{1,2}$)

^{31}P{^{1}H}-NMR (101.3 MHz, $CDCl_3$): **8.3** (s, P_o and P'_o), **61.9** (s, P_1), **62.8** (s, P_2)

^{13}C{^{1}H}-NMR (75.5 MHz, $CDCl_3$): **25.3** ($C^{(2/4)}H_2$), **28.9** ($C^{(3)}H_2$), **31.8** (d, P_2-N-CH_3, $^2J_{CP}$ = 13.1 Hz), **33.1** (2d, P_1-N-CH_3, $^2J_{CP}$ = 12.9 Hz), **34.6** (d, $C^{(2/4)}H_2$), **35.1** (d, CH_2Ar), **36.4** (CH_2CO), **38.5** (CH_2S), **40.3** ($C^{(6)}H_2$), **40.5** (CH_2NH [T]), **56.5** (CH-S), **121.0** (C_o^2 [T]), **121.4** (d, C_o^2, $^3J_{CP}$ = 6.2 Hz), **121.9** (d, C_2^1, $^3J_{CP}$ = 4.3 Hz), **128.3** (C_o^3), **128.8** (C_1^3), **129.8** (C_o^3 [T]), **131.6** (C_1^4), **131.9** (C_o^4), **135.9** (C_o^4 [T]), **138.9** (m, CH=N-N-P_1), **140.6** (d, CH=N-N-P_1, $^2J_{CP}$ = 18.7 Hz), **151.4** (m, C_o^1), **151.8** (d, C_1^1, $^2J_{CP}$ = 7.2 Hz), **172.6** (NCO [T])

11. G_2^+

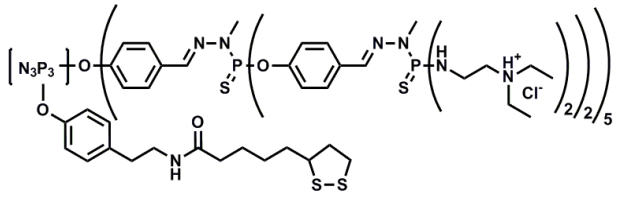

$C_{256}H_{462}N_{74}O_{17}P_{18}S_{17}Cl_{20}$

MW=6658

In a Schlenk tube, 1.00 g of compound **10** (0.231 mmol, 1.0 eq) was dissolved in 150 mL THF to which 650 µL of N,N-diethylethylenediamine (4.59 mmol, 19.9 eq) was added dropwise. The reaction was stirred overnight at room temperature. The precipitate was washed twice with dry THF, yielding 1.00 g (0.15 mmol, 65%) of product as a pale yellow solid).

^{1}H-NMR (300 MHz, $CDCl_3$): **1.30** (m, 122H, $C^{(3)}H_2$ and $NCH_2\mathit{CH_3}$), **1.51** (m, 4H, $C^{(4)}H_2$ + $C^{(2)}H_2$), **1.88** (1H, $C^{(6)}H_2$), **2.10** (t, 2H, CH_2CO), **2.36** (m, 1H, $C^{(6)}H_2$), **2.86** (t, 2H, CH_2Ar), **3.07** (2H, CH_2S), **3.20-3.40** (m, 208H, CH-S and CH_2NH [T] and $P_{1,2}$-N-CH_3 and CH_2), **6.65-7.93,** (m, 79H, arom. and CH=N-N-$P_{1,2}$)

^{31}P{^{1}H}-NMR (121.5 MHz, $CDCl_3$): **8.9** (s, P_0 and P'$_0$), **62.4** (s, P_1), **70.2** (s, P_2)

^{13}C{^{1}H}-NMR (75.5 MHz, $CDCl_3$): **7.9** ($NCH_2\mathit{CH_3}$), **25.4** ($C^{(2/4)}H_2$), **28.5** ($C^{(3)}H_2$), **31.3** (d, P_2-N-CH_3, $^2J_{CP}$ = 9.4 Hz), **32.5** (d, P_1-N-CH_3, $^2J_{CP}$ = 12.2 Hz), **34.4** (d, $C^{(2/4)}H_2$), **35.6** (d, CH_2Ar), **36.2** (CH_2-N-P_2), **36.4** (CH_2CO), **38.1** (CH_2S), **40.1** ($C^{(6)}H_2$ and CH_2NH [T]), **49.5** (N-$\mathit{CH_2}CH_3$), **52.2** (d, P_2-N-$CH_2\mathit{CH_2}$, $^3J_{CP}$ = 6.9 Hz), **56.3** (CH-S), **121.0** (C_0^2), **121.4** (C_1^2), **128.0** (C_1^3), **128.3** (C_0^3), **130.0** (C_0^3 [T]), **132.6** (C_0^4), **133.3** (C_1^4), **137.5** (d, CH=N-N-$P_{1,2}$, $^2J_{CP}$ = 13.4 Hz), **151.0** (m, $C_{0,1}^1$),

12. G_2'

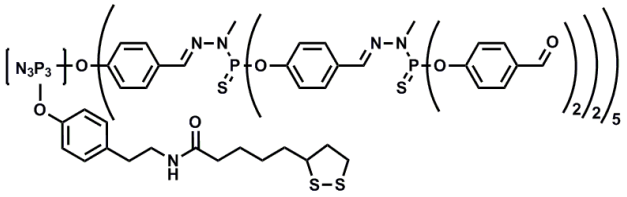

$C_{276}H_{242}N_{34}O_{57}P_{18}S_{18}$
MW=6047

In a Schlenk tube, 4.00 g of **10** (0.916 mmol, 1.0 eq), 2.45 g of p-hydroxybenzaldehyde (20.1 mmol, 22 eq) and 11.92 g Cs_2CO_3 (36.6 mmol, 40 eq) were dissolved in 600 mL THF. The reaction was stirred overnight at room temperature. The solution was filtered, its volume was reduced and the dendrimer was precipitated from pentane several times until all excess of p-hydroxybenzaldehyde was removed. This quantitatively yielded the product as a pale yellow solid (5.54 g).

^{1}H-NMR (300 MHz, $CDCl_3$): **1.35** (m, 2H, $C^{(3)}H_2$), **1.66** (m, 4H, $C^{(4)}H_2$ + $C^{(2)}H_2$), **1.88** (m, 1H, $C^{(6)}H_2$), **1.99** (t, 2H, CH_2CO, $^3J_{HH}$ = 7.2 Hz), **2.34** (m, 1H, $C^{(6)}H_2$), **2.66** (t, 2H, CH_2Ar, $^3J_{HH}$ = 7.2 Hz), **3.07** (m, 2H, CH_2S), **3.25-3.39** (m, 48H, CH-S and CH_2NH and $P_{1,2}$-N-CH_3), **5.75** (s, 1H, NH), **6.84-7.84** (m, 159H, aromatic and CH=N-N-$P_{1,2}$), **9.90** (CHO)

^{31}P{^{1}H}-NMR (121.5 MHz, $CDCl_3$): **8.3** (s, P_o and P'_o), **60.3** (s, P_2), **62.3** (s, P_1)

^{13}C{^{1}H}-NMR (75.5 MHz, $CDCl_3$): **25.3** ($C^{(2/4)}H_2$), **28.9** ($C^{(3)}H_2$), **33.0** (2d, $P_{1,2}$-N-CH_3, $^2J_{CP}$ = 12.8 Hz), **34.5** (d, $C^{(2/4)}H_2$), **35.0** (d, CH_2Ar), **36.3** (CH_2CO), **38.5** (CH_2S), **40.3** ($C^{(6)}H_2$ and CH_2NH [T]), **56.5** (CH-S), **120.7** (C_o^2 [T]), **121.3** (C_o^2), **121.3** (d, C_1^1, $^3J_{CP}$ = 4.0 Hz), **122.0** (d, C_2^1, $^3J_{CP}$ = 4.8 Hz), **128.4** ($C_{o,i}^3$), **129.6** (C_o^3 [T]), **131.5** (C_2^3), **132.0** ($C_{o,i}^4$), **133.7** (C_2^4), **135.9** (C_o^4 [T]), **139.6** (2d, CH=N-N-$P_{1,2}$, $^2J_{CP}$ = 15.1 Hz), **151.5** (2d, $C_{o,i}^1$, $^2J_{CP}$ = 7.1 Hz), **155.1** (d, C_2^1, $^2J_{CP}$ = 7.2 Hz), not observed (NCO [T]), **190.7** (CHO)

13. G_2^-

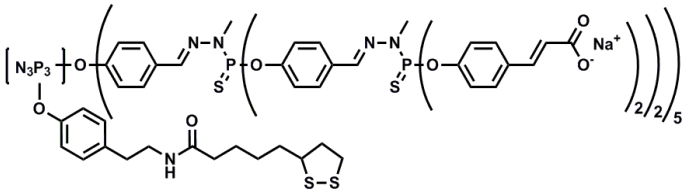

$C_{316}H_{262}N_{34}O_{77}P_{18}S_{18}$
Na_{20}
MW=7327

A mixture of 1.00 g of compound **12** (0.165 mmol, 1.0 eq), 0.86 g of malonic acid (8.27 mmol, 50 eq) and 24.5 µL of piperidine (freshly distilled over CaH_2) was stirred in 15 mL of pyridine at 95°C overnight. After 15 minutes of reflux to remove the CO_2, the mixture was cooled down and precipitated from ice-cold HCl (37%). The precipitate was washed 3 times with water and twice with ether before it was dried under reduced pressure. After dissolution in water and subsequent ion exchange with 12 mL of 0.1996 M NaOH (aq) (14.5 eq), the solution was lyophilisated. This yielded 0.858 g of product (0.117 mmol, 71%) as a pale yellow solid.

^{1}H-NMR (300 MHz, DMSO-d6): **1.23** (m, 2H, $C^{(3)}H_2$), **1.36** (m, 4H, $C^{(4)}H_2$ + $C^{(2)}H_2$), **1.75** (m, 1H, $C^{(6)}H_2$), **1.90** (t, 2H, CH_2CO), **2.18** (m, 1H, $C^{(6)}H_2$), **2.57** (t, 2H, CH_2Ar), **2.99** (m, 2H, CH_2S), **3.12-3.59** (m, 48H, CH-S and CH_2NH and P_1-N-CH_3), not observed (s, 1H, NH), **6.40-7.92** (m, 199H, aromatic and CH=N-N-$P_{1,2}$ and CH=CH), **12.4** (COOH, 20H)
^{31}P{^{1}H}-NMR (121.5 MHz, DMSO-d6): **8.4** (s, P_o and P'_o), **62.0** (s, P_2), **62.4** (s, P_1)
^{13}C{^{1}H}-NMR (75.5 MHz, DMSO-d6): **25.4** ($C^{(2/4)}H_2$), **28.7** ($C^{(3)}H_2$), **33.4** (m, $P_{1,2}$-N-CH_3), **34.0** ($C^{(2/4)}H_2$), **34.5** (CH_2Ar), **35.6** (CH_2CO), **38.4** (CH_2S), **40.3** ($C^{(6)}H_2$) (DMSO), **40.5** (CH_2NH [T]) (DMSO), **56.5** (CH-S), **119.8** (Ar-*CH*=CH), **120.6** (C_o^2), **121.3** (C_1^2), **121.8** (d, C_2^2, $^3J_{CP}$ = 4.8 Hz), **128.8** ($C_{o,i}^3$), **130.3** (C_2^3), **132.2** (C_2^4), **132.5** ($C_{o,i}^4$), **141.1** (m, CH=N-N-$P_{1,2}$), **143.1** (CH=*CH*-COOH), **151.3** (d, $C_{o,i}^1$, $^5J_{CP}$ = 6.9 Hz), **151.7** (C_2^1, $^5J_{CP}$ = 6.9 Hz), **167.9** (COOH), **172.4** (NCO [T])

3.5.2 Sample preparation

Cleaning procedure

Glass cover slips (3.8 x 2.5 cm) were first thoroughly cleaned. They were submerged twice in a 2% aqueous solution of the detergent Hellmanex and once in HPLC grade ethanol and sonicated for 15 minutes. In between, the samples were rinsed with an excess of water and ethanol, respectively. Finally they were dried with a stream of nitrogen gas.

Template stripped gold

The gold samples were prepared as described in literature [68].

Dendrimer coating

The freshly prepared gold samples were mounted into a Teflon SPR cell that allows the flow of liquid through the cell for the application of solutions. A 1 mg/mL aqueous dendrimer solution was applied to the cell and the adsorption process was followed in real time with SPR spectroscopy and stopped by rinsing with water after the no more dendrimers adsorbed.

3.5.3 Contact angle goniometry

The water contact angles were measured with an OCA 15+ (DataPhysics, Filderstadt, Germany) goniometer equipped with a CCD camera and an electronic dosing unit. For the determination of the contact angle, SCA 20 software was used that automatically recognises the droplet, fits a curve around the silhouette (LaPlace fitting) and calculates the contact angle. The droplet volume was 3 µL and the water was degassed before usage. At least 5 measurements per surface were done in order to obtain a statistically sound result.

3.5.4 Surface Plasmon Spectroscopy

The glass slides (high refractive index, $n \approx 1.82$, $LaSFN_9$) were cleaned and coated as described in section 3.5.2. The sample slide was attached to the $LaSFN_9$ prism using refractive index matching oil ($n=1.7$, Cargille Labs, USA). The dendrimer adsorption was carried out using a flow cell. The laser used was a HeNe laser with one spectral line at 632.8 nm.

3.6 Bibliography

[1] M. Kind, C. Woll, Prog Surf Sci 84/7-8 (2009) 230.
[2] A. Kuhnle, Curr Opin Colloid In 14/2 (2009) 157.
[3] M. Rosso, A. Arafat, K. Schroen, M. Giesbers, C.S. Roper, R. Maboudian, H. Zuilhof, Langmuir 24/8 (2008) 4007.
[4] M. Rosso, M. Giesbers, A. Arafat, K. Schroen, H. Zuilhof, Langmuir 25/4 (2009) 2172.
[5] B.J. Melde, B.J. Jonhnson, P.T. Charles, Sensors 8 (2008) 5202.
[6] G.R. Newkome, K.S. Yoo, C.N. Moorefield, Des Monomers Polym 5/1 (2002) 67.
[7] H. Tsutsumi, S. Furumoto, M. Morita, Y. Matsuda, Journal of Electrochemical Society 139/6 (1992) 1522.
[8] I. Yildiz, S. Ray, T. Benelli, F.M. Raymo, J Mater Chem 18/33 (2008) 3940.
[9] G. Schmid, E. Emmrich, J.P. Majoral, A.M. Caminade, Small 1/1 (2005) 73.
[10] G. Schmid, W. Meyer-Zaika, R. Pugin, T. Sawitowski, J.P. Majoral, A.M. Caminade, C.O. Turrin, Chem-Eur J 6/9 (2000) 1693.
[11] A. Schenning, E. Peeters, E.W. Meijer, J Am Chem Soc 122/18 (2000) 4489.
[12] B.W. Koo, C.K. Song, C. Kim, Sensor Actuat B-Chem 77/1-2 (2001) 432.
[13] M. Kawase, T. Shiomi, H. Matsui, Y. Ouji, S. Higashiyama, T. Tsutsui, K. Yagi, J Biomed Mater Res 54/4 (2001) 519.
[14] A.U. Bielinska, A. Yen, H.L. Wu, K.M. Zahos, R. Sun, N.D. Weiner, J.R. Baker, B.J. Roessler, Biomaterials 21/9 (2000) 877.
[15] F. Gao, B.F. Pan, W.M. Zheng, L.M. Ao, H.C. Gu, J Magn Magn Mater 293/1 (2005) 48.
[16] G.J. Wang, Y.N. Fang, P. Kim, A. Hayek, M.R. Weatherspoon, J.W. Perry, K.H. Sandhage, S.R. Marder, S.C. Jones, Adv Funct Mater 19/17 (2009) 2768.
[17] V. Le Berre, E. Trevisiol, A. Dagkessamanskaia, S. Sokol, A.M. Caminade, J.P. Majoral, B. Meunier, J. Francois, Nucleic Acids Res 31/16 (2003) E88.
[18] L.M. Prisant, B. Bottini, J.T. DiPiro, A.A. Carr, Am J Med 93/2A (1992) 45S.
[19] L. Qin, D.R. Pahud, Y. Ding, A.U. Bielinska, J.F. Kukowska-Latallo, J.R. Baker, Jr., J.S. Bromberg, Hum Gene Ther 9/4 (1998) 553.
[20] K.P. Rao, J Biomater Sci Polym Ed 7/7 (1995) 623.
[21] E.C. Wiener, M.W. Brechbiel, H. Brothers, R.L. Magin, O.A. Gansow, D.A. Tomalia, P.C. Lauterbur, Magnet Reson Med 31/1 (1994) 1.
[22] M. Beier, J.D. Hoheisel, Nucleic Acids Res 27/9 (1999) 1970.
[23] G.P. Perez, W.G. Yelton, R.W. Cernosek, R.J. Simonson, R.M. Crooks, Anal Chem 75/14 (2003) 3625.
[24] M.K. Park, S.X. Deng, R.C. Advincula, J Am Chem Soc 126/42 (2004) 13723.
[25] Sangermano, Macromolecular Materials and Engineering 293 (2008) 964.
[26] X.Y. Shi, K. Sun, L.P. Balogh, J.R. Baker, Nanotechnology 17/18 (2006) 4554.
[27] E.C. Cutler, E. Lundin, B.D. Garabato, D. Choi, Y.S. Shon, Mater Res Bull 42/6 (2007) 1178.
[28] L.O. Brown, J.E. Hutchison, J Am Chem Soc 1997 (1997) 12384.
[29] G. Schmid, R. Pugin, J.O. Malm, J.O. Bovin, Eur J Inorg Chem (6) (1998) 813.
[30] G. Schmid, R. Pugin, W. Meyer-Zaika, U. Simon, Eur J Inorg Chem (11) (1999) 2051.
[31] E. Emmrich, S. Franzka, G. Schmid, Nano Lett 2/11 (2002) 1239.

[32] O. Vidoni, S. Neumeier, N. Bardou, J.L. Pelouard, G. Schmid, J Clust Sci 14/3 (2003) 325.
[33] P. Wu, X. Chen, N. Hu, U.C. Tam, O. Blixt, A. Zettl, C.R. Bertozzi, Angew Chem Int Edit 47/27 (2008) 5022.
[34] X. Chen, G.S. Lee, A. Zettl, C.R. Bertozzi, Angew Chem Int Ed Engl 43/45 (2004) 6111.
[35] X. Chen, U.C. Tam, J.L. Czlapinski, G.S. Lee, D. Rabuka, A. Zettl, C.R. Bertozzi, J Am Chem Soc 128/19 (2006) 6292.
[36] Y. Kim, S.C. Zimmerman, Curr Opin Chem Biol 2/6 (1998) 733.
[37] C.C. Lee, J.A. MacKay, J.M. Frechet, F.C. Szoka, Nat Biotechnol 23/12 (2005) 1517.
[38] S. Svenson, D.A. Tomalia, Adv Drug Deliv Rev 57/15 (2005) 2106.
[39] M.J. Cloninger, Curr Opin Chem Biol 6/6 (2002) 742.
[40] W.B. Turnbull, J.F. Stoddart, Reviews in Molecular Biotechnology 90/3 (2002) 231.
[41] P. Wu, M. Malkoch, J.N. Hunt, R. Vestberg, E. Kaltgrad, M.G. Finn, V.V. Fokin, K.B. Sharpless, C.J. Hawker, Chem Commun (Camb)/46 (2005) 5775.
[42] S. Campidelli, C. Sooambar, E. Lozano Diz, C. Ehli, D.M. Guldi, M. Prato, J Am Chem Soc 128/38 (2006) 12544.
[43] D.H. Kim, P. Karan, P. Goring, J. Leclaire, A.M. Caminade, J.P. Majoral, U. Gosele, M. Steinhart, W. Knoll, Small 1/1 (2005) 99.
[44] C.L. Feng, X.H. Zhong, M. Steinhart, A.M. Caminade, J.P. Majoral, W. Knoll, Small 4/5 (2008) 566.
[45] Y.P. Sun, W.J. Huang, Y. Lin, K.F. Fu, A. Kitaygorodskiy, L.A. Riddle, Y.J. Yu, D.L. Carroll, Chem Mater 13/9 (2001) 2864.
[46] M. Holzinger, J. Abraha, P. Whelan, R. Graupner, L. Ley, F. Hennrich, M. Kappes, A. Hirsch, J Am Chem Soc 125/28 (2003) 8566.
[47] G. Decher, Science 277 (1997) 1232.
[48] Y.M. Yu, C.L. Feng, A.M. Caminade, J.P. Majoral, W. Knoll, Langmuir 25/23 (2009) 13680.
[49] J.L. Hernandez-Lopez, H.L. Khor, A.M. Caminade, J.P. Majoral, S. Mittler, W. Knoll, D.H. Kim, Thin Solid Films 516/6 (2008) 1256.
[50] D.H. Kim, O.J. Lee, E. Barriau, X. Li, A.M. Caminade, J.P. Majoral, H. Frey, W. Knoll, J Nanosci Nanotechnol 6/12 (2006) 3871.
[51] B.S. Kim, O.V. Lebedeva, K. Koynov, H.F. Gong, A.M. Caminade, J.P. Majoral, O.I. Vinogradova, Macromolecules 39/16 (2006) 5479.
[52] B.S. Kim, O.V. Lebedeva, D.H. Kim, A.M. Caminade, J.P. Majoral, W. Knoll, O.I. Vinogradova, Langmuir 21/16 (2005) 7200.
[53] F. Yu, S. Ahl, A.M. Caminade, J.P. Majoral, W. Knoll, J. Erlebacher, Anal Chem 78/20 (2006) 7346.
[54] W.B. Zhao, J. Park, A.M. Caminade, S.J. Jeong, Y.H. Jang, S.O. Kim, J.P. Majoral, J. Cho, D.H. Kim, J Mater Chem 19/14 (2009) 2006.
[55] C.L. Feng, X.H. Zhong, M. Steinhart, A.M. Caminade, J.P. Majoral, W. Knoll, Adv Mater 19/15 (2007) 1933.
[56] A.M. Caminade, J.P. Majoral, Prog Polym Sci 30/3-4 (2005) 491.
[57] A.M. Caminade, C.O. Turrin, R. Laurent, A. Maraval, J.P. Majoral, Current Organic Chemistry 10/18 (2006) 2333.
[58] J. Leclaire, Université Paul Sabatier, Toulouse, 2003.
[59] M. Blanzat, C.O. Turrin, A.M. Aubertin, C. Couturier-Vidal, A.M. Caminade, J.P. Majoral, I. Rico-Lattes, A. Lattes, Chembiochem 6/12 (2005) 2207.
[60] M. Blanzat, C.O. Turrin, E. Perez, I. Rico-Lattes, A.M. Caminade, J.P. Majoral, Chem Commun/17 (2002) 1864.
[61] F. Vogel, Vogel's Textbook of Practical Organic Synthesis, Longman, London, 1989.
[62] J. Voros, Biophys J 87/1 (2004) 553.
[63] M.J. Dudek, J.W. Ponder, Journal of Computational Chemistry 16 (1995) 791.
[64] J. Leclaire, Y. Coppel, A.M. Caminade, J.P. Majoral, J Am Chem Soc 126 (2004) 2304.
[65] S. Loi, U.M. Wiesler, H.J. Butt, K. Mullen, Macromolecules 34/11 (2001) 3661.
[66] W.H. Chuang, J.C. Lin, J Biomed Mater Res A 82A/4 (2006) 820.
[67] R. Schweiss, P.B. Welzel, C. Werner, W. Knoll, Langmuir 17/14 (2001) 4304.
[68] R. Naumann, S.M. Schiller, F. Giess, B. Grohe, K.B. Hartman, I. Karcher, I. Koper, J. Lubben, K. Vasilev, W. Knoll, Langmuir 19/13 (2003) 5435.

4 Synthesis of Ferrocene modified water-soluble dendrimers

Since their first appearance in 1991, hybrid organometallic dendrimers have already found numerous applications ranging from electrochemistry (bio-sensing) and catalysis to nano-optics and radiotherapy. In this chapter, the synthesis of water-soluble ferrocene containing dendrimers is discussed. The newly synthesised G_3 dendrimers contain 24 ferrocene groups in the branches and bear 48 either cationic or anionic charges. Dendrimers of the second family carry one ferrocene as their core and were grown until G_0 and G_1 bearing 4 or 8 peripheral cationic or anionic charges. Cyclic Voltammetry on the G_0 species revealed a small diffusion coefficient, which indicates that the dendrimers tend to aggregate in water.

4.1 Introduction

Since G.R. Newcome [1] and V. Balzani [2-4] synthesised the first dendrimers that contained metallic centres, a wealth of synthetic novelties, molecular properties and applications arose [5-9]. This can be explained by the large number of different applications for their ability to reversibly interact with, accept or donate electrons: electrochemistry (reduction and oxidation reactions), catalysis [10-12], optics (chirality [13-14], as contrast agent in MRI and molecular imaging [15-17]). The following introduction shows how all possible dendritic architectures and the nearly unlimited synthetic ways to include metals in organic molecules can be taken advantage of. It deals with different dendrimers that carry metallic centres at different locations: at the core, in the branches, encapsulated inside the dendrimer voids or at the periphery.

4.1.1 Metals in dendrimer cavities

Due to the fact that dendrimer molecular mass grows exponentially with the generation number, the periphery is relatively crowded with respect to the dendrimer interior. This implies that dendrimers possess internal voids that can take up small molecules or particles and therewith form a macromolecular cage [18]. Dendrimers can also act as a template for metal nanoparticle synthesis [19] where the nanoparticle is shielded from the outside and stabilised and solubilised by the dendritic shell. Dendrimer-templated and encapsulated metal nanoparticles thus present a valuable alternative to nanoparticles with an organic coating [20]. PAMAM (polyaminoamide) and PPI (polypropyleneimine) dendrimers take up metals ions such as Cu^{2+}, Pd^{2+}, Pt^{2+} and $AuCl_4^-$, either by complexation of the cations or by electrostatic attraction of anions. The metal ions can subsequently be chemically reduced (for example with $NaBH_4$ or hydrazine) resulting in clustering of the metal atoms into nanoparticles that are buried in the dendrimer interior. These

dendrimer encapsulated nanoparticles are efficient catalysts for a wide variety of chemical reactions [10, 19].

4.1.2 Metals at a dendrimer core and branches

The core of a dendrimer is highly shielded from its environment by the (multiple) dendritic wedges and the dendrimer can be regarded a protective shell [21]. As such, dendrimers were made carrying metallo-porphyrins grafted with dendritic shells [22]. The larger dendrimers show a prolonged lifetime of the O_2 adduct, even in presence of carbon monoxide. Dendritic branches can also exclude solvents by steric crowding. Accordingly, the core is completely shielded from the dendrimer environment and shows solvent-independent behaviour. This was shown for the luminescent properties of a metallo-porphyrin core dendrimer [23] and a lanthanide ion core dendrimer [24].

In a convergent approach, dendrimers can be constructed by the self-assembly of dendritic wedges by metal coordination [25-28]. By using Pd^{2+} and SCS pincer ligands, generation three dendrimers can be constructed with a

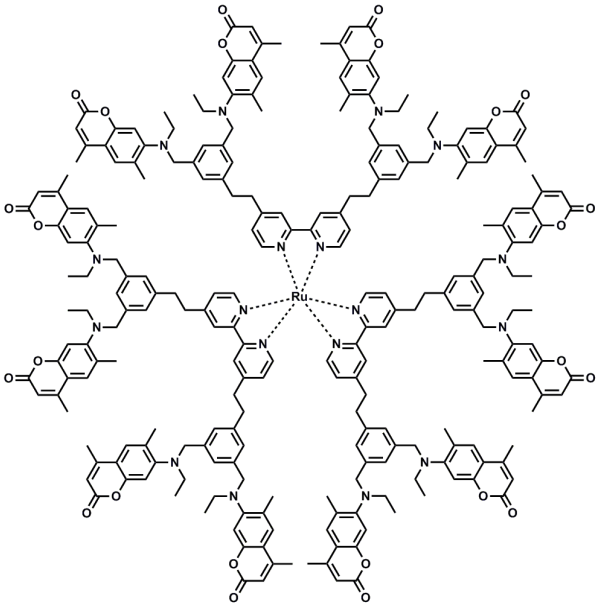

Fig. 4.1 – Light harvesting dendrimer with a Ru^{2+} tri-bipyridine complex core [25]

molecular mass of 24 kD, entirely driven by self-assembly [29]. Similarly, bipyridine ligands can coordinate to Os^{2+} and/or Ru^{2+} ions resulting in dendrimers that can carry as much as 22 metal ions [30] at the branch points. Dendrimers that are based on Ruthenium ion cores or, in particular, Iridium ion cores show remarkable charge transport and light emission capabilities. Their excellent luminescent properties have already found an application in the field of organic light emitting devices (OLEDS) [31].

Among many others, Balzani [33], Kaifer [32] and Gorman [21, 34] have synthesised dendrimers with one ferrocene at the core. They showed that electrochemical properties can be tuned through the dendrimer generation number and peripheral functionalisation. Normally, ferrocene exhibits very fast and reversible electrochemical kinetics in its one-electron oxidation process. However, burying it inside a dendritic shell results in slower diffusion dynamics (decreased diffusion constant) and therefore in lower currents. The slow dynamics limits the mass-transport towards the electrode. Also the electron transfer (ET) rate k^o is negatively affected by the size of the dendritic

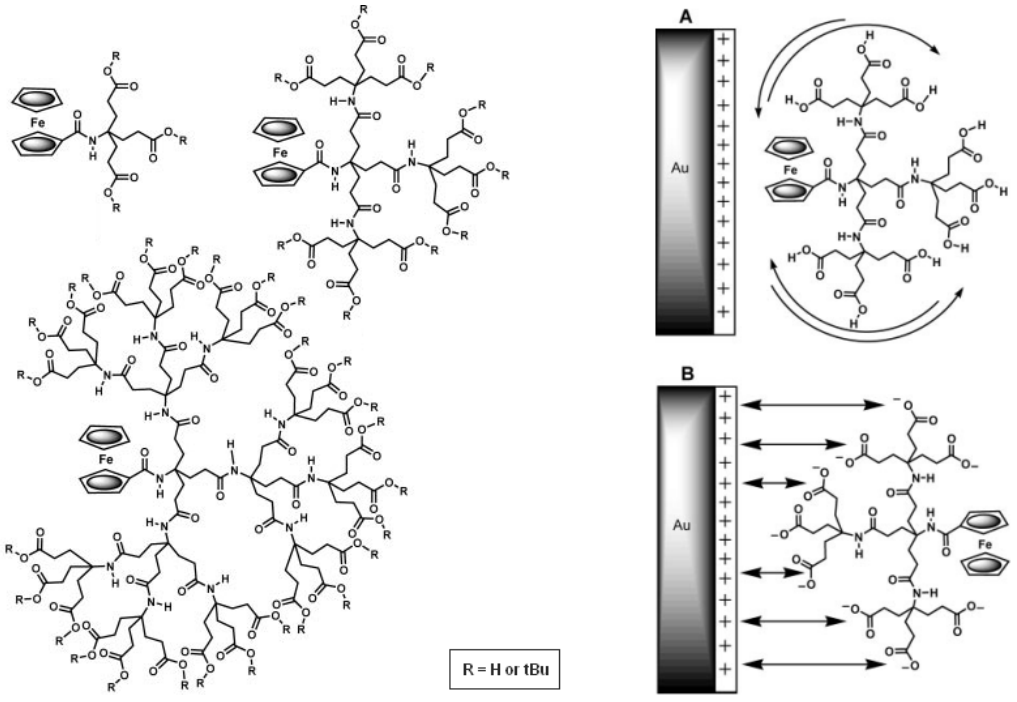

Fig. 4.2 – Left: Tuning the redox properties of ferrocene with a dendritic shell. Right: specific interactions with the electrode surface lead to different ET kinetics (from [32]).

shell, which can be explained by the increased average distance between ferrocene and surface. As the ET rate decays exponentially with the distance to the electrode [35], the ET rate will decrease with increasing dendrimer generation size. At lower generations, the dendrimers depicted in Fig. 4.2 exhibit a rather asymmetric shape that leads to heterogeneous behaviour close to the electrode. The distance of the ferrocene to the electrode thus depends on the conformation and orientation of the dendrimer. Peripheral functionalisation can further influence the orientation through electrostatic or specific host-guest interactions that might be mediated by the solution pH.

Encapsulation of the core, however, is not only dependant on dendrimer size, but also on wedge conformation and the efficiency with which the wedges cover the core [34, 36-37]. This structure-property relationship is not entirely investigated.

There are many dendrimers containing metallic centres within the cascade structure. Phosphorus dendrimers for example have been synthesised with many different arrangements of different metals [38-39]. The metals were either located at every branch point, at a branch point at a generation of choice or selectively in wedges of choice. All architectures have different properties and applications. Phosphorus containing dendrimers are usually synthesised using either a P=N-P=S branch point or a N-N(Me)-P=S branch point. Either has its own advantage. The former (Fig. 4.3A) has two phenyl groups on the first phosphorus that stabilizes a negative charge on the sulphur. This sulphur can therefore be used to complex gold to the backbone of the dendrimer. The latter P=S branch unit is chemically more stable than its oxygen analogue and does not react. The type of branch unit can be chosen for every generation independently, allowing for the selective complexation of gold at a certain location in the dendrimer. Also ferrocenes can be included into the dendrimer cascade structure. This principle has been shown by Majoral *et al* [14, 39-40] by making a ferrocene derivative into a basic building block of the dendrimer. Using their strategy it is also possible to exclusively introduce ferrocenes at the generation of preference. In Fig. 4.3B such a dendrimer is depicted bearing ferrocenes at each generation. It appeared that

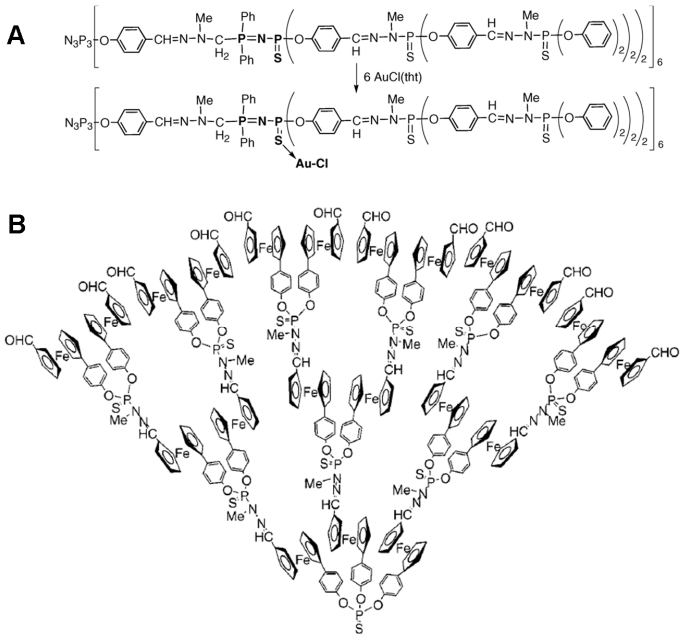

Fig. 4.3 – A: Metals coordinated to the branch point, B: Ferrocene as a part of the branches (from [38-39])

all ferrocenes have an identical oxidation potential. Some of these ferrocene derivatives could be obtained in enantiomerically pure form as well as others [41]. Because of their chirality, the dendrimers could find potential applications in optoelectronic devices.

4.1.3 Metals at the dendrimer periphery

As discussed in section 1.3.2, higher generation peripherally functionalised dendrimers have a higher density of functional groups than their linear or randomly (hyper-) branched analogues [42]. They expose all their functionality outwards, resulting in very strong and efficient interactions with their environment.

Dendrimers carrying ferrocene derivatives at their periphery constitute a very popular group of metal containing macromolecules [43-46]. The characteristic redox chemistry is maintained [39]. Upon oxidation of the numerous ferrocenes in and on those dendrimers into ferrocenium ions, a large amount of charge (electrons) is set free. Reduction restores the original ferrocene in an

entirely reversible manner. Exploitation of this remarkable property may result in a new generation rechargeable batteries [44, 47]. Although starting from generation 6, these dendrimers started having a number of defects that increases with generation number, generation 7 bore 14.000 ± 1000 ferrocenes at its periphery (instead of the theoretical maximum of 19.683 ferrocenes). It shows that extreme numbers of electrons can be stored and withdrawn from dendritic batteries without compromising the dendrimers' structural integrity. Nearly identical dendrimers were prepared containing metallocenes with cobalt, which also show reversible electrochemistry [48]. Similarly, dendronised linear polymers have been synthesised that are loaded with a large number of ferrocenes [49-52]. Ferrocene moieties can also interact with molecules like β-cyclodextrin and cucurbiturils [53] (Fig. 4.4), resulting in water-soluble macromolecular host-guest assemblies. The cyclodextrin is electrochemically released upon oxidation of the ferrocene. Dendrimers with many ferrocenes at their periphery were shown to recognise anions with a positive dendritic effect [54], i.e. the binding efficiency increases strongly with generation number. This is interesting for waste water treatment and can be applied for the recognition of biologically relevant anions (ATP^{2-}). The combination of electrostatic attraction between the ferrocenium and the anion and the hydrogen bonding with a near amido group does not suffice for a significant shift in redox potential of the ferrocene, but the dendrimer topology strongly enhances this interaction. The selectivity of the anion type can also be tuned. Whereas amidoferrocene dendrimers recognise oxoanions ($H_2PO_4^-$, HSO_4^-) [55], amino-attached pentamethylferrocene terminated dendrimers bind halides with a positive dendritic effect.

Furthermore, ferrocene terminated G4 PAMAM dendrimers have been used as an interface between a SAM functionalised electrode and a redox enzyme, Glucose oxidase [56]. The dendrimers allowed for a three times higher protein loading of the electrode surface as compared to the electrode that only bore the SAM (mercaptoundecanoic acid), probably by preventing the protein from unfolding upon its adsorption to the surface. The peripheral ferrocenes bridged the electron transport from the enzyme to the electrode, wiring the system into a fully active, stable and efficient biosensor.

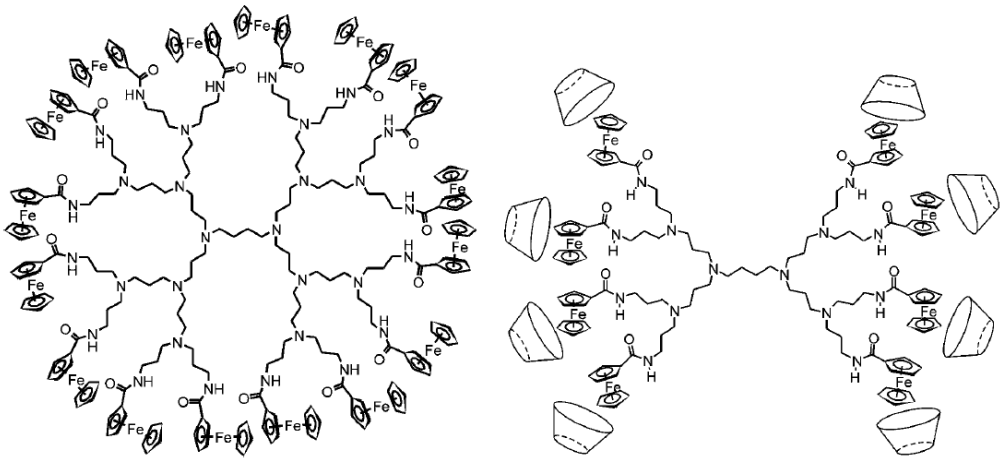

Fig. 4.4 – <u>Left:</u> Ferrocene dendrimers by Reinhoudt and co-workers [46]. Third generation polypropyleneimine (PPI) dendrimer coated with ferrocene end groups. <u>Right:</u> Second generation PPI dendrimer with ferrocene end groups complexed to β-cyclodextrin resulting in a water-soluble 8:1 supramolecular assembly (from [9])

Also other metals can be grafted on the dendrimer periphery. For catalysis [10] dendrimers combine their high loading of complexed catalyst (metal) with the fact that they are easily separated from the products. Examples of metals that have been grafted on dendrimers and their catalytic application include Nickel (addition reactions [57]), Ruthenium complexes (alkene metathesis [58]), Palladium complexes (Heck reactions [59]) and Co(salen) complexes (kinetic resolution of epoxides [60]).

For biomedical purposes, Gadolinium ion (Gd^{3+}) containing dendrimers have been tested for their ability to act as contrast agents in magnetic resonance imaging (MRI) [15, 61]. Currently, only low molecular weight Gd^{3+} complexes are allowed and higher molecular weight analogues based on (hyperbranched) polymers have not entered clinical trials for reasons including toxicity, incomplete renal excretion and size distribution. Dendrimers, however, are monodisperse and are therefore candidates to enter clinical trials. Due to their increased size they remain longer in the vascular system. They can carry multiple Gd^{3+} ions, which increases the contrast and reduces the required dosage. Additionally, dendrimers allow for specific interactions with other molecules by adding a functionalisation to the dendrimer periphery.

Finally, many different light harvesting dendrimers have been synthesised [25, 30, 62-64] where Aida and co-workers [62] used Zn-porphyrins that act as antennae with a high absorption cross-section similar to natural light harvesting complexes constructed from proteins. The porphyrins were located at the periphery or they were part of the dendrimer branches.

4.2 Research Objectives & Approach

Many different dendrimers containing ferrocene derivatives have been synthesised over the past decades. Their applications reached from chiral ferrocenes for dendrimer supported asymmetric catalysis and optics to electrochemistry exploiting the reversible redox transitions of ferrocene derivatives. However, most of the ferrocene containing dendrimers that have

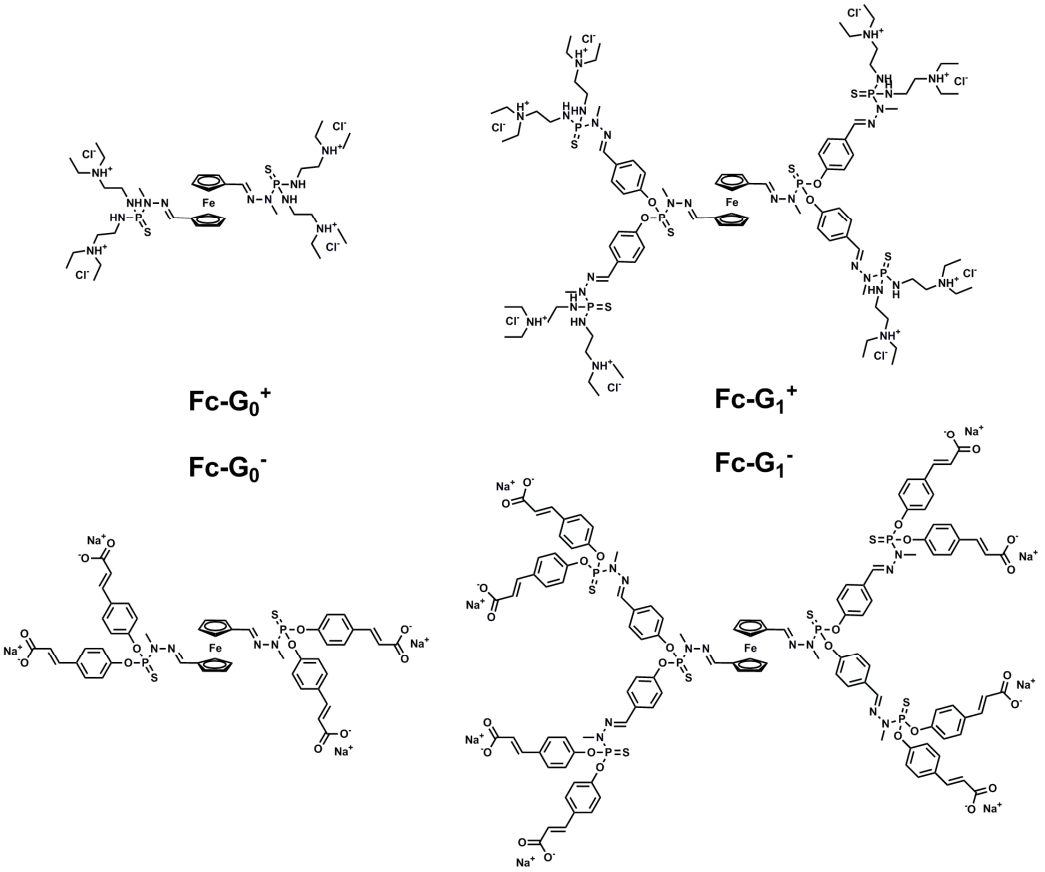

Fig. 4.5 – G_o and G_1 dendrimers with a ferrocene core carrying either 4 or 8 peripheral charges: diethylethylene diamine hydrochloride (polycationic, $G_{o,1}^{+}$) or sodium carboxylates (polyanionic, $G_{o,1}^{-}$).

been synthesised are soluble in organic solvents. This chapter focuses on the synthesis of two types of water-soluble dendrimers for applications in electrochemistry. Oppositely charged dendrimers can be assembled in a multilayer fashion with a layer-by-layer approach. The ferrocenes could then be used for electron relaying purposes between electrode and electrolyte. To that end, two different types of dendrimers were synthesised. The first family has one ferrocene as a core whereas the second family bears 24 ferrocenes in the branches. The target dendrimers are:

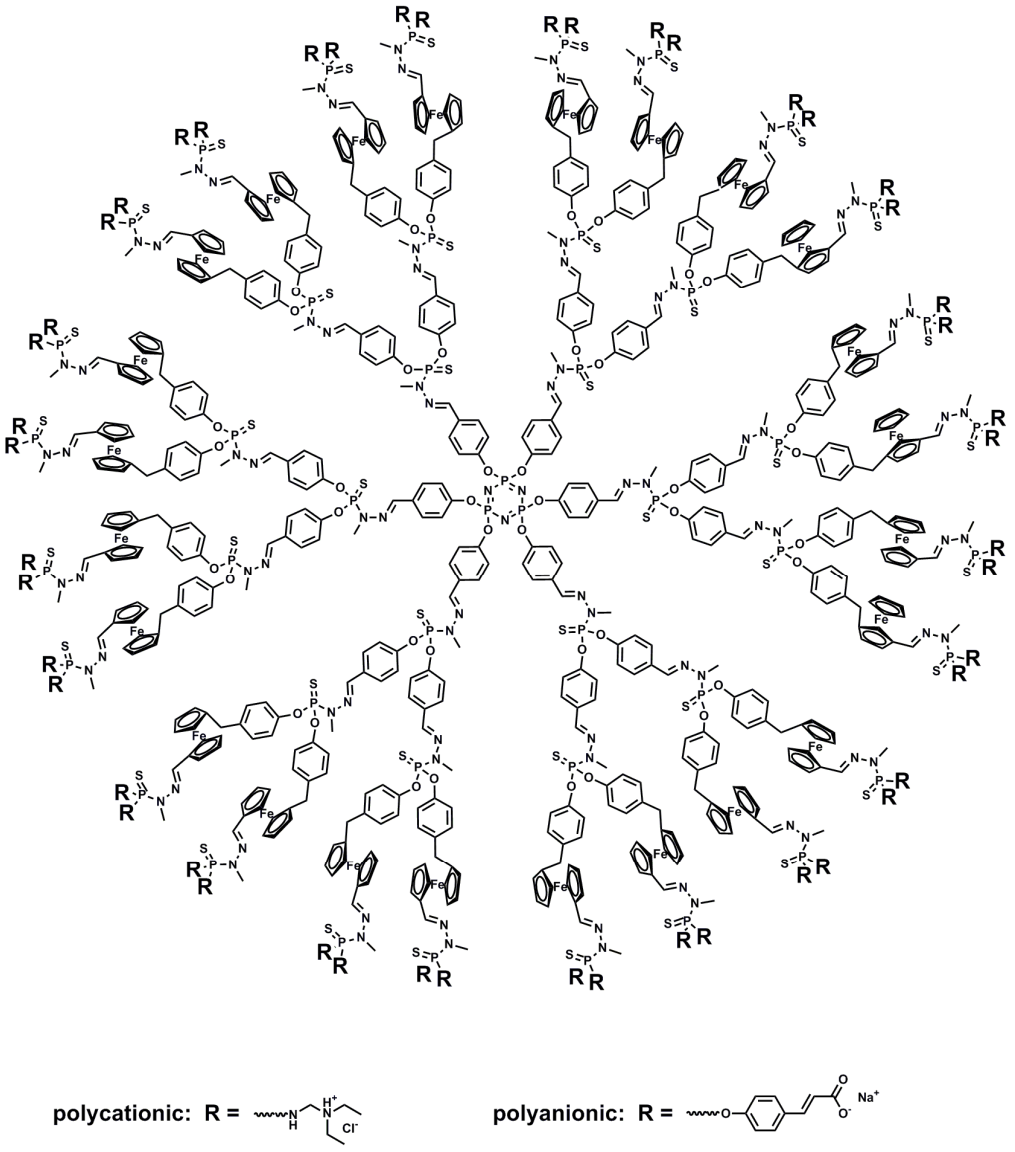

Fig. 4.6 – G3 dendrimer carrying 24 ferrocenes in the branches (at G2) and 48 peripheral charges: diethylethylene diamine hydrochloride (polycationic, G_3^+) or sodium carboxylates (polyanionic, G_3^-).

Family 1: ferrocene at the core

- ✓ Generations 0 and 1
- ✓ Polycationic (peripheral quaternary amines) and polyanionic (peripheral sodium carboxylates)

Family 2: ferrocenes in the branches

- ✓ Generation 3
- ✓ Polycationic (peripheral tertiary amines, HCl form) and polyanionic (peripheral sodium carboxylates)

The synthetic route towards these dendrimers largely followed the general Majoral's approach [65-66]. The target dendrimers are depicted in Fig. 4.5 and Fig. 4.6.

4.3 Results and Discussion

In this section the synthesis of six different ferrocene containing dendrimers and their individual building blocks is described.

4.3.1 Synthesis of Ferrocene building block

The objective is synthesising phosphorus dendrimers that contain ferrocenes in the branches. Therefore a ferrocene derivative is required that imitates the commonly used p-hydroxybenzaldehyde in order to be incorporated exactly the same way via a nucleophilic substitution reaction between a phenol and a P-Cl bond and a condensation reaction between an amine and an aldehyde. At the same time, the ferrocene derivative must be sufficiently large and flexible in order to not impose sterical and flexibility limitations when advancing with the dendrimer synthesis into higher generations. The target ferrocene building

block **18** that should meet all requirements and the synthetic route towards it are presented in Fig. 4.7.

This synthetic route is derived from the PhD thesis of Jérôme Chiffre [67]. In a five step synthesis, the commercially available ferrocene carboxaldehyde can be transformed into the target ferrocene derivative. The overall yield after five steps of 2.5%, however, was much lower than reported by Chiffre (15%). The synthesis of **14** requires a large excess of tributyltin chloride (4-fold), implying that during a large scale process (90 g $SnBu_3Cl$), which is necessary considering the number of ferrocenes that will be required for incorporation into dendrimers, a large amount of $SnBu_3Cl$ has to be eliminated from the mixture. This requires several cycles of column chromatography, resulting in a relatively high loss of product and high rate of destannylation. Also the instability of **17** and the destannylation during the other steps contributes to a reduced overall yield.

The first reaction stannylates the commercially available ferrocene carboxaldehyde [68], following the depicted scheme (Fig. 4.8). First, lithiation of the secondary amine of N-methylpiperazine with *tert*-butyl lithium (*t*BuLi)

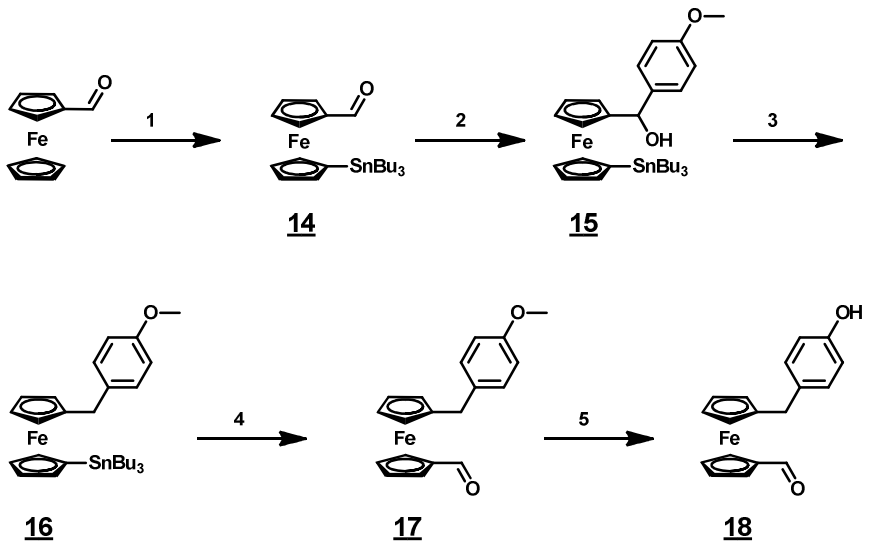

Fig. 4.7 – The synthesis of the target ferrocene (18) derivative that mimics p-hydroxybenzaldehyde. (1) a/ *t*BuLi / N-methylpiperazine b/ $SnBu_3Cl$ in THF at -80°C to *RT*, (2) bromoanisole / *n*BuLi in THF at -64°C to *RT*, (3) $BH_3.SMe_2$ in THF 30 min reflux, (4) a/ *n*BuLi b/ DMF in THF at -80°C to *RT*, (5) BBr_3 in THF at -80°C to *RT*.

turns it into a nucleophile that attacks the carbonyl of the ferrocene carboxaldehyde. In the resulting intermediate the oxygen forms an ion pair with the lithium. This intermediate can form a Lewis acid-base complex with another *t*BuLi whose lithium is coordinated mainly towards the other cyclopentadienyl (Cp) ring. As *t*BuLi is a base, it deprotonates and lithiates the ring at the 1' position. When an electrophile, like tributyltinchloride, is now added it substitutes both lithiums, of which the one bound to the oxygen can be removed by hydrolysis. This procedure yields the product, with a selectivity of 95% to the 1' position (5% on the 2-position).

In the second reaction (Fig. 4.7), lithiated bromoanisole makes a nucleophilic attack on the carbonyl readily yielding the alcohol **15**. Reproducing [67] the reduction of this alcohol **15** during step 3 using a mixture of $TiCl_4$ and $NaBH_3CN$ as reported imposed major complications with destannylation. Reduction with the rather reactive borane (as a dimethylsulfide complex) directly, however, appeared to be a straightforward way to obtain the product without the destannylation side effects [69].

In step four, the tributylstannyl group is removed by *n*BuLi after which the corresponding Cp carbon makes a nucleophilic attack on the carbonyl of dimethylformamide (DMF). The Li^+-alkoxyamide intermediate is then hydrolysed resulting in the formylated ferrocene derivative **17** obtained as an oil. The last step, to be carried out directly afterwards as **17** is not sufficiently stable for long term storage, comprises the deprotection of the methoxy group with boron tribromide. The last two steps could not be swapped as BBr_3 also destannylates the product.

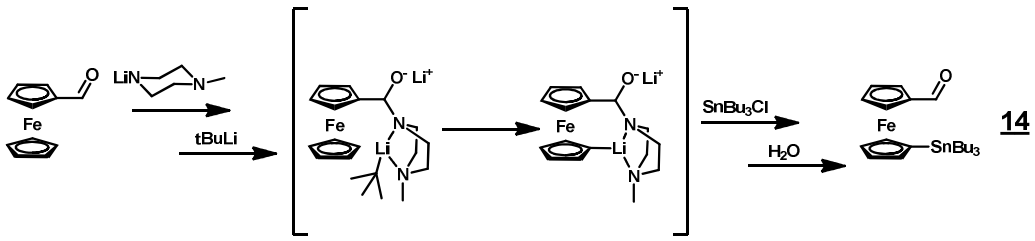

Fig. 4.8 – Selective stannylation of the ferrocenyl 1' position

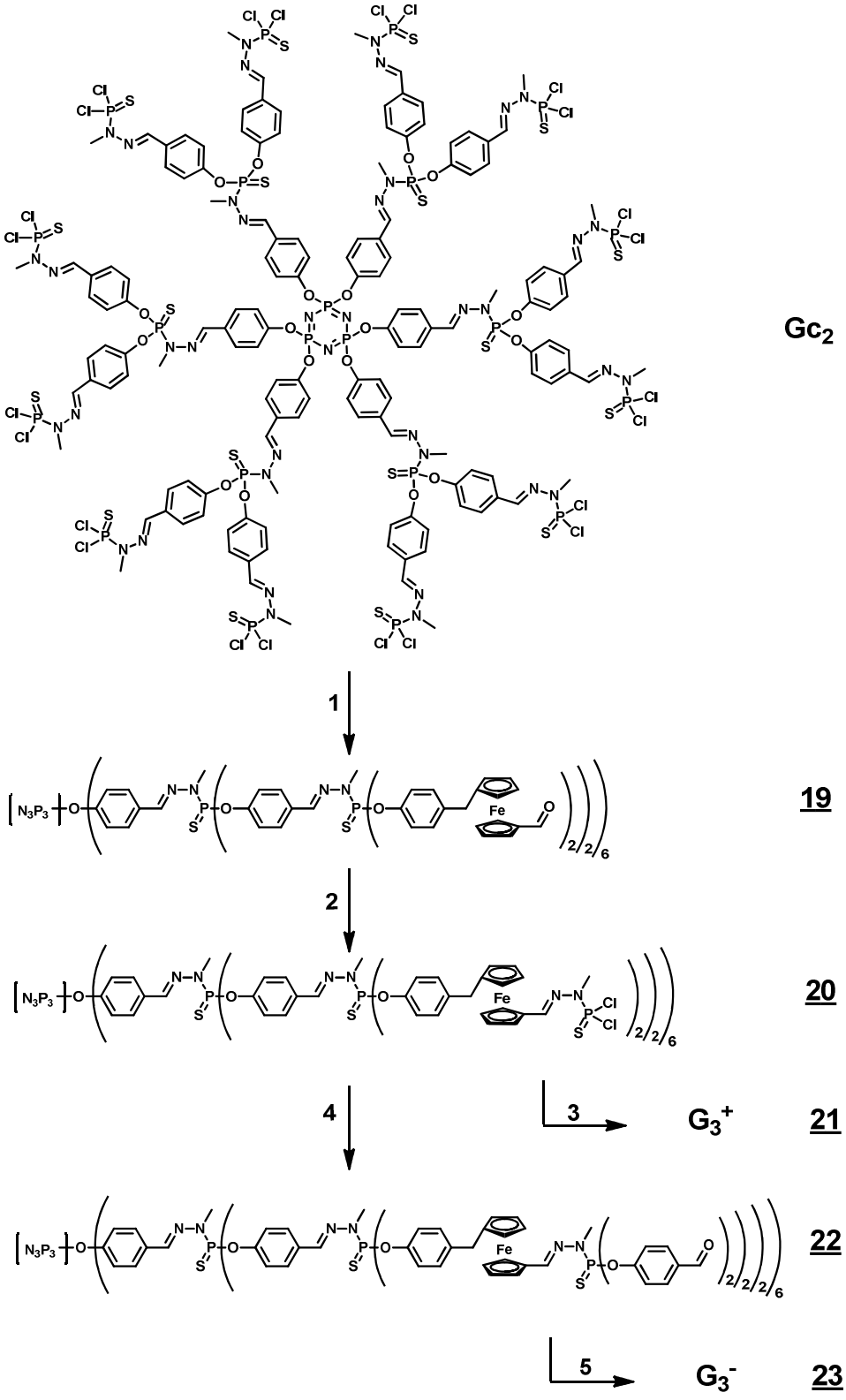

Fig. 4.9 – Reaction scheme towards G_3 water-soluble dendrimers with 24 ferrocene derivatives in the branches at G_2. (1) a/ NaH and 18 in THF at 0°C, b/ Gc_2 in THF at 0°C, (2) 2 in $CHCl_3$ at *RT*, (3) DEEDA in THF at 0°C, (4) pHBA/ Cs_2CO_3 at *RT*, (5) malonic acid/piperidine in pyridine at 95°C.

4.3.2 Synthesis of dendrimers having Ferrocenes in the branches

Despite the low yields, having product **18** in hand enabled their grafting on the Gc_2 dendrimer, which is defined in Fig. 4.9. The phenol of **18** was deprotonated with sodium hydride, turning it into a stronger base that substitutes the dendrimers' peripheral chlorines more easily and this approach does not require an excess of base (usually Cs_2CO_3). The small excess of the ferrocene derivative could be recycled and the reaction was performed with an overall yield of 74% of highly stable product **19**.

From this point on, the dendrimers were grown and functionalised with water solubilising moieties as described in section 3.3.3 with high to quantitative yields. Product **19** is then grown to the G_3 dendrimer that carries 48 chlorines. Substitution with diethylethylene diamine (DEEDA) in THF makes the dendrimers precipitate from the mixture in the course of the reaction, resulting in dendrimers that are soluble in water only. In order to synthesise the polyanionic analogues, **19** was quantitatively grown to G_3' and subsequently functionalised via a Doebner-like condensation [70-73].

4.3.3 Dendrimers with a Ferrocene core

Based on the work by C.-O. Turrin [13-14, 39-40, 74-75], new water-soluble dendrimers with a ferrocene core were synthesised. Whereas Turrin applied the dendrimers as solutions in organic solvents, this chapter focuses on rendering similar dendrimers water-soluble. The ferrocene dicarboxaldehyde core was synthesised as described by Balavoine [76] from the commercially available ferrocene.

The methylhydrazine was reacted with the core in slight excess to generate G_0 dendrimers bearing four chlorines to be substituted. In a reaction with the diethyl amine DEEDA, polycationic dendrimers were obtained. For G_0 polyanionic dendrimers, **19** was grown to G_0' and subsequently modified to

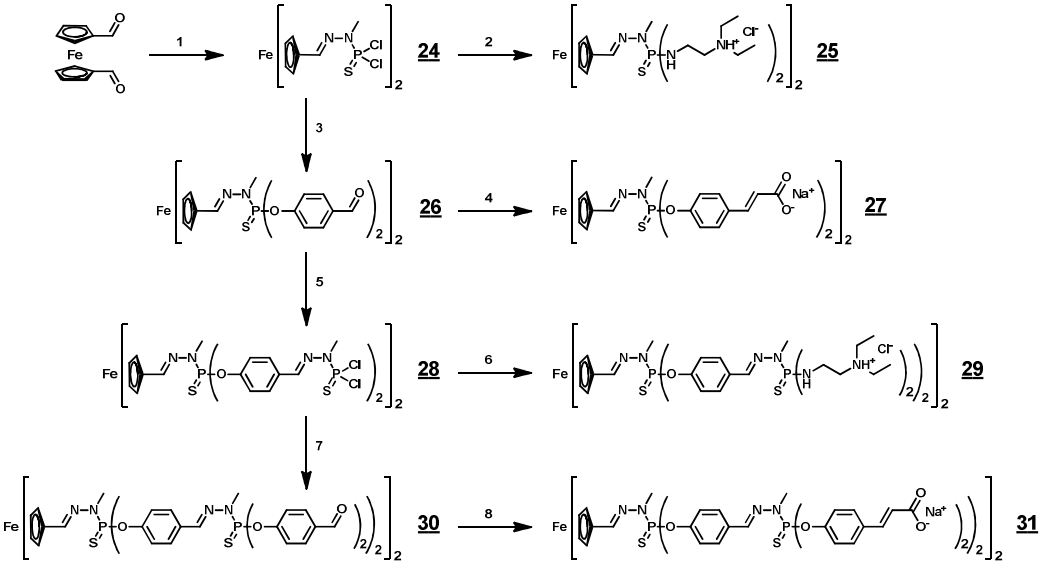

Fig. 4.10 – Reaction scheme towards water-soluble G_0 and G_1 dendrimers with a ferrocene at the core. (1,5) 2 in $CHCl_3$ at *RT*, (2,6) DEEDA in THF at *RT*, (3,7) 1 inTHF at *RT*, (4,8) malonic acid/piperidine in pyridine at 95°C.

cinnamic acid terminated dendrimers via a Doebner-like reaction yielding dendrimers with 4 anionic charges after ion exchange with NaOH. For the G_1 analogues the same chemistry was applied, resulting in polycationic and polyanionic dendrimers with eight terminal ion pairs.

4.3.4 Preliminary characterisation

In order to electrochemically characterise the synthesised dendrimers, the redox behaviour was measured with Cyclic Voltammetry (CV). As described in more detail in section 2.3, with CV an alternating voltage is applied in potential region in which the molecule undergoes its reduction and oxidation reactions. The current response shows peaks around the redox potential. Below, the preliminary results are shown for Fc-G_0^+ and Fc-G_0^-. The scales of the graphs are different as working electrodes with very different surface areas were used.

In Fig. 4.11, the preliminary results are shown for the G_0 dendrimers with a ferrocene at the core. In these voltammograms the redox current is plotted against the voltage at different scan rates. Both dendrimers show a quasi-

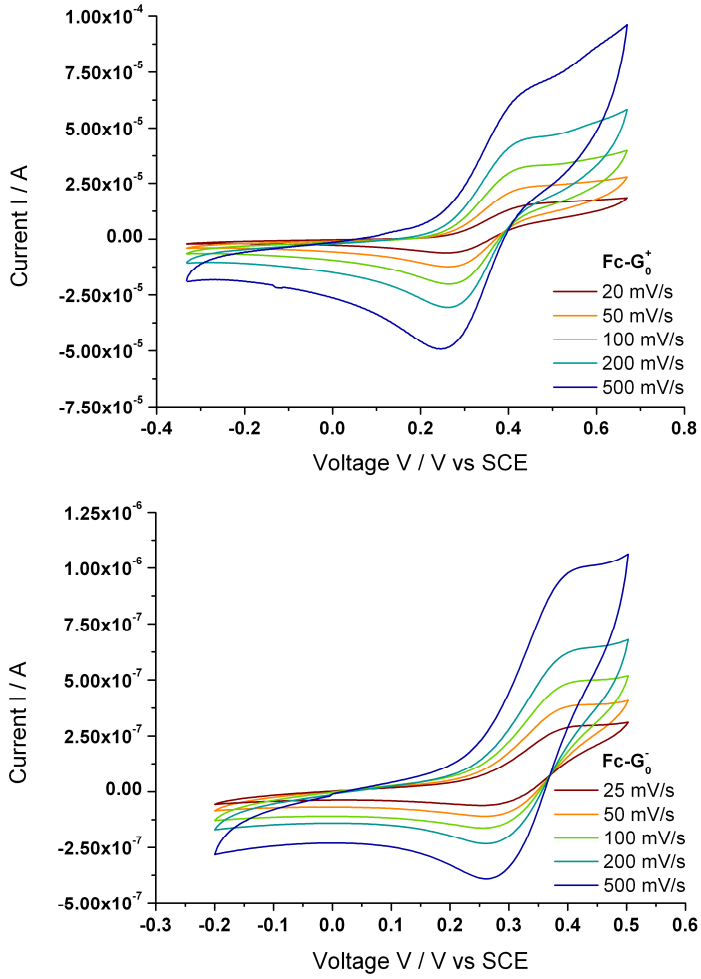

Fig. 4.11 – Cyclic voltammograms of Fc-G_0^+ (top) and G_0^- (bottom) dendrimers that bear a ferrocene at the core.

reversible reduction and oxidation behaviour as the ratio between reduction peak current and oxidation peak current almost equals unity. The dendrimers have very similar standard redox potentials (0.36 V for G_1^+ and 0.34 V for G_1^-). The polycationic dendrimers have a slightly larger peak separation (0.19 V compared to 0.16 V for Fc-G_0^-), which could be explained by a slightly reduced solubility or by the possibility that the electron transfer rate can no longer be completely neglected compared to the mass transport rate. In order to determine whether the mass transport is diffusion controlled or surface bound, the oxidation peak current must be plotted as a function of (the square root of) the scan rate (Fig. 4.12). Both dendrimers showed a linear relationship between peak current and the square root of the scan rate, which indicates a

diffusion controlled process. This linear relation is called the Randles-Sevcik relation and the diffusion constant can be calculated from its slope:

$$i_p = (2.69 \cdot 10^5) n^{\frac{3}{2}} A c D^{\frac{1}{2}} \upsilon^{\frac{1}{2}} \qquad \textbf{Eqn. 4.1}$$

with i_p the peak current (A), n being the number of transferred electrons (1), A the working electrode surface area (cm^2), D the diffusion constant ($cm^2.s^{-1}$), c the dendrimer concentration ($mol.cm^{-3}$) and n the scan rate ($V.s^{-1}$). Assuming the dendrimers adopt a spherical shape, the Stokes-Einstein relation provides the dendrimer radius:

$$D = \frac{k_B T}{6\pi\eta r} \qquad \textbf{Eqn. 4.2}$$

with k_B being the Boltzmann constant, T the temperature, η the solution viscosity and r the dendrimer radius. The diffusion constants and radii of both dendrimers are provided below.

dendrimer	***D* (cm^2s^{-1})**	***r* (nm)**
Fc-G_0^+	$2.5\ 10^{-8}$	96
Fc-G_0^-	$5.6\ 10^{-7}$	4

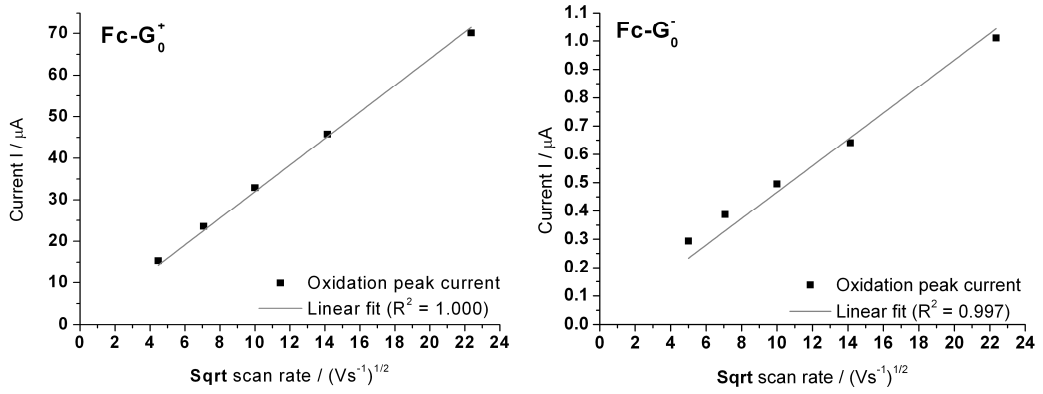

Fig. 4.12 – Oxidation peak currents of Fc-G_0^+ (left) and Fc-G_0^- (right) plotted against the square root of the scan rate. The linear fit, with a zero intercept, is the Randles-Sevcik relation.

Both dendrimers, but in particular the polycationic one, appear much larger than the expected value (approximately 1 nm). Despite the fact that aggregates are not necessarily spherical and therefore not best described by the Stokes-Einstein equation, these results clearly indicate that the dendrimers are only poorly soluble in water and are present as larger aggregates. This is in agreement with the larger peak separation for the polycationic dendrimers, which were found to be larger.

4.4 Synopsis and Conclusion

Six different ferrocene containing phosphorus dendrimers were synthesised. All dendrimers were water-soluble. One class contained 24 ferrocene derivatives in the branches at G2 and the dendrimers were prepared in polycationic and polyanionic form. The second class of dendrimers contained a ferrocene at the core and the wedges were attached on both Cp rings. Generations G_0 and G_1 were prepared in both polycationic and polyanionic form. The G_0 species were electrochemically characterised with cyclic voltammetry and they show reversible redox behaviour. Their measured radius in water, however, appeared 4 and 96 nm (Fc-G_0^- and Fc-G_0^+), which suggests that the dendrimers form aggregates due to their hydrophobic interior.

4.5 Materials and Methods

In this section all technical and experimental details are described. All water used is demineralised using MilliQ equipment and the resistivity was 18 MΩ.cm. All reactions are carried out under argon atmosphere and in freshly distilled solvents. All column chromatography was carried out with silica gel 60 as the static phase. All starting compounds were purchased from Aldrich, Merck or Fluka and used as received.

4.5.1 Synthesis of Ferrocene building block

14. 1'-tributylstannylferrocenecarboxaldehyde

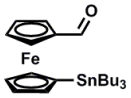

$C_{23}H_{36}FeOSn$
MW=503.1

In a Schlenk tube, *n*BuLi (45 mL, 1.7 M in pentane, 76.5 mmol, 1.1 eq) was added dropwise to a 150 mL THF solution of methylpiperazine (9.72 mL, 87.63 mmol, 1.25 eq, freshly distilled over Na_2CO_3) and was stirred for 15 minutes. Ferrocene carboxaldehyde (15.0 g, 70.1 mmol, 1.0 eq) in 20 mL THF was added dropwise to the lithiated piperazine. Another 51.5 mL of *n*BuLi solution (1.7 M in pentane, 87.63 mmol, 1.25 eq) were added dropwise at -20°C. This mixture was stirred for 1 hr at room temperature. The mixture was finally cooled down to -78°C and 76 mL of tributyltin chloride (280.4 mmol, 4.0 eq) were added dropwise. The reaction mixture was kept at this temperature for 30 minutes before it was stirred overnight at room temperature. THF was evaporated and the compound was dissolved in dichloromethane. This was washed with distilled water until the organic phase was clear. The DCM phase was dried over Na_2SO_4. The product was purified (several times) by column chromatography (5% ethyl acetate in hexane, increasing amounts of ethyl acetate). The yield was extremely low: 5.02 g (9.98 mmol, 14%) of a red oil.

^{1}H-NMR (250 MHz, $CDCl_3$): **0.94-1.57** (m, 27H, $SnBu_3$), **4.11** (s, 2H, Cp), **4.48** (s, 2H, Cp), **4.53** (s, 2H, Cp), **4.74** (s, 2H, Cp), **9.96** (s, 1H, CHO)
^{13}C{^{1}H}-NMR: See [67].

15. (4-methoxyphenyl)-(1'-tributylstannylferrocenyl)-methanol

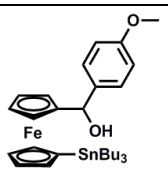

$C_{30}H_{44}FeO_2Sn$
MW=612.2

In a Schlenk tube, a solution of 5.0 g bromoanisole (34.9 mmol, 3.5 eq) in 10 mL THF was cooled down to -64°C. To this 13.56 mL of *n*-butyllithium (2.5 M in hexane, 33.9 mmol, 3.4 eq) were added and the mixture was stirred for 1 hour at this temperature. At -64°C a 80 mL THF solution containing 5.02 g of compound **14** (9.98 mmol, 1.0 eq) was added. This mixture was stirred for 15 minutes at -64°C and was allowed to stir for two hours at room temperature. The THF was evaporated and the product was dissolved in DCM and washed several times with distilled water till both phases were clear. The organic phase was dried over $MgSO_4$ and filtered with a Büchner funnel. The crude material was purified by column chromatography (several percent of ethyl acetate in hexane, increasing to 10%, with a few drops of triethylamine) yielding 2.65 g of a red oil (4.34 mmol, 43%).

^{1}H-NMR (250 MHz, $CDCl_3$): **0.94-1.59** (m, 27H, $SnBu_3$), **2.55** (OH), **3.78** (s, 3H, OMe), **4.04** (s, 2H, Cp), **4.40** (s, 2H, Cp), **4.50** (s, 2H, Cp), **4.88** (s, 2H, Cp), **5.66** (s, 1H, CH-O), **6.99** (d, 2H, arom. CH, $^3J_{HH}$ = 8.8 Hz), **7.95** (d, 2H, arom. CH, $^3J_{HH}$ = 8.8 Hz).
^{13}C{^{1}H}-NMR: See [67].

16. (4-methoxyphenyl)-(1'-tributylstannylferrocenyl)-methane

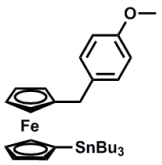

$C_{30}H_{44}FeOSn$
MW=595.2

In a Schlenk tube, a 25 mL THF solution of compound **15** (3.91 mmol, 1.0 eq) was preheated to 90°C to reflux conditions before 3.91 mL of a borane dimethylsulphide complex (1.0 M in DCM, 3.91 mmol, 1.0 eq) were added. The mixture was refluxed for 30 minutes and directly quenched with water. The product was extracted with pentane and the organic phase was dried over $MgSO_4$. The product was further purified on column using pentane as eluent. This procedure yielded 1.68 g of product (2.83 mmol, 73%) as a red oil.

^{1}H-NMR (250 MHz, $CDCl_3$): **0.94-1.59** (m, 27H, $SnBu_3$), **3.71** (s, 2H, CH_2), **3.83** (s, 3H, OMe), **4.05** (m, 2H, Cp), **4.08** (m, 2H, Cp), **4.10** (m, 2H, Cp), **4.36** (m, 2H, Cp), **6.87** (d, 2H, arom. CH, $^{3}J_{HH}$ = 8.7 Hz), **7.16** (d, 2H, arom. CH, $^{3}J_{HH}$ = 8.4 Hz)
^{13}C{^{1}H}-NMR: See [67].

17. 1'-[(4-methoxyphenyl)methyl]ferrocenecarboxaldehyde

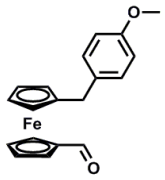

$C_{19}H_{18}FeO_2$
MW=334.2

In a Schlenk tube, a 20 mL THF solution of 0.84 g of compound **16** (1.41 mmol, 1.0 eq) was cooled to -78°C before 791 µL a *n*-butyllithium (2.5 M in hexane, 1.98 mmol, 1.4 eq) was added. This mixture was stirred for 15 minutes at this temperature, and subsequently for 1 hour at room temperature. Then it was cooled again to -78°C and 593 µL of freshly distilled (on CaH_2) DMF (7.045 mmol, 5.5 eq) was added. This mixture was stirred at this temperature for 15 minutes and then stirred at room temperature overnight. The reaction was quenched by the addition of water followed by extraction with ether, washing with brine and drying on Na_2SO_4. After column purification (up to 30% ether in hexane) the product was yielded as 0.363 g (1.09 mmol, 77%) of a red oil.

^{1}H-NMR (250 MHz, $CDCl_3$): **3.57** (s, 2H, CH_2), **3.80** (s, 3H, OMe), **4.22** (s, 4H, Cp), **4.59** (2H, Cp), **4.77** (2H, Cp), **6.84** (d, 2H, arom. CH, $^{3}J_{HH}$ = 8.6 Hz), **7.09** (d, 2H, arom. CH, $^{3}J_{HH}$ = 8.6 Hz), **9.95** (s, 1H, CHO)
^{13}C{^{1}H}-NMR: See [67]

18. 1'-[(4-hydroxyphenyl)methyl]ferrocenecarboxaldehyde

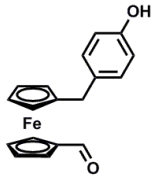

$C_{18}H_{16}FeO_2$
MW=320.2

In a Schlenk tube, a 6 mL DCM solution of 207 mg of compound **17** (622 µmol, 1.0 eq) was cooled to -78°C and 2.2 mL of boron tribromide (1.0 M in DCM, 2.2 mmol, 3.5 eq) were added. The reaction was stirred at room temperature and in the dark for 45 minutes. The reaction mixture was added to vigorously stirred ice water and stirred for 15 minutes. The product was extracted with DCM, washed three times with an aqueous 1.0 M $Na_2S_2O_3$ solution, three times with brine and finally dried over Na_2SO_4. After column chromatography (30% ether in pentane) the product was yielded as a red solid (143 mg, 447 µmol, 72%).

^{1}H-NMR (250 MHz, $CDCl_3$): **3.54** (s, 2H, CH_2), **4.22** (s, 4H, Cp), **4.60** (s, 2H, Cp), **4.78** (s, 2H, Cp), **5.36** (s, 1H, OH), **6.78** (d, 2H, arom. CH, J=8.2 Hz), **7.02** (d, 2H, arom. CH, 8.2 Hz), **9.94** (s, 1H, CHO)
^{13}C{^{1}H}-NMR: See [67]

4.5.2 Synthesis of G_3 dendrimers with 24 ferrocenes

The second generation Gc_2 dendrimer was synthesised as described in literature [65]. These dendrimers are used as a template for ferrocene containing dendrimers as described below.

19. G_2'-Fc_{24}

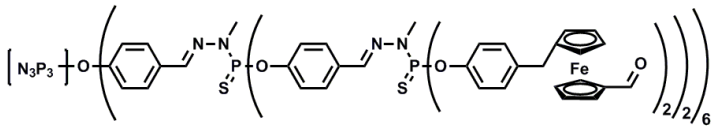

$C_{576}H_{504}N_{39}O_{66}$
$P_{21}S_{18}Fe_{24}$
MW=11590.2

To a suspension of 5.1 mg NaH (215 µmol, 27 eq) in 5 mL THF, a solution of 71.5 mg of product **18** (223 µmol, 28 eq) in 5 mL THF was added at 0°C. This was stirred for one hour at room temperature. Subsequently it was cooled again to 0°C and a 5 ml THF solution of Gc_2 (7.69 µmol, 1.0 eq) was added. The reaction was stirred overnight at room temperature. The solution volume was reduced and the dendrimer was precipitated from ether pentane (1:3). This yielded 66 mg (5.69 µmol, 74%) of an orange powder.

^{1}H-NMR (300 MHz, $CDCl_3$): **3.22** (d, 54H, $P_{1,2}$-N-CH_3, Cp), **3.49** (s, 48H, CH_2Fc), **4.13** (s, 96H, Cp), **4.49** (s, 48H, Cp), **4.68** (s, 48H, Cp), **6.92-7.61** (m, 186H, Ph + $CH{=}N_{1+2}$-N), **9.86** (s, 24H, CHO)
$^{31}P\{^1H\}$-NMR (121.5 MHz, $CDCl_3$): **8.4** (s, P_0), **62.6** (s, P_1), **62.9** (s, P_2)
$^{13}C\{^1H\}$-NMR (75.5 MHz, $CDCl_3$): **33.1** (d, CH_3-N-$P_{1,2}$, $^2J_{CP}$ = 12.3 Hz), **34.6** (CH_2), **69.4** (Cp), **70.2** (Cp CH), **70.3** (Cp), **74.0** (Cp), **79.6** (Cp^{quat}), **89.5** (Cp^{quat}), **121.2** (d, $C_2{}^2$, $^3J_{CP\text{-}2}$ = 4.5 Hz), **121.8** ($C_{0,1}{}^2$), **128.3** ($C_{0,1}{}^3$), **129.3** ($C_2{}^3$), **132.2** ($C_0{}^4$), **132.4** ($C_1{}^4$), **138.1** ($C_2{}^4$), **138.6** (m, CH=N-N-$P_{1,2}$), **148.9** (d, $C_2{}^1$, $^2J_{CP\text{-}2}$ = 7.1 Hz), **151.2** ($C_{0,1}{}^1$), **193.4** (CHO)

20. G_3-Fc_{24}

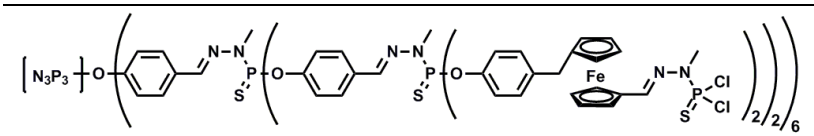

$C_{600}H_{576}N_{87}O_{42}$
$P_{45}S_{42}Cl_{48}Fe_{24}$
MW=15453.7

To a solution of 100 mg (8.6 µmol, 1.0 eq) in 8 mL of chloroform were added 0.9 mL 0.24 M MHTPC (265 µmol, 25 eq). After 45 minutes the product was precipitated from pentane twice. This yielded 128 mg (8.3 µmol, 96%) of an orange solid.

^{1}H-NMR (300 MHz, $CDCl_3$): **3.23** (s, 48H, CH_2Fc), **3.35** (d, 72H, =N-N_3-CH_3, $^3J_{HP}$ = 15 Hz), **3.51** (m, 54H, =N-$N_{1,2}$-CH_3), **4.05** (2s, 96H, Cp), **4.31** (s, 48H, Cp), **4.59** (s, 48H, Cp), **6.95-7.62** (m, 212H, arom. + $CH{=}N_{1+2}$-N),
$^{31}P\{^1H\}$-NMR (121.5 MHz, $CDCl_3$): **8.6** (s, P_0), **62.3** (s, $P_{1,2}$), **63.0** (s, P_3)

$^{13}C\{^1H\}$-NMR (75.5 MHz, $CDCl_3$): **32.1** (d, CH_3-N-P_3, $^2J_{CP}$ = 12.5 Hz), **33.1** (d, CH_3-N-$P_{0,1}$, $^2J_{CP}$ = 12.6 Hz), **34.9** (CH_2), **68.7** (Cp), **69.0** (Cp), **70.1** (Cp), **71.0** (Cp), **79.0** (Cp^{quat}), **88.6** (Cp^{quat}), **121.2** (d, C_2^2, $^3J_{CP-2}$ = 4.5 Hz), **121.8** ($C_{o,1}^2$), **128.3** ($C_{o,1}^3$), **129.3** (C_2^3), **132.2** (C_o^4), **132.4** (C_1^4), **138.5** (C_2^4), **143.6** (d, CH=N-N-$P_{1,2,3}$, $^3J_{CP-1,2,3}$ = 18.9 Hz), **148.8** (d, C_2^1, $^2J_{CP-2}$ = 6.8 Hz), **151.2** (d, $C_{o,1}^1$, $^2J_{CP-o,1}$ = 6.0 Hz)

21. G_3^+ -Fc_{24}

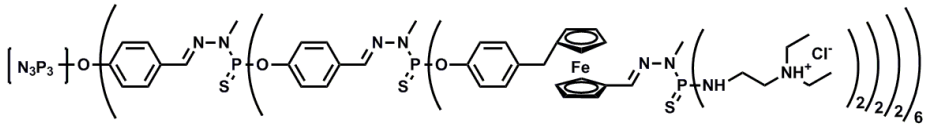

$C_{888}H_{1344}N_{183}O_{42}P_{45}S_{42}Cl_{48}Fe_{24}$, MW=21028.5

To a 5 mL THF solution of 47 mg of compound **20** (3.69 µmol, 1.0 eq) were added 24.6 µL of N,N-diethylethylenediamine (173 µmol, 47 eq) at 0°C. It was washed twice with dry THF (partly soluble!). This yielded 37 mg, (1.76 µmol, 48%) of an orange solid.

^1H-NMR (300 MHz, MeOD): **1.23** (m, 24H, N-CH_2-*CH3*), **3.21** (m, 32H, CH_2), **3.23** (2s, 48H, CH_2Fc), **3.35** (d, 72H, =N-N_3-CH_3, $^3J_{HP}$ = 15 Hz), **3.51** (m, 54H, =N-$N_{1,2}$-CH_3), **4.02** (2s, 96H, Cp), **4.21** (s, 48H, Cp), **4.58** (s, 48H, Cp), **6.98-7.63** (m, 212H, arom. + CH=N_{1+2}-N),

$^{31}P\{^1H\}$-NMR (121.5 MHz, MeOD): **8.6** (s, P_o), **61.3** (s, P_1), **62.7** (s, P_2), **69.5** (s, P_3)

$^{13}C\{^1H\}$-NMR (75.5 MHz, MeOD): **9.0** (*CH_3*CH_2-N), **32.1** (d, CH_3-N-P_3, $^2J_{CP}$ = 12.5 Hz), **33.1** (d, CH_3-N-$P_{1,2}$, $^2J_{CP}$ = 12.6 Hz), **34.9** (CH_2), **36.3** (*CH_2*-N-P_3), **49.6** (CH_3*CH_2*-N), **52.2** (d, *CH_2*CH_2-N-P_3, $^3J_{CP}$ = 6.9 Hz), **68.7** (Cp), **69.0** (Cp CH), **70.1** (Cp), **71.0** (Cp), **79.0** (Cp^{quat}), **121.2** (d, C_2^2, $^3J_{CP-2}$ = 4.5 Hz), **121.8** ($C_{o,1}^2$), **128.3** ($C_{o,1}^3$), **129.3** (C_2^3), **132.2** (C_o^4), **132.4** (C_1^4), **138.5** (C_2^4), **143.6** (d, CH=N-N-$P_{1,2,3}$, $^3J_{CP-1,2,3}$ = 18.9 Hz), **148.8** (d, C_2^1, $^2J_{CP-2}$ = 6.8 Hz), **151.2** (d, $C_{o,1}^1$, $^2J_{CP-o,1}$ = 6.0 Hz)

22. G_3' -Fc_{24}

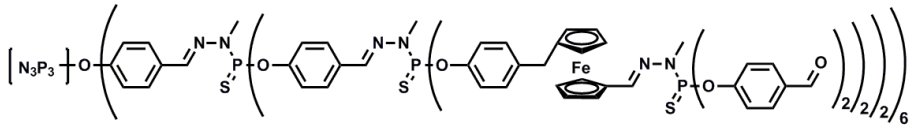

$C_{936}H_{816}N_{87}O_{138}P_{45}S_{42}Fe_{24}$, MW=19561.7

A solution of 71 mg of compound **20** (4.59 µmol, 1.0 eq), 27.8 mg p-hydroxybenzaldehyde (228 µmol, 50 eq) and 149 mg Cs_2CO_3 (457 µmol, 100 eq) in 5 mL THF was stirred overnight at room temperature. The product was precipitated from pentane yielding 91 mg (4.65 µmol, 100%) of an orange powder.

^{1}H-NMR (300 MHz, $CDCl_3$): **3.24-3.32** (2s+d, 48H, CH_2Fc and =N-N_3-CH_3, $^3J_{HP}$ = 15 Hz), **3.41** (m, 54H, =N-$N_{1,2}$-CH_3), **3.95** (s, 96H, Cp), **4.26** (s, 48H, Cp), **4.52** (s, 48H, Cp), **6.95-7.82** (m, 402H, arom. + CH=N_{1+2}-N), **9.86** (s, 48H, CHO)

^{31}P{^{1}H}-NMR (121.5 MHz, $CDCl_3$): **8.36** (s, P_0), **59.9** (s, P_3), **62.5** (s, P_1), **63.0** (s, P_2),

^{13}C{^{1}H}-NMR (75.4 MHz, $CDCl_3$): **32.9** (d, CH_3-N-$P_{1,2,3}$, $^2J_{CP}$ = 13.5 Hz), **34.8** (CH_2), **68.3** (Cp), **68.9** (Cp) **69.9** (Cp), **70.8** (Cp), **79.7** (Cp^{quat}), **88.3** (Cp^{quat}), **121.2** (d, $C_{o,1,2}^2$, $^3J_{CP-o,1,2}$ = 4.2 Hz), **121.8** (d, C_3^2, $^3J_{CP-3}$ = 5.1 Hz), **128.3** ($C_{o,1}^3$), **129.3** (C_2^3), **131.4** (C_3^3), **132.2** (C_o^4), **132.5** (C_3^4), **133.5** (C_4^4), **138.4** (C_2^4), **141.4**(d, CH=N-N-$P_{1,2,3}$, $^3J_{CP-1,2,3}$ = 13.5 Hz), **148.8** (d, C_2^1, $^2J_{CP-2}$ = 6.9 Hz), **151.2** ($C_{o,1}^1$), **155.2** (d, C_3^1, $^2J_{CP-3}$ = 6.7 Hz), **190.7** (CHO)

23. G_3^- -Fc_{24}

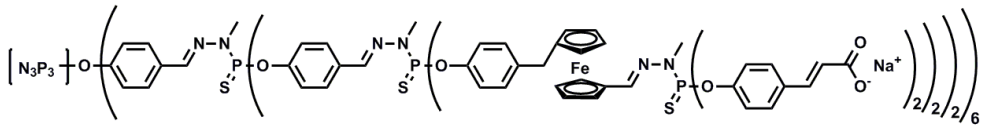

$C_{1032}H_{864}N_{87}O_{186}P_{45}S_{42}Na_{48}Fe_{24}$, MW=22633.6

In 2 mL freshly distilled (on CaH_2) pyridine were dissolved 60 mg of product **22** (3.07 µmol, 1.0 eq), 32 mg malonic acid (307 µmol, 100 eq) and 1.5 mL piperidine (freshly distilled over CaH_2) and stirred overnight at a temperature of 95°C. The reaction mixture was refluxed for 15 minutes to remove the CO_2 and precipitated from HCl (37%). The precipitate was washed three times with water and twice with ether before it was lyophilised. Ion exchange with 579 µL (0.1996 M, 116 µmol, 48 eq) NaOH yielded 27 mg of product (1.19 µmol, 39%) as an orange powder.

^{1}H-NMR (300 MHz, DMSO-d6): **3.22-3.41** (m, 102H, =N-$N_{1,2,3}$-CH_3), **3.90** (s, 48H, Cp), **3.97** (s, 48H, Cp), **4.21** (s, 48H, Cp), **4.48** (s, 48H, Cp), **6.39** (d, 48H, *CH*=CH-COOH, $^3J_{HH}$ = 15.6 Hz), **7.39** (d, 48H, CH=*CH*-COOH, $^3J_{HH}$ = 15.6 Hz), **6.95-7.82** (m, 402H, arom. + CH=N_{1+2}-N), **12.39** (s, 48H, COOH),
^{31}P{^{1}H}-NMR (121.5 MHz, $CDCl_3$): **8.17** (s, P_0), **60.8** (s, P_1), **61.4** (s, P_3), **62.9** (s, P_2)
A ^{13}C spectrum could not be taken due to a limited solubility and low concentration.

4.5.3 Synthesis of ferrocene core

For the dendrimers having a ferrocene as a core, the 1,1'-ferrocenedicarboxaldehyde core was synthesised as reported [76].

4.5.4 Synthesis of dendrimers with ferrocene core

24. Fc-G_0 (from [39])

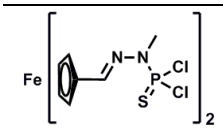

$C_{14}H_{16}N_4P_2S_2Cl_4Fe$
MW=563.9

A solution of 500 mg 1,1'-ferrocene dicarboxaldehyde (2.07 mmol, 1.0 eq) in 5 mL of THF was cooled to 0°C before 18.2 mL of MHTPC (0.24 M, 4.36 mmol, 2.1 eq) were added dropwise. This reaction mixture was stirred for approx. 2hrs at room temperature. The solvent volume was reduced and the dendrimers were precipitated from pentane/ether (± 10:1) and were washed several times with pentane/ether. This yielded 1.15 g (2.04 mmol, 99%) of a red solid.

^{1}H-NMR (250 MHz, $CDCl_3$): **3.42** (d, 6H, P_o-N-CH_3, $^{3}J_{HP}$ = 14.6 Hz), **4.43** (s, 4H, Cp), **4.72** (s, 4H, Cp), **7.6** (s, 2H, CH=N-N-P_o)
^{31}P{^{1}H}-NMR (101.3 MHz, $CDCl_3$): **62.1** (s, P_o)
^{13}C{^{1}H}-NMR: [77]

25. Fc-G_0^+

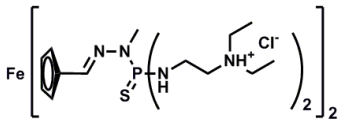

$C_{38}H_{80}N_{12}P_2S_2Cl_4Fe$
MW=1028.5

A solution of 600 mg of compound **24** (1.06 mmol, 1.0 eq) in 10 mL THF was cooled to 0°C and to this 590 µL N,N-diethylethylenediamine (4.16 mmol, 3.9 eq) was added dropwise. The reaction mixture was kept stirring overnight at room temperature. The solvent was evaporated and after two washing steps with ether 472 mg (459 µmol, 43%) of an orange powder was obtained.

^{1}H-NMR (300 MHz, MeOD): **1.32** (m, 24H, N-CH_2-*CH3*), **3.21** (m, 32H, CH_2), **3.35** (d, 6H, P_o-N-CH_3, $^{3}J_{HP}$ = 10.2 Hz), **4.36** (s, 4H, Cp), **4.75** (s, 4H, Cp), **7.6** (s, 2H, CH=N-N-P_o)
^{31}P{^{1}H}-NMR (121.5 MHz, $CDCl_3$): **69.8** (s, P_o)
^{13}C{^{1}H}-NMR (75.5 MHz, MeOD): **8.3** (N-CH_2*CH_3*), **31.2** (d, P_o-N-CH_3, $^{2}J_{CP}$ = 9.9 Hz), **36.6** (CH_2-N-P_o), **49.2** (N*CH_2*CH_3) (MeOD), **52.6** (d, P_o-N-CH_2*CH_2*, $^{3}J_{CP}$ = 6.6 Hz), **68.1** (Cp), **70.5** (Cp), **82.3** (Cp^{quat}), **138.8** (d, CH=N-N-P_o, $^{3}J_{CP}$ = 14.1 Hz)

26. Fc-G$_0$'

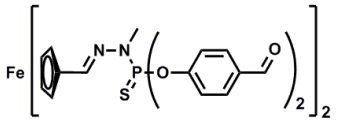

$C_{42}H_{36}N_4O_8P_2S_2Fe$
MW=19561.7

A mixture of 880 mg of compound **24** (1.56 mmol, 1.0 eq) and 940 mg of p-hydroxybenzaldehyde **1** (sodium salt, 6.6 mmol, 4.2 eq) dissolved in 20 mL THF was kept stirring overnight at room temperature. The unreacted excess of hydroxybenzaldehyde was removed by centrifugation and by subsequent quick washings of the dendrimer powder (2 minutes) with very cold methanol. This procedure yielded 1.13 g (1.25 mmol, 80%) of a dark orange solid.

^{1}H-NMR (250 MHz, $CDCl_3$): **3.28** (d, 6H, P_o-N-CH_3, $^3J_{HP}$ = 11.0 Hz), **4.28** (s, 4H, Cp), **4.58** (s, 4H, Cp), **7.42** (s, 10H, arom. and CH=N-N-P_o), **7.93** (d, 8H, arom., $^3J_{HH}$ = 7.5 Hz), **9.99** (s, 4H, CHO)
^{31}P{^{1}H}-NMR (101.3 MHz, $CDCl_3$): **60.1** (s, P_o)
^{13}C{^{1}H}-NMR: [77]

27. Fc-G$_0^-$

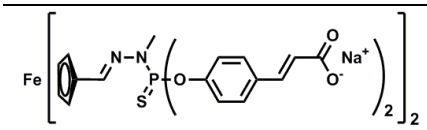

$C_{50}H_{40}N_4O_{12}P_2S_2Na_4Fe$
MW=1162.2

A mixture of 486 mg of compound **26** (537 µmol, 1.0 eq), 895 mg of malonic acid (8.6 mmol, 16 eq) and 45 µL piperidine (freshly distilled over CaH_2) was dissolved in 30 mL pyridine (freshly distilled over CaH_2) and kept stirring overnight at 95°C. The reaction mixture was refluxed for 15 minutes and precipitated with 37% HCl (in the dark). The precipitate was washed several times with water and ether and subsequently lyophilised. The dendrimer was turned into a sodium salt with 9.08 mL NaOH (0.1996 M aq, 4 eq). This quantitatively yielded 624 mg of a dark brown solid.

^{1}H-NMR (300 MHz, DMSO-d6): **3.22** (d, 6H, P_o-N-CH_3, $^{3}J_{HP}$ = 11.4 Hz), **4.29** (s, 4H, Cp), **4.55** (s, 4H, Cp), **6.48** (d, 4H, CH=CH, $^{3}J_{HH}$ = 15.9 Hz), **7.23** (d, 8H, arom.), **7.58** (d, 6H, CH=CH and CH=N-N-P_o, $^{3}J_{HH}$ = 16.2 Hz), **7.77** (d, 8H, arom.)

^{31}P{^{1}H}-NMR (121.5 MHz, DMSO-d6): **61.5** (s, P_o)

^{13}C{^{1}H}-NMR (75.5 MHz, DMSO-d6): **33.2** (d, P_o-N-CH_3), **68.8** (Cp), **71.7** (Cp), **81.1** (Cp^{quat}), **119.8** (Ar-*CH*=CH), **121.7** (d, C_o^2, $^{3}J_{CP}$ = 5.1 Hz), **130.3** (C_o^3), **132.1** (C_o^4), **142.2** (CH=N-N-P_o), **143.2** (CH=*CH*-COOH), **151.8** (d, C_o^1, $^{2}J_{CP}$ = 6.7 Hz), **167.9** (COOH)

28. Fc-G$_1$

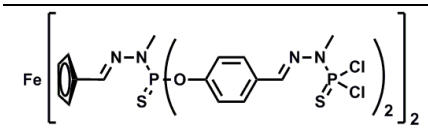

$C_{46}H_{144}N_{12}O_4P_6S_6Cl_{84}Fe$

MW=1550.1

In a mixture of 50 mL of THF and 200 mL chloroform, 950 mg of compound **28** (1,05 mmol, 1.0 eq) was dissolved and cooled down to -20°C. It is important to use concentrations this low to avoid cross condensation. In a dropwise manner 18.4 mL of MHTPC (0.24 M, 4.41 mmol, 4.2 eq) were added and the reaction mixture was allowed to come to room temperature. The reaction was strictly followed by NMR and immediately terminated upon completion. This took approx. 2 hrs. The volume of solvent was reduced and the dendrimers were precipitated with pentane and washed a couple of times with pentane/ether to remove the unreacted MHTPC. This yielded 1.38 g (890 µmol, 85%) of an orange solid.

^{1}H-NMR (300 MHz, $CDCl_3$): **3.36-3.47** (m, 18H, $P_{o,i}$-N-CH_3), **4.38** (s, 4H, Cp), **4.70** (s, 4H, Cp), **7.33-7.77** (m, 18H, arom. and CH=N-N-$P_{o,i}$)

^{31}P{^{1}H}-NMR (101.3 MHz, $CDCl_3$): **61.6** (s, P_o), **63.0** (s, P_i)

^{13}C{^{1}H}-NMR: [77]

29. Fc-G$_1^+$

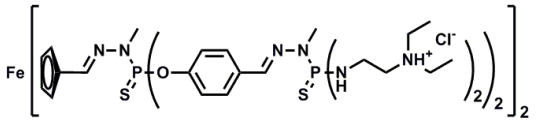

$C_{94}H_{176}N_{28}O_4P_6S_6Cl_8Fe$
MW=2479.3

To a solution of 720 mg of compound **28** (465 µmol, 1.0 eq) in 20 mL THF was added 520 µL N,N-diethylethylenediamine (3.67 mmol, 7.9 eq) at 0°C. This was kept stirring overnight at room temperature. The solvent volume was reduced and the dendrimers were precipitated from ether and washed several times with ether. This yielded 1.00 g (403 µmol, 87%) of an orange solid.

^{1}H-NMR (300 MHz, MeOD): **1.31** (m, 48H, N-CH_2*CH_3*), **3.26** (d, 18H, $P_{0,1}$-N-CH_3, $^3J_{HP}$ = 7.8 Hz), **3.33**, (64H, CH_2), **4.41** (s, 4H, Cp), **4.70** (s, 4H, Cp), **7.28** (d, 8H, arom., $^3J_{HH}$ = 8.1 Hz), **7.65** (s, 2H, CH=N-N-P_0), **7.74** (s, 4H, CH=N-N-P_1), **7.86** (d, 8H, arom.)
^{31}P{^{1}H}-NMR (121.5 MHz, MeOD): **62.4** (s, P_0), **70.2** (s, P_1)
^{13}C{^{1}H}-NMR (75.5 MHz, MeOD): **7.9** (N-CH_2*CH_3*), **31.1** (d, $P_{0,1}$-N-CH_3), **36.2** (CH_2-N-P_2), **49.6** (N-*CH_2*CH_3), **52.2** (d, P_1-N-CH_2*CH_2*, $^3J_{CP}$ = 6.9 Hz), **68.5** (Cp), **71.1** (Cp), **81.2** (Cp^{quat}), **121.3** (d, C_o^2, $^3J_{CP-o}$ = 5.1 Hz), **127.8** (C_o^3), **133.2** (C_o^4), **137.5** (d, CH=N-N-P_o, $^3J_{CP}$ = 12.5 Hz), **151.1** (d, C_o^1, $^2J_{CP}$ = 6.9 Hz)

30. Fc-G$_1$'

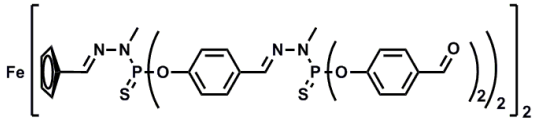

$C_{102}H_{88}N_{12}O_{20}P_6S_6Fe$
MW=19561.7

A solution of 660 mg of compound **28** (426 µmol, 1.0 eq) and 552 mg of p-hydroxybenzaldehyde (sodium salt, 3.83 mmol, 9 eq) in 20 mL THF was stirred overnight at room temperature. The unreacted excess of sodium salt was removed by means of centrifugation and several quick washings with very cold methanol. This yielded 750 mg (335 µmol, 79%) of an orange solid.

^{1}H-NMR (300 MHz, $CDCl_3$): **3.26** (d, 6H, P_0-N-CH_3, $^{3}J_{HP}$ = 10.8 Hz), **3.40** (d, 12H, P_1-N-CH_3, $^{3}J_{HP}$ = 10.9 Hz), **4.29** (s, 4H, Cp), **4.63** (s, 4H, Cp), **7.29-7.87** (m, 54H, arom. and CH=N-N-$P_{0,1}$), **9.95** (s, 8H, CHO)
^{31}P{^{1}H}-NMR (101.3 MHz, $CDCl_3$): **60.3** (s, P_0), **61.7** (s, P_0)
^{13}C{^{1}H}-NMR: [77]

31. Fc-G_1^-

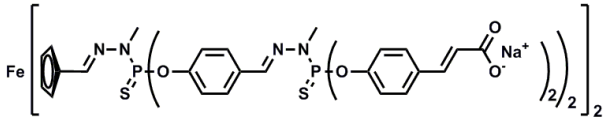

$C_{118}H_{96}N_{12}O_{28}P_6S_6Na_8Fe$
MW=2746.8

In 50 mL pyridine (freshly distilled over CaH_2) were dissolved 750 mg of compound **30** (335 µmol, 1.0 eq), 558 mg malonic acid (5.36 mmol, 16 eq) and 70 µL piperidine (freshly distilled over CaH_2). This was stirred overnight at 95°C. The mixture was refluxed for 15 minutes, the dendrimers were precipitated from 37% HCl and washed several times with water and ether. The dendrimers were transformed into their sodium salt analog by means of ion exchange with 13.5 mL NaOH (0.1996 M, 2.70 mmol, 8 eq), which yielded 868 mg (338 µmol, 100%) of an orange solid.

^{1}H-NMR (300 MHz, DMSO-d6): **3.23** (d, 6H, P_0-N-CH_3, $^{3}J_{HP}$ = 10.8 Hz), **3.31** (d, 12H, P_1-N-CH_3, $^{3}J_{HP}$ = 10.5 Hz), **4.28** (s, 4H, Cp), **4.58** (s, 4H, Cp), **6.45** (2d, 8H, CH=CH, $^{3}J_{HH}$ = 15.9 Hz), **7.22** (m, 24H, arom.), **7.53** (2d, 8H, CH=CH, $^{3}J_{HH}$ = 15.9 Hz), **7.68** (m, 24H, arom.), **7.93** (s, 6H, CH=N-N-$P_{0,1}$)
^{31}P{^{1}H}-NMR (121.5 MHz, DMSO-d6): **61.8** (2s, $P_{0,1}$)
^{13}C{^{1}H}-NMR (75.5 MHz, DMSO-d6): **33.2-33.5** (2d, $P_{0,1}$-N-CH_3), **68.7** (Cp), **71.7** (Cp), **81.2** (Cp^{quat}), **120.0** (C_o^2), **121.8** (d, C_1^2, $^{3}J_{CP}$ = 3.2 Hz), **128.8** (C_o^3), **130.3** (C_o^3), **132.2** (C_1^4), **132.4** (C_o^4), **141.3** (d or 2m, CH=N-N-$P_{0,1}$, $^{3}J_{CP}$ = 16.4 Hz), **143.0** (CH=*CH*-COOH), **151.3** (d, C_o^1, $^{2}J_{CP}$ = 6.6 Hz), **151.6** (d, C_o^1, $^{2}J_{CP}$ = 4.8 Hz), **168.0** (COOH)

4.5.5 Cyclic Voltammetry

Two different measurement setups have been used for the characterization of $Fc\text{-}G_0^+$ and $Fc\text{-}G_0^-$.

For the $Fc\text{-}G_0^-$, the CV measurements were carried out with an Autolab PGSTAT100 and a three electrode system. The reference electrode was a saturated calomel electrode, separated from the solution by a bridge compartment. The counter electrode was a platinum wire with an approximate surface area of 1 cm^2. The working electrode was a platinum electrode (0.5 mm diameter). The dendrimer concentration was 3.73 mM and the background electrolyte (KCl) concentration was 100 mM. Before each measurement, the solution was degassed with Argon and the working electrode was polished with a polishing machine (Presi P230).

For the $Fc\text{-}G_0^+$, CV was performed in a Teflon (PTFE) cell containing three electrodes: a reference electrode (Ag/AgCl wire in 3M KCl), a counter electrode (platinum wire, 1 cm^2 surface) and a gold coated glass substrate was used as the working electrode (0.78 cm^2). The potentiostat was an Autolab (PGSTAT12). The dendrimer concentration was 3 mM and the supporting electrolyte (KCl) concentration was 100 mM.

4.6 Bibliography

[1] G.R. Newkome, C.N. Moorefield, G.R. Baker, M.J. Saunders, S.H. Grossman, Angewandte Chemie-International Edition in English 30/9 (1991) 1178.
[2] S. Campagna, G. Denti, S. Serroni, M. Ciano, A. Juris, V. Balzani, Inorg Chem 31/13 (1992) 2982.
[3] G. Denti, S. Campagna, S. Serroni, M. Ciano, V. Balzani, J Am Chem Soc 114/8 (1992) 2944.
[4] G. Denti, S. Serroni, S. Campagna, V. Ricevuto, V. Balzani, Inorg Chim Acta 182/2 (1991) 127.
[5] P.A. Chase, R.J.M.K. Gebbink, G. van Koten, J Organomet Chem 689/24 (2004) 4016.
[6] I. Cuadrado, M. Moran, C.M. Casado, B. Alonso, J. Losada, Coordin Chem Rev 195 (1999) 395.
[7] S.H. Hwang, C.D. Shreiner, C.N. Moorefield, G.R. Newkome, New J Chem 31/7 (2007) 1192.
[8] G.R. Newkome, E.F. He, C.N. Moorefield, Chem Rev 99/7 (1999) 1689.
[9] B.J. Ravoo, Dalton T/12 (2008) 1533.

[10] D. Astruc, F. Chardac, Chem Rev 101/9 (2001) 2991.
[11] D.L. Jiang, T. Aida, Abstr Pap Am Chem S 214 (1997) 153.
[12] C. Valerio, S. Rigaut, J. Ruiz, J.L. Fillaut, M.H. Delville, D. Astruc, B Pol Acad Sci-Chem 46/3 (1998) 309.
[13] C.O. Turrin, J. Chiffre, J.C. Daran, D. de Montauzon, A.M. Caminade, E. Manoury, G. Balavoine, J.P. Majoral, Tetrahedron 57/13 (2001) 2521.
[14] C.O. Turrin, J. Chiffre, D. de Montauzon, G. Balavoine, E. Manoury, A.M. Caminade, J.P. Majoral, Organometallics 21/9 (2002) 1891.
[15] S. Langereis, A. Dirksen, T.M. Hackeng, M.H.P. van Genderen, E.W. Meijer, New J Chem 31/7 (2007) 1152.
[16] E. Toth, D. Pubanz, S. Vauthey, L. Helm, A.E. Merbach, Chem-Eur J 2/12 (1996) 1607.
[17] E.C. Wiener, M.W. Brechbiel, O.A. Gansow, G. Foley, P.C. Lauterbur, Abstr Pap Am Chem S 214 (1997) 221.
[18] A.W. Bosman, H.M. Janssen, E.W. Meijer, Chem Rev 99/7 (1999) 1665.
[19] R.M. Crooks, M. Zhao, L. Sun, V. Chechik, L.K. Yeung, Acc Chem Res 34/3 (2001) 181.
[20] M.C. Daniel, D. Astruc, Chem Rev 104/1 (2004) 293.
[21] C.B. Gorman, J.C. Smith, Acc Chem Res 34/1 (2001) 60.
[22] D.L. Jiang, T. Aida, Chem Commun/13 (1996) 1523
[23] K.W. Pollak, J.W. Leon, J.M.J. Frechet, M. Maskus, H.D. Abruna, Chem Mater 10/1 (1998) 30.
[24] M. Kawa, J.M.J. Frechet, Chem Mater 10/1 (1998) 286.
[25] D.S. Tyson, C.R. Luman, F.N. Castellano, Inorg Chem 41/13 (2002) 3578.
[26] J.J. Becker, M.R. Gagne, Organometallics 22/24 (2003) 4984.
[27] G. Chessa, L. Canovese, F. Visentin, C. Santoa, R. Seraglia, Tetrahedron 61/7 (2005) 1755.
[28] K.J. van Bommel, G.A. Metselaar, W. Verboom, D.N. Reinhoudt, J Org Chem 66/16 (2001) 5405.
[29] W.T.S. Huck, F.C.J.M. vanVeggel, D.N. Reinhoudt, Angewandte Chemie-International Edition in English 35/11 (1996) 1213.
[30] V. Balzani, S. Campagna, G. Denti, A. Juris, S. Serroni, M. Venturi, Accounts Chem Res 31/1 (1998) 26.
[31] P.L. Burn, S.C. Lo, I.D.W. Samuel, Adv Mater 19/13 (2007) 1675.
[32] A.E. Kaifer, Eur J Inorg Chem/32 (2007) 5015.
[33] P.R. Ashton, V. Balzani, M. Clemente-Leon, B. Colonna, A. Credi, N. Jayaraman, F.M. Raymo, J.F. Stoddart, M. Venturi, Chem-Eur J 8/3 (2002) 673.
[34] C.S. Cameron, C.B. Gorman, Adv Funct Mater 12/1 (2002) 17.
[35] A.J. Bard, L.R. Faulkner, Electrochemical Methods: Fundamentals and Applications, Wiley, New York, 2001.
[36] R. Toba, J.M. Quintela, C. Peinador, E. Roman, A.E. Kaifer, Chem Commun (9) (2001) 857.
[37] V. Vicinelli, M. Maestri, V. Balzani, W.M. Muller, U. Muller, U. Hahn, F. Osswald, F. Vogtle, New J Chem 25/8 (2001) 989.
[38] A.M. Caminade, J.P. Majoral, Coordin Chem Rev 249/17-18 (2005) 1917.
[39] C.O. Turrin, J. Chiffre, D. de Montauzon, J.C. Daran, A.M. Caminade, E. Manoury, G. Balavoine, J.P. Majoral, Macromolecules 33/20 (2000) 7328.
[40] C.O. Turrin, J. Chiffre, J.C. Daran, D. de Montauzon, G. Balavoine, E. Manoury, A.M. Caminade, J.P. Majoral, Cr Chim 5/4 (2002) 309.
[41] N.S. Khrushcheva, V.I. Sokolov, Russ Chem B+ 57/6 (2008) 1244.
[42] A.S. Abd-El-Aziz, E.K. Todd, Coordin Chem Rev 246/1-2 (2003) 3.
[43] J. Alvarez, T. Ren, A.E. Kaifer, Organometallics 20/16 (2001) 3543.
[44] D. Astruc, Pure Appl Chem 75/4 (2003) 461.
[45] R. Castro, I. Cuadrado, B. Alonso, C.M. Casado, M. Moran, A.E. Kaifer, J Am Chem Soc 119/24 (1997) 5760.
[46] C.A. Nijhuis, F. Yu, W. Knoll, J. Huskens, D.N. Reinhoudt, Langmuir 21/17 (2005) 7866.
[47] D. Astruc, C. Ornelas, J. Ruiz, Chem-Eur J 15/36 (2009) 8936.
[48] C. Ornelas, J. Ruiz, D. Astruc, Organometallics 28/9 (2009) 2716.
[49] E. Boisselier, A.C.K. Shun, J. Ruiz, E. Cloutet, C. Belin, D. Astruc, New J Chem 33/2 (2009) 246.
[50] D.A. Foucher, B.Z. Tang, I. Manners, J Am Chem Soc 114/15 (1992) 6246.
[51] M. Tanabe, I. Manners, J Am Chem Soc 126/37 (2004) 11434.

[52] M. Tanabe, G.W.M. Vandermeulen, W.Y. Chan, P.W. Cyr, L. Vanderark, D.A. Rider, I. Manners, Nat Mater 5/6 (2006) 467.
[53] W. Wang, A.E. Kaifer, Advanced Polymer Sciences (2009).
[54] D. Astruc, C. Ornelas, J. Ruiz, Accounts Chem Res 41/7 (2008) 841.
[55] C. Ornelas, J. Ruiz, D. Astruc, Organometallics 28/15 (2009) 4431.
[56] M. Frasconi, D. Deriu, A. D'Annibale, F. Mazzei, Nanotechnology 20/50 (2009) 505501.
[57] J.W.J. Knapen, A.W. Vandermade, J.C. Dewilde, P.W.N.M. Vanleeuwen, P. Wijkens, D.M. Grove, G. Vankoten, Nature 372/6507 (1994) 659.
[58] S.B. Garber, J.S. Kingsbury, B.L. Gray, A.H. Hoveyda, J Am Chem Soc 122/34 (2000) 8168.
[59] M.T. Reetz, G. Lohmer, R. Schwickardi, Angew Chem Int Edit 36/13-14 (1997) 1526.
[60] R. Breinbauer, E.N. Jacobsen, Angew Chem Int Edit 39/20 (2000) 3604.
[61] E.C. Wiener, M.W. Brechbiel, H. Brothers, R.L. Magin, O.A. Gansow, D.A. Tomalia, P.C. Lauterbur, Magnet Reson Med 31/1 (1994) 1.
[62] M.S. Choi, T. Yamazaki, I. Yamazaki, T. Aida, Angew Chem Int Edit 43/2 (2004) 150.
[63] S.L. Gilat, A. Adronov, J.M.J. Frechet, Angew Chem Int Edit 38/10 (1999) 1422.
[64] J. Hofkens, M. Maus, T. Gensch, T. Vosch, M. Cotlet, F. Kohn, A. Herrmann, K. Mullen, F. De Schryver, J Am Chem Soc 122/38 (2000) 9278.
[65] A.M. Caminade, J.P. Majoral, Prog Polym Sci 30/3-4 (2005) 491.
[66] A.M. Caminade, C.O. Turrin, R. Laurent, A. Maraval, J.P. Majoral, Current Organic Chemistry 10/18 (2006) 2333.
[67] J. Chiffre, Université Paul Sabatier, Toulouse, 2000.
[68] G.G.A. Balavoine, J.C. Daran, G. Iftime, E. Manoury, C. Moreau-Bossuet, J Organomet Chem 567/1-2 (1998) 191.
[69] L. Routaboul, J. Chiffre, G.G.A. Balavoine, J.C. Daran, E. Manoury, J Organomet Chem 637 (2001) 364.
[70] M. Blanzat, C.O. Turrin, A.M. Aubertin, C. Couturier-Vidal, A.M. Caminade, J.P. Majoral, I. Rico-Lattes, A. Lattes, Chembiochem 6/12 (2005) 2207.
[71] M. Blanzat, C.O. Turrin, E. Perez, I. Rico-Lattes, A.M. Caminade, J.P. Majoral, Chem Commun/17 (2002) 1864.
[72] G.J.D.A. Soler-Illia, L. Rozes, M.K. Boggiano, C. Sanchez, C.O. Turrin, A.M. Caminade, J.P. Majoral, Angew Chem Int Edit 39/23 (2000) 4250.
[73] F. Vogel, Vogel's Textbook of Practical Organic Synthesis, Longman, London, 1989.
[74] C.O. Turrin, Université Paul Sabatier, Toulouse, 2000.
[75] C.O. Turrin, B. Donnadieu, A.M. Caminade, J.P. Majoral, Z Anorg Allg Chem 631/13-14 (2005) 2881.
[76] G. Balavoine, G. Doisneau, T. Fillebeen-Khan, J Organomet Chem 412/3 (1991) 381.
[77] C.O. Turrin, Université Paul Sabatier, Toulouse, 2000.

5 Lipid bilayer membranes on Dendrimer Supports

Artificial lipid bilayer membranes are applied in sensor technologies and for studying membrane protein structure and functions. One of the applications is to study membrane proteins in their natural or in a biomimetic environment. In this chapter, the attempt to construct stable and well-defined lipid bilayers on a solid dendrimer coated support is described. The membranes and dendrimer coatings were characterised with optical and electrochemical techniques and it was concluded that, regardless of the fabrication method, the lipids could not be organised into robust and well-defined membranes. Immobilisation of Cytochrome C Oxidase on negatively charged dendrimers using a His-tag did not enhance lipid organisation and was found to be inactive. With a water contact angle of 50°, the dendrimer coating was neither sufficiently hydrophilic nor hydrophobic in order to enforce lipid organisation. Hence it was impossible to construct lipid membranes on dendrimer support. As GUVs did adhere to the dendrimers but not fuse into a bilayer, these dendrimer coated surfaces could be interesting candidates for cell applications.

5.1 Introduction

5.1.1 Biomembranes

In biology, a membrane defines a semi-impermeable border between the content of a cell or organelle and the outside, one of the most fundamental considerations in biological organisation. It permits biochemical reactions to take place in confined environments and therewith separate compartments with different functions. As most biological processes take place in the aqueous medium, the sole prerequisite for good segregation is impermeability towards solutes. A membrane is therefore comprised of phospholipids; small amphiphiles that spontaneously orient themselves into a bilayer with a hydrophobic interior and two hydrophilic interfaces with the surrounding water. It can be considered a two dimensional fluid in which lipids are free to diffuse and whose fluidity is controlled by the lipid type and cholesterol.

Apart from segregation, membranes have countless other functions as accounted for by the vast number of different integral membrane proteins inside or peripheral membrane proteins associated with the membrane. Examples include ion channels regulating ionic strength inside the cell or electrical signal transduction between neuron cells, ATPases synthesising ATP (a cellular energy carrier) by exploiting a proton gradient over the membrane and various kinds of receptors for cell-cell interaction and communication. Organelles in eukaryotic cells also have a membrane. As such, the nuclear membrane forms a protective envelope around the chromosomes, the inner and outer mitochondrial membranes facilitate the *respiratory chain* (see 5.1.3) and there are many more examples. For all the numerous and complex functions they have to accomplish, biological membranes contain an incredible amount of different proteins, lipids and other molecules and are therefore extremely difficult to mimic.

5.1.2 Artificial bio-mimicking membranes

For many applications and studies it is necessary to create an artificial lipid bilayer membrane that approximates the "natural situation" as closely as possible. There are several reasons for mimicking the natural environment. Many biological processes, like light-energy conversion and molecular recognition, are unbeatably efficient, specific and sensitive. Therefore, exploiting bio-components like proteins for their specialised properties and incorporating them into devices is the only feasible way of achieving similar performances as analogous biological processes. In other cases, where for example membrane proteins are being studied for their function, structure, interactions and dynamics, a natural environment is required to observe the natural behaviour of the protein. Obviously, the more biomimetic the system must be, the more complicated it is to fabricate, use and characterise. The next sections discuss different lipid bilayer membrane systems.

Liposomes and Vesicles

In the 1960s the first membrane systems were fabricated, all without a solid support. They included liposomes, giant vesicles and black lipid membranes (BLMs) and they were used for the investigation of channel proteins and receptors. Liposomes and vesicles are spheroid capsules with a lipid bilayer membrane that as the outer border (Fig. 5.1). Vesicles can be fabricated in different sizes and with one or more bilayer lamellae. Unilamellar vesicles vary in size from Small Unilamellar Vesicles (SUV, 20-50 nm diameter) until Giant Unilamellar Vesicles (GUV, 1-200 μm diameter) and are used for different purposes. Due to the strong curvature of their membrane, SUVs experience mechanical stress, from which can be easily relieved by fusing together or onto surfaces. This can be applied for the construction of lipid bilayers on solid supports [1-2]. GUVs on the other hand have a significant internal volume and can be used for the release of solutions upon fusion or collapse. When fusion with a cell membrane takes place (endocytosis), GUVs can transfer their contents into cells without leaving lipid residues [3-4]. Furthermore, vesicles can be used to reconstitute integral membrane proteins

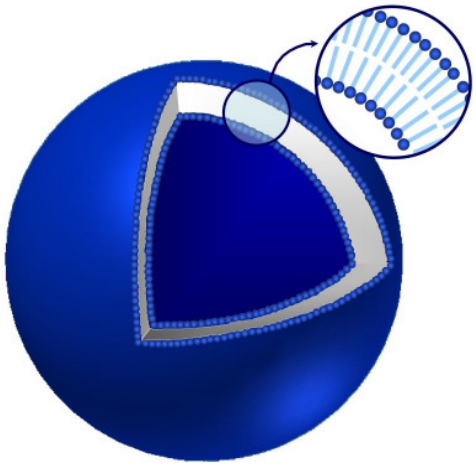

Fig. 5.1 – Schematic of a unilamellar vesicle

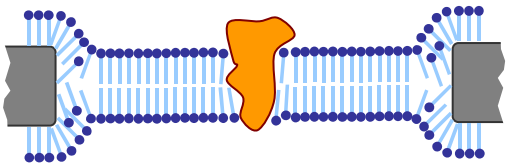

Fig. 5.2 – Schematic of a BLM with an integrated membrane protein

into lipid bilayers in order to study them directly in the vesicles or on planar substrates [5-9].

Black Lipid membranes

Black Lipid membranes (BLM's, Fig. 5.2) are built by spanning lipid bilayers across an aperture between two compartments containing aqueous solutions. The name refers to their black appearance due to the destructive interference of the reflected light off the two lipid monolayers. The separation of two volumes by the BLM allows for the characterisation of membrane proteins and in particular of those that electrochemically active and those that are involved in ion transport [10-13], unlike for vesicle systems [14]. The usually extremely high resistance (or impedance) of the membrane decreases dramatically when embedded proteins transport charge across it. Together with the membrane capacity (charge separation), this information may reveal protein gate sizes, ion selectivity and protein electron turnover. BLM construction allows for an asymmetric experimental setup: bilayers made from two sheets of different lipids, different buffers on each side and selective orientation of asymmetric proteins. One of the main issues with vesicles and BLMs is their stability in time and under mechanical stress [15].

Supported membranes

Another approach to study membranes and incorporated proteins is by depositing them on a solid substrate. This substrate offers mechanical stability and provides the opportunity to use a wealth of experimental techniques that require a solid support. It is possible to characterise the membrane system with QCM-D, SPR, EIS, FRAP, AFM and other optical or microscopic techniques, each providing a different kind of information on topology, mechanical strength, electrical impedance, layer thicknesses, refractive indices, vibrational energy dissipation, molecular diffusion and fluorescence. The most straightforward approach would be depositing a bilayer directly onto a bare hydrophilic surface. The negative surface charge of siliceous materials (due to the proton dissociation of the silanols) can attract the hydrophilic lipid head groups and therewith make vesicles break and fuse into a continuous lipid bilayer on the surface. However, the next sections show that there are more sophisticated methods that yield highly stable membranes.

Hybrid and tethered bilayer membranes

The name hybrid Bilayer Membranes refers to the two different monolayer sheets that together comprise the membrane. The membrane is built in two distinct steps of which the first is the (quasi-) covalent self-assembly of an alkane-like molecule and step two is the adsorption of a lipid layer by for example vesicle fusion or the Langmuir-Schaefer method [16]. This approach yields very stable and highly sealing membranes because of the almost defect free packing of the alkanes and lipids. If the membrane is to be applied for studying membrane proteins, hBLMs do not offer the protein a water layer at both sides of the membrane, which is required for many proteins and are therefore less attractive.

In order to make the membrane more biomimetic by introducing water between the solid support and the membrane, a spacer is required that is able to bind water and that in specific cases acts like an ionic reservoir [17-27]. The membrane thus formed is called a tethered membrane (tBLM). This approach also reduces the risk of denaturation of embedded proteins upon contact with the surface [17, 25, 28-29]. The molecules comprising the first layer contain a

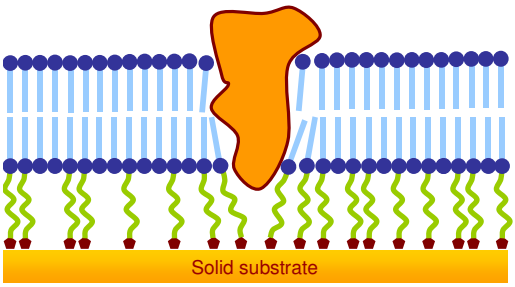

Fig. 5.3 – A tethered (green) lipid bilayer membrane (tBLM)

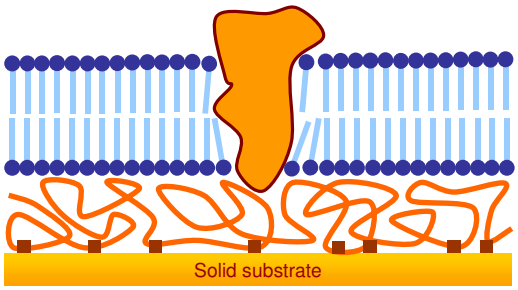

Fig. 5.4 – Schematic of a polymer supported lipid bilayer membrane

lipid group, a spacer (or tether unit) and an anchoring group that covalently binds to the solid surface and whose chemistry depends on the surface material. In case of a gold support, a sulphur containing group is used, whereas for silicon oxide silanes are used. Despite the chemical and mechanical robustness of the film, the spacer introduces flexibility into the membrane support, allowing for a smooth incorporation of large molecules. The first monolayer is usually not fully packed and therefore allows for introduction extra lipids during the deposition of the second, outer monolayer. The outer lipid leaflet can be deposited by Rapid Solvent Exchange [30], Vesicle Fusion or Langmuir Schaefer deposition. The aqueous reservoir created by the spacer material allows incorporated proteins to function optimally. Such a tethered system is schematically depicted in Fig. 5.3.

The resulting lipid bilayer membrane is highly resistant to electrical currents ($M\Omega cm^2$) and shows an electrical capacity below 1 $\mu F cm^{-2}$ [18, 21, 24, 27, 31]. This allows for measuring sensitively the (selective) ion permeation through channelling proteins [18, 32-33]. For an electrochemical investigation of the protein-membrane system, the solid support acts like an ultra-flat planar electrode. Gold is the ideal support material as it is chemically inert (also to oxidation) and it can be applied in combination with other techniques that require a gold film (SPR, EIS).

Membranes on polymer supports

Polymers can be utilised as soft supports for lipid membranes. With a film thickness of 1-10 nm they act like deformable cushions that are able to adapt

to the incorporation of membrane by their altering conformation. When a hydrophilic polymer or a copolymer with hydrophilic units is used, the resulting cushion contains a large amount of water and therefore enhances membrane protein functionality. The lipid membrane can be deposited on top of the polymer film by vesicle fusion [34] or LB transfer [35]. The most commonly used polymers are polyethyleneimide (PEI), polyethyleneglycol (PEG) and cellulose [29, 36-39]. A schematic depiction is provided in Fig. 5.4.

5.1.3 Cytochrome C Oxidase

A relatively new concept of tethering lipid membranes is using immobilised membrane proteins on a surface [40-42]. The stability and functionality is guaranteed by surfactant molecules that cover the membrane spanning part of the protein to shield it from the surrounding water. Upon application of a lipid containing solution, the surfactant molecules are replaced by the lipids and a stable lipid bilayer membrane is formed. An additional advantage of this system is that tethering molecules, which can restrict lipid dynamics and protein conformational freedom, are not necessary anymore. This leaves more space to the protein (as well as water and ions), which is required for its full biological activity.

Protein tethering

The attachment of the protein occurs *via* chelating a His-tag to chemical surface functionalities. This follows the principle of metal ion affinity chromatography [43], which is now nearly standard protocol for protein purification. A gold surface is modified with two different small thiols with one bearing three carboxylates (responsible for the chelation) and the other being an “inert” compound that enables the regulation of the relative surface coverage by the first thiol. The functionalised surface is subsequently incubated with a solution that contains either Copper or Nickel cations that coordinate with the carboxylates. The protein of interest (Cytochrome c, Cytochrome c Oxidase) contains a His-tag whose imidazole side chains coordinate to the immobilised cations. The surface coverage of the carboxylate

bearing thiol therewith determines the final protein coverage on the surface. The protein is applied as an aqueous solution containing surfactant molecules that stabilise the apolar regions of the protein. In the last step a lipid membrane is formed by the addition of lipids that replace the surfactants while the latter are absorbed by biobeads. This approach is described in more detail in section 5.3.3.

Cytochrome C Oxidase

In this chapter Cytochrome c Oxidase (CcO) was used. CcO is a transmembrane enzyme that is involved in the respiratory (electron transport) chain that takes place in bacteria and the mitochondrion of eukaryotic cells. It collects four electrons from four Cytochrome c proteins (after a process involving three precedent steps) and shuttles them to the other side of the membrane to reduce molecular oxygen to water by reacting with four protons. Simultaneously, CcO transports four protons across the membrane into the mitochondrial interlamellar space. The consequence of three processes in the respiratory chain (including the activity of CcO) is an electrochemical (proton) gradient across the membrane that drives the enzyme ATPase to conduct the oxidative phosphorylation of adenosine diphosphate to adenosine triphosphate, the energy currency of the cell.

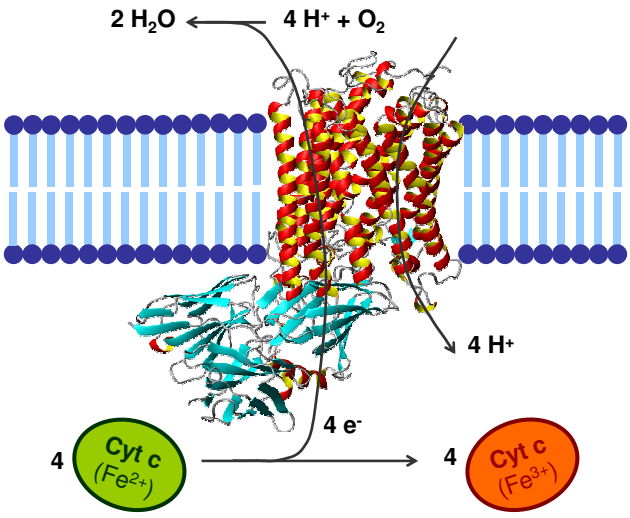

Fig. 5.5 – Cytochrome c in the inner mitochondrial membrane: the creation of proton concentration gradient across the membrane by the reduction of molecular oxygen and oxidation of Cytochrome c. (CcO image was made using Molmol [44])

5.2 Research Questions & Approach

Bio-mimicking membranes have been extensively studied and applied in research on integral membrane proteins. The deposition of a membrane on a dendrimer cushion, however, has never been described before. In this chapter the attempts to fabricate stable and well-defined lipid bilayer architectures on a soft dendrimer support are described. Here, the following research questions were addressed:

- ✓ Is it possible to construct a lipid membrane on a dendrimer coated solid support? What is the most appropriate method to deposit the membrane?
- ✓ Are there differences between polyanionic and polycationic dendrimer cushions?
- ✓ Is it possible to use immobilised Cytochrome c Oxidase (CcO) as a tethering unit on dendrimers and is the protein active in the resulting membrane?

In order to answer the first two questions, a simple experimental architecture was designed. Chromium and gold were evaporated onto a glass slide and subsequently coated with either polycationic or polyanionic dendrimers, which are depicted in Fig. 5.6.

A lipid bilayer membrane was reconstituted from a solution containing the zwitterionic DPhyPC (1,2-di-O-phytanoyl-sn-glycero-3-phosphocholine, for the molecular structure see 5.6.2) by means of vesicle fusion and/or solvent exchange. The final and intermediate layered systems were characterised by contact angle measurements (CA, hydrophilicity/hydrophobicity), surface plasmon resonance spectroscopy (SPR, layer thickness, refractive index) and electrochemical impedance spectroscopy (EIS, electrical DC conductivity and capacity). All SPR and EIS experiments were conducted on extremely flat gold surfaces (Template stripped gold, roughness < 1 nm).

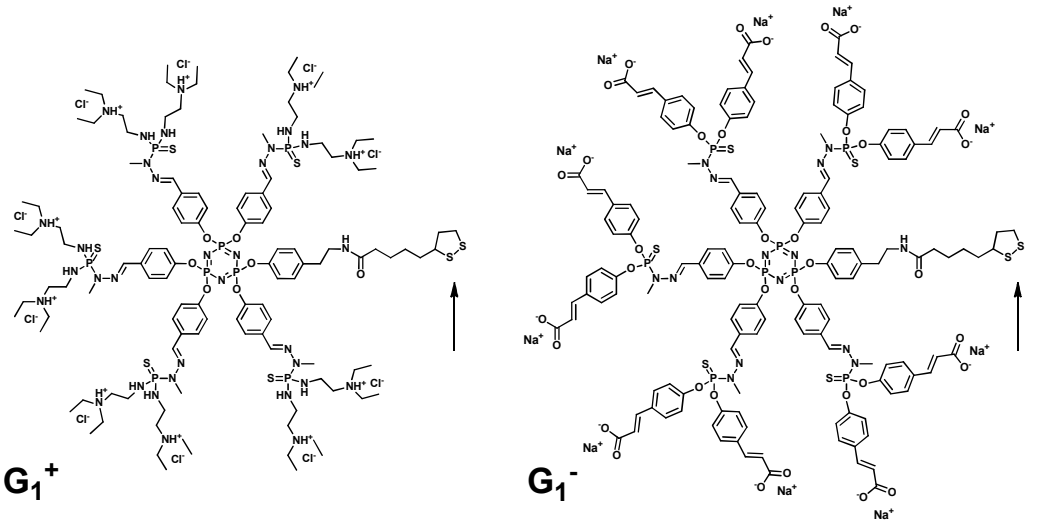

Fig. 5.6 — Left: G1 polycationic dendrimer, Right: G1 polyanionic dendrimer, each bearing 10 peripheral charges and one dithiolane moiety at its core (indicated with an arrow).

The third question could be answered by immobilising CcO on a gold surface coated with polyanionic dendrimers and reconstituting a lipid membrane (DPhyPC) around it (Fig. 5.8). The protein was expected to facilitate the lipid organisation and membrane formation, as described in the introduction to this chapter. The immobilisation of the His-tagged CcO was carried out by chelating the His-tag to Ni^{2+} ions that are coordinated to the carboxylates of the dendrimers. The dendrimer-protein-membrane system was characterised with SPR and EIS. For a detailed study of the CcO activity, Cyclic Voltammetry

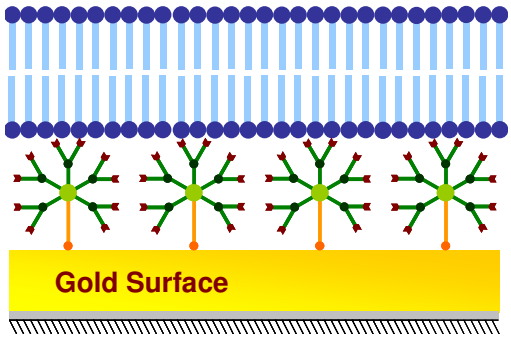

Fig. 5.7 – A lipid membrane deposited on a soft dendrimer cushion

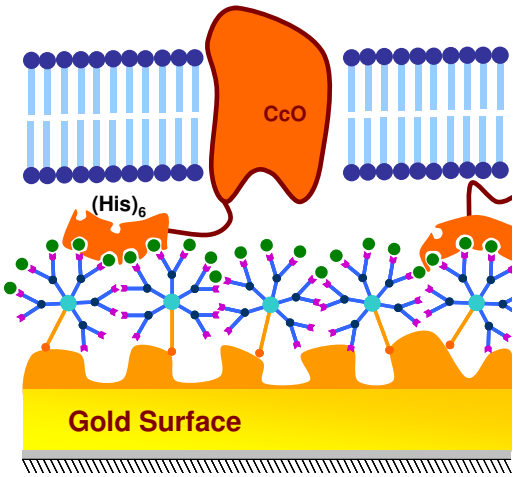

Fig. 5.8 – CcO coupled to a gold-dendrimer-Ni^{2+} coated surface *via* a His-tag, embedded in lipid membrane

(CV), Surface Enhanced InfraRed Absorption spectroscopy (SEIRAS) and SEIRAS with static potential titration were employed. The IR surface enhancement was achieved by growing gold nanoparticles from solution to the flat gold surface before the fabrication of the dendrimer-protein-membrane system. All techniques mentioned together characterise the systems' physical properties and the protein activity.

5.3 Results and Discussion

In this chapter, two different experiments are described. The first experiment is the deposition of a DPhyPC lipid bilayer membrane directly on a flat gold surface that is coated with dendrimers. This system is depicted in Fig. 5.7. In the second experiment, the His-tagged protein CcO is immobilised on a gold surface that is modified with gold nanoparticles, dendrimers and Nickel cations. This system is depicted in Fig. 5.8.

5.3.1 Membranes on dendrimer supports

This experiment investigated the possibility to directly couple a lipid membrane on a dendrimer support. Additionally, GUVs were fabricated and investigated for their interaction with the different dendrimer coatings using optical microscopy.

The water contact angles measured on dendrimer coatings were already discussed in section 3.3.5. The results indicated that the coated surfaces are neither hydrophilic nor hydrophobic. This suggests that the formation of a membrane on such a surface may be very difficult, as that generally requires either a hydrophobic or hydrophilic surface. Applying lipids in an unordered fashion, like with solvent exchange, will presumably not be successful to create a well-defined membrane. This presumption was confirmed with experimental data. However, with vesicle fusion and Langmuir related techniques, lipids are pre-organised in a (semi) membrane, which may help to

achieve a better organisation in the adsorbed lipids and which may lead to a better defined membrane.

Solvent Exchange and Vesicle Fusion

The template stripped gold (TSG) surface was coated with either positively charged or negatively charged dendrimers. The resulting dendrimer layers were always 1.0 nm thick. For all organic material, the refractive index is approximated to be 1.5 [45]. The most straightforward way to deposit lipids on these surfaces is solvent exchange [30]. The adsorption process was followed by SPR spectroscopy. After the solvent exchange (indicated with RSE), DPhyPC vesicles were applied to the surface (indicated with VF). This resulted on both dendrimer coated surfaces in an increased adsorbed amount of lipids. All results are shown in Fig. 5.9.

During the solvent exchange, lipids adsorb to the dendrimer coated surfaces. The adsorbed amount depended on the dendrimer charge. On the positively charged dendrimers, the lipids formed a layer with an average thickness of only 1.2 nm, whereas the negatively charged dendrimers harboured 4.7 nm of lipids. Apparently, the negatively charged dendrimers attracted more lipids, which can be explained by the presumed orientation of the lipids on the dendrimers. In ethanol, during the adsorption process, the lipids have their zwitterionic head groups oriented towards the dendrimer, with the positively

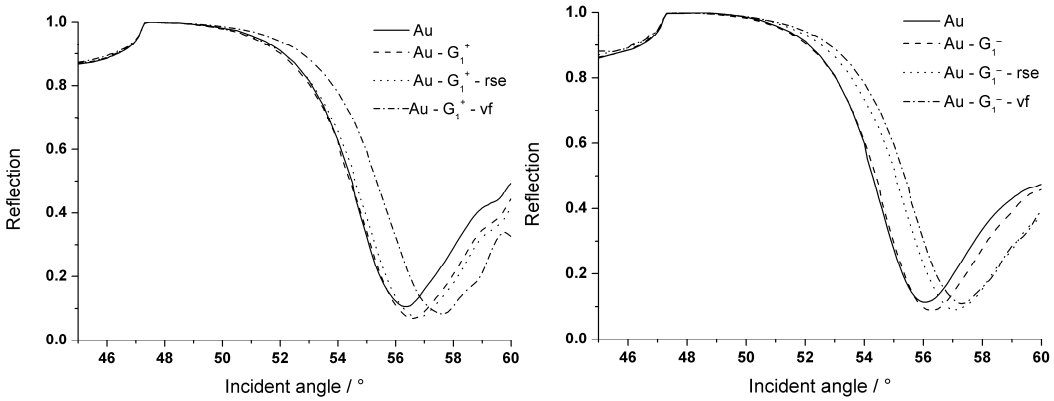

Fig. 5.9 – Two step lipid deposition on dendrimer coated surfaces, probed by SPR. step 1: rapid solvent exchange (rse), step 2: vesicle fusion (vf). <u>Right:</u> G_1^+ dendrimer, <u>Left:</u> G_1^- dendrimer

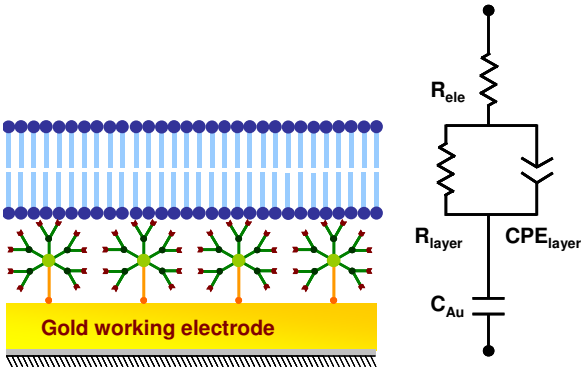

Fig. 5.10 – The equivalent circuit used for all samples with dendrimers and lipid bilayer membranes comprises an electrolyte resistance (R_{ele}), a bilayer resistance and constant phase element (R_{layer} and CPE_{layer}) and an electrode interface capacitor (C_{Au}).

charged choline closer to the dendrimer than the anionic phosphate and their tails are solubilised in ethanol. Initially, this orientation does not change during the solvent exchange and the lipids having an attractive electrostatic interaction with the (polyanionic) dendrimers will stick more, whereas the ones experiencing a repulsive interaction will be flushed off the surface again. This explains why hardly any lipid stays on the dendrimer surface. However, the amount of adsorbed lipids on negatively charged dendrimers represents nearly the equivalent amount of a lipid bilayer (expected value 6 nm).

During the second part of the experiment, lipid vesicles were applied to the surface. Again lipid deposition took place on both dendrimers. This time, however, the adsorption on positively charged dendrimers was much higher, but in both cases the total adsorbed amount of lipids levelled off to 6 nm. The fact that the thickness increment is twice the theoretical length of a lipid molecule suggests that the lipids may be organised in a bilayer fashion. However, this must be proven by a complementary method like EIS. The obtained spectra were fitted to the equivalent circuit depicted in Fig. 5.10.

This equivalent circuit comprises an electrolyte resistance (R_{ele}), a bilayer resistance and constant phase element (R_{layer} and CPE_{layer}) and an electrode interface capacitor (C_{Au}). In comparison to what was described in section 2.2, the bilayer capacitance has been replaced with a CPE element. A CPE acts like an imperfect capacitor and has two parameters, of which the T-parameter represents the actual capacitance and the P-parameter (values between 0-1) is a measure for the imperfectness. For P = 0, the CPE acts like a pure resistor

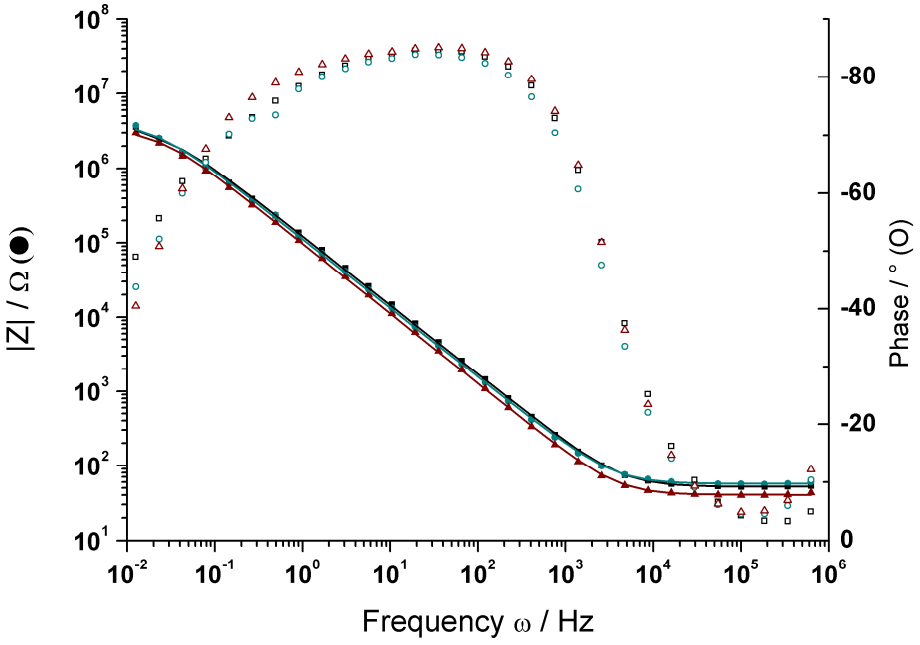

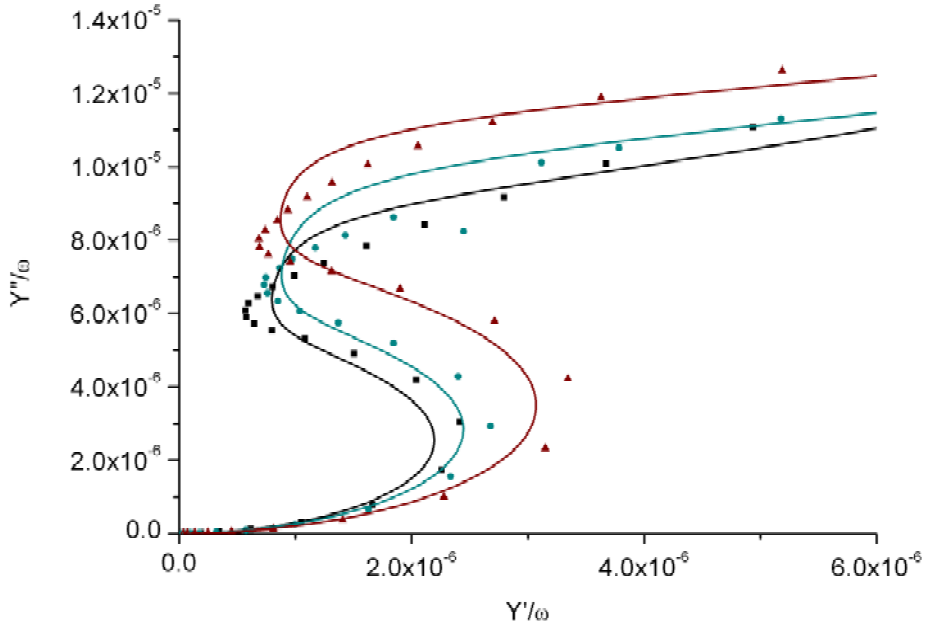

Sample	R_{ele} (Ωcm²)	R_{layer} (MΩ cm²)	CPE_{layer}-T (μFcm^{-2})	CPE_{layer}-P	C_{Au} (μFcm^{-2})
G_1^+ (■)	52	2.4	10	0.92	44
G_1^+/RSE (●)	57	3.4	10	0.92	83
G_1^+/RSE/VF (▲)	40	2.8	11	0.94	99

Fig. 5.11 – EIS data of solvent exchange followed by vesicle fusion on G_1^+ dendrimers. Left: Bode plot, right: admittance plot. Fits are indicated with solid lines.

and for P = 1 it represents a pure capacitor. The CPE takes into account system (surface) heterogeneities, which usually leads to a better fit. It must be noted, however, that P-values below 0.9 may improve the fit, but are essentially considered physically inappropriate.

The obtained data are presented as a Bode plot and a frequency-normalised Nyquist admittance plot. The background on these plots was discussed in section 2.2. The latter is necessary for observing whether the model fit is appropriate and useful to directly obtain the membrane capacitance. This capacitance approximately equals the value on the imaginary axis where the real part shows a minimum.

In Fig. 5.11 the EIS plots and fit results of lipid deposition on positively charged dendrimers are shown. The data of the deposition on negatively charged dendrimers were nearly identical and will therefore not be discussed here. The dendrimer layer shows a high resistance of 2.5 $M\Omega cm^2$. This can be explained by the hydrophobic interior of the dendrimers, which does not allow ions or electrons to pass. The Bode plot shows that lipid addition does not increase the impedance at low frequencies and the admittance plot shows a capacitance increase to 10 μFcm^{-2}. This implies that the adsorbed lipids are not organised into a well defined bilayer membrane and it could be therefore concluded that solvent exchange, even followed by vesicle fusion, is not an appropriate method for constructing lipid bilayer membranes.

The resulting 6 nm lipid deposition as observed with SPR can be explained by an unordered, perhaps even patch-wise architecture of lipids. It may well be that vesicles are adsorbing but do not fuse to a bilayer and stay intact. With dilute vesicle coverage on the surface, SPR could return an average film thickness much lower than the actual 50 nm vesicle diameter.

Vesicle Fusion

As solvent exchange did not result in the desired lipid bilayer membrane, a new approach is required. With direct vesicle fusion on the dendrimer coated

surfaces, pre-ordered lipid membranes are offered to the surface, which may enhance the possibility of well ordered membranes on the dendrimers.

In Fig. 5.12 the SPR results are shown. It could be observed that DPhyPC vesicles did not adhere and spread on positively charged dendrimers. The surface plasmon minimum did not shift to higher angles indicating that no material was deposited. On the negatively charged dendrimers the thickness increment was 1.4 nm, which is much less than the expected value for a complete bilayer membrane (approximately 6 nm). This indicates that vesicle fusion does not deposit sufficient amounts of lipids. A possible explanation will be given in section 5.3.2, where the interaction between dendrimers and vesicles was studied microscopically.

EIS spectroscopy confirmed our suspicion that vesicle fusion was not a successful approach for membrane construction either.

The impedance spectra of the experiments on positively and negatively charged dendrimers were again very similar and therefore only the results on G_1^+ are given in Fig. 5.13. As SPR did not show any lipid deposition on the positively charged dendrimers, it was not expected that the impedance spectra showed a difference between the surface with dendrimers and lipids and surfaces with only dendrimers. However, fitting the EIS parameters revealed

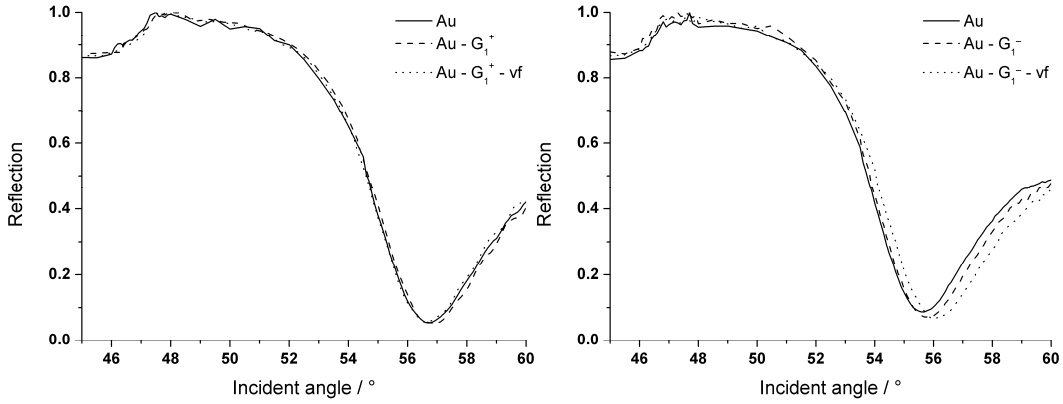

Fig. 5.12 – Vesicle fusion (vf) on dendrimer (G_1^+ and G_1^-) coated surfaces, probed by SPR. <u>Right:</u> G_1^+ dendrimer, <u>Left:</u> G_1^- dendrimer

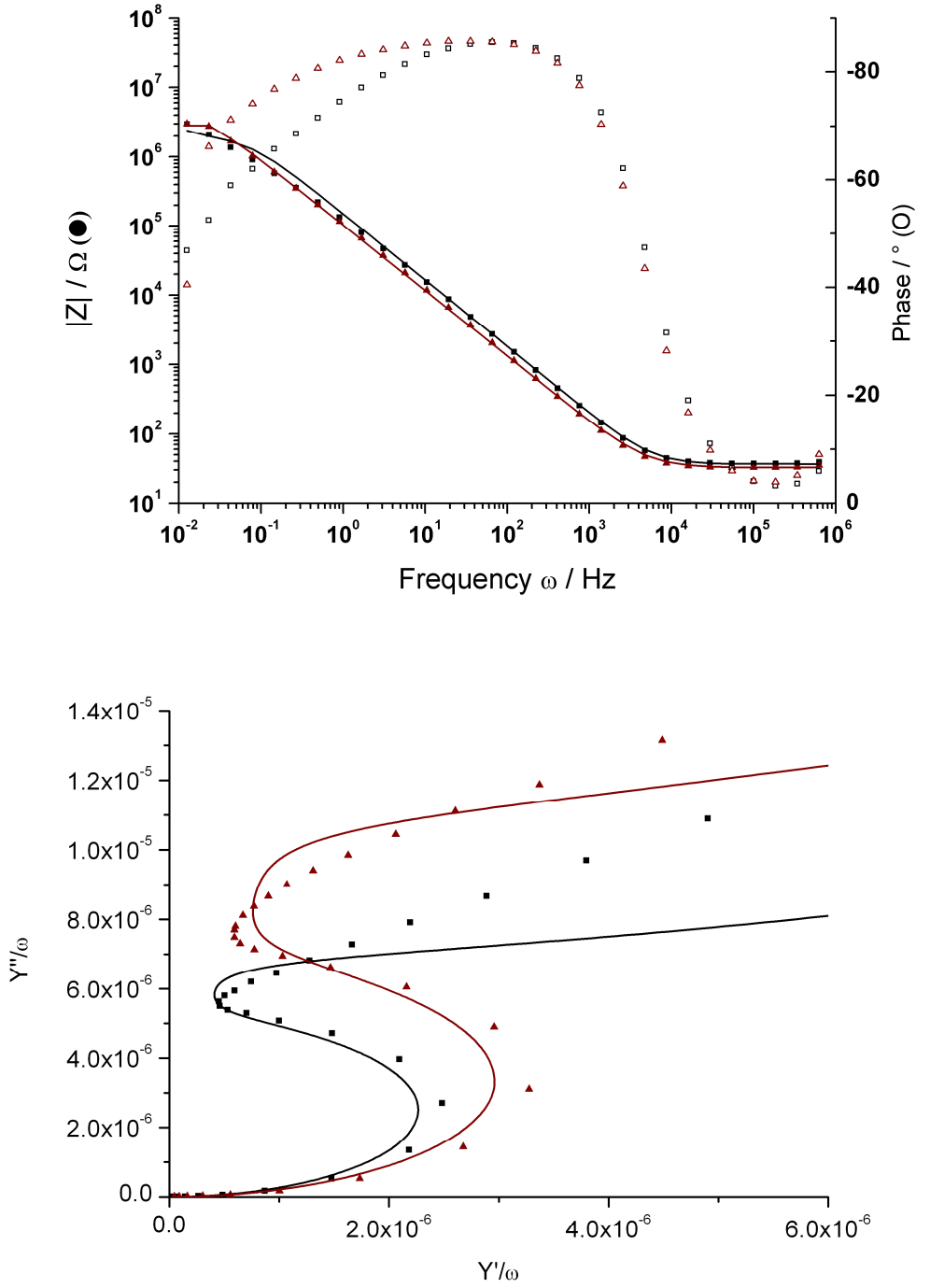

Sample	R_{ele} (Ωcm^2)	R_{layer} ($M\Omega cm^2$)	CPE_{layer}-T (μFcm^{-2})	CPE_{layer}-P	C_{Au} (μFcm^{-2})
G_1^+ (■)	36	1.8	7.5	0.96	56
G_1^+/VF (▲)	32	3.9	12	0.94	56

Fig. 5.13 – EIS data of vesicle fusion on G_1^+ dendrimers. Left: Bode plot, right: admittance plot. Fits are indicated with solid lines.

that the resistance remained constant and the capacitance increased. From this it could be concluded that both dendrimers did not allow vesicles to fuse and to form a lipid bilayer membrane.

5.3.2 GUV fusion on dendrimer supports

In order to further investigate the interactions between vesicles and dendrimer coated surfaces, GUVs were prepared and deposited on the different surfaces. GUVs have the advantage that they can be observed with optical microscopy. If the interaction between the GUV and a surface is sufficiently favourable, the GUV membrane breaks open and fuses onto the surface. This is observed as a sudden disappearance of the GUV. On the other hand, when the interaction is not attractive enough, the GUV remains intact and at most flattens into a pancake shaped object that is still clearly visible under the microscope.

A control experiment with GUVs exposed to a clean BK7 glass substrate (hydrophilic) resulted in the fusion of the membrane onto the substrate. On negatively charged dendrimers, which seemed to have the strongest attractive

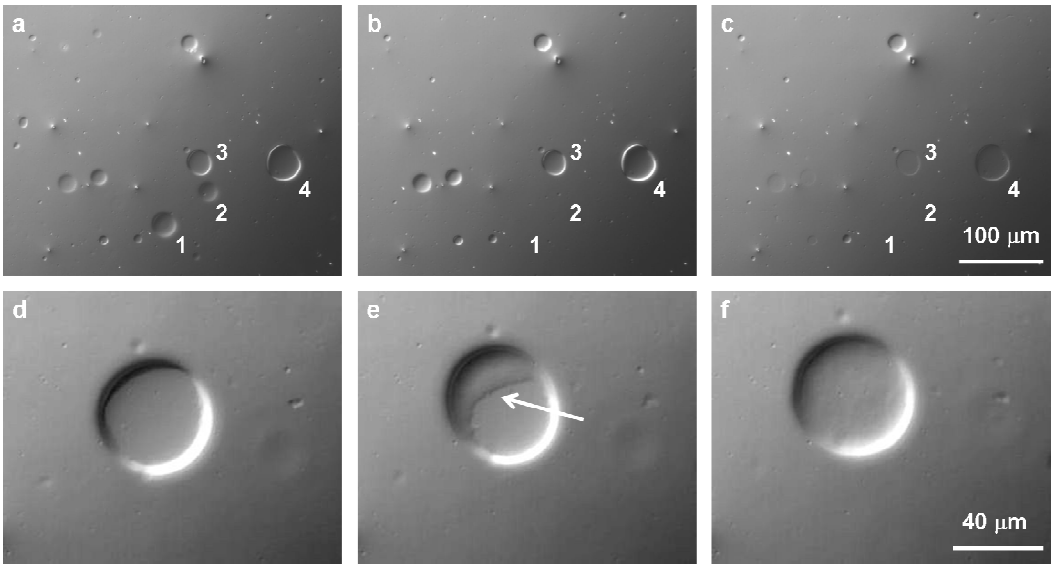

Fig. 5.14 – GUV adhesion to G_1- dendrimer coated surfaces. Images a-c: before (a) and after rinsing with buffer. Vesicles 1 and 2 are flushed off, vesicles 3 and 4 adhere strongly and flatten. Images d-f: before (d), during (e) and after (f) adhesion of GUV.

interaction with the lipids during the previous experiments, the GUVs did not burst, which is shown in Fig. 5.14.

In order to expose the vesicles to mechanical stress, the sample was rinsed with buffer. This is demonstrated in images a-c. The vesicles that had been on the surface for a while already (vesicles 3 and 4) stayed where they were, but the newly arrived vesicles (vesicles 1 and 2) were flushed off the surface. Image c shows that vesicles tend to flatten upon adhesion. Images d-f show the same vesicle undergoing different stages of adhesion. The GUV membrane is first loosely positioned on the dendrimer surface. If at a certain location on the membrane lipids start to strongly interact with the dendrimers, the area that is in intimate contact with the surface increases until the maximum contact area is reached. In image e the adhesion front of the membrane, which moves over the surface like a wave, can be observed. This process takes less than a second and does not lead to vesicle bursting or membrane fusion.

Despite the fact that this method of depositing a lipid bilayer was not successful, this result is very interesting. There are many applications that require the adhesion of vesicle-like bodies (cells) to a surface that does not introduce any side effects like cell membrane rupture or inhibition of cellular functions. Applications could include the adhesion of living cells for an active bio-interface (bio-sensing), for tissue engineering or for medical implants.

5.3.3 Protein tethered membranes on dendrimer support

As an alternative to the direct construction of free standing membranes on dendrimer supports, a membrane protein was immobilised on the dendrimers that enhances lipid organisation. This concept was shown to be successful on gold surfaces that bear a very thin thiol coating with carboxylate functionality [42, 46]. It was attempted to use the same concept on a dendrimer coated surface.

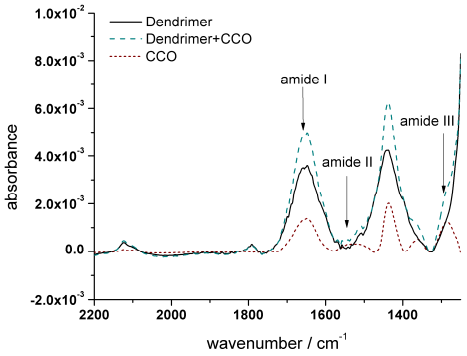

Fig. 5.15 – SEIRAS spectra of CcO immobilisation

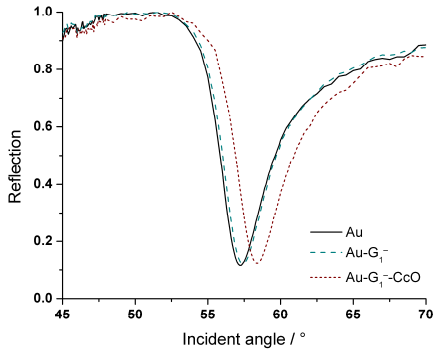

Fig. 5.16 – SPR spectroscopy on CcO immobilisation

Dendrimer support

An ATR crystal (for SEIRAS) was coated with 25 nm gold and gold nanoparticles were grown from an $AuCl_3$ solution in order to create a slightly roughened surface that gives an IR absorption signal enhancement of about a factor 5 [42, 46]. During the incubation with the polyanionic dendrimers G_1-SEIRAS spectra were recorded and the adsorption process was followed in real time until dendrimers did not adsorb anymore. The same procedure was performed on a gold coated $LaSFN_9$ glass slide in order to follow the construction by SPR.

Protein immobilisation

After coating the gold substrates with polyanionic dendrimers, a slightly acidic (pH 5.5) $NiCl_2$ solution was applied to the coated surface and Ni^{2+} ions complexed to the carboxylates of the dendrimers. Cytochrome c Oxidase (CcO) was then immobilised as a protein-surfactant complex by its His-tag, which strongly binds to the Ni^{2+} ions. This process was also followed by SEIRAS (Fig. 5.15) and SPR (Fig. 5.16). Due to the surface enhancement, the dendrimer adsorption is probed with high sensitivity. This enhancement, however, occurs only very locally (the first few nm above the surface) and thus the protein adsorption cannot be followed with the same sensitivity. As a consequence, despite the large amount of adsorbed proteins (3.6 nm, as observed with SPR), the IR response is relatively weak. The 3.6 nm thickness increment measured with SPR reflects the amount of immobilised protein.

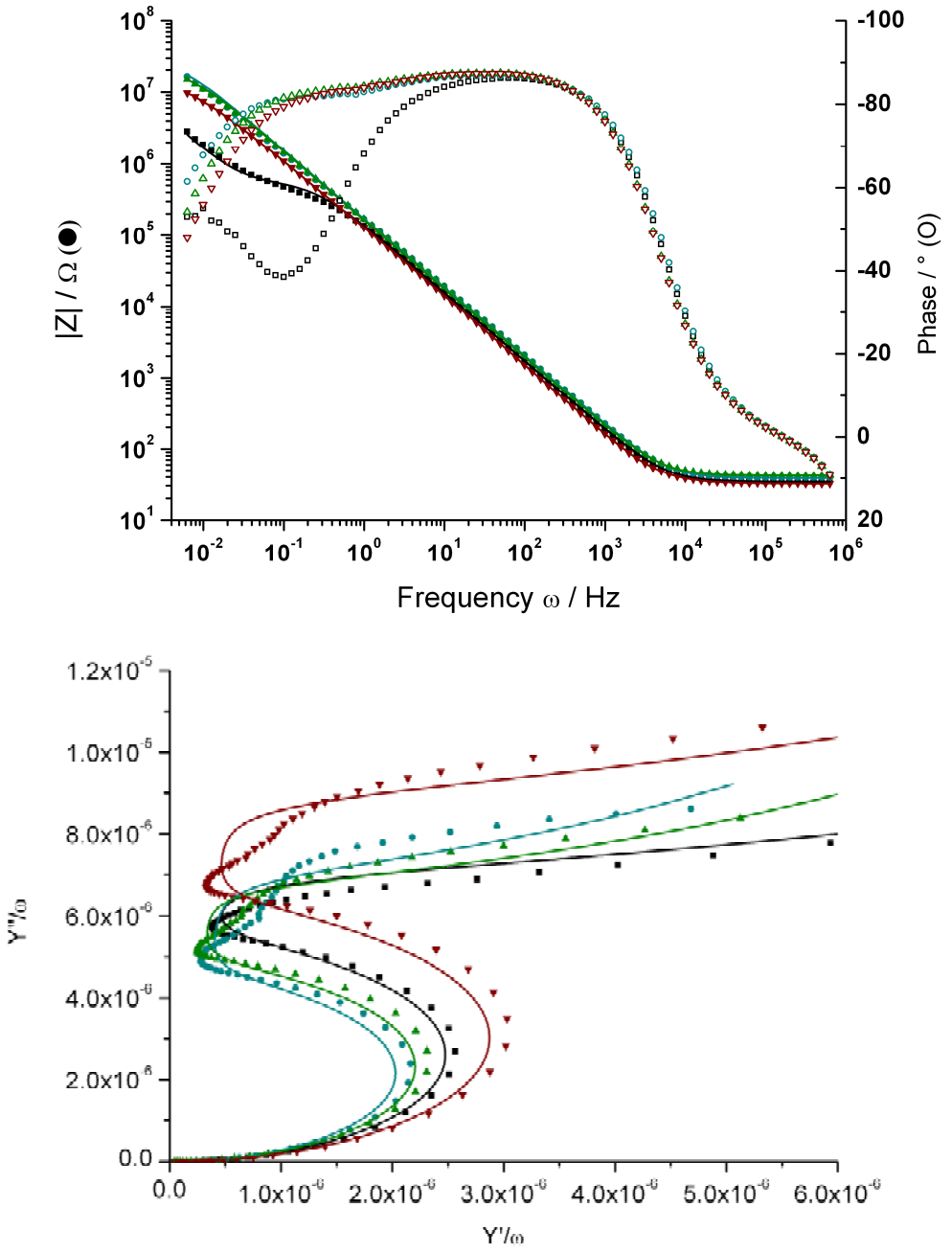

Sample	R_{ele} (Ωcm²)	R_{layer} (MΩcm²)	CPE_{layer}-T (μFcm⁻²)	CPE_{layer} -P	C_{Au} (μFcm⁻²)
G_1^- (■)	34	0.49	7.9	0.96	63
G_1^--CcO (●)	39	26	6.3	0.96	90
G_1^--CcO-DPhyPC (▲)	42	17.8	6.9	0.96	50
G_1^--CcO-DPhyPC* (▼)	33	8.3	9.7	0.95	47

Fig. 5.17 – EIS data of CcO immobilisation on G_1^- dendrimers. Left: Bode plot, right: admittance plot. Fits are indicated with solid lines. * sample re-measured after 15 hrs.

The protein shape can be approximated by a spheroid with a diameter of 10 nm. This implies that the surface coverage is 40%, which is much higher than on a very similar carboxy-thiol sample described in literature [42]. This can be explained by the comparatively large amount of chelated Ni^{2+} ions. Whereas every dendrimer on the surface complexes Ni^{2+}, the carboxy-thiols covered much less of the surface as they were mixed with a non-functionalised thiol.

Impedance studies (Fig. 5.17) on the samples revealed a clear protein deposition on the surface, which was observed as a significant increase in resistance. The admittance plot shows a decrease in capacitance during CcO immobilisation, but it increases again with the addition of lipids. This suggests that organic material is first deposited but then partly removed again. This might correspond to the replacement of DDM by the lipids. The next day, the sample was measured again and the lipid-protein film was found to be instable: the resistance decreased significantly and the capacitance increased, indicating an additional loss of organic material.

Protein Functionality

In order to test whether the protein was still fully active after immobilisation on the dendrimer surface, its redox behaviour was monitored. CcO contains two heme groups and two copper atoms complexed inside its polypeptide

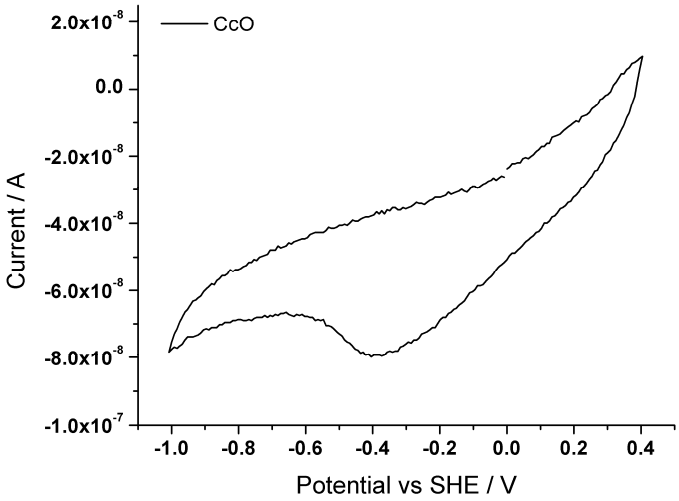

Fig. 5.18 – CV scan of immobilised CcO activity on G_1- dendrimers.

backbone which only show their characteristic redox behaviour when the protein is folded in its active conformation. After the DDM surfactants were exchanged with DPhyPC lipids and caught off by bio-beads, the system was rinsed with PBS buffer and directly tested for its protein functionality with cyclic voltammetry (Fig. 5.18). Whereas the protein normally displays a reversible electrochemical response with different oxidation and reduction peaks that correspond to the different redox centres, it appeared inactive when immobilised on the dendrimers. This suggests that the protein may be irreversibly damaged during the experiments, which can be explained by a strong interaction between its hydrophobic regions and the interior of the dendrimers. Additionally, a very low current was observed, which is in agreement with the high resistance of the dendrimer layer. This implies that a dense layer of this type of dendrimers cannot be applied in electrochemical sensory devices. In other studies [42], the protein activity was studied by a potentiostatic titration of the sample on top of the ATR crystal in the SEIRAS setup. The protein adapts its conformation upon oxidation or reduction of its redox centres, giving rise to a change in relative intensity of the amide bands in the SEIRAS spectrum. However, as can be observed in Fig. 5.15, the amide I band overlaps with the carboxylates of the dendrimers. Therefore it is impossible to assign any change in that region to either the protein or dendrimer. The results of the potentiostatic titration are therefore omitted.

5.4 Discussion

In this chapter, the application of generation 1 phosphorus dendrimers as polymeric supports for bio-mimicking membranes was discussed. For the assembly of supported membranes on dendrimers, different dendrimers and lipid deposition methods were deployed. It was possible to adsorb lipids by solvent exchange and it was observed that more lipids adsorbed on negatively charged dendrimers than on positively charged dendrimers. This can be explained by the attractive electrostatic interaction between the choline moiety of the lipid and the carboxylates of the dendrimers. By subsequent vesicle fusion, more lipids were deposited and the deposited amount was self-

limiting to 6 nm. This value agrees with the expected amount for a lipid bilayer. However, impedance spectroscopy showed unambiguously that the lipids were not ordered for it showed neither a decreased capacitance nor an increased membrane resistance.

It was attempted to exploit the hydrophobic domains of Cytochrome c Oxidase (CcO) to bring order to the lipids and support the formation of a well-defined bilayer membrane. Therefore CcO was successfully immobilised to polyanionic dendrimers *via* a His-tag. This process was followed real-time by SPR and SEIRAS. The surfactants that stabilise the protein were exchanged by DPhyPC as described in literature [40-42], but Cyclic Voltammetry showed that the protein was inactive. This may be explained by an interaction between the hydrophobic parts of the dendrimer coating and the protein. As the proteins were present in large amounts on the surface, they may have interacted with each other, which ultimately may have led to protein aggregation. This may cause the protein to irreversibly lose its active conformation. Additionally it could be concluded that also this architecture did not enhance the lipid order into a well-defined membrane. This can be explained by the large number of proteins on the surface and by the fact that they were not organised (standing up) themselves. The proteins were therefore unable to enhance lipid organisation.

The deposition of GUVs on polyanionic dendrimers gave an interesting result. The interaction was insufficient to make the vesicles spread and fuse into a bilayer, but it was strong enough to immobilise them on the surface. The application of mechanical force on the vesicles (by introducing a solution flow) did not lead to a release of the vesicles from the dendrimers. This can be particularly interesting for applications where vesicle-like bodies with lipid bilayers should adhere but not break. Examples of such an application are the adhesion of living cells for an active bio-interface (bio-sensing), for tissue engineering or for medical implants. This is further investigated in the next chapter.

5.5 Synopsis and Conclusion

Different methods and approaches have been used for the construction of a biomimetic lipid membrane on a dendrimer support. SPR, EIS and SEIRAS have shown that it is possible to adsorb lipids to dendrimer coated gold surfaces by solvent exchange and vesicle fusion. However, EIS showed unambiguously that the lipids had not organised themselves into a well-ordered membrane. It was attempted to enhance lipid order by tethering proteins to the dendrimer surface. EIS, however, showed again the low degree of lipid organisation. In all cases, the semi-hydrophobic character of the dendrimers was held responsible for the lack of lipid organisation. GUVs did not spread and fuse on dendrimers into a lipid bilayer either, but this property could be exploited for medical applications like tissue engineering and implant incorporation.

5.6 Materials and Methods

In this section all technical and experimental details are described. All water used is demineralised using MilliQ equipment and the resistivity was 18 MΩ.cm.

5.6.1 Sample preparation

Cleaning procedures

The glass cover slips (3.75 x 2.5 cm) were first thoroughly cleaned. They were twice submerged in a 2% aqueous solution of the detergent Hellmanex and once to HPLC grade ethanol and exposed to ultrasonic waves for 15 minutes. In between, the samples are rinsed with an excess of water and ethanol, respectively. Finally they are dried with a stream of nitrogen gas.

Silicon wafers were cleaned using hot basic piranha solution (1:1:5 NH_3 (35%): H_2O_2 (35%): H_2O) at 75°C for 30 minutes. They were subsequently rinsed with water and HPLC grade ethanol and stored under inert gas until their processing into TSG.

The surface of the silicon ATR crystal (for SEIRAS) was polished prior to use with a polishing machine (Buehler PHOENIX 4000) using the polishing cloth TexMet P, VerduTex, and MicroCloth and MetaDi Supreme and polycrystalline diamond suspension, grain size 9 µm, 3 µm, and 1 µm, in that order. The polished trapezoid crystal was ultrasonically cleaned with ethanol for 15 min.

Template stripped gold (TSG) samples

Using electrothermal evaporation at reduced pressure (ca. 5.10^{-6} mbar) 50 nm gold was evaporated onto ultra smooth Silicon wafers (Crystec, roughness < 1 nm). The equipment used was an Edwards Auto 306 and it allows the samples to turn around to guarantee a homogenously distributed gold layer. Cleansed BK7 glass were pressed to the gold using an expoxy glue (EPO-TEK, Epoxy Technology, USA) that was degassed for 1 hour at 10^{-3} mbar prior to application. The glue was cured in an oven at 150°C. Shortly before usage, the TSG samples were stripped from the silicon wafers to avoid any contamination.

ATR Crystal preparation

By electrothermal evaporation (Edwards FL 400) a 25 nm gold layer was deposited on the flat surface of the ATR crystal (for SEIRAS) and the crystal was carefully rinsed with ethanol and dried under a stream of nitrogen. It was subsequently immersed into a 50 mL aqueous solution of hydroxylamine hydrochloride ($NH_2OH{\cdot}HCl$, 0.4M) to which a 500 µL 0.3 mM $AuCl_3$ (gold(III) chloride hydrate) was added. After 2 minutes an equal amount of $AuCl_3$ was added. This step is repeated 5 times so that the crystal spent in total 10 minutes in this growth solution. The samples were removed from the solution, carefully rinsed with water and dried with a stream of nitrogen.

Dendrimer, Nickel, Protein and Lipid coating

The freshly prepared gold samples were exposed to a 1 mg/mL aqueous solution of the generation 1 (G1) polyanionic dendrimers bearing one dithiolane functional group connected to the core (Fig. 5.6). The samples were exposed to this solution until the real time kinetic mode of SPR or SEIRAS showed a stable plateau value and were then excessively rinsed with water.

A 40 mM $NiCl_2$ solution was prepared using water that contains 3 mL/L acetic acid. This solution is titrated to pH 5.5 using KOH. The previously dendrimer coated surface is exposed to this solution for 15 minutes, which is long enough to complexate a sufficient amount of Nickel cations to the dendrimers' carboxylates. The sample is then first rinsed with water of pH 5.5 before rinsing with neutral pH water. This prevents sedimentation of $NiCl_2$.

The His-tagged bacterial CcO protein was provided by Prof. B. Gennis (University of Illinois) and Prof. S. Ferguson-Miller (Michigan State University). The protein samples contained DDM as a stabilising agent (dodecyl-β-D-maltoside). The protein was dissolved in a 1 mg/mL PBS buffer (100 mM K_2HPO_4, 50 mM KCl, 0.1% DDM, pH 8) to a concentration of 10 nM. The sample surfaces are exposed to the protein solution (500 µL) until the adsorption kinetics, as observed from SPR or SEIRAS, reached a stable value. The sample is then rinsed with the PBS solution containing DDM.

For the experiments on an ATR crystal, the lipids were deposited by applying a PBS solution that contains 10 µg/mL DPhyPC and 1 mg/mL DDM. The lipid deposition of the other experiments is discussed below.

5.6.2 Lipid deposition methods

DPhyPC

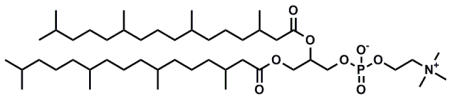

Fig. 5.19 – DphyPC: 1,2-di-*O*-phytanoyl-*sn*-glycero-3-phosphocholine

DPhyPC was obtained from Avanti Polar Lipids (USA) and used without further purification.

Vesicle Fusion

A 2 mg/mL aqueous DPhyPC suspension was prepared, heated to 75°C for one hour and stored cool. From this solution, a 250 µL aliquot was taken and extruded using a 50 nm filter. The resulting solution is clear and contains SUVs of 50 nm. From this solution, 50 µL was taken and transferred into the sample holder that contains water or PBS solution. The binding process of the lipids is followed in kinetic mode SPR and was terminated when a plateau value was reached. The sample was rinsed with water.

Rapid Solvent Exchange

An ethanolic solution containing 5 mg/mL DPhyPC lipids was prepared. From this solution 50 µL was transferred into a sample holder already containing ethanol. The sample was exposed to this solution for 10 minutes and subsequently rinsed, quickly and extensively, with water.

GUV preparation and deposition

Two ITO (Indium Tin Oxide) slides and a PDMS (polydimethylsiloxane) ring were thoroughly cleaned with the usual procedure. A 1 mg/mL DPhyPC solution in chloroform was prepared and spread on one side of each ITO slide. The chloroform was evaporated under reduced pressure during 15 hours. The two slides, spaced by the ring, were pressed together with the lipid-coated side towards each other. The space between the slides was filled with a 200 mM

aqueous saccharose solution (which will avoid osmotic stress and which makes the GUVs having a higher density than water). The ITO slides were connected to the electrodes of a DC power source, which applied a differential potential to it (base potential 0 V, amplitude 1 V. frequency 10 Hz (1.5 hrs) and 5 Hz (subsequent 30 minutes). This procedure yields GUVs with rather variable sizes (500 nm-50 μm), but by far the most observed vesicles were approximately 10 μm. A similar approach is decribed in [47].

The dendrimer coated slides were mounted onto a Zeiss Axioskop microscope table and a water (100 mM KCl) droplet connected the slide with the objective (Zeiss Achroplan 40x 0.8W). To this droplet, a small amount of GUV solution was added and the GUVs were followed (by manual focus) on their way sinking to the substrate. Images were taken using a CMOS camera (μEye UI-1540).

5.6.3 Characterisation techniques

Surface Plasmon Resonance spectroscopy experiments and contact angle measurements were carried out as described in 3.5.4.

Surface Enhanced InfraRed Absorption Spectroscopy

The SEIRAS experiments were performed with a Bruker Vertex 70. Every scan contained 5555 scans and the measurements were carried out with a mirror velocity of 120 kHz. The obtained data were corrected for the base line (linearly) and for the presence of water (with a spectrum of pure water: bands at 1240 cm^{-1} and 1648 cm^{-1}).

Electrochemical Impedance Spectroscopy

The EIS experiments are conducted simultaneously with the SPR experiments. The sample surface is connected to a PTFE cell that allows for flowing different solvents over the surface without having to dismantle the setup. This flow cell has thus two connections for liquids, but also two holes into which an Ag/AgCl reference electrode and a platinum counter electrode

can be inserted. The sample surface itself acts as the working electrode. The Impedance Spectrometer (Autolab, PGSTAT12, The Netherlands) applied a base potential of zero Volts and a differential potential with an amplitude of 10 mV at frequencies logarithmically distributed over the frequency range of interest (10^6 until 10^{-2} Hz). All experiments are conducted with 100 mM KCl present in the flow cell, or with 100 mM PBS buffer.

All data were analysed with ZView 3.0 (Scribner Associates, Inc.) and fitted with equivalent circuits.

Cyclic Voltammetry

Cyclic Voltammetry (CV) is a technique that offers information about the dynamics of redox processes. It provides the redox potentials and insight into the reversibility of the redox reactions. In this chapter, CV was performed simultaneously with SPR by mounting electrodes (Ag/AgCl reference and counter electrode) to the flow cell. The gold surface acted like the working electrode. The potentiostat (Autolab, PGSTAT12) scanned at a rate of 50 mVs^{-1} and in a potential window between -1.0 and +0.4 V (vs SHE).

5.7 Bibliography

[1] S. Lingler, I. Rubinstein, W. Knoll, A. Offenhäusser, Langmuir 13/26 (1997) 7085.
[2] E. Kalb, S. Frey, L.K. Tamm, Biochimica et Biophysica Acta (BBA) - Biomembranes 1103/2 (1992) 307.
[3] R.E. Pagano, J.N. Weinstein, Annual review of biophysics and bioengineering|Annual review of biophysics and bioengineering (1978) 435.
[4] R.A. Schwendener, P.A. Lagocki, Y.E. Rahman, Biochim Biophys Acta 772/1 (1984) 93.
[5] J.L. Rigaud, D. Levy, Methods in Enzymology 372 (2003) 65.
[6] J. Lindstrom, R. Anholt, B. Einarson, A. Engel, M. Osame, M. Montal, Journal of Biological Chemistry 255/17 (1980) 8340.
[7] K.H. Leung, P.C. Hinkle, Journal of Biological Chemistry 250/21 (1975) 8467.
[8] Y. Kagawa, A. Kandrach, E. Racker, Journal of Biological Chemistry 248/2 (1973) 676.
[9] R.C. Carroll, E. Racker, Journal of Biological Chemistry 252/20 (1977) 6981.
[10] P. Mueller, D.O. Rudin, Nature 217/5130 (1968) 713.
[11] P. Mueller, D.O. Rudin, Nature 213/5076 (1967) 603.
[12] W.I. Gruszecki, A. Wardak, W. Maksymiec, Journal of Photochemistry and Photobiology B-Biology 39/3 (1997) 265.
[13] G. Belmonte, L. Cescatti, B. Ferrari, T. Nicolussi, M. Ropele, G. Menestrina, European Biophysics Journal with Biophysics Letters 14/6 (1987) 349.
[14] J. Vecer, P. Herman, A. Holoubek, Biochimica Et Biophysica Acta-Biomembranes 1325/2 (1997) 155.
[15] M. Winterhalter, Curr Opin Colloid In 5/3-4 (2000) 250.

[16] W.C. Bigelow, D.L. Pickett, W.A. Zisman, Journal of Colloid Science 1/6 (1946) 513.
[17] E.K. Sinner, W. Knoll, Current Opinion in Chemical Biology 5/6 (2001) 705.
[18] S.M. Schiller, R. Naumann, K. Lovejoy, H. Kunz, W. Knoll, Angew Chem Int Edit 42/2 (2003) 208.
[19] B. Raguse, V. Braach-Maksvytis, B.A. Cornell, L.G. King, P.D.J. Osman, R.J. Pace, L. Wieczorek, Langmuir 14/3 (1998) 648.
[20] R. Naumann, E.K. Schmidt, A. Jonczyk, K. Fendler, B. Kadenbach, T. Liebermann, A. Offenhausser, W. Knoll, Biosensors & Bioelectronics 14/7 (1999) 651.
[21] R. Naumann, S.M. Schiller, F. Giess, B. Grohe, K.B. Hartman, I. Karcher, I. Koper, J. Lubben, K. Vasilev, W. Knoll, Langmuir 19/13 (2003) 5435.
[22] R. Naumann, T. Baumgart, P. Graber, A. Jonczyk, A. Offenhausser, W. Knoll, Biosensors & Bioelectronics 17/1-2 (2002) 25.
[23] G. Krishna, J. Schulte, B.A. Cornell, R.J. Pace, P.D. Osman, Langmuir 19/6 (2003) 2294.
[24] G. Krishna, J. Schulte, B.A. Cornell, R. Pace, L. Wieczorek, P.D. Osman, Langmuir 17/16 (2001) 4858.
[25] W. Knoll, C.W. Frank, C. Heibel, R. Naumann, A. Offenhausser, J. Ruhe, E.K. Schmidt, W.W. Shen, A. Sinner, J Biotechnol 74/3 (2000) 137.
[26] R. Guidelli, G. Aloisi, L. Becucci, A. Dolfi, M.R. Moncelli, F.T. Buoninsegni, Journal of Electroanalytical Chemistry 504/1 (2001) 1.
[27] F. Giess, M.G. Friedrich, J. Heberle, R.L. Naumann, W. Knoll, Biophys J 87/5 (2004) 3213.
[28] E. Sackmann, M. Tanaka, Trends Biotechnol 18/2 (2000) 58.
[29] M.L. Wagner, L.K. Tamm, Biophys J 79/3 (2000) 1400.
[30] C. Miller, P. Cuendet, M. Gratzel, Journal of Electroanalytical Chemistry 278/1-2 (1990) 175.
[31] C. Peggion, F. Formaggio, C. Toniolo, L. Becucci, M.R. Moncelli, R. Guidelli, Langmuir 17/21 (2001) 6585.
[32] B.A. Cornell, V.L.B. BraachMaksvytis, L.G. King, P.D.J. Osman, B. Raguse, L. Wieczorek, R.J. Pace, Nature 387/6633 (1997) 580.
[33] T. Stora, J.H. Lakey, H. Vogel, Angew Chem Int Edit 38/3 (1999) 389.
[34] J. Spinke, J. Yang, H. Wolf, M. Liley, H. Ringsdorf, W. Knoll, Biophys J 63/6 (1992) 1667.
[35] H. Sigl, G. Brink, M. Seufert, M. Schulz, G. Wegner, E. Sackmann, European Biophysics Journal with Biophysics Letters 25/4 (1997) 249.
[36] H. Hillebrandt, G. Wiegand, M. Tanaka, E. Sackmann, Langmuir 15/24 (1999) 8451.
[37] J. Majewski, J.Y. Wong, C.K. Park, M. Seitz, J.N. Israelachvili, G.S. Smith, Biophys J 75/5 (1998) 2363.
[38] J.C. Munro, C.W. Frank, Langmuir 20/24 (2004) 10567.
[39] J.Y. Wong, J. Majewski, M. Seitz, C.K. Park, J.N. Israelachvili, G.S. Smith, Biophys J 77/3 (1999) 1445.
[40] K. Ataka, F. Giess, W. Knoll, R. Naumann, S. Haber-Pohlmeier, B. Richter, J. Heberle, J Am Chem Soc 126/49 (2004) 16199.
[41] M.G. Friedrich, J.W.F. Robertson, D. Walz, W. Knoll, R.L.C. Naumann, Biophys J 94/9 (2008) 3698.
[42] C. Nowak, C. Luening, D. Schach, D. Baurecht, W. Knoll, R.L.C. Naumann, Journal of Physical Chemistry C (2009) 2256.
[43] E. Hochuli, H. Dobeli, A. Schacher, Journal of Chromatography 411 (1987) 177.
[44] R. Koradi, M. Billeter, K. Wuthrich, Journal of Molecular Graphics 14/1 (1996) 51.
[45] J. Voros, Biophys J 87/1 (2004) 553.
[46] C. Nowak, C. Luening, W. Knoll, R.L.C. Naumann, Applied Spectroscopy 63/9 (2009) 1068.
[47] R. Dimova, S. Aranda, N. Bezlyepkina, V. Nikolov, K.A. Riske, R. Lipowsky, Journal of Physics-Condensed Matter 18/28 (2006) S1151.

6 Biocompatibility of dendrimer coatings towards Human Osteoblast Cells

Organic surface coatings are applied in many fields of research and applications. For example, they are used to treat medical implants. Implant surfaces must either enhance or obstruct cell and/or protein adhesion, depending on the type of application. In this work, the response of Human Osteoblast (HOB) cells to gold-coated glass slides with a layer of covalently bound dendrimers was tested. HOB cells did initially adhere, spread, grow and proliferate on the dendrimer coatings. However, when polycationic dendrimers were applied, the cells showed a gradually increasing rate of apoptosis. In contrast, on the negatively charged dendrimers no apoptosis was observed. Cells that grew on positively charged dendrimers showed a twice to three times reduced cell number, viability, confluence and generation number. This difference was attributed to the stronger electrostatic attraction between the peripheral cationic tertiary amines of the dendrimers and the negatively charged cell membrane, reducing the necessary cell mobility.

6.1 Introduction

6.1.1 Osteoblasts

Osteoblast (greek: bone germ) cells play an important role in bone formation (osteogenesis). They produce collagen and are responsible for the mineralisation of the osteoid matrix, the calcium rich matrix that gives bones their mechanical strength. Osteoblasts are constantly involved in renewing and reshaping bone tissue, until elderly age when the production of new Osteoblasts retards.

6.1.2 Cell adhesion on polymer coated surfaces

Medical implants have to be integrated into various types of tissue. Therefore, an optimal interaction between the surrounding tissues and the surface of the implant is necessary. Therefore, it is important to understand the factors that govern these interactions. As different cell types often react entirely different to an environment [1], there is a wealth of parameters to study for the optimisation of surfaces to serve their purpose as implants or solid support for tissue generation. This section shortly discusses the recent developments made in understanding the interplay between surface properties such as surface chemistry and morphology and the cell response (Osteoblast in particular [2-3]), on both a cellular and molecular scale.

For some applications in biomedicine (temporary implants), the term “biocompatibility” implies that a surface must not provoke cell adhesion, inflammatory reactions, protein adsorption and it should show minimal biological response. In other cases, where full body incorporation of implants is required, “biocompatibility” features strong cell adhesion, proliferation and/or protein adsorption. There have been extensive studies on surface-cell interactions and an enormous number of surface properties can affect a cell

response in contact with a substrate. Among those properties are hydrophilicity [4], surface charge, surface energy [5], protein adsorption [6] and surface topography and morphology [3, 7-12], which all can influence cell-surface interaction. A selection of these parameters, polymer coatings, the influence of surface charge and proteins and peptides will be discussed in more detail below.

Polymer coatings and surface charge

Charge neutral phosphorylcholine polymer coatings can be used to prevent bioadhesion [1]. Rose *et al.* developed cationic phosphorylcholine coated surfaces and the cationic charge seemed to enhance the cell attachment, possibly through electrostatic attraction [13-16]. This finding was confirmed for human umbilical vein endothelial cells [17], Osteoblasts [18-19], to a lesser extent for fetal cortical neurons on dendrimers [20] and other cells [21-22]. For example, the sign of the surface charge did not greatly influence the number of adhered smooth muscle cells, but significantly affects the cell morphology. Zwitterionic surfaces appeared to be less favourable for cell adhesion [23]. For Osteoblasts it was found that positively charged amino coated titanium surfaces enhanced the first steps towards Osteoblast adhesion [19]. This could be related to the negative charge of hyaluronan that is involved in the early adhesion process [24]. In some cases, cell adhesion was minimal, irrespective of the charge of the (metacryloyloxyethyl) polymer coating [25], probably because other parameters such as the chemical nature of the polymer or the surface roughness prevented cell adhesion.

Results on polymer multilayers were more diverse. On dendrimer multilayers, either carboxy or amine terminated, neurons attach and proliferate [20]. On elastin-like polypeptide multilayers [26], cells grow better on thicker multilayers. However, for PLL-DS (poly-L-lysine and dextran sulphate) systems, less layers seemed preferred by the cells [17]. In other cases [27], the layer number had no influence on cell adhesion.

Protein and peptide coatings for osteogenesis

On a molecular scale, recent approaches have been concentrated on designing "biomimetic" surfaces, which would be attractive for (Osteoblast) cells. Substrates have been coated with special ligands that, sometimes specifically, actively trigger the cell to adhere and proliferate through recognition by a receptor protein in the cell membrane. This can be done using proteins or oligopeptides [28-32] that contain the partial amino acid sequence of an extracellular matrix protein (Fibronectin [17, 33-34], Vitronectin [28] or Osteopontin [32]). This principle has even been shown to be applicable to hydrophobic surfaces [32], despite the fact that cells have a strong preference for hydrophilic surfaces.

One type of ligand is an oligopeptide which is covalently attached to the surface [28-31]. When the peptide contains the tripeptide RGD motif, it specifically evokes a signalling pathway via the interaction with the integrin receptor. Integrins are involved in cell signalling and thereby in defining cell shape, mobility and cell cycle regulation. This receptor also mediates the attachment of the cell to surrounding tissue or the extracellular matrix *via* so-called cell adhesion molecules. Another peptide, which reproduces the (352-360) sequence of Vitronectin, indirectly (*via* heparins) provokes the excretion of Vitronectin, a glycoprotein that is usually found in the extracellular matrix to promote cell adhesion and spreading. This second sequence appears to function in a more specific way, as Osteoblasts do adhere and endothelial cells were shown not to adhere.

On a cellular scale, Osteoblasts appear to adhere into intimate layers on smooth surfaces, though their adhesion strength appears to be much higher on rough surfaces [11]. Surface morphology and its roughness order, more than the roughness amplitude, affects the response of cells [11, 35-38] and in particular their adhesion.

Fig. 6.1 gives a clear indication of the subtleness of the balance between good and poor cell adhesion. In this case surfaces coated with different amounts of a RGD-sequence, showed entirely different fibroblast morphologies. The

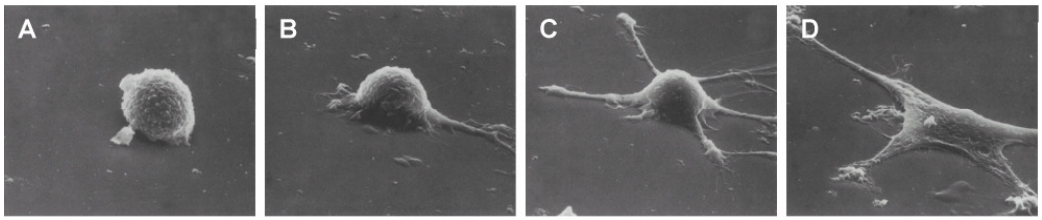

Fig. 6.1 – SEMs of adherent fibroblast cells on surfaces with increasing RGD content (A → D) showing different morphologies. A spheroid, B spheroid with 1-2 filapodial extensions, C spheroid with many filapodial extensions, D flattened and well spread. [39]

stretched cells have a large contact surface, indicating a good interaction of the cell with the surface. Where the cells are rounded, the interaction is poor.

Cells on dendrimer-coated surfaces

Only very few reports on cell adhesion to dendrimer coated or dendronised surfaces can be found. Neurons have a good affinity and proliferation on multilayered G4 phosphorus dendrimer surfaces, irrespective of the charge of the outer layer [20]. On (G1-G4) dendronised surfaces with a hydroxyl extremity (non-ionic) and a PAMAM-like cascade structure, human corneal epithelial cells and mouse fibroblasts were found to adhere very well [40].

6.1.3 Apoptosis

In essence, two types of cell death can be distinguished. The first is necrosis [41], a process that can be provoked by injuries, infections, cancer, poisoning and other external causes. It usually causes inflammatory reactions in the particular cell and surrounding tissue. Because necrotic cells are sometimes unable to communicate their suffering with the immune system, the body cannot react appropriately to the trauma, for instance by removing the dead cells. This may have fatal consequences for the organism.

Under certain circumstances, cells are triggered to undergo programmed cell death, which is called apoptosis [41-42]. It is a form of suicide that is beneficial for the organism as a whole. It can be evoked by many different stimuli, including (UV) radiation, starvation, DNA damage, toxic chemicals

and other compromising conditions. The body or the cell itself decides via chemical signalling (NGF, Interleukin-2) for dismantling into its separate components before it becomes dangerous for surrounding cells. However, also healthy tissue and organisms show apoptosis and it seems to play a vital role in the well-being of the organism. One task is keeping the balance between cell division and cell death in order to keep the body dimensions stable and to replace old cells with new ones. In special cases, apoptosis even forms a key process behind the development of the multicellular organism, like the termination of cells between the fingers on a hand.

In apoptosis three phases can be distinguished: the induction phase, execution phase and end phase. Each of them will be shortly described here.

Induction phase

This phase is activated by intrinsic and extrinsic factors that enable a cell to determine itself whether it is redundant or compromising the organism's health. Those factors include the

- ✓ internal stress: ATP level, pH value, Ca^{2+} concentration and the glucose level,
- ✓ external stress: UV radiation, toxins and mutagens, lack of cell-cell contact.

Three different signalling pathways can be distinguished. If the cell receives an extrinsic signal, this signal is processed by receptors and Caspase 8. Intrinsic signals lead to the other two pathways: mitochondrial damage leads to a Cytochrome C release (followed by Caspase 9) and stress in the Endoplasmatic Reticulum results in a Ca^{+2} release (followed by Caspase 12). The initiator Caspases (8, 9 and 12) are enzymes that activate effector Caspases (3, 6 and 7), which are responsible for carrying out the actual apoptosis process.

For example, Cytochrome C is located in the intermembrane space of mitochondria (between the inner and outer membrane) and is a crucial redox

mediator in the respiratory chain where it transports one electron between Complex III and Complex IV (5.1.3). Its release is usually preceded by an elevated Calcium level (due to a malfunctioning Endoplasmic Reticulum, ER) and it accelerates the release of Calcium and thereby its own release in large amounts. Free Cytochrome C activates the initiator Caspase 9, a protease that mediates in the activation of Caspase 3 and Caspase 7. The latter proteases are responsible for the destruction of all proteins and thereby all cell activity from inside.

Execution phase

The Caspase cascade system is activated by either intrinsic or extrinsic factors and the initiator Caspases are activated by proteolytic cleavage. They activate the effector Caspases, which dismantle the cell from inside. All proteins and the cytoskeleton are being cut to pieces. Nucleases are activated to cleave the nucleosomes and the nuclear membrane starts leaking.

End phase

Once the apoptosis process is activated, all proteins and DNA are being destroyed. Chromatin condensation takes place and the cell nucleus starts fragmenting. Furthermore cell shrinkage and “membrane blebbing” (the

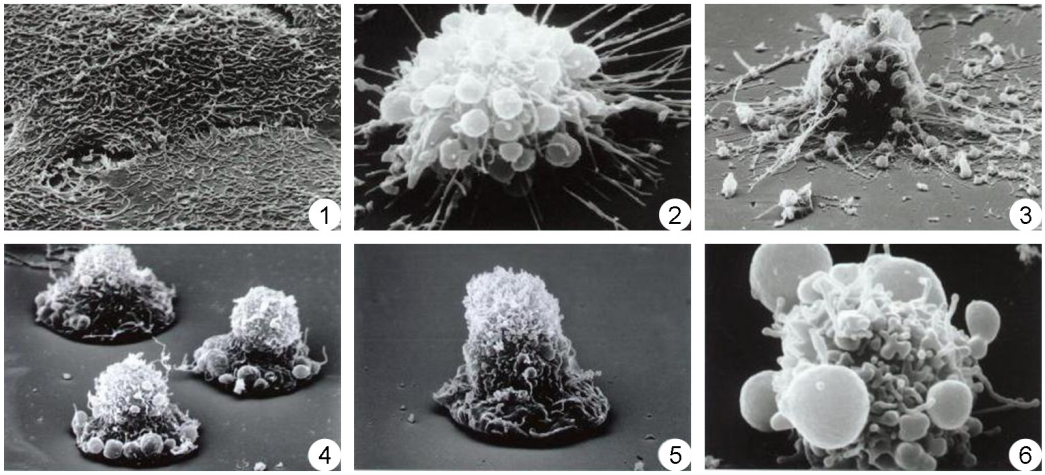

Fig. 6.2 – EM images of healthy spread cells (1) and of advancing apoptosis with retraction, membrane blebbing and apoptotic body formation (2-6) (edited from [43]).

formation of quasispherical protrusions [44]) can be observed, as well as that cells lose contact with their neighbouring cells. Ultimately the dead cells decay into so-called apoptotic bodies and neighbouring cells and macrophages start consuming the rest materials by phagocytosis.

Apoptosis and polymers

Polyelectrolytes in solution were also shown to be able to trigger apoptosis. Several studies on different cell types (human lung cells [45], macrophages [46], ovarian cancer cells [47] and human breast cancer cells [48]) revealed that polycationic PAMAM (polyamidoamine) and polypropylenimine [49] dendrimers negatively affect several cellular functions and can induce apoptosis mediated through a massive drop of the mitochondrial membrane potential. This is explained by the fact that positively charged dendrimers easily diffuse through biomembranes and compromise the mitochondrial membranes' integrity, which results in the release of Cytochrome C. This activates the Caspase cascade, the typical apoptotic reaction. Polyanionic dendrimers appear to be completely harmless.

Also linear polymers can have cytotoxic effects. In one study [50], different polycationic polymers were tested (linear, dendritic and cationised proteins) for their relative cytotoxicity to different cell types. Normally, cytotoxicity increases with the molecular weight [51-54], substitution degree of amines (tertiary > secondary > primary) [50, 55], charge density [56-57], degree of branching [56] and flexibility [57-58]. The G3 starburst PAMAM dendrimers appeared to be relatively harmless, unlike the reports discussed above. However, in this comparative study the cell viability was monitored for only 24 hours (which possibly excludes the observation of a longer term apoptotic cell death induced by dendrimers) whereas the specific dendrimer studies above were conducted for at least 72 hours.

Surface-mediated apoptosis

There are not many reports on cells that show apoptosis as a direct consequence of surface properties. One study states that the cell response is very different among different cells [59]. In this study, monocytes died on the

surface when cell adhesion was not explicitly stimulated with a precoating of fibrinogen, regardless of the surface topography. Mouse macrophages seemed unaffected. A study of bacterial viability [60] showed that an increasing amino content (and hence surface charge) resulted in faster bacterial adsorption, but also in a reduced viability. A third study [61] showed an increased rate of apoptosis among Osteoblast-like cells when they are in contact with a metal oxide surface, which was correlated to cell clustering. On the other hand, polystyrene surfaces coated with fructose-modified PAMAM dendrimers were found to actively reduce apoptosis among hepatocytes with increasing generation number [62].

6.2 Research Questions & Approach

Surface topology, -charge and –chemistry are determining factors in the process of cell adhesion and response. It is crucial to understand and to control these surface properties and cell responses if they are to be applied in biomedical situations, such as implants.

Here, the response of Human Osteoblast (HOB) cells to low-roughness planar surfaces that are functionalised with different biomimetic dendritic coatings is described. The coated surfaces were investigated for their

- ✓ Biocompatibility,
- ✓ Promotion of cell proliferation,
- ✓ Long term cell viability / cytotoxicity.

Only very few studies investigated the cell response to dendritic coatings on surfaces. Here, the following research questions were addressed:

- ✓ Do HOB cells adhere, grow and proliferate on dendrimer coated surfaces?

- ✓ Are there differences between the responses to polycationic and polyanionic coatings?
- ✓ Are polycationic dendrimers cytotoxic, like the PAMAM dendrimers discussed above, or do they enhance Osteoblast adhesion through a favourable electrostatic attraction?

In order to address these questions and to be able to compare the observations to literature, a simple experimental approach was designed (Fig. 6.3).

In short, thin glass cover slides commonly used for optical microscopy were coated with thin layers of chromium and gold. This surface now allowed for the attachment of molecules with a thiol-like functional group. The gold surface was thus coated with water-soluble dendrimers whose cores bear one dithiolane moiety (Fig. 6.4), which strongly binds to the gold via quasi-covalent bonds. This attachment process was be monitored by Contact Angle measurements (CA) and Surface Plasmon Resonance spectroscopy (SPR). The peripheral functionality of the dendrimers was either the sodium salt of a carboxylic acid or the hydrochloric acid salt of a diethyl amine. This yielded surfaces that were, under neutral pH conditions, either polyanionic or polycationic, respectively.

The employed dendrimers have an amphiphilic character. As described before (sections 0 and 3.3.5), they have a hydrophobic interior, dominated by aromatic rings and methyl groups and a hydrophilic periphery that bears numerous ionic groups, which are dissociated in an aqueous environment at neutral pH values. These groups are responsible for the dendrimers' overall

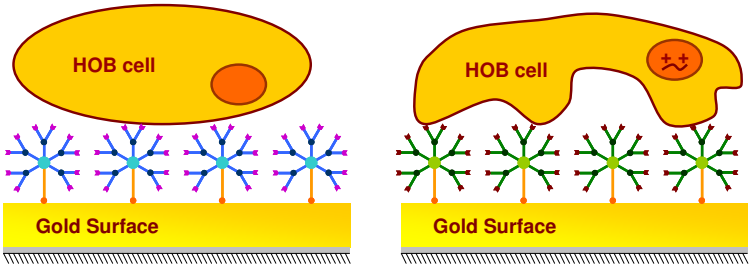

Fig. 6.3 — Cell adhesion and response to different dendrimer coated surfaces

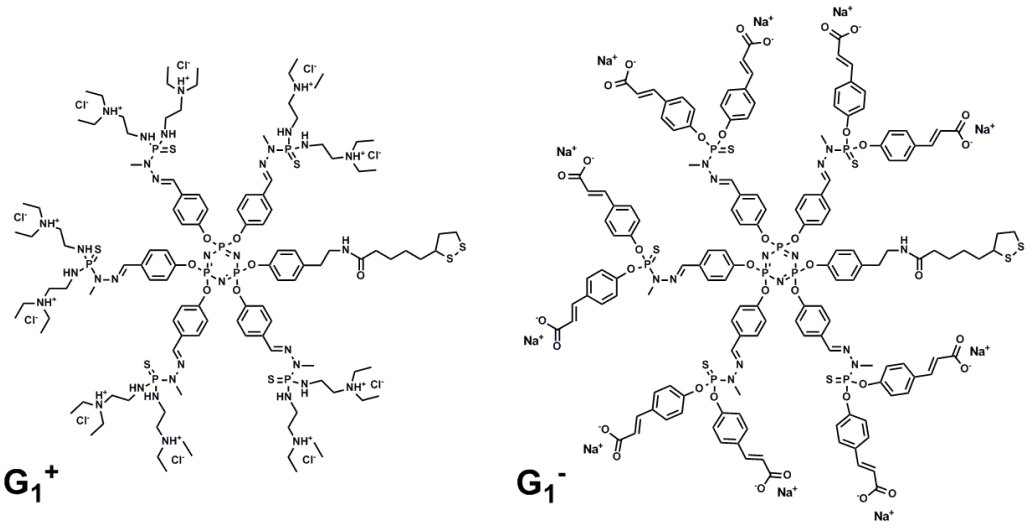

Fig. 6.4 — Left: G1 polycationic dendrimer, Right: G1 polyanionic dendrimer, each bearing 10 peripheral charges and one dithiolane moiety at its core.

solubility in water. This ambivalent character together with the flexibility of the dendritic wedges gives the dendrimers the ability to adapt to their environment. They can expose their hydrophobic interior to hydrophobic objects; they may even take up smaller hydrophobic molecules into their interior. The dendrimers' flexibility allows for positioning the peripheral charges depending on their environment.

These special properties may also allow for stronger interactions with cells that adhere to the dendrimer coating. Now, it is not only electrostatic interactions that play a role in the cell's attachment, but also the hydrophobic interactions with the cell's exteriors and their excreted proteins (Fibronectin, Vitronectin, Osteopontin and other proteins) that are responsible for an improved adhesion.

The dendrimer coated surfaces were incubated with a cell culture medium and tested for their biocompatibility. Cell counting and the determination of viability, confluence and generation number and time indicated how the cells adhered to the surface coating and how fast they adapted and proliferated. These parameters are indirect measures for the interactions between surface

and cells. All cell experiments were part of the diploma thesis of Nicole Deloch (MPI-P).

6.3 Results and Discussion

Here, results obtained on the adhesion of HOB cells onto dendrimer coated surfaces are discussed. In total, we have followed the adhesion process and the different parameters on 3 samples coated with polycationic dendrimers and 5 samples with polyanionic dendrimers over a time span of 13 days. Three control experiments were done on glass substrates coated with only chromium and gold. Only one of them is taken into the discussion, as their results were nearly identical.

6.3.1 Cell adhesion and morphology

Optical microscopy is a valuable method for assessing cell morphology during the cell adhesion and proliferation. During the first 24 hours, the cells were observed several times in order to assess the cell attachment and spreading process. The Osteoblasts spread readily on all surfaces and there was no obvious difference between either of the surfaces. After 24 hours most of the cells had adopted their typical stretched shape and they seemed to try and make contact with neighbouring cells. This contact is vital for survival and is usually made within the first few days. A selection of the results is provided in Fig. 6.5.

The cell proliferation was followed until the confluence rate was 80-100%, meaning that (nearly) the whole surface is covered with cells. After the first few days, the cells started to show a different behaviour on the samples coated with positively charged dendrimers. There was no obvious difference between the observations on the control surfaces (Au coated glass or the Petri dish plastic), which suggests that cells did attach, stretch and proliferate similarly easily on these surfaces. On the positively charged dendrimers, however, many rounded cells appeared and the surface coverage was relatively low. This

indicates that the cells did not proliferate as well as on the other surfaces. The rounded cells may have been dead cells, which concurs with the decreased proliferation. Also on the other samples, a few rounded cells were observed, but most of them spread again. This is a common process and is related to mitosis (cell division): The cell relaxes its contact to the surface, rounds up, divides and the two new cells re-attach and spread again. Moreover, on the positively charged dendrimers it was observed that all cells were retracting on

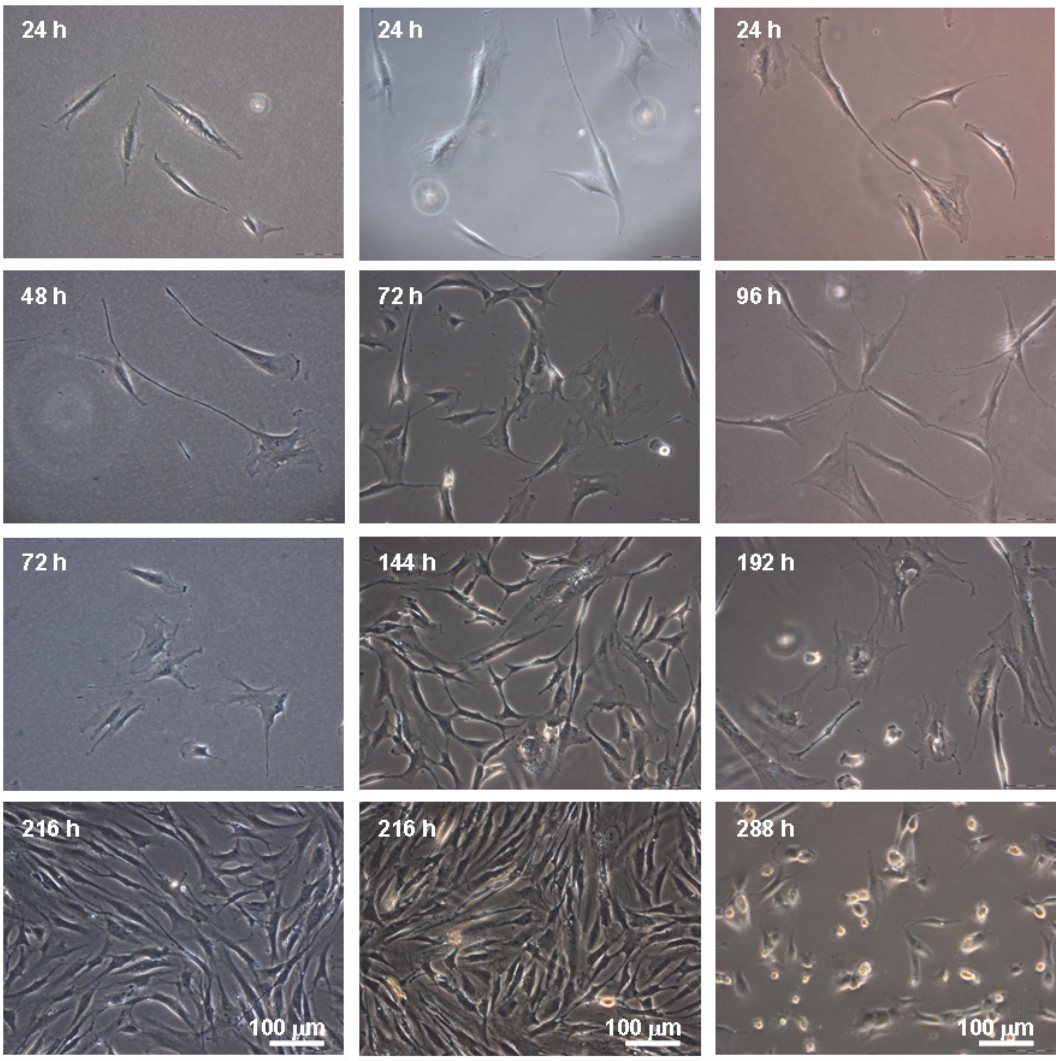

Fig. 6.5 – HOB cell proliferation on different surfaces (left: control, middle: G_1^-, right: G_1^+) at different moments. On the control and G_1^- surfaces, the cells spread and multiply, indicating healthy behaviour. On the G_1^+ samples, cells initially spread, but do not multiply and ultimately die. The image sizes are all identical.

longer time scales. In the bottom right image of Fig. 6.5 only rounded cells could be observed.

Apoptosis

The microscopic images of the cells on positively charged dendrimer have been studied in more detail for the visualisation of the dead cells. The results are shown in
Fig. 6.6. In these images it becomes obvious that most cells die through apoptosis, rather than necrosis.

It was possible to observe the main morphological hallmarks for apoptosis concerning their appearance: cell shrinkage, nuclear leakage, membrane blebbing and the final phase where apoptotic bodies are formed. Cell shrinkage manifests itself with irregular cell shape and shady areas around the cells. When chromatin condensation takes place, it is possible to observe an inhomogeneous nucleus content, giving rise to a contrast differences within the nucleus. Membrane blebbing is an advanced form of cell shrinkage where as a result the membrane starts to deform heavily, showing large wrinkles. It is possible to observe the excretion of vesicles containing old cell material that will later be subject to phagocytosis. This manifests itself as small blobs quasi-attached to the cell membrane. Apoptotic bodies are the leftovers of the entire process and show up under the microscope as condensed, ring-like features.

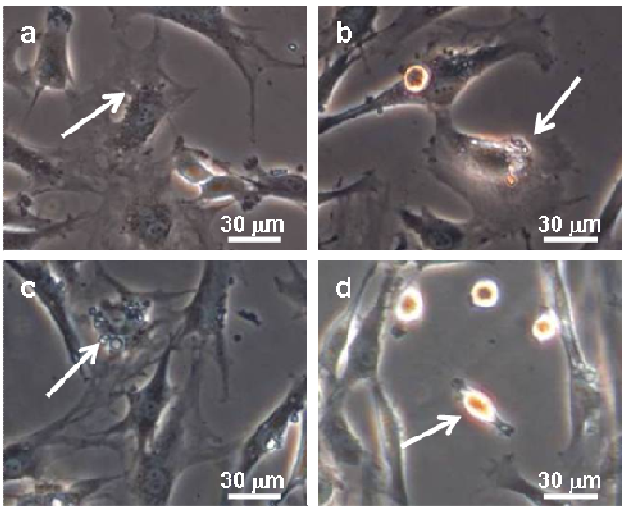

Fig. 6.6 – HOB cell morphology on polycationic dendrimers. Nearly all dead cells show hallmarks of apoptosis: a: cell retraction / shrinkage, b: membrane blebbing/apoptotic body formation, c: apoptotic body formation, d: apoptotic bodies.

However, more details could be obtained from a separate study by specific staining. These results clearly show all apoptotic phenomena, which were discussed in section 6.1.3.

In short

During the first days of cell adhesion, no differences were observed among the different samples. However, after a few days, microscopic studies revealed a clear difference in proliferation behaviour on positively charged dendrimers as compared to the negatively charged ones and the control surfaces. Cells became smaller and showed a high rate of apoptosis.

6.3.2 Viability test

In this experiment, the viability of the cells is determined as the ratio of living cells on a surface and the total number of cells on the surface. The dendrimer coated (or control) surfaces were transferred into a Petri dish containing growth medium and HOB cells. In order to have an internal positive control in every experiment, the cells that adhered to the Petri-dish plastic were also counted and evaluated for their viability. In Fig. 6.7 it can be observed that for all samples (except #1) the cells showed approximately the same viability on

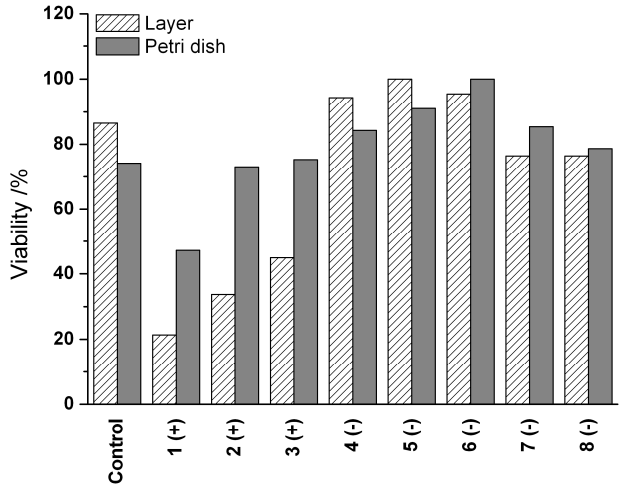

Fig. 6.7 – Cell viability on the three different surface types: control surface (gold), polycationic dendrimers (G_1^+), indicated with (+) and polyanionic dendrimers (G_1^-), indicated with (-). The numbers indicate the sample number.

the plastic of the Petri dish. Secondly, it was observed that HOB cells had no different viability on the plastic of the Petri dish or the samples coated with negatively charged dendrimers, nor on the control surfaces. In these cases, the viability was between 80% and 100%, which indicates a good health of the cells on all these surfaces. However, the difference in viability between cells on the plastic and on positively charged dendrimers is very significant. On positively charged dendrimers, the viability was twice as low as on the dish itself. The viability on polycationic dendrimers was around 30%, which indicated that the cells had a very poor viability.

In short

All these results indicate clearly that HOB cells preferred growing and proliferating on negatively charged dendrimers, rather than on positively charged dendrimers. On the latter, cell viability is severely compromised.

6.3.3 Cell counting test

Cell counting gave the same unambiguous results (Fig. 6.8). The total cell numbers within each sample (surface + plastic) varied from 85 until 140 thousand cells, which shows that a direct comparison between the different

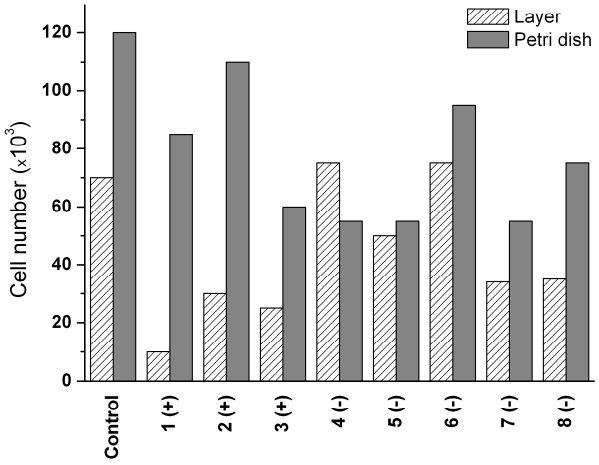

Fig. 6.8 – Cell number adhered to three different surface types: control surface (gold), polycationic dendrimers (G_1^+), indicated with (+) and polyanionic dendrimers (G_1^-), indicated with (-).The numbers indicate the sample number.

samples cannot be made. However, within each Petri dish, the results are clear: HOB cells show no preference for negatively charged dendrimers or the plastic, but there were only relatively few cells to be found on the positively charged dendrimers. But also on an absolute scale there were 2-3 times more HOB cells growing on the negatively charged dendrimers than on the positively charged ones. This all indicates that HOB cells have no affection for the polycationic dendrimers.

In short

The cell numbers on positively charged dendrimers was significantly lower than on all other surfaces. This indicates that they do not proliferate very well on these surfaces.

6.3.4 Generation time and number test

The generation time and number together give an indication for the proliferation rate. The generation time tells us the time needed for doubling the population size, whereas the generation number gives information on how many times the cells have multiplied on a particular sample. As they are mathematically interrelated and deduced from the same cell counting

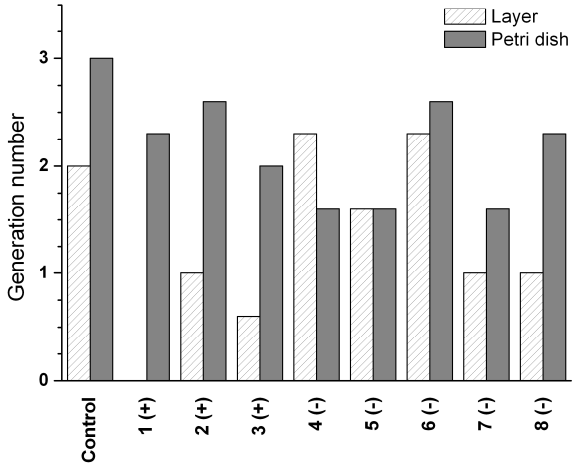

Fig. 6.9 – Generation number for each sample: control surface (gold), polycationic dendrimers (G_1^+), indicated with (+) and polyanionic dendrimers (G_1^-), indicated with (-). The numbers indicate the sample number.

experiment, only the results for generation number are shown (Fig. 6.9).
On sample #1, the viability of the cells was so low (22%) due to the high rate of apoptosis, that it was not possible to determine the generation time and number. For this sample, only the value for the cells on the Petri dish is given.
The generation time was for all Petri dishes very similar, suggesting that the proliferation behaviour of the HOB cells was for all Petri dishes the same, regardless of the type of sample it contained. The cells took on average approximately 5 days to divide. On the samples, the cells show different behaviour. Whereas the observations are not very unambiguous for the samples coated with polyanionic dendrimers, it is obvious that cells on positively charged dendrimers take a very long time to proliferate. This logically resulted in a low generation number.

These results confirm to the earlier observations that HOB cells have a reduced viability on the coatings made of polycationic dendrimers and conform to the fact that they show a high degree of apoptosis on these surfaces.

In short

HOB cells grow and proliferate slower on positively charged dendrimers than on negatively charged dendrimers. This is in good agreement with the reduced viability on the positively charged dendrimers.

6.3.5 Confluence test

This experiment shows to which extent the cells grow, proliferate and fuse into a dense layer. The confluence can be easily visualised with optical microscopy.

After one hour of incubation, HOB cells show good adhesion on all samples. There are no differences observed between either of the samples. The confluence rate is approximately 5%.

At 40-60% confluence, cell division was observed. As a result, they shortly exhibited spheroid topography. After 90-100% confluence was reached on

negatively charged dendrimers (and on the control sample), the cells showed their usual cell shape and very good spreading. However, on the positively charged dendrimers, very many of the cells showed apoptosis and these samples never reached full confluence as can be judged from Fig. 6.5.

6.3.6 Caspase assay test

The optical microscopy data strongly suggest a high degree of apoptosis on positively charged dendrimers. The observations include typical hallmarks of apoptosis: apoptotic body formation, cell shrinkage and membrane blebbing. This, however, has to be confirmed by a test on molecular level. To this end, a Caspase 3/7 assay was carried out that proofs the presence or absence of activated Caspase 3 and/or 7 activity and therewith, unambiguously, whether apoptosis is taking place or not.

Therefore, a new set of samples was prepared, coated with either positively or negatively charged dendrimers. The control surfaces possess again a bare gold surface. The samples were incubated with HOB cells until they showed signs of apoptosis and subsequently tested for their Caspase activity.

As the luminescence is proportional to the Caspase activity, it is also

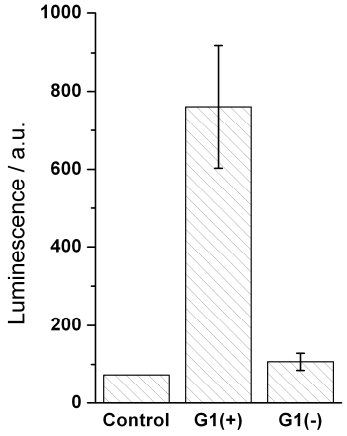

Fig. 6.10 – Caspase 3/7 assay on HOB cells that were cultured on the three different samples: control surface (gold), polycationic dendrimers (G_1^+) and polyanionic dendrimers (G_1^-)

proportional to the number of apoptotic cells. As the cells on the control surfaces and surfaces coated with negatively charged dendrimers did not show any clear sign of apoptosis, their response in the Caspase assay are very minimal, which can be considered background luminescence. However, the cells that had been in contact with the positively charged dendrimer surface coating showed a high Caspase activity, indicating that they suffer from apoptosis.

In short

Also on a molecular scale apoptosis among HOB cells was proven to be provoked by positively charged dendrimers and not by negatively charged dendrimers.

6.3.7 DAPI staining test

Additionally to the wealth of microscopic data, apoptosis was visualised in more detail with a DAPI staining. DAPI (4',6-diamidino-2-phenylindole dihydrochloride) selectively stains the genetic material in the cell (AT rich regions). As the concentration of RNA (compared to DNA) is very low, this method selectively visualises the DNA in the nucleus. This allows for recording fluorescence images that show apoptotic hallmarks like chromatin condensation and nuclear breakdown.

The nuclear material diffuses into the cytoplasm upon leakage of the nucleus. Therefore, cells containing recognisable nuclei with sharply defined dimensions are healthy, whereas the cells suffering from apoptosis have their DNA diffusing through their cytoplasm, which gives rise to a faintly recognisable nucleus and fluorescence intensity distributed throughout the cell. In Fig. 6.11, three DAPI fluorescence images with their corresponding overlay with a phase-contrast microscopic image (a+b) or magnification (c). Two living cells can be observed with their nuclear membranes still intact (arrow 1). In the same image and also in the other images, most cells are suffering from apoptosis. This manifests itself in irregular nucleus shapes, membrane blebbing and apoptotic body formation (arrows 2-5). In a less

advanced state of apoptosis, chromatin condensation could be observed in two occasions in *image c*, where the nuclear content has a rather granular appearance (arrow 5). All images support the conclusion that apoptosis occurs on positively charged dendrimer coated surfaces.

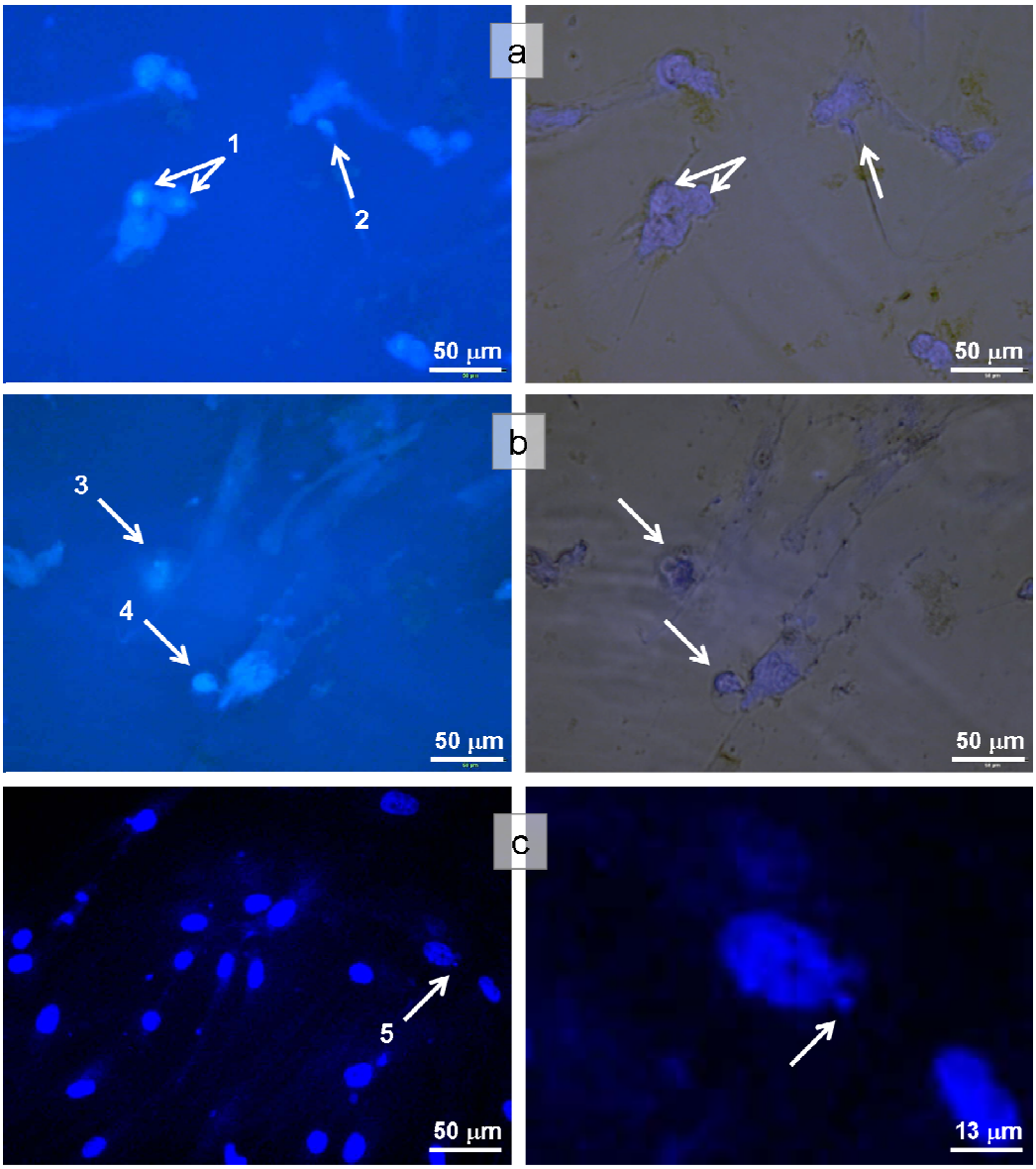

Fig. 6.11 – <u>Left:</u> Fluorescent DAPI staining images with their corresponding overlay with a phase-contrast microscopic image (right, a+b) or magnification (right, c). HOB cells on polycationic dendrimer coated surfaces show signs of apoptosis, indicated by the numbered arrows. 1: two intact cell nuclei, 2-5: membrane blebbing and/or apoptotic body formation, 5: chromatin condensation (granular appearance of the nucleus)

6.4 Discussion

All the above described experiments have proven that surface coatings of polycationic dendrimers bearing diethylammonium moieties at their periphery provoke apoptosis among HOB cells. Cells grew and proliferated normally on coatings comprised of dendrimers with carboxylic peripheral functionalities (and identical interior composition), like on the bare gold and the Petri plastic control samples. This highly selective HOB response to one of the dendrimers indicates that it is the peripheral diethylammonium groups that are cytotoxic.

As extensively described in the introduction to this chapter, water-soluble positively charged dendrimers (PAMAM starburst type) and linear polymers are able to induce apoptosis among many cell types [45-58]. However, the main difference with the work described here is that these studies investigated the cytotoxicity of polycations in solution, whereas our experiments were carried out on a solid support. PAMAM dendrimers and linear polycations were found to diffuse through the cell membrane and to integrate into the mitochondrial membrane where they are responsible for the destruction of the organelle's integrity, for setting free Cytochrome c (which directly triggers apoptosis by the activation of Caspase 9) and for inhibiting the respiratory chain from functioning. It was described that the amine content as well as the amine substitution degree (primary - quaternary) affect cytotoxicity, where higher substitution degrees were found to be more lethal [50, 55]. It was shown by other studies that dendrimers and linear polymers containing tertiary amines can be cytotoxic to cells when applied as a solution. In the present study, however the dendrimers were fixed to the surface via a quasi-covalent dithiolane-gold linkage, which was assumed to hold during the whole experiment. Under the assumption that the dendrimers were released from the surface during the experiment, they might have been taken up by the cells and have compromised the mitochondrial integrity, which ultimately would lead to an apoptotic response like PAMAM dendrimers do.

There are only a few literature reports on apoptosis specifically induced by surface coatings as described in the introduction [59-61]. In general, cells are unaffected by amines or by positively charged surfaces. In fact, cells adhere preferentially to cationic surfaces due to the favoured electrostatic interaction between surface and cell membrane. The most relevant factor that provoked apoptosis was related to amine content. Although this study was carried out with another cell type, it shows that amines can also be cytotoxic to cells when applied as a surface functionality. This is in agreement with the finding in this chapter and it shows that the dendrimers do not have to be released from the surface in order to evoke apoptosis. Furthermore, it is noteworthy that surfaces coated with thiols (-SH) were reported to be harmless [21]. This suggests that, if the dendrimers were released from the gold surface, it was not the SH functionality that led to a cytotoxic response. In another study, almost identical cationic dendrimers were applied electrostatically bound coatings for enhancing neuron cell adsorption. They bore diethylammonium groups as well, but were not found to be cytotoxic to neurons [20]. This suggests that it strongly depends on the cell type whether a chemical is cytotoxic or not.

During cell division, adsorbed cells retract and adopt a globular shape. This process requires a certain mobility that allows the cells to retract and reshape. Positively charged dendrimers, however, are oppositely charged to the cell membrane and have therefore a stronger attractive electrostatic interaction with the cells. This may hamper the required retraction and reformation thereby obstructing cell division. This subsequently triggers the activation of the apoptosis pathway.

Altogether, the findings presented in this chapter strongly suggest that it is the peripheral tertiary amines that cause the apoptosis of HOB cells on positively charged dendrimers due to reduced cell mobility and a possible cytotoxicity.

6.5 Synopsis and Conclusion

Glass supported gold surfaces could be coated with two different water-soluble dendrimers that bear a dithiolane moiety at the core and either polyanionic or polycationic functional groups at their periphery. Their film thickness of 1 nm indicated an approximate surface coverage of nearly 100%. The charged moieties were unable to render the surface very hydrophilic, which resulted in a 50° water contact angle, indicating that the dendrimer interior is in both cases exposed to the aqueous medium. To these surfaces, Human Osteoblast (HOB) cells were applied and their proliferation behaviour was compared. On negatively charged dendrimers, the HOB cells behave like on the reference samples (bare gold and Petri dish plastic). On the positively charged dendrimers, HOB cells showed a high rate of apoptosis (as proven with a Caspase activity test, DAPI staining). Optical microscopy and DAPI staining revealed all symptoms of apoptosis (as opposed to necrosis): chromatin condensation, membrane blebbing, cell shrinkage and apoptotic body formation. The cells showed a drastically decreased cell number, proliferation rate and viability. Therefore it can be concluded that peripheral diethylammonium functionalities of the dendrimers induce apoptosis among HOB cells, whereas on polyanionic dendrimers HOB cells appear to grow and proliferate normally. The apoptosis process was triggered by a reduced cell mobility (required for cell division) and/or cytotoxicity of the dendritic cations. The negatively charged dendrimers allowed for good cell proliferation and are therefore suitable candidates for coatings on medical devices when permanent cell adhesion is required (implants).

6.6 Materials and Methods

In this section, all technical and experimental details are described. All water used was demineralised using MilliQ equipment and the resistivity was 18 MΩ.cm.

6.6.1 Sample preparation

Cleaning procedure

Glass cover slips (2.5 x 2.5 cm) were first thoroughly cleaned. They were submerged twice in a 2% aqueous solution of the detergent Hellmanex and once in HPLC grade ethanol and sonicated for 15 minutes. In between, the samples were rinsed with an excess of water and ethanol, respectively. Finally they were dried with a stream of nitrogen gas.

Chromium and gold evaporation

Chromium and gold can be evaporated onto the glass slides using electrothermal evaporation at reduced pressure (ca. 5.10^{-6} mbar). The equipment used was an Edwards Auto 306 and it allows rotating the samples to guarantee a homogenously distributed gold layer. The 2 nm thick chromium layer acted as an adhesion layer between the 50 nm gold and glass substrate.

Dendrimer coating

The freshly prepared gold samples were immersed into a 1 mg/mL aqueous solution of either the generation 1 (G1) polycationic or polyanionic dendrimers bearing one dithiolane functional group connected to the core (Fig. 5.6). The samples were exposed to this solution for at least 15 hours at room temperature. Subsequently the slides were rinsed with an excess of water and HPLC grade ethanol. Under sterile conditions, the samples were rinsed with a 70% aqueous ethanol solution to sterilise the surfaces right before their application.

6.6.2 Surface Plasmon Resonance Spectroscopy

Glass slides (high refractive index, $n \approx 1.82$, $LaSFN_9$) were cleaned and coated as described in section 5.6.1. The sample slide was attached to the $LaSFN_9$ prism using refractive index matching oil (n=1.7, Cargille Labs, USA). The

dendrimer adsorption was carried out using a flow cell. The laser used was a HeNe laser with one spectral line at 632.8 nm.

6.6.3 Contact Angle measurements

The water contact angles were measured with an OCA 15+ (DataPhysics, Filderstadt, Germany) goniometer equipped with a CCD camera and an electronic dosing unit. For the determination of the contact angle, SCA 20 software was used that automatically recognises the droplet, fits a curve around the silhouette (LaPlace fitting) and calculates the contact angle. The droplet volume was 3 µL and the water was degassed before usage. At least 5 measurements per surface were performed in order to obtain a statistically sound result.

6.6.4 HOB cells

The cell line used (HOB, Human Hipbone Osteoblasts,) is commercially available from Promocell. First a cell bank was created with these cells. For culturing the HOB cells, we employed the commercially available HOB Growth medium also containing a supplement mix, as described in the technical bulletin of the supplier. All cell experiments have been performed under strictly sterile conditions in a S1 type laboratory.

Cell culture

Before their usage, the HOB cells were defrosted and transferred to a sterile T75 flask. The flask was stored in an incubator at 37 °C and 5% CO_2 for a couple of days depending on the condition of the cells (as observed with optical microscopy). The growth medium was exchanged every 48 hours to ensure the optimum conditions for cell growth.

Sample incubation

The gold coated glass substrates, covered with a monolayer of dendrimers (or the reference samples lacking the dendrimer layer) were transferred in a 60 mm Petri-dish containing 3 mL growth medium and $2.0.10^4$ HOB cells per

mL. During the experiment, the growth medium was also exchanged every second day.

6.6.5 Methods

Here, the different measurements and used equipment (if applicable) are described. Cell experiments were part of the diploma thesis of Nicole Deloch (MPI-P).

Confluence

By means of optical microscopy it was possible to follow the growth and proliferation of the cells. The confluence rate was determined by approximating the relative surface area occupied by the cells.

Trypsination

Trypsination is a method to release adhered cells from a surface. In this procedure, the sample surfaces were taken out of the Petri dishes, transferred to a new Petri dish, washed with Hepes BSS buffer (which is removed afterwards) and subsequently exposed to a trypsination solution (Detach kit, Promocell) containing 2.5 mL Trypsin / EDTA. The cell detachment (rounding) was followed by optical microscopy and when they had been released from the sample surface, they were treated with 2.5 mL TNS to quench the trypsin/EDTA activity. This 5 mL cell solution was centrifuged at 400 g for 5 minutes (at room temperature). The supernatant was separated from the cell pellet and the pellet is re-suspended into 2 mL HOB growth medium.

In case of trypsinating the cells that adhered to the Petri dish itself, the above described procedure was applied to the Petri dishes.

Cell counting

After trypsination, cell counting was done after approx. 300 hrs, when 80-100% confluence was reached. From the solution left after trypsination 20 µL

was taken and mixed with an equal amount of Trypan Blue stain (GIBCO, 0.4%). The cell suspension was transferred to a Neubauer cell counter for counting.

Viability determination

After the trypsination and counting procedure described above, the relative number of living cells (stained brightly blue) with respect to the dead cells (dark blue) was determined.

Cell generation number and generation time

After cell counting it was possible to determine the generation time and number by the following equations:

$$n = \log\left(\frac{N}{N_0}\right) \Big/ \log 2 \qquad \textbf{Eqn. 6.1}$$

$$tg = t \log 2 \Big/ \log\left(\frac{N}{N_0}\right) \qquad \textbf{Eqn. 6.2}$$

with n being the generation number, tg being the generation time, N being the final number of cells, N_0 the initial number of cells and t the time elapsed between N and N_0. This approach presumes an exponential growth of the number of cells.

DAPI staining

DAPI (4',6-diamidino-2-phenylindole dihydrochloride) is a fluorescent dye that specifically and strongly intercalates in the minor groove between the two strands of DNA molecules. It is water-soluble and easily passes through cell membranes due to its two positively charged diamidino groups. Because of its specific binding, it is widely used for staining cell nuclei and for instance viral DNA. This allows for the recognition of the cell cycle (proliferation) of single cells and also for checking the condition of a whole cell culture. This indirectly gives information about possible contaminations and the quality of the nutrient supplies. Another application of this stain is the staining of apoptotic

cells, as their cell nuclei open up and DNA is located everywhere in the cell. The absence of a clearly stained nucleus is then a powerful suggestion for apoptotic cell death.

For the visualisation of the stained cells a fluorescence microscope was used. The excitation wavelength was around 358 nm in the UV range and the DAPI emission was at 454 nm (blue), as a DNA-DAPI complex. The microscope filters were selected accordingly (UV Filter M-MNU2 360-370 nm, Olympus). Extreme care must be taken when handling and disposing this chemical because of its toxicity and mutagenic properties. DAPI is commercially available and it was purchased from Carl Roth GmbH. The powder was diluted into water (2 mg/mL) and 50 µL was added to the cell culture. The microscope used was an Olympus IX 70. Images were taken at a 400-fold magnification and were recorded using a CCD camera.

Apoptosis Caspase-Glo® 3/7 Assay

The purpose of this assay is to determine the activity of Caspase 3 and/or Caspase 7 in cells. These two Caspases are the key proteins in the apoptosis process (section 6.1.3) in mammalian cells. They are proteases that specifically attack cysteine and aspartic acid residues.

The assay first evokes cell lysis after which all cell contents are exposed to the other components of the assay. Then, if either of the caspases is present, the Z-

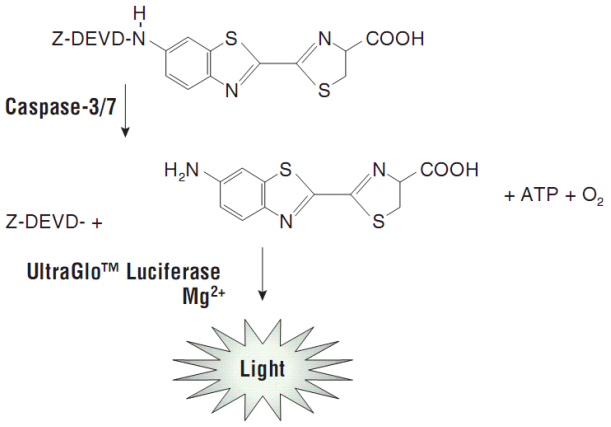

Fig. 6.12 – Functioning of the Caspase-Glo® 3/7 Assay schematically [63]

DEVD (a tetra-peptide) labelled aminoluciferin is relieved of its tetra peptide, yielding the luciferin analog. This latter molecule is ultimately recognised by the luciferase protein present in the assay and this leads to luminescence that can be detected by a luminometer. The assay conditions ensure the full functionality of all its components due to additives like Mg^{2+} ions and appropriate buffers. The assay was purchased from Promega and was used as described in the technical bulletin.

From each sample cells were taken by the trypsination method described above, selectively from the sample surface or the Petri-dish surface and transferred to a 96-wells Elisa plate. The cells were put to re-attach to the Elisa walls for approximately 24 hours in HOB growth medium. 100 µL medium was left in each Elisa well and mixed with another 100 µL of the Assay solution. Subsequently, the Elisa plate was kept in the dark for 30 minutes for the assay to reach full activity and then measured with a luminometer (GloMax Multi, Promega, Mannheim).

6.7 Bibliography

[1] S.F. Rose, A.L. Lewis, G.W. Hanlon, A.W. Lloyd, Biomaterials 25/21 (2004) 5125.
[2] K. Anselme, Biomaterials 21/7 (2000) 667.
[3] V.I. Sikavitsas, J.S. Temenoff, A.G. Mikos, Biomaterials 22/19 (2001) 2581.
[4] T.A. Horbett, J.J. Waldburger, B.D. Ratner, A.S. Hoffman, J Biomed Mater Res 22/5 (1988) 383.
[5] B. Hopp, N. Kresz, J. Kokavecz, T. Smausz, H. Schieferdecker, A. Doring, O. Marti, Z. Bor, Appl Surf Sci 221/1-4 (2004) 437.
[6] A. Dekker, T. Beugeling, A. Poot, J. Feijen, A. Bantjes, W.G. Vanaken, Abstr Pap Am Chem S 201 (1991) 188.
[7] R. Nicholov, N. Lum, R.P.N. Veregin, F. Dicosmo, Acs Sym Ser 602 (1995) 280.
[8] A. Thapa, D.C. Miller, T.J. Webster, K.M. Haberstroh, Biomaterials 24/17 (2003) 2915.
[9] S.J. Lee, J.S. Choi, K.S. Park, G. Khang, Y.M. Lee, H.B. Lee, Biomaterials 25/19 (2004) 4699.
[10] V. Sollazzo, A. Palmieri, F. Pezzetti, A. Scarano, M. Martinelli, L. Scapoli, L. Massari, G. Brunelli, E. Caramelli, F. Carinci, J Biomed Mater Res B Appl Biomater 85/1 (2008) 29.
[11] K. Anselme, M. Bigerelle, Acta Biomater 1/2 (2005) 211.
[12] K. Anselme, M. Bigerelle, B. Noel, E. Dufresne, D. Judas, A. Iost, P. Hardouin, J Biomed Mater Res 49/2 (2000) 155.
[13] K. Kato, S. Sano, Y. Ikada, Colloid Surface B 4/4 (1995) 221.
[14] J.S. Mao, Y.L. Cui, X.H. Wang, Y. Sun, Y.J. Yin, H.M. Zhao, K. De Yao, Biomaterials 25/18 (2004) 3973.
[15] G. Rainaldi, P. Filippini, A. Ferrante, P.L. Indovina, M.T. Santini, J Biomed Mater Res 55/1 (2001) 104.
[16] M. Wahlgren, T. Arnebrant, Trends Biotechnol 9/6 (1991) 201.

[17] C.R. Wittmer, J.A. Phelps, W.M. Saltzman, P.R. Van Tassel, Biomaterials 28/5 (2007) 851.
[18] K.Y. Cai, M. Frant, J. Bossert, G. Hildebrand, K. Liefeith, K.D. Jandt, Colloid Surface B 50/1 (2006) 1.
[19] B. Finke, F. Luethen, K. Schroeder, P.D. Mueller, C. Bergemann, M. Frant, A. Ohl, B.J. Nebe, Biomaterials 28/30 (2007) 4521.
[20] J.L. Hernandez-Lopez, H.L. Khor, A.M. Caminade, J.P. Majoral, S. Mittler, W. Knoll, D.H. Kim, Thin Solid Films 516/6 (2008) 1256.
[21] R.K. Aithal, D.P. Kumaraswamy, D.K. Milis, D. Kuila, J Biomed Nanotechnol 3/3 (2007) 254.
[22] A.P. Zhu, N. Fang, Biomacromolecules 6/5 (2005) 2607.
[23] A.P. Zhu, F. Zhao, N. Fang, J Biomed Mater Res A 86A/2 (2008) 467.
[24] B. Nebe, B. Finke, F. Luthen, C. Bergemann, K. Schroder, J. Rychly, K. Liefeith, A. Ohl, Biomol Eng 24/5 (2007) 447.
[25] Y. Xu, M. Takai, K. Ishihara, Biomaterials 30/28 (2009) 4930.
[26] M. Swierczewska, C.S. Hajicharalambous, A.V. Janorkar, Z. Megeed, M.L. Yarmush, P. Rajagopalan, Acta Biomaterialia 4/4 (2008) 827.
[27] D. Vautier, V. Karsten, C. Egles, J. Chluba, P. Schaaf, J.C. Voegel, J. Ogier, J Biomat Sci-Polym E 13/6 (2002) 713.
[28] A. Bagno, A. Piovan, M. Dettin, A. Chiarion, P. Brun, R. Gambaretto, G. Fontana, C. Di Bello, G. Palu, I. Castagliuolo, Bone 40/3 (2007) 693.
[29] M. Dettin, A. Bagno, R. Gambaretto, G. Iucci, M.T. Conconi, N. Tuccitto, A.M. Menti, C. Grandi, C. Di Bello, A. Licciardello, G. Polzonetti, J Biomed Mater Res A 90A/1 (2009) 35.
[30] M. Dettin, M.T. Conconi, R. Gambaretto, A. Bagno, C. Di Bello, A.M. Menti, C. Grandi, P.P. Parnigotto, Biomaterials 26/22 (2005) 4507.
[31] A.J. Garcia, C.D. Reyes, J Dent Res 84/5 (2005) 407.
[32] Y.J. Lee, S.J. Park, W.K. Lee, J.S. Ko, H.M. Kim, Biomaterials 24/6 (2003) 1059.
[33] J.R. Potts, I.D. Campbell, Matrix Biol 15/5 (1996) 313.
[34] F.C. Soumetz, L. Pastorino, C. Ruggiero, J Biomed Mater Res B 84B/1 (2008) 249.
[35] B.D. Boyan, C.H. Lohmann, D.D. Dean, V.L. Sylvia, D.L. Cochran, Z. Schwartz, Annu Rev Mater Res 31 (2001) 357.
[36] B.D. Boyan, S. Lossdorfer, L. Wang, G. Zhao, C.H. Lohmann, D.L. Cochran, Z. Schwartz, Eur Cell Mater 6 (2003) 22.
[37] D.D. Deligianni, N. Katsala, S. Ladas, D. Sotiropoulou, J. Amedee, Y.F. Missirlis, Biomaterials 22/11 (2001) 1241.
[38] R. Lange, F. Luthen, U. Beck, J. Rychly, A. Baumann, B. Nebe, Biomol Eng 19/2-6 (2002) 255.
[39] S.P. Massia, J.A. Hubbell, J Cell Biol 114/5 (1991) 1089.
[40] S.R. Benhabbour, H. Sheardown, A. Adronov, Biomaterials 29/31 (2008) 4177.
[41] H. Lodish, A. Berk, S.L. Zipursky, P. Matsudaira, D. Baltimore, J.E. Darnell, Molecular Cell Biology, New York, 2001.
[42] J.F.R. Kerr, A.H. Wyllie, A.R. Currie, Brit J Cancer 26/4 (1972) 239.
[43] W. Malorni, http://www.cyto.purdue.edu/flowcyt/research/cytotech/apopto/data /malorni/malorni.htm#electron.
[44] M. Bovellan, M. Fritzsche, C. Stevens, G. Charras, Febs J 277/1 (2010) 58.
[45] J.H. Lee, K.E. Cha, M.S. Kim, H.W. Hong, D.J. Chung, G. Ryu, H. Myung, Toxicol Lett 190/2 (2009) 202.
[46] J.H.S. Kuo, M.S. Jan, H.W. Chu, J Pharm Pharmacol 57/4 (2005) 489.
[47] T. Gabryelak, A. Rucinska, K. Maczynska, B. Klajnert, S. Rozalska, Febs J 276 (2009) 309.
[48] K. Winnicka, K. Bielawski, M. Rusak, A. Bielawska, J Health Sci 55/2 (2009) 169.
[49] N.A. Stasko, C.B. Johnson, M.H. Schoenfisch, T.A. Johnson, E.L. Holmuhamedov, Biomacromolecules 8/12 (2007) 3853.
[50] D. Fischer, Y.X. Li, B. Ahlemeyer, J. Krieglstein, T. Kissel, Biomaterials 24/7 (2003) 1121.
[51] D. Fischer, T. Bieber, Y.X. Li, H.P. Elsasser, T. Kissel, Pharm Res 16/8 (1999) 1273.
[52] J. Haensler, F.C. Szoka, Bioconjugate Chem 4/5 (1993) 372.
[53] D.M.L. Morgan, J. Clover, J.D. Pearson, J Cell Sci 91 (1988) 231.
[54] D.M.L. Morgan, V.L. Larvin, J.D. Pearson, J Cell Sci 94 (1989) 553.

[55] P. Ferruti, S. Knobloch, E. Ranucci, R. Duncan, E. Gianasi, Macromol Chem Physic 199/11 (1998) 2565.
[56] S. Choksakulnimitr, S. Masuda, H. Tokuda, Y. Takakura, M. Hashida, J Control Release 34/3 (1995) 233.
[57] H.J.P. Ryser, Nature 215/5104 (1967) 934.
[58] A.K. Singh, B.S. Kasinath, E.J. Lewis, Biochim Biophys Acta 1120/3 (1992) 337.
[59] C. Gretzer, M. Werthen, P. Thomsen, Biomaterials 23/7 (2002) 1639.
[60] A. Terada, A. Yuasa, T. Kushimoto, S. Tsuneda, A. Katakai, M. Tamada, Microbiology 152/Pt 12 (2006) 3575.
[61] E. Czarnowska, A. Sowinska, B. Cukrowska, J.R. Sobiecki, T. Wierzchon, Mater Sci Forum 475-479 (2005) 2415.
[62] M. Kawase, T. Shiomi, H. Matsui, Y. Ouji, S. Higashiyama, T. Tsutsui, K. Yagi, J Biomed Mater Res 54/4 (2001) 519.
[63] Promega, Technical Bulletin, 2009.

7 Conclusions

This thesis describes the synthesis and application of new dendritic materials at the interface of materials science and biology. Ten new phosphorus containing dendrimers have been synthesised which are all exclusively water-soluble through their either polycationic or polyanionic peripheral functional groups. Most of them have been obtained in large (1 gram) quantities. Two families of dendrimers are distinguished; the first carries ferrocenyl derivatives at either the core or in the branches and the second bears a dithiolane linker at the core that binds to gold surfaces.

The first family comprises a set of electrochemically active building blocks. The Fc-G_0 dendrimers were electrochemically characterised for their standard redox potential. In both cases, Cyclic Voltammetry showed reversible redox behaviour of the ferrocenes, but the scan rate study revealed that the diffusion coefficient was very low, indicating possible dendrimer aggregation. This can be explained by a reduced water solubility of the dendrimers due to their hydrophobic interior. The reduced solubility makes these dendrimers less attractive for application in aqueous systems.

In the second family, generation 1 and 2 dendrimers have been synthesised of which only the G_1 series covalently bound to gold. This shows that G_2 buries its dithiolane linker inside the hydrophobic dendrimer interior, effectively shielding it from the aqueous environment. Therefore, these dendrimers could not be used as coatings on gold surfaces. Both polyanionic and polycationic G_1 dendrimers were found to strongly bind to gold and assemble into a 1 nm thick monolayer at a surface coverage of nearly 100%. Water contact angle measurements (50°) showed that the resulting coating is neither very hydrophilic nor a clearly lipophilic character. This reveals that the terminal ionic moieties do not completely cover the dendrimer's periphery and that the hydrophobic interior is exposed to the aqueous environment.

The integration of Surface Plasmon Spectroscopy and Electrochemical Impedance Spectroscopy into one setup allowed for the investigation of membrane formation on dendrimer coated gold surfaces. The attempts to construct dendrimer tethered lipid bilayer membranes with a high Ohmic resistance failed. This finding confirms that lipids require pre-organisation and a homogenous surface chemistry in order to organise themselves into a well-defined membrane, whereas the dendrimer film surface has a chemically heterogeneous character. In order to improve the pre-organisation for membrane formation, the His-tagged membrane protein cytochrome c oxidase was successfully immobilised on a film of polyanionic dendrimers by the double complexation of Nickel cations. The clear separation of a hydrophobic and hydrophilic region on the protein appeared, however, insufficient for obtaining a well-defined lipid bilayer membrane.

Giant Unilamellar Vesicles, however, attached firmly to the dendrimer film without fusing into a lipid bilayer. This result paved the way for investigating the adhesion of cells, which are in first approximation large vesicles as well. Human Osteoblast (HOB) cells were adhered and cultured on the films and the polyanionic dendrimers proved themselves perfectly appropriate for applications where good cell adhesion is required (permanent medical implants in bone tissue). The cationic dendrimers, however, appeared to be cytotoxic to the cells, which can be explained by two independent parameters. Firstly, tertiary ammonium groups are toxic as they compromise the cell membrane integrity. Secondly, a strong electrostatic attraction between the dendrimers and cell membranes reduces the usually required cell mobility and in particular during cell division.